BALANCED FLAP TYPE SUPERSONIC CONTROL SURFACES

Thesis by

Harry J. Heimer

In Partial Fulfillment of the Requirements

For the Degree of

Doctor of Philosophy

California Institute of Technology

Pasadena, California

1958

ACKNOWLEDGEMENTS

The author would like to acknowledge the guidance and support of Dr. Homer J. Stewart in this research. The author is also grateful to the Hughes Aircraft Company which permitted him to do the experimental work necessary for this thesis as part of the development testing of its guided missile projects. Without its support this research would not have been possible. Among those at the Hughes Aircraft Company who were instrumental in this project and to whom the author expresses gratitude are: Allen E. Puckett for his general support, Richard S. Faucett for his fine work in design and construction of the model, and Bohdan I. Wandzura for his assistance with the tests.

Gratitude must also be expressed to the Jet Propulsion Laboratory's staff of the 12 Inch Wind Tunnel for their cooperativeness during the testing and to James Edberg, the project engineer.

ABSTRACT

The purpose of this investigation is to qualitatively explain the flow phenomena which occur on a balanced flap type control surface at supersonic speeds and to find means of calculating the pressure distributions occurring. The popular and generally useful linearized flow theory, and in fact any inviscid theory, cannot be used since viscosity plays a predominant part in the determination of the flow. It is shown that the flow often involves shock induced separation and reflection of shock waves by these separated wakes. Experimental data in the form of pressure distributions and shadowgraph pictures of the flow are used to arrive at a description of the flow. By use of the empirical results given, a method of predicting the pressure distributions for this type of surface is derived. This procedure is then used to calculate several pressure distributions which are compared with those experimentally determined.

The separation effects that occur at the larger angles of attack and/or control surface deflection angles cause the control effectiveness and hinge moments to be very non-linear. It is shown that the use of a gap between the wing and control surface delays or eliminates separation depending on the size of the gap used. Data are presented for a typical control surface, in which the hinge moments were reduced by a factor of 8 or 10 by using a gap between the wing and control surface. A method is given for estimating the size gap necessary to achieve this reduction.

TABLE OF CONTENTS

I. PURPOSE

To understand the flow phenomena which occur on a balanced flap type control surface configuration at supersonic speeds, and to determine a suitable method of predicting the pressure distribution.

II. INTRODUCTION

While the author was in charge of wind tunnel testing at the Hughes Aircraft Company, wind tunnel tests of numerous control surface configurations showed that their effectiveness and hinge moments were considerably different from what would be expected from classical theory. These effects were first noticed in 1951 and were most apparent at Mach numbers above 3. Testing was continued through 1953 during which time force tests on a large number of control surface configurations were made. However, the force tests were not sufficient to give a detailed picture of the flow from which an understanding of the flow phenomenon could be obtained. Many of the results of the force tests which were quite puzzling at the time are now obvious from the knowledge gained in the current series of tests.

The lack of understanding of the force results obtained in these control surface tests suggested the subject of this research project. The Hughes Aircraft Company, being interested in this work, permitted the author to use its facilities to design and build the necessary models and to run the tests in the Jet Propulsion Laboratory 12 Inch Wind Tunnel.

Balanced control surfaces are used to reduce the hinge moments and thus the forces required to move the surface. In guided missiles and in current aircraft using hydraulically actuated control surfaces, this can result in a considerable weight reduction in the hydraulic system. Because of the high growth

factor that occurs on some missiles, it has been estimated in some instances that the use of unbalanced control surfaces instead of balanced surfaces would double the overall weight of the vehicle if the same performance were maintained. Therefore it is felt that it is important to understand the character of the flow over such surfaces.

In the force tests performed while at the Hughes Aircraft Company, it was found that one could ameliorate the flow changes with Mach number by using a gap between the control surface and the main surface. This idea was further investigated in the present tests to determine and understand the advantageous changes that result from the use of a gap.

In order to explain the flow phenomenon on a balanced flap type control surface, it was decided that both visual and pressure distribution data would be useful. The tunnel available for these tests was the 12 Inch Supersonic Wind Tunnel at the Jet Propulsion Laboratory. It was decided that the simplest model that would represent the flow conditions adequately would be a two dimensional model with wedge cross sections. In designing the model, it was found to be more practical to use two models, one for the visual tests and one for the pressure measurements. Details of the models will be given in the next section.

At the beginning of this program, it was only known that the force tests, available on a large number of configurations, did not agree with any of the known theories. After the

basic flow phenomena had been identified from the test data as one of shock induced separation, it was found that there were a few papers that discussed this effect to some extent, but not specifically as applied to control surfaces. Also the present configuration was different in that it was an actual control surface model whereas the previous authors had primarily investigated the effect with steps and wedges mounted on flat plates. However the results of other authors were useful after the shock induced separation was identified in the control surface problem. While this investigation has been in progress, several papers have been published on the general shock induced separation problem.

III. MODEL CONSTRUCTION

To accommodate the two dimensional model in the Jet Propulsion Laboratory 12 Inch Supersonic Wind Tunnel, a special support system was designed and built to replace the usual windows in the tunnel sidewalls. For the pressure model the new "windows" were made of steel to facilitate bringing the pressure leads out of the tunnel. Photographs of these windows on either side of the tunnel are shown in Figures 1 and 2. The wing mounts in the rectangular slot at the center of the window using spacer blocks to fill the remainder of the opening. These blocks were provided in different sizes to permit the wing to be moved fore and aft to provide a gap between the wing and control surface. Blocks were built to give gaps of 0.020" (called zero gap), 1/4", 1/2", 1" and 2". The control surface remained in a fixed position in the tunnel for all gap settings. A photograph of the pressure wing showing the pressure tubes emanating from the ends is shown in Figure 3. The tubes are connected by short lengths of tygon tubing to a cover which encloses the entire rectangular opening shown in Figure 1. This cover has short tubes protruding from its inner and outer surfaces and is the means of bringing the pressure lines out of the tunnel. This cover also provides a seal for the tunnel. Pressure lines are brought out of both sides of the tunnel so there are similar cover plates on both sides.

Behind the main rectangular slot is a cylinder that holds the control surface and brings its pressure leads from the surface in the tunnel to the external tubing, while sealing the tunnel. This

cylinder rotates to provide the control surface deflections. The cylinder is on one side of the tunnel only and all control surface pressure leads are brought out on this side. The window on the other side of the tunnel has a small hole for the shaft that is on the other end of the control surface, as shown in Figure 4. The cylinder is driven by a worm gear that in turn is geared to a small reversible D.C. motor.

The windows were rotated to change the angle of attack. Since each end of the wing is rigidly connected to a window, it is imperative that these windows move together; otherwise the wing will be twisted. To accomplish this, windows were driven by a single motor located under the tunnel through a series of worm gears and chain drives. Because of the large gear reduction, the play occurring in the chain drive is negligible. As may be noticed from the photographs, Figures 1 and 2, the drive system was very conservatively designed and gave excellent service. The system moved the model at about one-quarter degree per second, but this could be varied by cone pulleys on the motor and initial drive shaft. The motor was reversible and could be driven in either direction by a lever switch mounted on a control box in the tunnel control room. The angle of attack was measured by a potentiometer, mounted on one of the "windows", connected in a bridge circuit with a multiturn potentiometer on the control box. The angle of attack could be set to an accuracy of better than 0.1 degree.

The visual windows are very similar to the pressure windows, except that they had a six inch optically ground high quality

glass insert in a location that made visible the entire control surface and the area approximately $2\frac{1}{2}$ inches ahead of the control surface's leading edge. A steel insert in the glass provided a support point for the control surface shafts. These windows were driven to change angle of attack in the same manner as the pressure windows.

The visual control surface was deflected by an arm attached to the shaft that is in line with the aft portion of the control surface so that it would not block any of the view of the flow. This arm had a worm gear attached that was driven by the same motor and drive system pictured in Figure 1. This motor was operated from a control box in the tunnel control room. A potentiometer mounted on the motor block was wired in a bridge circuit to indicate the control deflection to the operator of the control box.

The visual model, a photograph of which is shown in Figure 5, was made of steel. A drawing of the aerodynamic configuration of the model is shown in Figure 6. The gap between the sidewalls and the model was held to about 0.005 inch or less to eliminate three dimensional effects. There was a second visual model with a larger chord to obtain the effects of turbulent flow on the wing. A drawing of the larger model is shown in Figure 7.

The pressure model had exactly the same aerodynamic configuration as the visual model. It was made of steel, in two halves, with slots cut into both halves to serve as pressure lines. These slots had an average size of about 0.05 by 0.09 inches but were both larger and smaller as the thickness of the surfaces would permit. The two halves were brazed together with a 0.010 inch steel

shim between them to separate the pressure slots for the upper and lower surface. Drawings of the model with the chordwise locations of the orifices are shown in Figures 8 and 9. The orifices had a diameter of 1/32 inch and are located in two rows 1/4 inch apart at the center of the span. The orifices were placed in two rows so that the center section would not be unnecessarily weakened. The pressure lines emerging from the cover plates on the windows were tied to the manometer through about 25 feet of 1/8" I.D. tygon tubing. The lag in the manometer response was calculated, and this size tubing was found to be close to the optimum for the volumes involved. In only one case was the lag appreciable and that was in the case of one tube whose orifice was located in the leading edge of the control surface so that it had to be made of stainless steel tubing with an I.D. of 0.010 inch. Even here the lag was not significant unless large changes in angle of attack or control surface deflection were made.

Some difficulty was experienced with the supporting shafts of the visual control surface model. The dynamic loads that this surface experienced due to separation and tunnel choking were apparently much larger than anticipated and required some minor redesign during the test to increase the strength. Near the choking condition, a control surface buzz developed which caused the shaft to pass the elastic limit in several cases prior to the redesign.

IV. WIND TUNNEL

The tests were made in the 12 Inch Supersonic Wind Tunnel at the California Institute of Technology, Jet Propulsion Laboratory. Reference 1 contains a description of this tunnel. The tunnel is capable of being run at Mach numbers between 1.25 and 4.04 by means of a flexible nozzle adjusted by manual jacks. At Mach numbers below 2.20 the tunnel has a 12 x 12-inch test section, whereas above this Mach number the test section is reduced to 9 x 12 inches. The supply pressure into the tunnel may be varied to change the Reynolds number. For most of these tests the supply pressure was varied with Mach number to provide a constant dynamic pressure in the test section. For a small portion of the second visual test the supply pressure was reduced to about one quarter of its usual value to give a reduced Reynolds number. The following table gives the nominal tunnel operating conditions for the tests.

Mach Number	1.70	2.60	3.52
Static pressure	8.1	3.4	1.86 psia
Stagnation pressure	40	68	146 psia
Dynamic pressure	16.3	16.1	16.1 psia
Reynolds Number per inch	.36	.42	$.54 \times 10^6$

The manometer board was equipped with 50 tubes filled with Meriam unity oil, 50 tubes of acetylene tetrabromide (TBE), and 30 tubes of mercury. Many orifices were connected to both the unity oil and TBE tubes or to the TBE and mercury in order to keep the accuracy high under all conditions. Usually only one of the two tubes

would be connected at a time, to keep the volume and thus the lag at a minimum. The manometer board was 250 cm. high. A photograph of the board is shown in Figure 10. The manifolds on the manometer were tied to a static pressure orifice in the test section upstream of the model so that the tubes read the difference between the local and free stream static pressure. Guillotines were used on all of the unity oil and TBE tubes so that they could be shut off for starting and stopping the tunnel.

Because the total pressures in the tunnel were as much as 15 times the capacity of the manometer board, it was necessary to employ a complex starting and shutting down procedure in order to avoid blowing the manometer fluids overboard into the lines. Since TBE is a very corrosive substance and its fumes toxic, traps made of chemical test tubes were included in the lines. By using extreme caution these were never needed. In general, the guillotines were used to cut off the pressure lines from the manometer whenever changes were made in angle of attack or control surface setting. These guillotines were electrically and hydraulically operated so that they could be used easily. At least one man watched the manometer board at all times who could instantly shut all guillotines to avoid exceeding the capacity of the manometer. The manometer board was photographed for later data reduction.

Several items influenced the accuracy of the pressures read. It is possible to read the photographs of the manometer to $\pm$ 1 mm. and because the pressure coefficient is formed from the difference of two readings the error may amount to $\pm$ 2 mm.

However, in the general course of data reduction the average error probably amounted to 3 mm. and in some instances may have been as much as 5 or 6 mm. The above reading accuracy determines the consistency of the results; however, the absolute accuracy was primarily influenced by a change in specific gravity of the manometer fluids which occurred during the test. The specific gravities of the unity oil and TBE were carefully measured by weighing a known quantity both before and after the test. These measurements were made by the JPL staff. The results of the measurements are given in the table below:

Fluid	S. G. before test	S. G. after test	Value used for results
Meriam Unity Oil	1.00	.958	.960
TBE	2.96	2.88	2.90

No satisfactory explanation has been found for the discrepancy between the before and after measurements. The manometer had been thoroughly cleaned and reworked just prior to the test and new fluid installed in all tubes. The tubes and the system were rinsed with alcohol as the last step in cleaning. Although it was several days between the time the manometer was cleaned and when the new fluid was added, it is possible that some alcohol had not evaporated and remained in the system to dilute the manometer fluids and lowered the specific gravity. Another possible explanation is that the fluids reacted chemically with some material used in the manometer system and changed their chemical composition. However, this is not too likely since the majority of the system is of stainless steel.

The manometers were drained soon after the test was completed and it was not possible to determine the reason for the change in specific gravity. The total period between the before and after measurements of the fluid specific gravities was not in excess of 30 days. This discrepancy can cause a 1 to 2% error in the pressure coefficients but does not appear to be too detrimental in explaining the flow phenomena that occur.

V. TEST PROGRAM

It was decided to run the models at three Mach numbers: M = 1.70, 2.60 and 3.52. It was planned to run the visual tests first and on the basis of knowledge gained, modify the proposed program for the pressure tests to give the most data. However, because of the difficulties encountered with the mounting shafts on the visual control surface model mentioned in the section on models, it was necessary to postpone these tests and to proceed to the pressure tests. The program of the pressure tests is given in Table I. This table and those similar are not arranged chronologically but rather in a manner that will more systematically show the data obtained.

The extreme conditions on angle of attack and control surface deflection were determined when the tunnel choked. Choking was measured by watching the pressure distribution on the floor and ceiling of the tunnel and noticing when the shock wave moved forward into the test section. Experimental curves showing the conditions which caused choking for this model are given in Figures 11 to 13. Approximately 60 hours of tunnel time were expended in running the pressure model.

At the completion of the pressure test the visual model was run under approximately the same conditions as the pressure model. The program is given in Table II. The visual system used, the standard one at the 12 Inch Supersonic Wind Tunnel, is a double mirror system, consisting of a light source, two 24 inch mirrors, a knife edge and a camera. Either a continuous BH-6 light source or a spark from a condenser discharge may be used. In this first

test both light sources were tried and also shadowgraphs were taken by moving the knife edge completely out of the light path. Initially schlierens were made but it was found that spark shadowgraph pictures gave much more detail to the flow phenomenon. The pictures were not of the best quality since the optical system was not in good alignment. It was in good enough condition to give satisfactory pictures for the usual type of test being run at the tunnel but did not give the detail desired to explain the flow phenomenon in this test. Samples of the photograph obtained are shown in Figures 14 and 15. The time available for the tests permitted the model to be run only at the two lower Mach numbers. It was therefore necessary to continue the tests at a later date. This first series of visual tests was made in August 1954 and required about 45 hours of tunnel time.

After the test was completed, it was found that the deflection of some of the light rays in passing through the 12 inches of the wind tunnel would be large enough to cause the rays to be completely off the second mirror and out of the field of view. Therefore the so-called shadowgraph pictures were really the result of a combination of the shadowgraph and schlieren phenomenon. On the second visual test it was decided to use a spark shadowgraph technique with the photographic plate located a few inches outside the tunnel. A frame to accept 8 x 10 film holders was attached to the steel "window" so that it rotated with the model on angle of attack changes. The spark light source and first parallel ray forming mirror were the standard ones in the JPL system. Much better pictures were obtained with this sytem than with that originally used. All of the

remaining photographs presented were obtained with this modified system. The run schedule for this test is in Table III. This test was run in January 1955 and required about 40 hours of tunnel time.

VI. RESULTS AND ANALYSIS OF ZERO GAP CONFIGURATION

The results of the tests are all contained in the shadowgraph pictures and in the pressure distribution graphs. Because there were about 575 usable shadowgraphs taken and data from 432 pressure distributions, it is impractical to present all these data in this thesis. Only a few selected shadowgraphs and pressure distributions will be presented as examples. The conclusions drawn in the analysis could not have been based on these selected data but represent information obtained from the complete set of data which is presented in Reference 2.

The first part of this discussion will be concerned with the data obtained from the configuration without a gap between the main surface and the control surface. These results will be discussed in detail and then the data obtained with a gap between the two surfaces will be used to show the changes resulting from the use of a gap. In the discussion, the main surface will be referred to as a wing or stabilizer interchangeably, and the control surface will often be called a flipper. The term flipper is used because the control surface may be an elevator, rudder, aileron or a combination of these.

Qualitative Tests

The zero gap configuration will be discussed first from the qualitative standpoint using the flow shadowgraphs to explain the details of the flow phenomena. Considering first the series of shadowgraphs at the highest Mach number at which tests were made,

M = 3.52. Figures 22 to 54, it is clear that the flow is separating from the wing ahead of the control surface in all cases when the control surface is deflected. Therefore the problem is one of shock wave-boundary layer interaction in which the higher pressures experienced behind a shock wave are being transmitted forward through the boundary layer to separate the flow. Although the flow is supersonic, pressures may still be transmitted upstream through the subsonic boundary layer. Shock-wave-boundary layer interaction has been the subject of a number of papers in the last few years since this research was begun. The configurations for which this problem has been discussed are simpler than that used for the tests to be discussed here; however, the general results that have been obtained experimentally and theoretically are applicable to the present configuration. Gadd has made numerous contributions to the literature on this subject from both the theoretical and experimental basis (References 3 to 7); Chapman in a recent paper has reported the most comprehensive series of experiments made to date (Reference 8). Several other authors have also written on some aspects of the subject (References 9 to 15).

The majority of the tests made for this investigation had a laminar boundary layer and therefore this case will be the one given the most consideration. It is immediately noticed that the flow separates for quite weak shock waves. Therefore it is not necessary to have a control surface behind a wing to separate the flow, as the shock wave at the trailing edge of most lifting surfaces will be strong enough to separate the flow. Figures 16 to 21 are shadowgraphs of the wing alone configuration at a Mach number of 3.52. No separation is visible at zero angle of attack, but as the angle of attack is

increased, separation begins to be apparent. In the discussion of the quantitative results which will follow, it will be shown that when the flow is turned through an angle greater than 2 or 3 degrees, a laminar boundary layer will separate. The exact turn angle necessary for separation is a function of the Mach number and Reynolds number. It does not require a very thick surface to cause the boundary layer to separate even when the surface is at zero angle of attack. The surfaces used in this investigation are quite thin; the wing used for this series of shadowgraphs being discussed is 4% thick and it has a trailing edge half angle of 2.16 degrees. Flow separation occurs first near the trailing edge, and the separation point moves gradually forward as the angle of attack is increased. It may be noticed from the aforementioned shadowgraphs that the flow direction behind the separation point is approximately constant, which indicates that the pressure is also constant, and this will be verified when the pressure distribution data are discussed.

We will consider some of the shadowgraphs in detail and explain the information that can be derived from them. The basic idea of the shadowgraph technique, explained in Reference 16, is that the light ray deflection is a function of the density gradient. If the gradient is constant, the rays are all deflected the same and the light intensity in the photograph is constant. However, if $\frac{\partial^2 \rho}{\partial y^2}$ is not zero, then a light and dark area will be formed on the photographic negative. Shock waves, expansion waves and boundary layers all have a second derivative in density and show on a shadowgraph. Some general observations about the photographs

may be helpful. They were taken on full scale negatives but have been reduced to about two thirds size in the figures. The circular pattern is due to the round glass windows having a diameter of approximately 6 inches on each side wall of the tunnel. The numbers shown at the bottom of the picture are the tunnel run and point numbers. The camera rotates with the model as the angle of attack is changed so the α can not be measured from the photographs. The small circular black area just downstream of the center of the window is the steel inserts in the windows which provide bearings for the supporting shafts of the control surface. These inserts were flush with the inner surfaces of the glass and did not have any influence on the flow. In the shadowgraphs the model appears to be considerably thicker than it really is. This may be explained by the presence of a boundary layer on the tunnel sidewalls that forms a fillet with the boundary layer of the model. The curvature of the fillet is such that it deflects the light rays away from the model's surface, leaving a dark area that is much wider than would occur from the model's boundary layer alone. The variation in light intensity is a function of the second derivative of the density so it is smaller when the tunnel pressure is reduced. Thus on shadowgraphs made with low tunnel pressure, the area near the wing is not as dark and the true size of the model is apparent. When the flow is separated, the true size of the model may usually be seen since the flow in the separated region does not deflect all the light rays away from the body.

Figure 16 is the shadowgraph of the wing alone at zero angle of attack. The leading edge shock waves are apparent in

the upper and lower right-hand corners. The expansion waves from the maximum thickness point on each side of the wing are visible in the center of the right-hand edge of the picture. The trailing edge shock waves, emanating symmetrically from either side of the trailing edge, near the center of the picture, are visible.

Figure 17 is very similar except that with an angle of attack separation occurs on the lower surface only, a short distance ahead of the trailing edge. This separation is the result of the higher pressure behind the shock wave that is initially attached to the trailing edge, feeding upstream through the subsonic boundary layer and causing the flow to separate. As the trailing edge shock grows stronger, the pressure is increased and the separation point moves further upstream. This result is apparent from a comparison of Figures 17 to 21. A shock wave emanates from the separation point, as will be noted from these figures. A study of Figure 20 shows that the flow on the upper surface expands at the trailing edge to a pressure approximately equal to that on the lower surface. Then in order for the flow to have the free stream pressure and direction far behind the wing, shock waves form on either side of the mixing region that extends from the end of the separated region. These waves however do not affect the pressures on the wing except that the one from the lower surface may be considered the cause of separation. The shock wave seen above and behind the model in Figure 21 is not part of the basic flow over the model. It is a shock wave formed in the tunnel by the choking effect of the wing at a high angle of attack. If the angle of attack were slightly larger, this shock wave would move forward, strike the model

and the tunnel would choke.

Looking now at the wing-control surface configuration, it is obvious that that separation will also occur here. In the zero angle of attack case, Figures 22 to 27, the increased pressure from the shock wave at the leading edge of the control surface is transmitted upstream through the boundary layer wake and separates the flow on both the upper and lower surfaces of the wing. At zero control surface deflection angle the flow is separated on the wing because the shock wave due to the thickness of the control surface is sufficient to cause separation. As the control surface deflection is increased, the pressure behind the shock wave increases and the separation point moves gradually upstream. The flows on the upper and lower surface of the wing are approximately symmetrical since the shock wave from the flipper affects both sides similarly.

The flow on the suction side of the control surface is only slightly affected by the separation and its characteristics may be calculated using the inviscid shock-expansion theory with excellent results except near the leading edge where the wake of the wing influences the flow and increases the pressure. On the pressure side of the control surface, separation has its major effect.

Except at very small control surface deflections, the shock wave from the leading edge of the flipper is reflected from the surface of the separated region as an expansion fan which then strikes the flipper and is re-reflected again as an expansion wave. This lowers the pressure on the control surface rapidly. When this expansion fan is again reflected by the surface of the separated

region, it becomes a series of compression waves that merge into a shock. This shock wave strikes the control surface, is reflected as a shock wave and causes an increase in pressure. At this point the pressure is approximately the same as it would have been if the separated region had not existed to reflect the leading edge shock wave. All this reflection may take place within the chord of the control surface or not, depending on the Mach number and the geometry. When the shock wave from the leading edge of the flipper strikes the wake of the separated region the amount that is reflected as an expansion wave and the amount transmitted depends on the pressure in the separated wake.

At very small control surface deflections the control surface lies completely in the wing's wake and the pressure on the leading edge of the flipper increases slowly because of the reduced velocity in the wake. The flow is turned more gradually, but somewhat back of the leading edge the flow is established parallel to the surface and the pressure is approximately the same value it would have been if it had been turned abruptly at the leading edge by a shock wave. The flow downstream of this point may be calculated by the inviscid shock-expansion theory except the pressure decrease at the maximum thickness point is more gradual with the real fluid.

We will now consider in detail some shadowgraphs that illustrate the points made in the preceding paragraphs. In Figure 24 the flow separates at approximately the same place on each surface of the wing. From a consideration of the light line at the edge of the separated area, one sees that transition occurs in the vicinity of the trailing edge on the upper surface. Upstream of that point

the light line is smooth and straight, whereas downstream it is wavy. The flow on the upper surface of the flipper is turbulent. It is difficult to see what is occurring on the upper surface of the flipper except that it turns the wake of the wing parallel to its surface thus requiring a shock wave. On Figures 25 to 27 there are no differences in the flow from that already described other than the fact that the separation and transition points move further upstream. When transition occurs, it is noted that the flow curves outward from the wing's surface, allowing the pressure to again increase. The flow separates from the lower surface of the flipper at deflection angles of -15, -20, and -25 degrees because of the shock wave that occurs at its trailing edge. The flow on this surface is laminar so separation is easily induced.

We will next consider the series of shadowgraphs made at an angle of attack of -4 degrees and for a range of control surface deflection from -15 to +25 degrees, Figures 28 to 36. Now it is clear that only the lower surface (suction side) of the wing is separated when there is a negative angle of attack. The suction side is more vulnerable to separation because of the larger pressure difference between the flow on this surface and the flow behind the shock wave from the leading edge of the flipper. Therefore only the suction side of the wing is separated in most cases and the flow on the pressure side remains attached. Considering Figure 28 it is noted that separation occurs upstream of the maximum thickness of the wing on the lower surface and that transition occurs slightly behind the maximum thickness point. From the shape of the boundary of the separated region, we conclude that

the pressure continues to increase downstream of transition. The leading edge of the control surface is in the separated region so it would appear that the pressure on its lower surface would only gradually fall to a lower pressure instead of expanding rapidly at the leading edge. The flow on the upper surface will act in a similar manner, in that the flow will only gradually turn in line with the surface and the resulting shock waves lie downstream instead of at the leading edge. Looking at Figures 29 to 36, one notices that the flow develops in a systematic manner as the control surface deflection angle is increased. In Figure 34 it is clear that separation occurs just downstream of the maximum thickness point on the lower surface and transition occurs about one inch ahead of the trailing edge. The upper surface of the wing is unseparated. The flow on the upper surface of the flipper is determined by the expansion of the flow around the leading edge so that the flow is attached to the surface. The flow on the lower surface of the flipper is more complex. It follows the discussion on page 21 about the reflection of the leading edge shock wave back and forth between the solid surface and the wake of the separated region. From this particular photograph this is difficult to see but after a study of many other photographs where this phenomenon occurs, one can see that the same pattern exists here also.

The remaining two shadowgraphs at this angle of attack, Figures 35 and 36, are further developments of the same flow phenomenon. From Figure 36 it is clear that separation has occurred on the forward half of the lower surface of the wing. (This is determined by extrapolation of the shock wave from the separation

point that is visible in the photograph.) Transition occurs in the neighborhood of maximum thickness and induces a continuing pressure rise. By inference one sees that the pressure at the trailing edge of the lower surface has increased to the extent that it exceeds the pressure on the upper surface. Therefore, the higher pressure is propagated forward in the boundary layer of the upper surface also, and induces separation. On the flipper the flow is uniform behind the leading edge expansion wave on the upper surface. Near the maximum thickness point the flow separates because of the shock wave that occurs at the trailing edge. On the lower surface, the leading edge shock wave is reflected back and forth between the flipper and the surface of the separated region. The flow from the upper surface of the wing flows over the lower surface of the flipper. The flow from the lower surface of the wing is separated from the lower surface of the flipper by the separated region and a mixing region in which the flow from the upper and lower surfaces of the wing are reunited. This mixing region is bounded by two shock waves that turn the flows into a uniform direction.

Considering now the shadowgraphs made at -8 degrees angle of attack, Figures 37 to 44, one observes that the flow follows very similar patterns to those at the lower angles of attack. Up to a flipper deflection of 15 degrees, no significant change is found from the shadowgraphs at the lower angles of attack. However, at flipper deflections of 20, 25 and 30 degrees, Figures 42, 43 and 44, a new phenomenon is noticed. The shock wave from the leading edge of the flipper's lower surface appears to be curved. At this Mach number we would not expect this wave to detach until

the flipper deflection exceeds 33 degrees if the flipper were in a free stream with the same Mach number that exists on the upper surface of the wing. It appears that the back pressure from the separated flow on the lower surface of the wing causes the shock wave to be of the strong type and therefore the flow on the front of the flipper will be subsonic.

Looking now at the shadowgraphs at the angles of attack of -12 and -16 degrees, Figures 45 to 54, it is seen that the characteristics of the flow are unchanged from that at the lower angles of attack except that the separation and transition points are further forward. It is important to realize in studying the photographs at -16 degrees angle of attack that the shock waves striking the upper surface of the flipper are not part of the flow about the surface but are due to the wind tunnel. This completes the discussion of the qualitative data obtained at M = 3.52 and the normal Reynolds number.

Reynolds Number Effects

The shadowgraphs obtained at a Reynolds number approximately one fourth that of the shadowgraphs already discussed show that basically the flow is very similar. The flow separates more easily at the lower Reynolds number and therefore the separation points are further forward on the wing. The change in flow direction that accompanies the separation is larger at the lower Reynolds number. The photographs are more easily analyzed since the boundary layer areas are not as dark as before. The change in density gradient which determines the light and dark area is proportional to the pressure which has been reduced by a factor of four for the low Reynolds number tests.

One change that should be noted is that the choking effect that appeared at the high angles of attack and flipper deflection and caused the shock wave from the flipper leading edge to be of the strong type, has disappeared. This may be explained by the fact that the pressure in the separated region on the lower surface of the wing is lower because the transition point is nearer the trailing edge and therefore the pressure rise in the turbulent flow regime is restricted. This lower pressure in the separated region reduces the back pressure on the flow passing through the gap between the wing and flipper and eliminates the choking effect. A few shadowgraphs at the reduced Reynolds number, Figures 55 to 59, have been selected to illustrate the similarities and differences in the flow. Table IV gives a comparison of the location of the separation points for the normal and reduced Reynolds number cases.

Mach Number Effects

At Mach numbers higher than 3.52, it is believed that the flow phenomenon is very similar, but the pressure distributions obtained may be quite different. Since the Mach angles are smaller, the reflections of the shock and expansion waves between the control surface and the surface of the separated region are stretched out in the flow direction and not all of the reflections will be completed ahead of the trailing edge. At a Mach number of 3.52, in most cases the final shock wave reflection from the wake did not strike the flipper. In some instances some of the initial expansion waves from the wake failed to strike the surface. At a Mach number of 4.0 or higher, the condition would exist to a greater extent

and it appears that at some Mach numbers none of the initial expansion wave will strike the surface and therefore the pressure on the entire pressure side of the control surface will vary only where the expansion wave from the trailing edge of the wing strikes the flipper and at the flipper's maximum thickness point. At large angles of attack this gives pressure distributions that appear very similar to those that have separation with the multiple reflections.

At lower Mach numbers, changes in the flow are very gradual. At the next lower Mach number at which tests were made, $M = 2.60$, the conditions are very similar to those at $M = 3.52$. Because the Mach angle is larger and all disturbances are transmitted with steeper angles, the phenomenon of the reflection of the waves back and forth between the flipper and the surface of the separated region is condensed in the flow direction. Separation takes place on the wing in much the same manner as at the higher Mach number. A few shadowgraphs of the flow are given in Figures 60 to 63.

As the Mach number is further reduced, the general flow phenomena are unchanged, but the magnitudes are quite different. From consideration of the data obtained at $M = 1.70$, the following conclusions are drawn. Separation occurs on the wing in a similar manner to that at the higher Mach numbers, however, the pressure rise is smaller as is the width of the separated region. The shock from the separated region is partially transmitted and partially reflected by the wake. At the lower control deflection angles, most of the shock wave is transmitted through the narrow wake and the flow is similar to that calculated with the inviscid theory with some change due to viscosity reducing the rate of change in

pressure at the corners.

Turbulent Boundary Layer

When there is a turbulent boundary layer on the wing, the flow is changed considerably. A turbulent boundary layer does not separate as readily as a laminar layer, and therefore, a stronger shock wave with its increased pressure rise is necessary to separate it. From the shadowgraphs it is found that the flow must be turned through 12 to 20 degrees to separate it when the flow is turbulent instead of the 2 or 3 degrees required to separate a laminar boundary layer. The important consideration that decides if the flow will separate as a laminar or turbulent boundary layer is the condition of the boundary layer at the trailing edge of the wing. The general conclusion from these tests is that a turbulent boundary layer delays separation to much larger angles of attack and/or flipper deflections, but the flow phenomena that occur are very similar.

In the experimental tests, turbulent flow was achieved by using a wing with a 10 inch chord instead of the standard 6 inch one. By noting the wavy appearance of the edge of the boundary layer one can see that the layer is turbulent in the vicinity of the trailing edge in Figure 68, the shadowgraph for $\alpha = 0$, $\delta = 0$ and $M = 3.52$. No separation is in evidence, whereas with the laminar boundary layer, separation occurred in this case due to the shock wave on the leading edge of the flipper. The shadowgraph for a flipper deflection of -25 degrees, the highest value tested at zero angle of attack is shown in Figure 69. It is noted that the flow is separated from the wing at a point a short distance

ahead of the trailing edge. Thus the pressures on the wing are altered only in this small region.

The next four figures show the flow over the larger wing at an angle of attack of -8 degrees. Figure 70, for $\delta = 0$, shows that the turbulent boundary layer is attached to the surface whereas separation occurs in this case when the boundary layer is laminar. In Figure 71, for $\delta = 10$ degrees, the flow is just beginning to separate. For the last two shadowgraphs of the group at this angle of attack, Figures 72 and 73, the turbulent boundary layer has separated and the separation points are very near the leading edge. In these final cases, the flow appears very similar to that occurring in the laminar boundary layer cases. The magnitude of the separation is determined by the geometry of the configuration and the requirement that the flow on the lower surface must be deflected sufficiently to flow around that which comes from the upper surface of the wing through the gap between the wing and flipper. This requirement is the same for both laminar and turbulent flows.

Quantitative Tests

The foregoing discussion of the shadowgraph flow pictures provides a general explanation of the flow phenomena that occur on a wing-control surface configuration. This investigation also included pressure distribution measurements on the basic configuration. The details of the model including the pressure orifice locations are given in the section on model construction. It was tested at the same three Mach numbers used for the shadowgraph

pictures and over the same range of angle of attack and control surface deflection. In all, 93 pressure distributions were obtained at the various angles of attack, flipper angles and Mach numbers for the zero gap configuration. Only a few of these will be presented here, but the complete set may be found in Reference 2.

The data will be discussed in the same order that the visual data were presented starting with that at the highest Mach number, $M = 3.52$. Data were not taken with the wing alone so comparisons of these pressure distributions can not be made with the shadowgraph results. The pressure distributions for the wing-control surface configuration at zero angle of attack are given in Figures 74 to 79. Separation on the wing is indicated by an increase in pressure on the surface of the wedge which would have a constant pressure if the flow remained attached. At zero flipper deflection, Figure 74, separation occurs on both surfaces 5 inches from the leading edge. Upstream of separation, the flow is attached to the surface and may be calculated by the inviscid shock-expansion theory. In this case and all others for which pressure distributions were measured the flow on the wing is laminar prior to separation. On the forward portion of the control surface, which is in the wake of the wing, the pressure is lower than anticipated by an inviscid calculation. The pressure at the leading edge is approximately the same as that at the trailing edge of the wing but it increases gradually as the thickness of the flipper increases. At the maximum thickness point it has increased to the value expected in inviscid flow on the forward portion of the flipper. The flow then expands as it turns at the maximum thickness point.

The fact that the pressures are slightly different on the upper and lower surface is probably because the control surface was not set to exactly zero degrees.

At a flipper deflection of 5 degrees, the pressure pattern does not differ basically from that obtained at zero degrees except in a manner that can be predicted by inviscid theory. However, at a control surface deflection angle of 10 degrees, the shock wave from the leading edge of the flipper is reflected from the wake of the separated region as expansion waves. These waves strike and are reflected from the flipper, lowering the pressure very rapidly. The waves are then reflected again by the surface of the separated region, this time as compression waves that merge to form a shock wave. When this shock wave strikes the flipper again and is reflected, the pressure rises rapidly and is returned to approximately the same value it would have had if the separated region were not present and the initial shock wave were transmitted away from the vicinity of the control surface without reflection. Figure 76 shows a pressure distribution that follows the explanation given above and is in complete agreement with the analysis given for the shadowgraphs. In this particular case the wake of the separated region is very near the surface of the flipper and therefore the reflection pattern takes place in a short longitudinal direction. The orifice located 0.050 inches from the leading edge of the flipper may not be completely reliable in this case or any of the others and must always be questioned. The leading edge was built up of two 0.020 steel tubes in tandem, filled in with solder. Therefore the smoothness and regularity of the surface in the

neighborhood of this orifice is in question and may influence the pressures measured there.

The pressure distribution measured at $\delta = 15$ degrees, Figure 77, follows the same flow pattern discussed for $\delta = 10$ degrees except that separation takes place somewhat further forward on the wing as would be expected. With a flipper deflection of 20 degrees, however, there is a larger change in the pressure distribution. The flow for this case, Figure 78, separates the laminar boundary layer ahead of the maximum thickness point on the wing. The pressure rises slightly and then about 1 to 2 inches downstream, the boundary layer on the surface of the separated region becomes turbulent and allows the pressure to increase again. A laminar boundary will support only a very small increase in pressure when it separates whereas when a turbulent boundary layer separates it may be accompanied by a much larger pressure rise. The magnitude of these pressure rises will be discussed in the next section of this thesis. On the lower surface of the flipper the pressure distribution follows the same pattern as that discussed for $\delta = 10$ degrees, but here the pattern extends over a larger part of the flipper because the surface of the separated region is further away from the flipper causing the reflection pattern to be spread out. A similar pressure distribution pattern exists for a flipper deflection of 25 degrees, Figure 79. Separation in this case is further upstream and the turbulent separation is more easily identified. Also note that the flow also separates from the upper surface of the flipper.

When the angle of attack is different from zero, there are no major changes in the pressure distributions. Usually only one surface of the wing is separated, as was discussed in the section on the analysis of the shadowgraphs, page 23. As examples of pressure distributions at angle of attack, the case of $\alpha = -8$ degrees, $\delta = 0$ degrees was selected. This pressure distribution, Figure 80, follows the inviscid shock-expansion theory calculation with some modifications. It is necessary to account for the laminar separation on the lower surface of the wing and for the effect of the wing's wake on the forward portion of the flipper.

A second example, $\alpha = -8$ degrees, $\delta = 20$ degrees, follows the previous discussion about this case in the section on the shadowgraphs. Figure 81, the pressure distribution for this case, has its initial laminar separation point far forward, followed by transition to turbulent flow and a further pressure rise. The flow on the upper surface of the wing and the flipper remains attached and follows inviscid theory. The lower surface of the flipper follows the multiple reflection pattern already discussed. The pressure near the leading edge is higher than anticipated from the shock-expansion theory but may be explained by a strong shock wave brought about by the choking of the flow that passes from the upper surface of the wing to the lower surface of the flipper. Downstream the pressure is decreased by the expansion as the flow aligns itself with the surface and by the expansion waves arising from the reflection of the leading edge shock wave by the surface of the separated region. This reflection pattern is not completed within the chord of the flipper and the pressure just

reaches its minimum value at the trailing edge, showing that the shock formed by the reflection of the expansion waves from the free surface never strikes the flipper.

Figure 82, for $\alpha = -8$ degrees, $\delta = 25$ degrees, is very similar to the preceding case except that the laminar separation and transition to turbulent flow takes place nearer the leading edge and thus the pressures on the lower surface of the wing are very much greater than anticipated by inviscid theory. It is believed that there is a small error in the angle of attack setting for this and the next figure, that causes the pressure on the wing's upper surface to be slightly in error. Figure 83, for $\alpha = -8$ degrees, $\delta = 30$ degrees, shows a further extension of the same idea with the laminar separation, the transition to turbulent flow, and the resulting pressure rise taking place very near the leading edge of the wing. It should be noticed that the pressure is approximately constant on the wing's lower surface and it is everywhere larger than that on the upper surface. Therefore the net force on the wing is positive in spite of the angle of attack of -8 degrees. This is a prime example of the importance of shock induced separation on the wing-control surface problem. The pressure distribution of the flipper is similar to the previous cases. Higher angles of attack produce a continuation of these flow patterns and pressure distributions.

Data are not available on pressure distribution at free stream Mach numbers above 3.52, but using the ideas set forth in the section on analysis of the shadowgraphs and extrapolating the data on separation, it should be possible to calculate pressure distributions with reasonable accuracy at the higher Mach numbers.

At lower Mach numbers, data are available at M = 2.60 and 1.70. At M = 2.60 the pressure distributions are very similar to those at the higher Mach number. To illustrate this, Figures 84 and 85 are the pressure distributions at flipper deflection angles of 0 and 15 degrees for zero angle of attack. Figures 86 to 88 are the pressure distributions at an angle of attack of -8 degrees and for flipper deflections of 0, 25, and 30 degrees.

At a Mach number of 1.70, the flow is somewhat changed. Although the laminar boundary layer separates from the wing, the shock from the flipper leading edge is not as readily reflected by the surface of the separated region. At zero angle of attack, pressure distributions are given for flipper deflection angles of 0 and -10 degrees in Figures 89 and 90. These pressure distributions are similar to those at the higher Mach numbers, except it appears that the flipper leading edge shock wave is not reflected by the separated region. Therefore the pressure distributions are very similar to those calculated by the inviscid shock-expansion theory.

Typical examples of pressure distributions at -4 degrees angle of attack are given by Figures 91 to 93. Figure 91, for a flipper deflection of zero, has a distribution very similar to that obtained from an inviscid flow calculation. The main differences are that the flow separates on the lower surface of the wing as previously discussed and that because of the wing wake, the pressure rise on the forward portion of the flipper is slow in developing. Figures 92 and 93 for flipper deflections of 10 and 12 degrees, respectively, reveal that the pressure gradient changes sign at least four times on its forward portion. This must be explained by

multiple reflections of compression and expansion waves from the separated region. These waves are visible in the shadowgraph at this angle of attack and flipper deflection but the exact mechanism of the flow is in question. It would be interesting to see pressure distributions at higher angles of attack and flipper deflections, but it was not possible to run these at the low Mach number without blocking the tunnel. It is not anticipated that there are any unpredictable changes in the flow that will change it basically.

This completes the discussion of the pressure distribution data at zero gap. It is unfortunate that data are not available at other Reynolds numbers and especially that none of the pressure measurements have a turbulent boundary layer, but it is thought that the flow phenomena are sufficiently understood to make possible calculations of pressure distributions with a turbulent boundary layer.

In general it was found that the pressure distributions were in very close agreement with the shadowgraphs. From the shadowgraphs, the pressure distributions could be calculated to a reasonable degree of accuracy, and in like manner, having the pressure distributions, the appearance of the shadowgraphs could be visualized. It is therefore apparent that the basic flow phenomena are understood and the following section is an attempt to give methods for calculating the pressure distributions using a combination of theoretical and empirical methods.

VII. METHODS OF PREDICTING PRESSURE DISTRIBUTION

This section will be devoted to a discussion of methods of computing the pressure distribution on a wing with a balanced flap type control surface at supersonic speeds. From the tests described in the foregoing sections, an understanding of the qualitative flow phenomenon was obtained and empirical means derived for estimating the pressure distribution. The basic method to be used is the shock-expansion calculation technique which is discussed in all textbooks on supersonic aerodynamics. The difference between the standard technique and the way it will be used here is in the analysis of the flow phenomena to include the effects of viscosity. Usually the method assumes an inviscid fluid. The major effect of the viscosity is that the higher pressure behind the shock wave emanating from the leading edge of the control surface is transmitted upstream in the subsonic portion of the wake and boundary layer, thereby causing the flow to separate from the surface of the wing. It is therefore necessary to determine the conditions under which separation will occur. These conditions are greatly influenced by the type of boundary layer, i.e., whether the flow is laminar or turbulent at the trailing edge of the wing or more precisely at the point just ahead of the high pressure region. The case in which the boundary layer is laminar will be discussed first. Figure 96 may be used as a criterion for separation. The experimental results only allowed an approximate determination of the necessary conditions for separation and this graph of the flow deflection that occurs when separation takes place appeared to be a good approximation. If the flow is turned through an angle larger than

given by Figure 96, separation will occur.

If separation does not occur, the pressure distribution may be calculated using the inviscid shock-expansion theory taking into account the effect of the expansion wave at the wing's trailing edge on the flipper. If desired, a small correction may be made in the vicinity of expansion corners where the rate of pressure change is finite instead of infinite as predicted by the inviscid theory. A detailed means of making this correction will not be discussed; it is suggested that it may be made by eye from a knowledge of experimental pressure distributions on similar configurations. For a more detailed picture, it would be necessary to make tests with pressure orifices located more closely spaced than those of the current experiments. It is anticipated that the downstream distance may be non-dimensionalized by use of the boundary layer displacement thickness.

When separation does occur, the pressures on the forward portion of the wing up to the separation point may be calculated by the inviscid shock-expansion theory. It will be noticed in all the pressure distributions presented in this thesis and in Reference 2 that when the laminar boundary layer separates, the pressure increases approximately in an exponential manner to a plateau, and remains there until it undergoes transition or reattaches. It would be useful to be able to predict this pressure increase by theoretical or empirical means. Using the data obtained from the current set of experiments and from several other published experiments on this subject, it was found that a good fit could be obtained by assuming that the Mach number ratio across

the shock at the separation point is a linear function of the initial Mach number. Because pressure data from the current tests were available at only one Reynolds number at each Mach number, it was not possible to account for variations in pressure increase due to Reynolds number. Recently, Chapman has published a paper, Reference 8, that gives more comprehensive data than available here. A comparison between the data of the current tests and Chapman's results, given in Figure 94, shows satisfactory agreement. Chapman's tests were aimed at a detailed measurement of the pressure change occurring with a shock induced separation, whereas the measurements made in the experiments being reported here were more general in order to explain the phenomena that occur on balanced flap control surfaces. Because of the more detailed measurements and because the measurements cover a much broader range of Reynolds number, Chapman's results are believed to be superior to those obtained here and are used for all calculations involving separation of the laminar boundary layer. The pressure rise occurring behind a shock induced separation may be expressed algebraically by

$$\frac{p-p_o}{p_o \sqrt{\tilde{c}_f}} = \frac{0.0427 M_o^2}{(M_o^2-1)^{1/4}} - 0.0183$$

where $\tilde{c}_f$ is the ratio of the local skin friction coefficient, c_f, at a given Reynolds number, R_{x_o}, to the corresponding value at $R_x = 10^6$. The subscript o refers to conditions just upstream of separation. This equation was used to draw Figures 95, 96 and 97 which show the pressure ratio, flow deflection and Mach number ratio that occurs at separation. As discussed earlier, Figure 96

is also used as a criterion for separation to occur. The Mach number used in these graphs is that just ahead of the separation point, and the Reynolds number is the value where the first effect of the separation is felt. As may be noticed from any of the experimental pressure distributions, the pressure does not abruptly jump to the separation pressure, but instead changes in a manner approximated by a double exponential curve. A detailed calculation of this variation can be made using Reference 17, but it is not thought necessary for calculations of this type since the calculations are lengthy, and an approximate variation estimated from a knowledge of experimental data from the current or similar tests provides all the accuracy required. If the angle of attack of the wing is zero, both sides of this surface will be separated by a pressure rise occurring on a control surface behind the wing. However if the wing is at an angle of attack, only the suction side of the wing, i.e., the low pressure side, will be separated in the usual case. One exception that can occur will be discussed later. The low pressure side is more susceptible to separation since the pressure difference is larger on this side causing the pressure disturbance to be more easily fed forward in the boundary layer on this surface.

The final item necessary to complete the calculation of the pressure distribution on the wing with a laminar boundary layer is to determine where separation will occur. Very few data are available on this subject in the literature so an attempt was made here to correlate data from the current test with those from Reference 18. Although the result of the correlation, Figure 98, has considerable scatter, it does give the approximate separation

point. Actually in this figure separation point is used to refer to the most upstream point of influence of the separation on the pressure. This point is more important in determining the pressure distribution than the actual point of separation, which is slightly downstream. It is believed that much of the scatter of the data results from difficulty in locating this point from the data available. Because of the spacing between pressure orifices it is frequently difficult to determine the extent of the upstream pressure influence to better than 10 to 20 percent. The Mach number and Reynolds number variations determined from the data appear to be significant. The parameter, $H = \frac{R_o^{3/8}}{G(M)} \frac{\Delta s}{x_o}$, used to obtain correlation is one suggested by a theoretical analysis of the problem in Reference 19. The function of Mach number, G(M), is plotted in Figure 99.

$$G(M) = 6.70 \frac{[1 + .365(\gamma-1)Pr^{\frac{1}{2}}M^2]^{\frac{5(1-\omega)}{8}}}{(1 + .277M^2)(M^2-1)^{3/8}} \left(\frac{T_w}{T}\right)^{\frac{1}{2}+\omega} \delta^*_*$$

where $\frac{T_w}{T} = 1 + \frac{\gamma-1}{2} Pr^{\frac{1}{2}}M^2$

Ratio of specific heats, $\gamma = 1.40$

Prandtl Number, $Pr = 0.72$

Variation of viscosity with temperature, $\mu \sim T^{\omega}$, $\omega = 0.75$

R_o is the Reynolds number at the point where the effect of separation is first felt, $R = \frac{Ux_o}{\nu}$

Δs is the distance ahead of the shock wave that separation is felt

x is the effective distance to the beginning of the laminar boundary layer

$\delta^*_* = \frac{\delta^* R^{\frac{1}{2}}}{L}$ = Mach number variation of displacement boundary thickness, Figure 100.

It will be noticed that the parameter, H, is non-dimensional. For the majority of the data used, a better correlation could be obtained by using a parameter $F = \frac{M^2-1}{M^3} \left(\frac{U}{\nu}\right)^{2/5} \Delta s$, but since this parameter is dimensional, it is felt that it will not apply over as wide a range in geometry and Reynolds number. To illustrate the improved correlation, Figure 101 is presented, but it is not used for further calculations. The Mach number variation of both of the parameters, F and H, is very similar in the range of Mach numbers between 1.25 and 4.25 differing by at most 5%.

There is no theoretical or experimental data available concerning the changes in a laminar boundary layer as it passes through a Prandtl Meyer expansion. In estimating the distance x_o in the Reynolds number and in the parameters F and H it was arbitrarily assumed that the boundary layer had its origin 0.75 inches ahead of the maximum thickness point.

Although it is thought that the curve given to determine the location of the separation effect is not very accurate and needs improvement, it does serve to give the approximate location for separation and quite satisfactory results when the overall pressure distribution is considered. The above results are all based on separation of a laminar boundary layer with zero pressure gradient. Without any experimental evidence in the current experiments to back up the claim, it is felt that the conditions in the separated region would be unaffected by a pressure gradient, but that the location of separation and the conditions under which

it would occur would be affected. This view is supported by the results of Reference 20. Therefore it was not expected that Figure 98 would apply when the separation point lies ahead of the maximum thickness point on a double wedge wing. This proved to be true and data from cases in which separation occurred ahead of the maximum thickness point could not be used in the preparation of this curve.

If the Reynolds number at separation is of the proper size, we may have laminar separation on the wing followed by a transition on the boundary of the separated flow to turbulent. It was found in the current set of experiments, that when the Reynolds number increased by approximately 800,000 behind the laminar separation point, transition would occur. Behind the transition point, the pressure again increases. The amount of the increase may be determined in the following manner. For purposes of the following discussion consider that the control surface has a positive deflection. There is flow from the upper surface of the wing to the lower surface of the flipper. Therefore the mass of fluid which passes below the trailing edge of the flipper is increased. One knows the necessary conditions to calculate the mass flow of fluid that flows from the upper surface of the wing to the lower surface of the flipper. Using this and an estimate of the pressure at the trailing edge of the control surface, one may approximate the extent of this flow into the area below the control surface. The flow from the lower surface of the wing must be turned because it cannot occupy this same area. From a consideration of the experimental data it was found that the flow begins to turn at

the transition point and assumes the direction determined by a line through the point where transition occurs and the estimated extent of the fluid from the wing's upper surface where it reaches the flipper trailing edge. A better picture of the means of estimating this will be obtained when the methods of calculating the pressure on the control surface are discussed. A useful equation in estimating the extent of the flow that comes from the wing's upper surface is derived from the continuity equation.

$$\frac{h_2}{h_1} = \frac{p_1}{p_2} \left(\frac{1 + \frac{\gamma-1}{2} M_1^2}{1 + \frac{\gamma-1}{2} M_2^2} \right)^{\frac{1}{2}} \frac{M_1}{M_2}$$

where h_1 = height of fluid at the wing's trailing edge that flows over the lower surface of the flipper

h_2 = height of fluid at the flipper trailing edge that came from the wing's upper surface

p_1 = pressure at trailing edge of wing's upper surface

p_2 = estimate of the average pressure in the area occupied by the flow from the wing's upper surface as it passes the trailing edge of the flipper's lower surface

M_1 = Mach number at wing's trailing edge

M_2 = average Mach number corresponding to the same location as p_2

In calculating h_1, it is necessary to account for the displacement boundary layer thickness. To assist with this, Figure 100, based on the methods of Crocco, Reference 21, is included. Use

of the above procedure gives the flow direction and in turn the pressure and Mach number on the portion of the wing following transition.

The one further case that must be considered is when the flow is turbulent on the wing. As discussed previously the flow is much less likely to separate in this case and it requires a flow deflection of about 20 degrees before it occurs at a Mach number of 3.5. In the present set of experiments, only qualitative visual data were obtained with a turbulent boundary layer, so it is necessary to depend on results of others for much of the quantitative information. Reshotko and Tucker in Reference 22 have given a simple means of calculating the flow resulting from shock induced turbulent separation which appears to give reasonable results when compared with the present experiments. They state that the Mach number ratio across the separated region is 0.81 for the case involving flow around a wedge and 0.76 for flow over a step. Our case is most closely approximated by the wedge and so a Mach number ratio of 0.81 was used to draw Figures 102 and 103 for the resulting pressure ratio and flow deflection. The data from References 10 and 11 suggest that variation of the Reynolds number does not affect the pressure in the separated region, but Reference 8 indicates that the pressure ratio is inversely proportional to the tenth root of the Reynolds number for a step shape configuration. The data given in this latter reference for the wedge shape configuration are quite meager but from that which is given, it appears that Reynolds number has no effect.

If the variation is inversely proportional to the tenth root of the Reynolds number, this would be consistent with the variation

in the laminar flow case since then the general conclusion could be drawn that the pressure is proportional to the square root of the skin friction coefficient in both cases. However there is no need to complicate the flow calculation more than necessary and since the evidence is conflicting on whether the pressure is influenced by Reynolds number, one might as well consider the simpler solution and assume that it has no effect.

Considering now the location of separation with a turbulent boundary layer, it is noticed that the upstream influence is much reduced. Table IX shows the location of the separation points for the 10 inch wing-control surface configuration on which the flow was turbulent. One notices that apparently separation begins very near the trailing edge and moves slowly forward as the shock strength is increased. However the data show that at the larger flipper deflections, the separation point jumps much further forward. It is believed that this latter phenomenon is similar to that explained for the cases involving transition after the laminar boundary layer was separated. When the flipper deflection is positive some of the flow from the upper surface of the wing flows over the lower surface of the flipper and causes the flow from the lower surface of the wing to turn aside. When the extent of this turning is larger than can be realized from the usual separation phenomenon of the turbulent boundary layer occurring near the wing trailing edge, the separation point is forced well forward so that the flow may turn through a smaller angle and still clear the flow from the upper surface. Since pressure distributions on a wing with turbulent flow are not available it was not possible to

verify the above postulated phenomenon which was based on the flow shadowgraphs and therefore it is felt that further discussion is not warranted until such data are available to check the theory.

Conditions necessary to initiate separation with a turbulent boundary layer have not been defined. From the flow shadowgraphs of the 10 inch wing-control surface model at a Mach number of 3.52 and with the ideas gained from other experiments, it was found that separation will be induced when a shock wave has a Mach number ratio across it of 0.65. Although this result was obtained entirely from the tests at a tunnel Mach number of 3.52, the Mach number ahead of the shock varied from 3.1 to 3.5 due to different angles of attack. It is believed that this figure is approximately independent of Mach number and Reynolds number based on the results obtained for experiments reported in references cited in the previous paragraphs. Therefore as an approximate criterion for shock induced separation it is suggested that a Mach number ratio across the shock of 0.65 be used. Figure 104 is a graph of the flow deflection occurring when the Mach number ratio across the shock is 0.65. This completes the discussion of the calculation of the pressures on the wing.

On the control surface the pressure distribution is calculated in the same manner for both a laminar and turbulent boundary layer. The conditions at the trailing edge of the wing serve as a starting point for the calculation. At the trailing edge the flow on the pressure side of the wing expands to the pressure occurring on the suction side.

Figures 105 and 106 are included to illustrate this expansion fan from the wing's trailing edge. These figures are for a configuration having a gap of $\frac{1}{2}$ inch between the surfaces because they give a clearer representation of the waves than the zero gap pictures. Figure 105, for $\alpha = -12$ degrees, $\delta = 20$ degrees, is a case in which the laminar separation is caused by the shock at the trailing edge of the wing. The shock from the flipper's leading edge is far enough downstream to prevent it from influencing the flow on the wing. A fuller explanation of this will be given in the section on the use of gaps. It suffices to say that the laminar separation is limited in extent as is its wake downstream of the wing. The beginning of the expansion fan is seen as a light line emanating from the trailing edge. One also sees that the shape of the wake in the immediate vicinity of the trailing edge indicates expansion from the high pressure occurring on the upper surface to the lower pressure in the separated region. The angle measured from this photograph is in agreement with that required by the pressures. The flow is turned through an angle larger than required to return it approximately to the original free stream direction and therefore a shock wave is seen above and below the wake that brings it to the correct angle. Figure 106, for $\alpha = -12$ degrees, $\delta = 25$ degrees, illustrates a case in which an extensive separated region exists because of the flipper's shock wave. It is noted that again the flow on the upper surface expands to the pressure in the separated region.

The expansion waves, discussed in the preceding paragraph will of course influence the flow on the flipper. Depending

on the geometry of the configuration and the Mach number, the leading edge of the flipper may or may not be affected. When separation has not been brought about by the flipper, the wake of the wing is turned into the free stream direction a short distance behind the wing. In many instances this requires a shock wave slightly downstream of the expansion waves just described to bring the flow to the proper direction. The above waves from the flow over the wing set the initial conditions for the flow over the flipper. On the suction side of the flipper, the flow is attached except at high deflection angles. It is easily determined by the shock-expansion theory. At the low deflection angles, where the leading edge of the flipper is in the wing's wake, the pressure only gradually assumes the value calculated by this method as the effects of the wake are dissipated downstream. The distance required may be estimated from the thickness of the wake at the wing's trailing edge and the thickness distribution of the flipper.

At large deflection angles there is the possibility of separation on this surface caused by the shock wave that occurs at the trailing edge of the flipper. The same criteria used to determine separation on the wing, Figures 96 and 104, are also applicable in this case. When the flipper's leading edge falls outside the wing's wake, the boundary layer on its suction side has a new start and is not influenced by the previous flow on the wing. If separation does occur on the flipper, the methods previously discussed for finding the pressure, Mach number and flow direction of the separated flow apply.

On the pressure side of the control surface, the largest changes from the inviscid theory take place. When the flow on the wing is not separated the flow on this surface may be calculated by a simplified characteristics method, taking into account the waves that emanate from the flow about the wing. When separation has occurred on the wing, then the surface of the separated region reflects the shock or expansion waves that are between it and the flipper's surface. The leading edge shock wave is reflected by the separated wake as an expansion fan. These expansion waves then strike the surface of the flipper and are reflected again as expansion waves. When they again strike the separated wake, they are reflected as compression waves which converge to form a shock wave. It is necessary to use the method of characteristics (Reference 16 for example) for the calculation of the above described flow. One of the required boundary conditions for this calculation is the pressure occurring in the separated region. Although this pressure varies in the streamwise direction, it has been found that a reasonable approximation may be obtained by assuming the pressure is constant and equal to the average of the pressure in the separated region at the trailing edge of the wing and an estimated static pressure that is found by assuming the flow of the separated region to be turned parallel to the surface of the aft portion of the flipper. Although this is a simple and somewhat crude approximation, it does appear to give satisfactory results in the majority of the cases checked. This completes the discussion of the suggested methods of calculating the pressure distribution on a balanced flap type control

surface. An outline of the above methods is given in Table X.

The ensuing paragraphs will be devoted to discussing the results obtained by using the above procedure and comparing these results with experimental pressure distributions. Twenty pressure distributions were calculated and compared with experiment. The calculations were made in two ways: 1) Assuming an inviscid fluid, and 2) assuming a viscous fluid using the methods described in the first portion of this section.

All of the initial figures to be discussed are for a Mach number of 3.52. Figure 74, for $\alpha = 0$, $\delta = 0$, shows that the inviscid calculation agrees with the experimental pressure distribution except at expansion corners, at the trailing edge of the wing where separation occurs, and at the leading edge of the flipper which is in the wing's wake. The viscous flow calculation agrees well everywhere with the experimental values. To avoid confusion, where the curve for the viscous calculation is in agreement with the inviscid solution, only the inviscid curve is drawn.

Figure 75, for $\alpha = 0$, $\delta = 5$ degrees, shows about the same agreement on the wing as the previous figure, but the flipper does not show good agreement with either the viscous or inviscid calculation. The major discrepancy lies in the upper surface where the measured pressures are much less than predicted. It is believed that this is because the leading edge of the flipper is in the separated wake from the wing. The air in this wake has a low velocity and only on its lower side is energy being fed in to increase this velocity. The upper side of the wake is cut off from the external flow by the presence of the flipper. Therefore

the pressure never does increase to the full theoretical value. It does not appear practical to try to determine an empirical means of estimating this decrease in pressure. Although a general method might be devised it does not seem to be of enough importance to warrant it.

Figure 76, for $\alpha = 0$, $\delta = 10$ degrees, has a pressure distribution on the wing which is similar to the preceding cases. The pressures on the flipper are here completely different from those calculated with inviscid theory. The distribution calculated with the empirical methods outlined in this thesis is, however, in general agreement with the measured values. The calculated pressure on the aft portion of the lower surface of the flipper is higher than the measured value; no satisfactory explanation for this is available. The viscous calculation was made by using the method of characteristics.

Figure 77, for $\alpha = 0$, $\delta = 15$ degrees, shows a pressure distribution similar to that in the preceding figure. Because of the lengthy procedure in the characteristics calculation, it was used only in selected cases. For the case in question only the initial maximum, the minimum and final pressure were calculated. These values can be easily obtained but to obtain the complete distribution requires three or more additional hours of work. Since the majority of these distributions are similar in shape it was felt that determination of the maximum and minimum value was sufficient for many of the cases. The large differences between the inviscid and viscous results become more and more apparent as the flipper deflection angle is increased.

Figure 78, for $\alpha = 0$, $\delta = 20$ degrees, shows a case in which the laminar separation appears on the forward half of the wing and is followed by transition and a further increase in pressure that is permitted by the turbulent separation. The pressures are calculated but the location at which laminar separation takes place cannot be estimated by the methods described. This is because sufficient data are not available to understand what occurs to the separated flow at a Prandtl-Meyer corner. Although the separation point moves gradually forward as the size of the triggering pressure rise increases, the process is discontinuous when an expansion corner is encountered. The pressure distribution obtained by the viscous calculation has the same shape and magnitude as the one determined experimentally. On the lower surface of the flipper, again only three pressure levels were found. It is noticed that the calculated minimum pressure is much less than the measured value; however the pressures at the leading and trailing edges are in excellent agreement. The upper surface of the flipper exhibits a laminar separation due to the strong shock occurring at its trailing edge. This is predicted satisfactorily by the viscous calculation.

Figure 79, for $\alpha = 0$, $\delta = 25$ degrees, represents a very difficult case to calculate. Because the laminar separation occurs in front of the maximum thickness point, the curve for the location of laminar separation is not valid, as discussed in the previous paragraph. Using the experimental data for its location, it is possible to calculate the pressure rise resulting from laminar separation and the location of the transition point; these calculations

agree well with the experiment. The turbulent separation pressure rise is determined from the required flow deflection for the fluid to clear the trailing of the flipper. The method as outlined states that the upper and lower surface distributions are the same since they are influenced by the same high pressure region. The experimental data show that the upper and lower surface have slightly different pressures but this error in the calculations is not serious. At least one can say that there is a very marked improvement over the inviscid calculation. Because of the turbulent separation the wake at the leading edge of the flipper completely envelopes the flipper and makes it very difficult to predict the pressures. Even the upper surface of the flipper is in the wake and therefore the full pressure change that would occur in a uniform velocity stream is not developed. Laminar separation does occur on this surface and this can be estimated satisfactorily. Because the lower surface of the flipper is completely buried in the wake the usual viscous calculations outlined do not give results that are reasonable. No attempt is made to show these results. This completes the calculations made at zero angle of attack.

The next group of pressure distributions are at -8 degrees angle of attack at the same Mach number, 3.52. Figure 80, for $\alpha = -8$ degrees, $\delta = 0$, shows that the calculated pressures with the inviscid assumption are quite satisfactory on the wing except near the trailing edge on the lower surface. Here laminar separation takes place in a manner predicted by the viscous theory. The pressures on the flipper are reasonably well predicted by the inviscid theory with some improvement noted by use of the viscous

method. The small discrepancy in the flipper pressures between the calculated value and experiment is likely caused by a small error in the flipper setting.

Figure 81, for $\alpha = -8$ degrees, $\delta = 20$ degrees, shows excellent agreement between the calculated and measured pressure distributions. On the flipper, the upper surface experimental values agree with the inviscid solution which is the same as the viscous solution in this case. On the lower surface of the flipper, only the maximum and minimum pressures are calculated for this case since the shape of the distribution will be similar to the $\alpha = -8$ degrees, $\delta = 25$ degrees case for which the complete calculation is given. One notices that the calculated maximum pressure on the forward portion of the lower surface of the flipper is considerably smaller than the measured value. The experimental pressure falls rapidly to the calculated values so that the agreement is very good from 0.65 back of the leading edge. Apparently the leading edge shock is stronger than necessary for the flow to be attached to the flipper and an expansion takes place immediately behind this shock. This phenomenon was noticed in the experimental data for several cases. However in many of the cases it was because a strong shock was occurring at the leading edge. The pressure measured for this case is much too small for that to be occurring here.

Figure 82, for $\alpha = -8$, $\delta = 25$ degrees, has a pressure distribution similar to the one discussed in the last paragraph. In this case, the complete calculation has been made and one sees that the agreement with the experimental data on the flipper is

excellent. On the stabilizer the calculated and measured results are also in good agreement. It should be noted, however, that the calculation method on the wing only predicts the plateaus of pressure, and the distribution between them is estimated from experience. Since separation of a turbulent boundary layer is involved, a theoretical analysis of the problem does not seem to be a fruitful project and it is expected that empirical data must be used to obtain the shape of the pressure distribution. Although this is not a desirable situation, the improvement in the pressure distribution, calculated by what has been referred to as the viscous method over that obtained with the inviscid shock-expansion theory, shows that the method is still attractive with all its approximations. The calculated pressure on the wing's upper surface is slightly larger than the measured value. This effect was noticed in other similar cases where the flipper deflections were large, but the reasons for it are not understood and no means of predicting it are at hand. The discrepancy is however a small one in all cases where it was noted.

Figure 83, for $\alpha = -8$ degrees, $\delta = 30$ degrees, has a somewhat different pressure distribution. The flow on the lower surface of the wing is separated very near the leading edge. Because of the lack of pressure orifices in this area, the exact location is not known. For practical purposes it is assumed that separation occurs at the leading edge and the full increase in pressure is developed immediately. This, of course, is not actually true and a somewhat better approximation would be that the pressure at the leading edge is the value shown for the inviscid

solution and separation occurs 1/4 to 1/2 inch back of the leading edge. The interesting thing about this distribution is that the normal force on the wing is up instead of in the expected down direction for a negative angle of attack, and the viscous calculation method predicts this change. The pressures on the flipper are also predicted satisfactorily. This completes the discussion of the calculated results at a Mach number of 3.52.

Next, five typical cases that have a free stream Mach number of 2.60 will be discussed. Figure 84, for $\alpha = 0$, $\delta = 0$, shows good agreement between the calculated and measured pressure distributions. In fact the inviscid solution gives reasonable results in this and similar cases. The major difference in the calculations is due to the separation near the trailing edge of the wing, and on the leading edge of the flipper because of the large wake. By estimating the width of the wake from the location of separation and the angle of the flow deflection, it is possible to estimate where the pressure on the flipper reaches its inviscid value with reasonable accuracy.

Figure 85, for $\alpha = 0$, $\delta = 15$ degrees, shows similar results on the wing as the previous case. On the lower surface of the flipper the calculated pressure distribution has the same shape as the experimental one and is a reasonable quantitative approximation.

Figure 86, for $\alpha = -8$ degrees, $\delta = 0$, shows fine agreement between the calculations and experiment. It appears that the angle of attack might have been larger than the stated 8 degrees to account for the slightly larger pressures on the wing.

Figure 87, for $\alpha = -8$ degrees, $\delta = 25$ degrees, is one of the cases for which the characteristic method was used. The calculations of the wave angles were made on a Burroughs E-102 Computer and the drawing of the expansion and compression waves made 30 times the actual scale of the model. Thus the method was applied with great care and it is felt that there are not significant errors in its application. In the case being discussed the discrepancies between the calculated and measured values are not too large. If this calculated pressure distribution were used to calculate normal force or hinge moment on the surfaces, they would be within a few per cent of the measured values. This is certainly as much as can be expected and all that is desired from a method of this sort.

Figure 88, for $\alpha = -8$ degrees, $\delta = 30$ degrees, indicates separation on the lower surface of the stabilizer very near the leading edge. From the geometry of the configuration, and using the methods described, the calculated pressure in this separated region is much smaller than measured in the experiments. It is believed that this discrepancy is not due to the basic ideas involved in the method; instead the difficulty is thought to be in the method of estimating the width of the flow from the upper surface of the wing as it passes the trailing edge of the lower surface of the flipper. This determination is best accomplished by making a characteristic solution of the flow over the flipper, but since the flow at the leading edge on the lower surface of the flipper is detached, no effort was made to solve the mixed flow region involved. The

estimate that was made for the size of the region containing the flow from the upper surface of the wing was apparently too small. The pressures calculated for the upper surface of the wing and flipper agree well with measurement. As stated previously, since there is a detached shock on the flipper's leading edge and thus subsonic flow, no effort was made to solve for the pressure distribution.

The final five pressure distributions studied are for a Mach number of 1.70. In Figure 89, for $\alpha = 0$, $\delta = 0$, the agreement between the calculated and measured pressure distribution is very good. Figure 90, for $\alpha = 0$, $\delta = -10$ degrees, also shows good agreement.

In Figure 91, for $\alpha = -4$ degrees, $\delta = 0$, both of the calculated distributions by the inviscid and viscous methods agree well with the experiment. In this and similar cases, there is only a slight difference between the two methods; the separation on the wing causes only a small change in the pressure and its wake causes the pressure on the flipper to rise more slowly.

Figure 92, for $\alpha = -4$ degrees, $\delta = 10$ degrees, is an example of the flow at a low Mach number in which the shock wave from the leading edge of the flipper is reflected by the separated wake to cause rapid variations in the pressure on the forward portion of the flipper's lower surface. Calculations were made using the method of characteristics and the shape of the resulting pressure curve is similar to that measured, but quantitatively the curves are not too similar. This discrepancy can be caused by very minor

errors in estimating the boundary layer thickness and/or how fast the wake spreads downstream of the wing's trailing edge. It is also not known if the curve of the measured pressures is faired properly, since the pressure orifices are too widely spaced for a case where the pressure changes as rapidly as it does here. The pressures calculated on the remainder of the surfaces of the wing and flipper are reasonable.

Figure 93, for $\alpha = -4$ degrees, $\delta = 12$ degrees, shows similar agreement between calculated and measured pressures as the preceding figure. On the flipper's lower surface, the method of characteristics is not used and thus only the maximum and minimum pressures are shown. It is anticipated that the agreement here is similar to that in the preceding figure also. In conclusion it is noted that the results obtained where separation occurs at the lower Mach numbers are not nearly as good as those obtained at the higher Mach numbers. In a way this is not too unfortunate as it was found that there were much larger discrepancies in hinge moment and elevator effectiveness between linearized theory and experiment at the higher Mach numbers than at the lower Mach numbers. Therefore it is more important that the method be applied best at the higher Mach numbers. Considering the general agreement obtained in the calculations made using the viscous method, one concludes that the method does in a majority of cases appear to give results that are very satisfactory for engineering purposes.

VIII. CONTROL SURFACE EFFECTIVENESS AND HINGE MOMENTS

The prime purpose in determining the wing and control surface pressure distributions is to be able to predict the control surface effectiveness and hinge moments. As stated in the introduction it was found that linearized theory or any inviscid flow theory was inadequate to predict the performance of supersonic control surfaces over a wide range of conditions. It has also been shown that the lift on a wing alone is seriously affected by shock-boundary layer interaction. This interaction will affect a wing in much the same manner as the normal stall phenomenon of a wing at subsonic speeds.

If the flow does not separate, a reasonable calculation of the control surface effectiveness may be made using inviscid linearized theory but much better results may be obtained by use of the shock expansion theory, taking into account the effect of the wing on the control surface. Linearized theory usually gives a value of effectiveness at high deflection angles that is too small. If the flow on the wing separates, the usual effect is to increase the control surface effectiveness especially at the larger deflections. In this case a careful calculation of the pressure distribution by the methods described previously in this thesis are required to obtain a reasonably accurate value of effectiveness. The major change in effectiveness due to separation results from the change in the force on the wing; the change in force on the flipper is not in general a large factor. At Mach numbers larger than 3.5, it has been found that the control effectiveness increases with Mach number, contrary to the anticipated decrease which is predicted by linearized theory. This result was obtained from unpublished force data of the Hughes

Aircraft Company on typical flippers of the type being discussed. The methods given for calculating pressure distribution will give values at the high Mach numbers that agree with this result.

Considering now means of obtaining hinge moments on a balanced flap type control surface, it becomes apparent that linearized theory cannot be used at any except very small deflection angles, and even here the results obtained will not be very good. Of course, if the pressure distribution can be accurately predicted by the methods described previously, then good hinge moment prediction may be obtained. To show the typical shape of the hinge moment curves for this type of flipper, some of the pressure distributions measured in the current tests were integrated. Figure 107 shows the hinge moment coefficient plotted versus control surface deflection, holding angle of attack constant. The shape of the curves is in excellent agreement with force measurements made on similar control surfaces (unpublished). One notes that the surfaces are unstable when the flipper deflection and angle of attack have opposite signs. This represents typical trim conditions when tail type control surfaces are used. With an unstable hinge moment the aerodynamic forces tend to increase the surface deflection without limit whereas with stable hinge moments the aerodynamic forces tend to return the surface to a unique trim value that depends on the angle of attack. Trim conditions, as used above, refer to steady state conditions with a constant angle of attack.

If the hinge moment curves are linear, it is easy to reduce the size of the hinge moments by moving the hinge line. This in effect rotates the line and if exact linearity is obtained, the hinge moments may be made zero. Of course this can probably not be accomplished at all angles of attack and at all Mach numbers, but much can be done to reduce the hinge moments if they are linear with deflection angle. However, when the curves are shaped as the ones are in Figure 107, a best hinge line location may be obtained, but it is not possible to achieve really small hinge moments. The shape of these curves in Figure 107 is typical of balanced flap type control surfaces and changes in hinge line and planform (on a three dimensional design) can do little to improve it. In the next section of this thesis, a method of linearizing these curves will be discussed.

Because separation has a very strong effect on the hinge moment of the flipper, it is imperative to simulate the proper type of boundary layer, i.e., laminar or turbulent, when making hinge moment measurements in a wind tunnel. In these tests it is also desirable to have full scale Reynolds numbers to obtain similar separation phenomena, but this is of course usually not possible. With a turbulent boundary layer, Reynolds number effects on separation are believed to be small and can probably be neglected, but with a laminar boundary layer, changes in Reynolds number can produce noticeable but not major changes in the hinge moments.

IX. EFFECT OF A GAP BETWEEN WING AND CONTROL SURFACE

In an effort to reduce the hinge moments on a control surface, several different planforms and balance modifications were tried by the author while at the Hughes Aircraft Company. One of these produced a considerable improvement in reducing overall hinge moments. The change was to move the balanced control surface downstream with respect to the main surface thereby leaving a gap between the two surfaces. When this gap is of sufficient size, separation will be delayed or forestalled and the variation in hinge moments considerably reduced. No precise gap size may be given as optimum because it appears that the larger the gap, the better; however, a point of diminishing returns is reached when the gap is 15 to 30 percent of the wing chord. Gap sizes of 1/4, 1/2, 1 and 2 inches were used for this test where the wing chord was 6 inches. A rather complete series of tests was run in which about 100 shadowgraphs and 80 complete pressure distributions were obtained at each gap setting. Only a small number of these will be shown in the body of the thesis, but the rest are available in Reference 2. In the following paragraphs the differences in flow conditions and pressure distributions will be emphasized and the lack of a discussion about some point will indicate that it is similar to the zero gap condition and needs no further discussion. In general a given condition of Mach number, angle of attack, and flipper deflection will be selected and then the changes with variation in gap size will be discussed.

We will begin by considering the highest Mach number first, $M = 3.52$. At zero angle of attack and zero control surface deflection angle, the laminar boundary layer on the wing separates for gaps of

1/4 and 1/2 inch and is attached for gaps of 1 and 2 inches, Figures 108, 109, 110 and 111. The larger gaps permit the wing wake to accelerate sufficiently so that the wake does not provide a means of propagating high pressures forward to the wing. When the control surface deflection was increased, thus increasing the shock strength, it was found that the separation point moved upstream in the same manner as it did for zero gap. In the case of the 1 inch gap, which did not separate at $\delta = 0$ degrees, separation has occurred by $\delta = 20$ degrees, Figure 112. For a gap of 2 inches, the boundary layer on the wing was still attached at $\delta = 25$ degrees, Figure 113. This was the highest control deflection angle at which tests were made.

There are two shock waves that affect the separation of the boundary layer from the wing. One is the shock wave at the trailing edge of the wing and the other is the shock from the leading edge of the flipper. Of course the existence of a gap cannot influence the effect of the shock at the trailing edge of the wing. The strength of this shock is a function of the wing thickness and the angle of attack. At this Mach number it requires a shock having a flow deflection angle of about 3 degrees to separate the laminar boundary layer. Because of the thickness of the wing this value is exceeded at an angle of attack of about 1 degree. This is borne out by the shadowgraphs, Figures 114 and 115, which show that at an angle of attack of zero degrees separation does not exist where there is a large gap, whereas at 4 degrees it does exist. Therefore we can conclude that the presence of a gap does not affect separation

resulting from the shock at the trailing edge of the wing, and the location of the separation point will move steadily upstream on the wing as the angle of attack increases. The gap, however, does reduce separation due to the shock wave from the leading edge of the flipper. At an angle of attack of zero, an increase in flipper deflection from zero, causes the separation point to move upstream when there is not a gap between the surfaces. With a gap of 1/4 inch, however, a flipper deflection of over 15 degrees is necessary before the separation point is adversely affected. With a gap of 1/2 inch it requires a flipper deflection larger than 20 degrees and with a larger gap the flipper deflection must be greater than 25 degrees before its effect is felt. Tables V, VI and VII give the separation points for all the tests run at normal Reynolds numbers. Data are included from both the visual and pressure tests. The data from the pressure tests are followed by an asterisk, whereas the visual data are presented unaccompanied. There is considerable scatter in the data, partly caused by the difficulty in reading the separation points and partly because small differences in surface conditions or tunnel conditions can cause the location of the separation point to shift. In many instances, it appears that the presence of the pressure orifices cause separation to occur further upstream than observed visually on the model without these orifices. All of the data given in these three tables are for separation of a laminar boundary layer. Table VIII shows the effect of Reynolds number on separation of the laminar boundary layer with a 2 inch gap. It should be noticed that even a small gap can reduce the

extent of the separation and when the gap is larger the effect of the shock wave on the leading edge of the flipper is isolated from the boundary layer on the wing. This is even more important when the boundary layer on the wing is turbulent. In this case the shock wave at the trailing edge of the wing for angles of attack of about 15 degrees or less will not cause the boundary layer to separate and if there is a gap of reasonable size present, flipper deflection angles up to 25 degrees will still not cause separation. Then in this case the adverse effects of separation will be eliminated and the pressures on the surfaces will closely follow the inviscid theory. Table IX gives the separation points at a Mach number of 3.52 for the turbulent boundary layer cases.

Figures 116 and 117 are presented to show the effect of a gap on the pressure distributions. They are both for cases having a 2 inch gap, and may be compared with the zero gap pressure distributions for similar conditions that are given in Figures 58 and 77 respectively. Figure 116 shows that separation did not occur on the wing at the rearmost orifice (station 5.25) whereas with zero gap, Figure 58 indicates that separation occurred near station 4.00. The pressure distributions on the lower surface of the flipper were completely different in the two cases. Since separation did not occur in the gapped case, one might expect the flipper's pressure distribution on its lower surface to be similar to that obtained with an inviscid calculation. This appears to be approximately the case, except that the pressure near the flipper's leading edge was modified by an expansion wave from the wing's

trailing edge striking the flipper and being reflected. This accounts for the dip in pressure between stations 8.0 and 8.8 on Figure 116.

Figure 117 for -8 degrees angle of attack, shows that there was only minor separation on the wing. This separation was caused by the shock wave at the wing's trailing edge and is much less severe than the separation that occurred in the zero gap case shown in Figure 77. On the flipper's lower surface, the pressure distributions were quite different in the two cases. The zero gap case has been discussed previously and its shape is explained primarily by the reflection of shock and expansion wave between the separated region and the surface of the flipper. In the 2 inch gap case the phenomenon is different. Here the variation in pressure on the flipper's surface is primarily caused by expansion wave emanating from the trailing edge of the wing, followed by a shock wave that occurs slightly downstream. The shadowgraphs corresponding to these gapped cases are given in Figures 118 and 119.

Figure 120 has been prepared from the data obtained at Mach numbers 2.60 and 3.52. It is an attempt to correlate the size of gap needed to eliminate laminar separation caused by the leading edge shock wave from the flipper. The wake from the wing is composed of lower velocity air than that surrounding it. As it progresses downstream the surrounding air accelerates the low velocity region back to the free stream conditions by a mixing phenomenon. When the wake strikes the shock wave from the flipper it must have sufficient energy to increase its pressure to the value behind the shock wave, if separation is to be avoided. A normal shock wave gives the maximum increase in pressure for a given

Mach number so this determines the minimum required Mach number in the wake just ahead of the shock to avoid separation. If the Mach number is lower than this minimum the flow in the wake cannot proceed downstream and pressure disturbances are transmitted back through the wake to the laminar boundary layer of the wing.

The downstream distance is non-dimensionalized by using the momentum thickness of the boundary layer at the trailing edge of the wing. This factor was used because when the boundary layer is thick it requires a longer mixing distance to accelerate the flow in the core of the wake. The abscissa of Figure 120 is the non-dimensional downstream distance from the trailing edge of the wing to the point at which the wake strikes the flipper's leading edge shock wave, divided by the Mach number outside the wake squared. In computing these distances the theoretical locations of the shock waves were used. The shock wave was calculated by assuming that the flow behind the wing is turned into the free stream direction and returns to the original free stream Mach number. There is a slight error in this assumption that becomes larger at the higher angles of attack, but it is not believed to be of importance. It is assumed that the flipper turns this flow into a direction parallel to its surface. The value used for the momentum boundary layer thickness, θ, is that calculated to occur at the wing's trailing edge, assuming the laminar boundary layer begins 3/4 inch ahead of the wing's maximum thickness point. A curve for finding the momentum thickness of a laminar boundary layer is given in Figure 121.

The ordinate of Figure 120, M_2/M_1, is the ratio of the Mach number in the wake just ahead of the normal shock wave portion of the flipper leading edge shock to the external flow field Mach number. The Mach number, M_2, is the minimum that can occur and still result in an increase in pressure of the air within the wake to the same pressure that occurs in the external flow. The Mach number of the external flow, M_1, may be approximated as the free stream Mach number. The ratio M_2/M_1 is equivalent to the sine of the wave angle of the shock wave occurring in the external flow.

In obtaining the data for Figure 120, Tables VI and VII were used to find the gap required to eliminate separation caused by the flipper. Because the gaps were spaced at intervals, the gaps on either side of this point were used. Thus it could only be determined that separation did not occur with a 1 inch gap and it did occur with a 1/2 inch gap, as an example. This accounts for the line representing each point of data. It is known that separation occurs for the condition at the left end of each line and that it does not occur at the right end. Somewhere between is the critical point of incipient separation. This method adds to the large scatter of the points, but the information obtained is a useful approximation to the gap required to avoid separation of a laminar boundary layer by the shock wave from a flipper. The line drawn on this graph is believed to be a conservative estimate for this requirement. If separation is avoided, the resulting pressure distributions will be closely approximated by the inviscid shock-expansion theory, with some modifications for viscous effects caused by the wake. However

since the shock wave at the trailing edge of the wing is sufficient to separate a laminar boundary layer in most cases, there will usually be a separated region. This region is smaller in extent when a gap is present and causes smaller changes in pressures so that considerable improvement is noticed in the similarity of the pressure distributions as the control surface angle is varied.

All of the foregoing discussion concerning the effect of a gap applies to the case with a laminar boundary layer. Some visual data are available for the turbulent boundary layer case at a Mach number of 3.52. It was obtained with the 10 inch chord wing and the separation points obtained are given in Table IX. It is noticed that separation occurs only at the extreme conditions of angle of attack and/or control surface deflection for the larger gaps. It is believed that for the cases where the flow is not separated, the pressure distributions will be close to those given by the inviscid shock-expansion theory. When separation does occur then the methods discussed previously in the zero gap case should be applied.

Figure 122 is included to illustrate the effectiveness of a gap in reducing and linearizing the hinge moment curves. This figure is for Mach number 3.52 and -8 degrees angle of attack, but it is indicative of the effect at other Mach numbers and angles of attack. It is noticed that as the size of the gap increases, the range of control surface deflections over which the hinge moment curves are linear increases. At a 2 inch gap the curve is nearly linear over the entire range for which data are available, namely from -10 degrees to 25 degrees. With a curve as linear as this, the

hinge line may be moved slightly aft to reduce the hinge moments still further. For the control surface used in these tests, the use of a gap reduced the hinge moment by a factor of about six for the range of control deflection angles considered. By shifting the hinge line to an optimum position for the gapped surface, it is expected that a full order of magnitude improvement over the ungapped surface could be realized.

CONCLUSIONS

1. Separation has a predominant effect on the pressure distributions for a balanced flap type control surface.
2. Inviscid theory will not give satisfactory results in most cases where separation is present.
3. Shock induced separation occurs for weak shock waves when a laminar boundary layer is present.
4. Turbulent boundary layers require a much stronger shock before separation occurs.
5. The pressure on a main surface is strongly affected by the control surface deflection.
6. The flow phenomena which occur have been explained in a manner that agrees qualitatively with the experimental data obtained.
7. A method of calculating the pressure distribution on this type of surface is given which agrees with experimental data well enough to be used for engineering calculations. Although this method is lengthy and requires further testing, it should be most useful in calculating modifications to designs for which test data are available.
8. Separation of the boundary layer introduces extreme non-linearity into the hinge moments for this type of surface, making it impossible to closely balance the surface for a wide range of angle of attack, control surface deflection, and Mach number.
9. It is shown that the use of a gap between the control surface and the main surface will ameliorate separation and thus make it possible to more closely balance a control surface and thus reduce the hinge moments by as much as an order of magnitude.

REFERENCES

1. Puckett, A. E., "Performance of the 12 Inch Wind Tunnel," JPL Memorandum Report 4-52, 1949.

2. Heimer, H. J., "Balanced Flap Type Supersonic Control Surfaces," Hughes Aircraft Co. Special Research Study (to be published).

3. Gadd, G. E., "Interactions Between Wholly Laminar or Wholly Turbulent Boundary Layers and Shock Waves Strong Enough to Cause Separation," Journal of the Aeronautical Sciences, Vol. 20, No. 10, November 1953.

4. Gadd, G. E., Holder, D. W., and Regan, J. D., "An Experimental Investigation of the Interaction Between Shock Waves and Boundary Layers," Proc. Roy. Soc. A, Vol. 226, pp. 227-253, 1954.

5. Gadd, G. E., "A Simple Theory for Interactions Between Shock Waves and Entirely Laminar Boundary Layers." Journal of the Aeronautical Sciences, Vol. 23, No. 3, March 1956.

6. Gadd, G. E., Holder, D. W., "Boundary Layer Separation in Two Dimensional Supersonic Flow," British ARC CP 270.

7. Gadd, G. E., "A Theoretical Investigation of Laminar Separation in Supersonic Flow." Journal of the Aeronautical Sciences, Vol. 24, No. 10, October 1957.

8. Chapman, D. R., Kuehn, D. M., Larson, H. K., "Investigation of Separated Flows in Supersonic and Subsonic Streams with Emphasis on the Effect of Transition," NACA TN 3869, 1957.

9. Donaldson, C., and Lange, R. H., "Study of the Pressure Rise Across Shock Waves Required to Separate Laminar and Turbulent Boundary Layers." NACA TN 2770, 1952.

10. Lange, R. H., "Present Status of Information Relative to the Prediction of Shock Induced Boundary Layer Separation." NACA TN 3065, 1954.

11. Love, E. S., "Pressure Rise Associated with Shock-Induced Boundary-Layer Separation." NACA TN 3601, 1955.

12. Holder, D. W., "The Interaction Between Shock Waves and Boundary Layers." Preprint of paper presented to Fifth International Aeronautical Conference June 20-24, 1955, Los Angeles.

13. Bogdonoff, S. M., and Kepler, C. E., "Separation of a Supersonic Turbulent Boundary Layer." Princeton Univ. Dept. of Aero. Eng. Report 249, 1954.

14. Crocco, L. and Probstein, R. F., "The Peak Pressure Rise Across an Oblique Shock Emerging from a Turbulent Boundary Layer Over a Plane Surface," Princeton Univ. Dept. of Aero. Eng., Report 254, 1954.

15. Bogdonoff, S. M., "Some Experimental Studies of the Separation of Supersonic Turbulent Boundary Layers." Princeton Univ. Dept. of Aero. Eng., Report 336, 1955.

16. Liepmann, H. W. and Puckett, A. E., "Introduction to Aerodynamics of a Compressible Fluid." John Wiley, New York, 1947.

17. Crocco, L. and Lees, L., "A Mixing Theory for the Interaction Between Dissipative Flows and Nearly Isentropic Streams." Journal of the Aeronautical Sciences, October 1952.

18. Sweeney, M. W., Jr., "An Experimental Study of Supersonic Hinge Moment and Control Effectiveness." MIT NSL Wind Tunnel Report 109, 1956.

19. Honda, M., "Theory of the Interaction Between Oblique Shock Waves and Laminar Boundary Layers." Report of the Institute of High Speed Mechanics, Tohoku University, Vol. 8, 1957.

20. Gadd, G. E., "Effects of Convex Surface Curvature on Boundary Layer Separation in Supersonic Flow." British ARC CP289.

21. Crocco, L., "The Laminar Boundary Layer in Gases." Monografie Scientifiche di Aeronautica No. 3, Dec. 1946. Translated by North American Aviation AL 684.

22. Reshotko, E. and Tucker, M., "Effect of a Discontinuity on Turbulent Boundary Layer-Thickness Parameters with Application to Shock Induced Separation." NACA TN 3454, 1955.

SYMBOLS

F Parameter used in estimating location of separation, alternate method, $F = \frac{M^2-1}{M^3}\left(\frac{u_o}{\nu}\right)^{2/5} \Delta s$; units $(\text{inches})^{3/5}$

G(M) Mach number parameter used in estimating the location of the separation of a laminar boundary layer. Equation given on page 42. Values given in Figure 99.

H Parameter used in estimating location of separation, $H = \frac{R_o^{3/8}}{G(M)} \frac{\Delta s}{x_o}$

L Length

M Mach number

Pr Prandtl number, for this report assumed to be constant at 0.72

RN/L Reynolds number per inch

R_x Reynolds number at point x

T Absolute temperature

U Velocity; feet per second

c_f Local skin friction coefficient

$\tilde{c}_f$ Local skin friction coefficient at a given Reynolds number divided by the skin friction coefficient at a Reynolds number of 10^6

g Distance from trailing edge of wing to shock wave from leading edge of the flipper measured along the wake; inches

p Pressure; pounds per square inch

Δs Distance from shock wave that induces separation to most forward position where its effect is felt; inches

α Angle of attack, positive direction is leading edge up

δ Control surface deflection angle, positive direction is leading edge up

β Wave angle of shock wave measured from flow direction ahead of shock

γ Ratio of specific heats, $C_P/C_V = 1.40$

δ^* Displacement boundary layer thickness; inches

δ^*_* Displacement thickness parameter where $\delta^* = \delta^*_* \frac{x}{\sqrt{R_x}}$

θ Momentum thickness of the boundary layer; inches

μ Coefficient of viscosity; pound seconds per square foot

ν Kinematic viscosity, feet squared per second

ω Exponent for variation of viscosity with temperature, $\mu \sim T^{\omega}$

SUBSCRIPTS

o Indicates condition far enough upstream to be unaffected by separation

w Indicates conditions at the wall

TABLE I

SCHEDULE OF DATA FROM PRESSURE DISTRIBUTION TEST

GAP	M	α	δ	RUN NO.
0	1.70	0	-10,-5,0,3,5	35
		-2	-5,0,5,10	36
		-4	0,5,10,12	37
		-6	5,10,12	38
		2,0,-2,-4	0	34
	2.60	0	-15,-10,-5,0,5,10,15	4
		-4	-15,-10,-5,0,5,10,15,20,25	5
		-8	-4,0,5,10,15,20,25,30	6
		-12	20,25	7
		2,0,-2,-6,-9	0	3
	3.52	0	-15,-10,-5,0,5,10,15,20,25	55
		-4	-15,-10,-5,0,5,10,15,20,25	56
		-8	-10,-5,0,5,10,15,20,25,30	57,58
		-12	0,5,10,15,20,25,30	59
		-16	15,20,25,30	60
		2,0,-2,-6,-10	0	54
1/4"	1.70	0	-10,-5,0,3,5	30
		-2	-5,0,5,10	31
		-4	0,5,10,12	32
		-6	5,10,12	33
		2,0,-2,-4	0	29
	2.60	0	-15,-10,-5,0,5,10,15	24
		-4	-10,-5,0,5,10,15,20	25
		-8	-5,0,5,10,15,20	26
		-12	15,20,25	27
		2,0,-2,-6,-9	0	23
	3.52	0	-15,-10,-5,0,5,10,15,20	79
		-4	-15,-10,-5,0,5,10,15,20,25	80
		-8	-10,-5,0,5,10,15,20,25,30	81
		-12	0,5,10,15,20,25,30	82
		-16	20,25,30	83
		2,0,-2,-6,-10	0	84
1/2"	1.70	0	-10,-5,0,3,5	50
		-2	-5,0,5,10	51
		-4	0,5,10,12	52
		-6	5,10,12	53
		0,2	0	49
	2.60	0	-15,-10,-5,0,5,10,15	19
		-4	-15,-10,-5,0,5,10,15,20,25	20
		-8	-5,0,5,10,15,20,25	21
		-12	15,20,25	22
		2,0,-2,-6,-9	0	18

GAP	M	α	δ	RUN NO.
1/2"	3.52	0	-15,-10,-5,0,5,10,15,20	73
		-4	-15,-10,-5,0,5,10,15,20,25	74
		-8	-10,-5,0,5,10,15,20,25,30	75
		-12	0,5,10,15,20,25,30	76
		-16	20,25,30	77
		2,0,-2,-6,-10	0	78
1"	1.70	0	-10,-5,0,5	45
		-2	-5,0,5,10	46
		-4	0,5,10	47
		-6	5,10	48
		2,0	0	44
	2.60	0	-15,-10,-5,0,5,10	14
		-4	-10,-5,0,5,10,15,20,25	15
		-8	-5,0,5,10,15,20,25	16
		-12	10,15,20,25	17
		2,0,-2,-6,-10	0	13
	3.52	0	-10,-5,0,5,10,15,20	68
		-4	-15,-10,-5,0,5,10,15,20	69
		-8	-10,-5,0,5,10,15,20,25	70
		-12	0,5,10,15,20,25,30	71
		-16	20,25,30	72
		2,0,-2,-4,-6,-8,-10	0	85
2"	1.70	0	-10,-5,0,3	40
		-2	-5,0,5,10	41
		-4	0,5,10	42
		-6	5,10	43
		2,0,-2,-4	0	39
	2.60	0	-15,-10,-5,0,5,10	9
		-4	-10,-5,0,5,10,15,20	10
		-8	-5,0,5,10,15,20,25	11
		-12	5,10,15,20,25	12
		2,0,-2,-6,-10	0	8
	3.52	0	-15,-10,-5,0,5,10,15	62
		-4	-15,-10,-5,0,5,10,15,20	63
		-8	-10,-5,0,5,10,15,20,25	64
		-12	0,5,10,15,20,25,30	65
		2,0,-2,-6,-10	0	61

TABLE II

TABLE OF SHADOWGRAPHS OBTAINED IN FIRST VISUAL TEST

GAP	M	α	δ	RUN NO.
0	1.70	0	-12,-9,-6,-3,0,3,6,9,12,15	4,55,56,58
		-2	-12,-9,-6,-3,0,3,6,9,12,15,18	5,57
		-4	-6,-3,0,3,6,9,12,15,18	6
		-6	0,3,6,9,12,15,18,21,24	7
	2.60	0	-10,-5,0,5,10,15	22
		-4	-10,-5,0,5,10,15,20	23
		-8	0,5,10,15,20,25	24
		2,0,-2,-6	0	21
	1.70	2,1,0,-1,-2,-3,-4,-6,-6,-7,-9,-8.5	No Flipper	59

TABLE III

TABLE OF SHADOWGRAPHS OBTAINED FROM SECOND VISUAL TEST

Wing Alone Configuration

M	α	RUN NO.
2.60	-10,-8,-6,-2,0,2,4,6,8,10	
3.52	-16,-12,-10,-8,-6,-4,-2,0,2,4,6,8,10,12,14	

Wing-Control Surface Configuration

GAP	M	α	δ	R.N.	RUN NO.
0	1.70	0	4,8,12	N	01
		-2	-8,-4,0,4,8,12	N	02
		-4	-4,0,4,8,12,16	N	03
		-6	4,8,12,16	N	04
	2.60	0	0,-5,-10,-15,-20,-25	N	21
		-4	-10,-5,0,5,10,15,20	N	22
		-8	0,5,10,15,20,25	N	23
		-12	15,20,25	N	24
	3.52	0	0,-5,-10,-15,-20,-25	N	43
		-4	-15,-10,-5,0,5,10,15,20,25	N	44
		-8	-5,0,5,10,15,20,25,30	N	45
		-12	5,10,15,20,25,30	N	46
		-16	15,20,25,30	N	47
		0	0,-5,-10,-15,-20,-25	L	51
		-4	-15,-10,-5,0,5,10,15,20,25	L	50
		-8	-5,0,5,10,15,20,25,30	L	49
		-12	5,10,15,20,25,30	L	48
		0	0,-5,-10,-15,-20	H	77
		-4	-15,-10,-5,0,5,10,15,20,25	H	78
		-8	-5,0,5,10,15,20,25,30	H	79
		-12	5,10,15,20,25,30	H	80
1/4"	1.70	0	0,4,8,12	N	17
		-2	-8,-4,0,4,8,12	N	18
		-4	-4,0,4,8,12,16	N	19
		-6	4,8,12,16	N	20
	2.60	0	0,-5,-10,-15,-20	N	37
		-4	-10,-5,0,5,10,15,20,25	N	38
		-8	0,5,10,15,20,25	N	39
		-12	15,20,25	N	40
	3.52	0	0,-5,-10,-15,-20,-25	N	72
		-4	-15,-10,-5,0,5,10,15,20,25	N	73
		-8	-5,0,5,10,15,20,25,30	N	74
		-12	5,10,15,20,25,30	N	75
		-16	15,20,25,30	N	76

GAP	M	α	δ	R.N.	RUN NO.
1/2"	1.70	0	0,4,8,12	N	100
		-2	-8,-4,0,4,8,12	N	101
		-4	-4,0,4,8,12,16	N	102
		-6	4,8,12,16	N	16
	2.60	0	0,-5,-10,-15,-20	N	33
		-4	-10,-5,0,5,10,15,20	N	34
		-8	0,5,10,15,20,25,30	N	35
		-12	15,20,25	N	36
	3.52	0	0,-5,-10,-15,-20,-25	N	67
		-4	-20,-15,-10,-5,0,5,10,15,20,25	N	68
		-8	-5,0,5,10,15,20,25,30	N	69
		-12	5,10,15,20,25,30	N	70
		-16	15,20,25,30	N	71
		0	0,-5,-10,-15,-20	H	89
		-4	-15,-10,-5,0,5,10,15,20,25	H	90
		-8	0,5,10,15,20,25	H	91
		-12	0,5,10,15,20,25,30	H	92
1"	1.70	0	0,4,8	N	09
		-2	-8,-4,0,4,8,12	N	10
		-4	-4,0,4,8,12	N	103
		-6	4,8,12	N	104
	2.60	0	0,-5,-10,-15	N	29
		-4	-10,-5,0,5,10,15,20	N	30
		-8	-5,0,5,10,15,20,25	N	31
		-12	10,15,20,25	N	32
	3.52	0	0,-5,-10,-15,-20,-25	N	62
		-4	-15,-10,-5,0,5,10,15,20	N	63
		-8	-5,0,5,10,15,20,25	N	64
		-12	15,20,25,30	N	65
		-16	15,20,25,30	N	66
		0	0,-5,-10,-15,-20,-25	H	85
		-4	-15,-10,-5,0,5,10,15,20,25	H	86
		-8	-5,0,5,10,15,20,25	H	87
		-12	0,5,10,15,20,25,30	H	88
2"	1.70	0	0,4,8	N	96
		-2	-8,-4,0,4,8,12	N	97
		-4	-4,0,4,8,12	N	98
		-6	4,8,12	N	99
	2.60	0	0,-5,-10,-15	N	25
		-4	-10,-5,0,5,10,15,20	N	26
		-8	-5,0,5,10,15,20,25	N	27
		-12	5,10,15,20,25	N	28
	3.52	0	0,-5,-10,-15,-20,-25	N	61
		-4	-15,-10,-5,0,5,10,15,20	N	60
		-8	-10,-5,0,5,10,15,20,25	N	57
		-12	0,5,10,15,20,25,30	N	58
		-16	15,20,25,30	N	59

GAP	M	α	δ	R.N.	RUN NO.
2"	3.52	0	0,-5,-10,-15,-20,-25	L	52
		-4	-15,-10,-5,0,5,10,15,20	L	53
		-8	-5,5,10,15,20,25	L	54
		-12	5,10,15,20,25,30	L	55
		-15	20,25,30	L	56
		0	0,-5,-10,-15,-20,-25	H	81
		-4	-15,-10,-5,0,5,10,15,20,25	H	82
		-8	-10,-5,0,5,10,15,20,25,30	H	83
		-12	0,5,10,15,20,25,30	H	84

TABLE IV

EFFECT OF REYNOLDS NUMBER ON SEPARATION

Laminar Flow Wing Chord = 6"
Gap = 0 M = 3.52

			Location of Separation Point Measured from Wing's Leading Edge. ~ Inches	
α	δ	Surface	Normal R.N.	Low R.N.
0	0	U	5.00	4.65
		L	5.15	4.65
	-5	U	4.90	4.37
		L	5.02	4.17
	-10	U	4.54	3.75
		L	4.57	3.55
	-15	U	3.70	3.52
		L	4.00	3.45
	-20	U	3.15	3.00
		L	3.35	3.00
	-25	U	3.00	2.30
		L	3.00	2.70
-4	-15	L	2.45	2.50
	-10	L	3.05	3.00
	-5	L	3.77	3.70
	0	L	4.33	4.17
	5	L	4.20	3.65
	10	L	4.20	3.00
	15	L	3.55	3.12
	20	U	5.03	----
		L	2.17	2.02
	25	U	3.70	3.40
		L	1.95	~.90
-8	-5	L	3.72	3.43
	0	L	4.38	4.25
	5	L	3.68	3.00

α	δ	Surface	Location of Separation Point Measured from Wing's Leading Edge. ~ Inches: Normal R.N.	Low R.N.
-8	10	L	3.55	2.85
	15	L	2.70	2.15
	20	L	1.35	1.15
	25	L	.85	.50
	30	U	5.00	4.00
		L	0	0
-12	5	L	3.15	2.80
	10	L	3.0	1.7
	15	L	1.3	1.1
	20	L	.6	.5
	25	L	.3	.3
	30	L	0	0

NOTE: Normal $RN_{/inch} = 0.54 \times 10^6$

Low $RN_{/inch} = 0.14 \times 10^6$

U - Upper Surface

L - Lower Surface

All data from visual tests

TABLE V

EFFECT OF GAP ON SEPARATION POINT

Laminar Boundary Layer
M = 1.70

α	δ	Surface	Location of Separation Point Measured from Wing's Leading Edge, ~Inches G=0	G=1/4"	G=1/2"	G=1"	G=2"
0	-10	U	4.95*	----*	----*	----*	----*
		L	4.70*	4.90*	----*	----*	----*
	-5	U	5.05*	----*	----*	----*	----*
		L	4.87*	----*	----*	----*	----*
	0	U	----	----*	----*	----*	----*
		L	4.95*	----*	----*	----*	----*
	3	U	----	----*	----*	----*	----*
		L	4.87*	----*	----*	----*	----*
	4	U	5.15	----	----	----	----
		L	5.25	----	----	----	----
	5	U	----*	----*	----*	----*	----*
		L	4.90*	----*	----*	----*	----*
	8	U	4.90	----	----	----	----
		L	4.90	----	----	----	----
	12	U	4.15	5.25	5.50	----	----
		L	4.25	5.60	5.50	----	----
-2	-8	U	5.10	----	----	----	----
		L	4.25	5.40	----	----	----
	-5	U	----*	----*	----*	----*	----*
		L	4.45*	5.20*	----*	----*	----*
	-4	U	5.12	----	----	----	----
		L	4.10	----	----	----	----
	0	U	----	----	----	----	----
		L	5.08	----	----	----	----
			4.80*	----*	----*	----*	----*
	4	U	----	----	----	----	----
		L	4.67	----	----	----	----

α	δ	Surface	Location of Separation Point Measured from Wing's Leading Edge. ~ Inches G=0	G=1/4"	G=1/2"	G=1"	G=2"
-2	5	U	----*	----*	----*	----*	----*
		L	4.88	----*	----*	----*	----*
	8	U	----	----	----	----	----
		L	4.67	----	----	----	----
	10	U	4.45*	5.00*	----*	----*	----*
		L	2.20*	2.15*	3.15*	3.15*	3.90*
	12	U	5.05	----	----	----	----
		L	4.28	----	----	----	----
-4	-4	U	----	----	----	----	----
		L	4.00	5.20	----	----	----
	0	U	----	----	----	----	----
		L	5.00	----	----	----	----
			4.72*	----*	----*	----*	----*
	4	U	----	----	----	----	----
		L	4.80	----	----	----	----
	5	U	----*		----*	----*	----*
		L	4.72*		----*	----*	----*
	8	U	----	----	----	----	----
		L	4.58	----	----	----	----
	10	U	----				
		L	4.45*				
	12	U	----	----	----	----	----
		L	4.35	----	----	----	----
		L	4.40*	3.00*	3.15*	----*	----*
	16	U	----	----	----	----	----
		L	4.05	5.00	----	----	----
-6	4	U	----	----	----	----	----
		L	4.80	----	----	----	----
	5	U	----*	----*	----*	----*	----*
		L	4.50*	4.70*	----*	----*	----*
	8	U	----	----	----	----	----
		L	4.50	----	----	----	----

			Location of Separation Point Measured from Wing's Leading Edge, ~ Inches				
α	δ	Surface	G=0	G=1/4"	G=1/2"	G=1"	G=2"
-6	10	U	----*	----*		----*	----*
		L	4.45*	3.60*	3.35*	----*	----*
	12	U	----	----	----	----	----
		L	4.45	----	----	----	----
			4.25*	3.00*	3.15*	----*	----*
	16	U	----	----	----		
		L	3.65	4.90	----		
2	0	U	----*	----*	----*	----*	----*
		L	----*	----*	----*	----*	----*
0	0	U	----	----	----	----	
		L	4.95	----	----	----	
-2	0	U	----	----		----	----
		L	4.75	----		----	----
		U	----	----			----
-4	0	L	4.70	5.00			----

NOTE: *, Pressure Data

No *, Visual Data

--- Data available, but separation not observed

TABLE VI

EFFECT OF GAP ON SEPARATION POINT

Laminar Flow
M = 2.60

α	δ	Surface	Location of Separation Point Measured from the Wing's Leading Edge. - Inches G=0	G=1/4"	G=1/2"	G=1"	G=2"	Flipper Off
0	-25	U	4.97					
		L	3.35					
	-20	U	3.53	3.15	4.05			
		L	5.20	4.68	3.95			
	-15	U	4.14		4.30	----	----	----
			3.70*	3.70*	4.15*	----*	----*	
		L	3.47		4.20	----	----	----
			3.35*	3.70*	4.15*	----*	----*	
	-10	U	4.54	----	----	----	----	----
			4.40*	4.45*	----*	----*	----*	
		L	4.39	4.20	----	----	----	----
			4.15*	4.20*	----*	----*	----*	
	-5	U	4.80	5.10	5.45	----	----	----
			4.95*	5.20*	----*	----*	----*	
		L	4.85	4.85	5.30	----	----	----
			4.60*	4.63*	4.60*	----*	----*	
	0	U	4.97	5.40	5.55	----	----	----
			4.96*	----*	----*	----*	----*	
		L	4.97	4.75	5.55	----	----	----
			4.63*	4.70*	4.95*	----	----	
	5	U	4.70	5.20	----	----	----	
		L	4.35	4.40	4.65	----	----	
	10	U	4.40	4.72	----	----	----	
		L	4.20	4.20	----	----	----	
	15	U	3.45	3.90	4.05			
		L	3.40	3.90	4.05			

Location of Separation Point Measured from the Wing's Leading Edge. - Inches

α	δ	Surface	G=0	G=1/4"	G=1/2"	G=1"	G=2"	Flipper Off
-4	-15	U	4.22		4.33			
		L	2.90		3.10			5.31
	-10	U	4.50	----	----	----	----	
			4.45*	----*	----*	----*	----*	
		L	3.22	3.35	5.30	5.37	5.35	5.31
			3.15*	3.42*	5.10*	4.95*	----*	
	-5	U	----	----	----	----	----	
			----*	----*	----*	----*	----*	
		L	3.76	4.08	5.45	5.32	5.35	5.31
			3.60*	3.90*	5.10*	4.90*	----*	
	0	U	----	----	----	----	----	
			----*	----*	----*	----*	----*	
		L	4.85	4.80	5.60	5.47	5.35	5.31
			4.62*	4.60*	5.20*	4.85*	----*	
	5	U	----	----	----	----	----	
			----*	----*	----*	----*	----*	
		L	4.20	5.35	5.40	5.29	5.35	5.31
			3.92*	4.67*		5.00*	----*	
	10	U	----	----	----	----	----	
			----*	----*	----*	----*	----*	----*
		L	4.23	5.45	5.38	5.28	5.35	5.31
			3.82*	----*	5.20*	4.95*	----*	
	15	U	----	----	----	----	----	
			4.90*	----*	----*	----*	----*	
		L	3.26	5.40	5.37	5.32	5.35	5.31
			3.20*	----*		5.15*	----*	
	20	U	----	4.30	----	----	----	
			4.20*	3.65*	4.15*	----*	----*	
		L	2.50	3.00	5.40	5.45	5.35	5.31
			3.00	0	0	5.10	----	
	25	U	3.00		>3.0	3.70		
		L	<1.00		0	<1.00		5.31

Location of Separation Point Measured from the Wing's Leading Edge. - Inches

α	δ	Surface	G=0	G=1/4"	G=1/2"	G=1"	G=2"	Flipper Off
-8	-5	U				----	----	4.57
			----	----	----	----	----	
		L				4.55	4.50	4.57
				3.50*	4.60*	4.60*	4.70*	
	-4	U	----					
		L	3.45*					
	0	U	----	----	----	----	----	
			----*	----*	----*	----*	----*	
		L	4.55	4.05	4.60	4.45	4.38	4.57
			4.15*	3.90*	4.95*	4.70*	4.60*	
	5	U	----	----	----	----	----	
			----*	----*	----*	----*	----*	
		L	4.00	4.45	4.63	4.55	4.45	4.57
			3.50*	3.95*	4.65*	4.70*	4.60*	
	10	U		----	----	----	----	----
			----*	----*	----*	----*	----*	
		L		4.35	4.57	4.60	4.45	4.57
			3.40*	4.60*	4.60*	4.70*	4.60*	
	15	U		----	----	----	----	----
			----*	----*	----*	----*	----*	
		L		4.50	4.58	4.35	4.40	4.57
			3.00*	4.65*	4.60*	4.70*	4.65*	
	20	U		----	----	----	----	----
			----*	----*	----*	----*	----*	
		L		2.25	4.58	4.47	4.40	4.57
			1.80*	1.25*	4.35*	4.60*	4.65*	
	25	U		----	----	----		----
			----*		----*	----*	----*	
		L		1.60	2.20	4.56		4.57
			.92*		.90*	4.65*	4.60*	

Location of Separation Point Measured from the Wing's Leading Edge. - Inches

α	δ	Surface	G=0	G=1/4"	G=1/2"	G=1"	G=2"	Flipper Off
-8	30	U	----					
		L	<1.0					
-12	5	U					----	
							----*	
		L					3.77	
							3.92*	
	10	U				----	----	
						----*	----*	
		L				3.80	3.82	
						3.75*	3.80*	
	15	U	----	----	----	----	----	
				----*	----*	----*	----*	
		L	1.75	3.85	3.93	3.80	3.85	
				3.85*	3.70*	3.75*	3.90*	
	20	U			----	----	----	
			----*	----*	----*	----*	----*	
		L			3.90	3.80	3.82	
			.75*	.88*	3.80*	3.75*	3.85*	
	25	U			----	----	----	
			----	----	----	----	----	
		L			1.00	3.84	3.90	
			.60*	1.0*	3.80*	3.75*	3.80*	
2	0	U	4.45*	4.45*	4.72*	----*	----*	
		L	----*	----*	----*	----*	----*	
0	0	U	4.93*	5.10*	----*	----*	----*	
		L	4.65*	4.65*	4.95*	----*	----*	
-2	0	U	----*	----*	----*	----*	----*	
		L	4.65*	4.72*	----*	----*	----*	
-6	0	U	----*	----*	----*	----*	----*	
		L	4.43*	3.95*		4.92*	4.90*	

Location of Separation Point Measured from the Wing's Leading Edge. - Inches

α	δ	Surface	G=0	G=1/4"	G=1/2"	G=1"	G=2"	Flipper Off
-9	0	U	——*	——*	——*	——*		
		L	4.15*	3.72*	4.45*	3.75*		
-10	0	U					——*	
		L					4.05*	

NOTE: *, Pressure Data

No *, Visual Data

—— Data available, but separation not observed

TABLE VII

EFFECT OF GAP ON SEPARATION POINT

Laminar Flow
M = 3.52

α	δ	Surface	Location of Separation Point Measured from the Wing's Leading Edge. - Inches					
			G=0	G=1/4"	G=1/2"	G=1"	G=2"	Flipper Off
0	-25	U	3.00	3.10	3.30			———
		L	3.00	3.10	3.40			———
	-20	U	3.15	3.25	3.55			———
		L	3.35	3.75	3.70			———
	-15	U	3.70	4.00	4.08	———	———	———
			4.15*	4.10*	4.70*	———*	———*	
		L	4.00	4.15	4.34	———	———	———
			3.89*	3.80*	4.70*	———*	———*	
	-10	U	4.54	4.54	4.83	———	———	———
			4.65*	4.90*	———*	———*	———*	
		L	4.57	4.86	5.29	———	———	———
			4.40*	4.60*	———*	———*	———*	
	-5	U	4.90	4.85	5.15	———	———	———
				———*	———*	———*	———*	
		L	5.02	5.28	5.70	———	———	———
				4.88*	———*	———*	———*	
	0	U	5.00	5.15	5.50	———	———	———
			5.15*	———*	———*	———*	———*	
		L	5.15	5.38	5.60	———	———	———
			4.95*	4.95*	———*	———*	———*	
	5	U	5.20*	———*	———*	———*	———*	
		L	4.93*	5.10*	———*	———*	———*	
	10	U	4.65*	4.80*	———*	———*	———*	
		L	4.45*	4.60*	———*	———*	———*	
	15	U	4.00*	4.00*	4.35*	———*	———*	
		L	3.83*	3.93*	4.35*	———*	———*	

Location of Separation Point Measured from the Wing's Leading Edge. - Inches

α	δ	Surface	G=0	G=1/4"	G=1/2"	G=1"	G=2"	Flipper Off
0	20	U	1.8*	3.00*	3.25*	——*		
		L	1.8*	3.00*	3.25*	3.0*		
	25	U	1.55*					
		L	1.35*					
-4	-20	U			5.05			——
		L			2.40		5.35	5.35
	-15	U	——	——	——	——	——	——
			——*	——*	——*	——*	——*	
		L	2.45	2.50	3.00		5.35	5.35
			2.70*	4.92*	3.0*	5.10*	5.15*	
	-10	U	——	——	——	——	——	——
			——*	——*	——*	——*	——*	
		L	3.05	3.18	3.50	5.00	5.35	5.35
			3.00*	3.15*	3.45*	5.10*	5.10*	
	-5	U	——	——	——	——	——	
			——*	——*	——*	——*	——*	——
		L	3.78	4.00	4.65	5.32	5.35	5.35
			3.70*	3.75*	4.45*	5.10*	5.05*	
	0	U		——	——	——	——	——
			——*	——*	——*	——*	——*	
		L	4.75	4.70	5.15	5.32	5.35	5.35
			4.72*	4.43*	5.0*	5.10*	5.05*	
	5	U	——	——	——	——	——	——
			——*	——*	——*	——*	——*	
		L	4.2	4.7	5.25	5.34	5.35	5.35
			3.93*	4.10*	5.20*	5.10*	5.05*	
	10	U	——	——	——	——	——	——
			——*	——*	——*	——*	——*	
		L	4.25	5.10	5.25	5.25	5.35	5.35
			3.87*	4.30*	5.20*	4.90*	5.05*	
	15	U	——	——	——	——	——	——
			——*	——*	——*	——*	——*	

Location of Separation Point Measured from the Wing's Leading Edge. - Inches

α	δ	Surface	G=0	G=1/4"	G=1/2"	G=1"	G=2"	Flipper Off
-4	15	L	3.55	5.25	5.14	5.32	5.35	5.35
			3.20*	4.20*	----	5.10*	4.95*	
	20	U	5.03	5.05	----	----	----	----
			4.88*	4.87*	4.95*	----	----	
		L	2.15	1.90	5.35	5.32	5.35	5.35
			1.57*	1.65*	1.9*	1.95*	4.95*	
	25	U	3.7		5.50			----
			3.0*		3.0*			
		L	1.9	.8	.8			5.35
			<1.0*	<1.0*	<1.0*			
-8	-10	U				----	----	----
			----*	----*	----*	----*	----*	
		L				4.43	4.20	4.40
			3.0*	3.0*	3.1*	4.80*	4.35*	
	-5	U	----	----	----	----	----	----
			----*	----*	----*	----*	----*	
		L	3.72	3.85	4.35	4.43	4.38	4.40
			3.55*	3.6*	4.3*	4.6*	4.35*	
	0	U	----	----	----	----	----	----
			----*	----*	----*	----*	----*	
		L	4.38	4.00	4.40	4.44	4.45	4.40
			4.30*	3.60*	4.45*	4.45*	4.60*	
	5	U	----	----	----	----	----	----
			----*	----*	----*	----*	----*	----*
		L	3.68	4.25	4.45	4.45	4.48	4.40
			3.10*	3.50*	4.45*	4.45*	4.35*	
	10	U	----	----	----	----	----	----
			----*	----*	----*	----*	----*	
		L	3.55	4.40	4.45	4.45	4.35	4.40
			3.10*	3.80*	4.45*	4.35*	4.25*	

Location of Separation Point Measured from the Wing's Leading Edge. - Inches

α	δ	Surface	G=0	G=1/4"	G=1/2"	G=1"	G=2"	Flipper Off
-8	15	U	———	———	———	———	———	———
			———*	———*	———*	———*	———*	
		L	2.70	4.50	4.45	4.43	4.38	4.40
			2.5*	4.60*	4.60*	4.45*	4.35*	
	20	U	———	———	———	———	———	———
			———*	———*	———*	———*	———*	
		L	1.35	1.3	4.45	4.45	4.55	4.40
			.85*	.90*	4.60*	4.60*	4.60*	
	25	U	———	———	———	———	———	———
			———*	———*	———*	———*	———*	
		L	.85	.40	.70	4.45	4.40	4.40
			<1.0*	<1.0*	<1.0*	<1.0*	4.60*	
	30	U	5.00	4.90	4.92			———
			5.00*	4.90*	4.95*			
		L	~0	~0	~0			4.40
			<1.0*	<1.0*	<1.0*			
-12	0	U					———	———
				———*	———*	———*	———*	
		L					3.63	3.70
				3.0*	3.80*		3.65*	
	5	U	———	———	———	———	———	———
			———*	———*	———*	———*	———*	
		L	3.15	3.75	3.7	3.7	3.61	3.70
			3.0*	3.0*	3.80*		3.85*	
	10	U	———	———	———	———	———	———
			———*	———*	———*	———*	———*	
		L	3.0	3.75	3.65	3.70	3.63	3.70
			3.0*	3.0*	3.80*		3.65*	
	15	U	———	———	———	———	———	———
			———*	———*	———*	———*	———*	

Location of Separation Point Measured from the Wing's Leading Edge. - Inches

α	δ	Surface	G=0	G=1/4"	G=1/2"	G=1"	G=2"	Flipper Off
-12	15	L	1.30	3.75	3.70	3.70	3.67	3.70
			1.25*	1.8*	3.80*	3.3*	3.65*	
	20	U	----	----	----	----	----	----
			----*	----*	----*	----*	----*	
		L	.60	.75	3.70	3.70	3.67	3.70
			<1.0*	<1.0*	<1.0*	3.6*	3.65*	
	25	U	----	----	----	----	----	----
			----*	----*	----*	----*	----*	
		L	.3	.4	.6	3.70	3.69	3.70
			<1.0*	<1.0*	<1.0*	<1.0*	3.70*	
	30	U	----	----	----	----	----	----
			----*	----*	----*	----*	----*	
		L	0	0	0	3.70	3.65	3.70
			<1.0*	<1.0*	<1.0*	<1.0*	<1.0*	
-16	15	U	----	----	----		----	----
			----*	----*				
		L	.60	.75	3.25		3.20	3.20
			2.8*	<1.0*				
	20	U	----	----	----	----	----	----
			----*	----*	----*	----*		
		L	.4	.5	.3	3.2	3.22	3.20
			<1.0*	<1.0*	3.0*	3.0*		
	25	U	----	----	----	----	----	----
			----*	----*	----*	----*		
		L	0	0	0	3.2	3.22	3.20
			<1.0	<1.0	<1.0	3.0		
	30	U	----	----	----	----	----	----
			----*	----*	----*	----*		
		L	0	0	0	3.15	3.20	3.20
			<1.0*	<1.0*	<1.0*	<1.0*		

α	δ	Surface	Location of Separation Point Measured from the Wing's Leading Edge. - Inches G=0	G=1/4"	G=1/2"	G=1"	G=2"	Flipper Off
2	0	U	4.9*	4.9*	----*	----*		
		L	----*	----*	5.1*	----*		
0	0	U	4.85*	----*	----*	----*		
		L	5.15*	----*	----*	----*		
-2	0	U	----*	----*	----*			
		L	4.60*	4.85*	----*			
-6	0	U	----*	----*	----*	----*		
		L	4.60*	3.85*	4.3*	5.1*		
-10	0	U	----*	----*	----*			
		L	3.95*	3.25*	4.3*			

NOTE: *, Pressure Data

No *, Visual Data

---- Data available, but separation not observed

TABLE VIII

EFFECT OF REYNOLDS NUMBER ON SEPARATION

Laminar Flow
Gap = 2"
M = 3.52

α	δ	Surface	Location of Separation Point Measured from Wing's Leading Edge. - Inches: Normal R.N.	Low R.N.
0	0	U	----	----
		L	----	----
	-5	U	----	----
		L	----	----
	-10	U	----	----
		L	----	----
	-15	U	----	----
		L	----	----
	-20	U		3.8
		L		4.2
	-25	U		3.4
		L		3.3
-4	-15	L	5.4	5.2
	-10	L	5.4	5.2
	-5	L	5.4	5.2
	0	L	5.4	5.2
	5	L	5.4	5.2
	10	L	5.4	5.6
	15	L	5.4	5.2
	20	L	5.4	5.3
-8	-10	L	4.2	3.0
	-5	L	4.4	3.8
	0	L	4.4	3.8
	5	L	4.5	3.8
	10	L	4.4	3.9
	15	L	4.4	3.7

α,	δ	Surface	Location of Separation Point Measured from Wing's Leading Edge. - Inches: Normal R.N.	Low R.N.
-8	20	L	4.5	3.7
	25	L	4.4	3.8
-12	5	L	3.6	3.3
	10	L	3.6	3.4
	15	L	3.7	3.4
	20	L	3.7	3.4
	25	L	3.7	3.4
	30	L	3.7	3.4
-16	20	L	3.2	3.1
	25	L	3.2	2.7
	30	L	3.2	2.7

NOTE: Normal $RN/_{inch} = 0.54 \times 10^6$

Low $RN/_{inch} = 0.14 \times 10^6$

All data from visual tests

TABLE IX

LOCATION OF SEPARATION POINT

M = 3.52
Wing Chord = 10 Inches
Turbulent Boundary Layer

α	δ	Surface	Location of Separation Point Measured from Wing's Leading Edge. - Inches G=0	G=1/2"	G=1"	G=2"
0	0	U				
		L				
	-5	U				
		L				
	-10	U				
		L				
	-15	U				
		L				
	-20	U	9.7			
		L	9.7			
	-25	U	9.4			
		L	9.5			
-4	-15	L	9.4			
	-10	L	9.5			
	-5	L				
	0	L				
	5	L				
	10	L				
	15	L	9.8			
	20	L	9.2			
	25	L	6.7	8.3	S	S
-8	-5	L	9.5			
	0	L				
	5	L	9.9			
	10	L	9.8			
	15	L	9.2			

α	δ	Surface	Location of Separation Point Measured from Wing's Leading Edge. - Inches G=0	G=1/2"	G=1"	G=2"
-8	20	L		----	----	----
	25	L		3.4	4.2	----
	30	L	0			S
-12	0	L		S	S	S
	5	L	S	S	S	S
	10	L	5.0	S	S	S
	15	L	4.0	S	S	S
	20	L	$\leq$3.0	S	S	S
	25	L	$\leq$3.0	$\leq$3.0	S	S
	30	L	$\leq$3.0	$\leq$3.0	$\leq$3.0	S

NOTE: All data from visual tests

TABLE X

Outline of Proposed Method for Calculating the Pressure Distribution on a Wing with a Balanced Flap Type Control Surface

WING

Laminar Boundary Layer

Determine occurrence of separation by Figure 96.

No Separation: Inviscid shock-expansion theory with minor modification at expansion corners.

Separated: Inviscid shock-expansion theory on forward portion. Location of separation from Figure 98. Conditions in separated region from Figures 95, 96, 97. Flow separates on both upper and lower surface at zero angle of attack but only on the surface having the lower pressure if angle of attack is not zero. Transition to turbulent boundary layer will occur when Reynolds number increases by approximately 800,000 from separation point. Pressure, Mach number and flow direction thereafter are determined by the fact that flow must be deflected around the control surface and flow from other side of the wing. If the pressure in the separated region becomes larger than that on the wing's pressure surface at the trailing edge, then the flow on this surface will experience laminar separation also.

Turbulent Boundary Layer

Determine occurrence of separation by Figure 104.

No Separation: Inviscid shock-expansion theory with modification at expansion corners.

Separated: Location of separation to be estimated from comparison with other results, such as those in Table IX. Conditions in separated region from Figures 102 and 103. If the flow direction by this method is not as large as required for the flow to clear the flow from

the wing's pressure surface as it flows over the control surface, then the flow direction of the separated region will be adjusted for this and the pressure and Mach number modified accordingly.

CONTROL SURFACES

Laminar and Turbulent Boundary Layer

Flow on wing not separated: Inviscid shock-expansion theory taking into account waves generated at the trailing edge of the wing. Flow on flipper may separate on the suction side due to the shock wave at its trailing edge.

Flow on wing separated: Inviscid shock-expansion theory on suction surface. Flow on this surface may separate due to the shock wave at the trailing edge. Flow on pressure surface determined by use of characteristics method considering that the flow is constrained between the surface of the flipper and the free surface of the separated region. These surfaces reflect shock and expansion waves back and forth between them. See p. 51.

If the leading edge of the control surface lies in the wake of the wing, the above reflections do not occur and instead the pressures only gradually reach values determined by the shock expansion theory because of the deficiency of velocity in the wake.

See Section VII for a more detailed discussion.

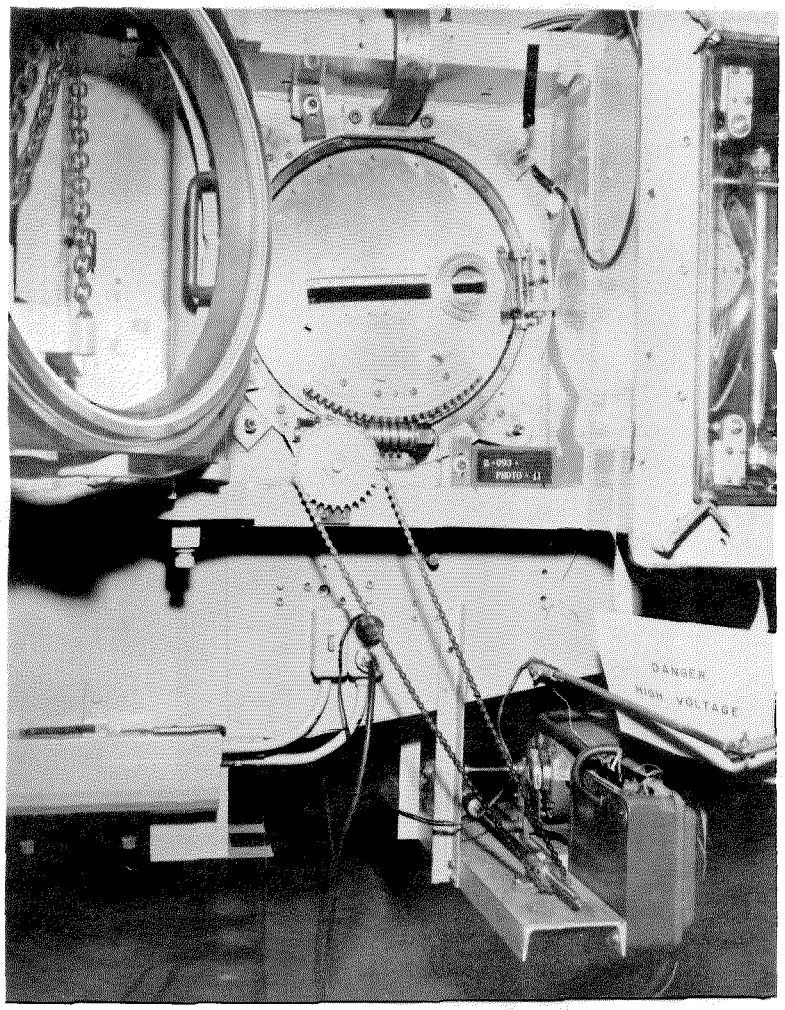

Figure 1. Photograph of the Support System on the East Side of the J. P. L. Wind Tunnel

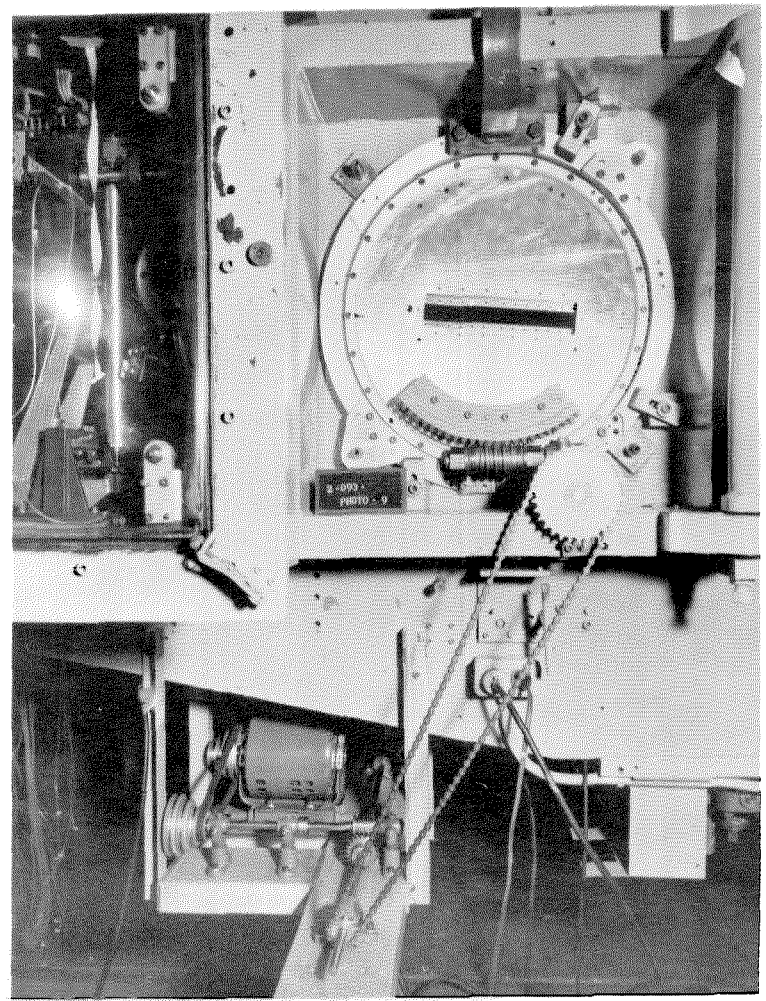

Figure 2. Photograph of the Support System on the West Side of the J. P. L. Wind Tunnel

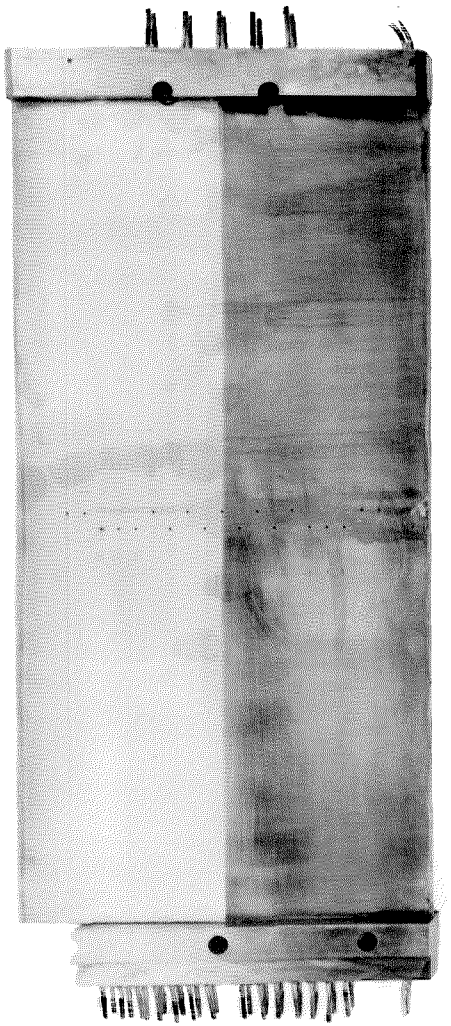

Figure 3. Photograph of the Wing Used for the Pressure Tests

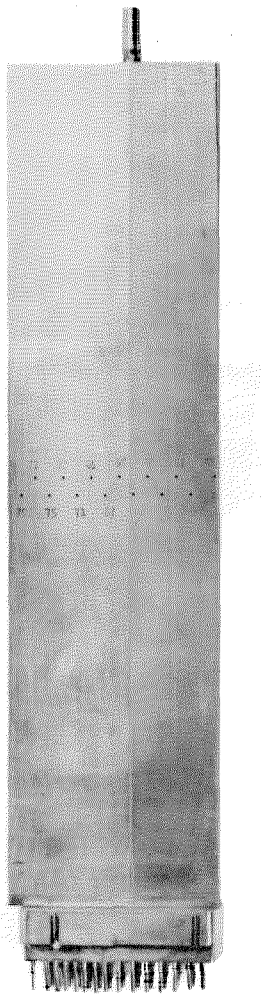

Figure 4. Photograph of the Control Surface Used for the Pressure Tests

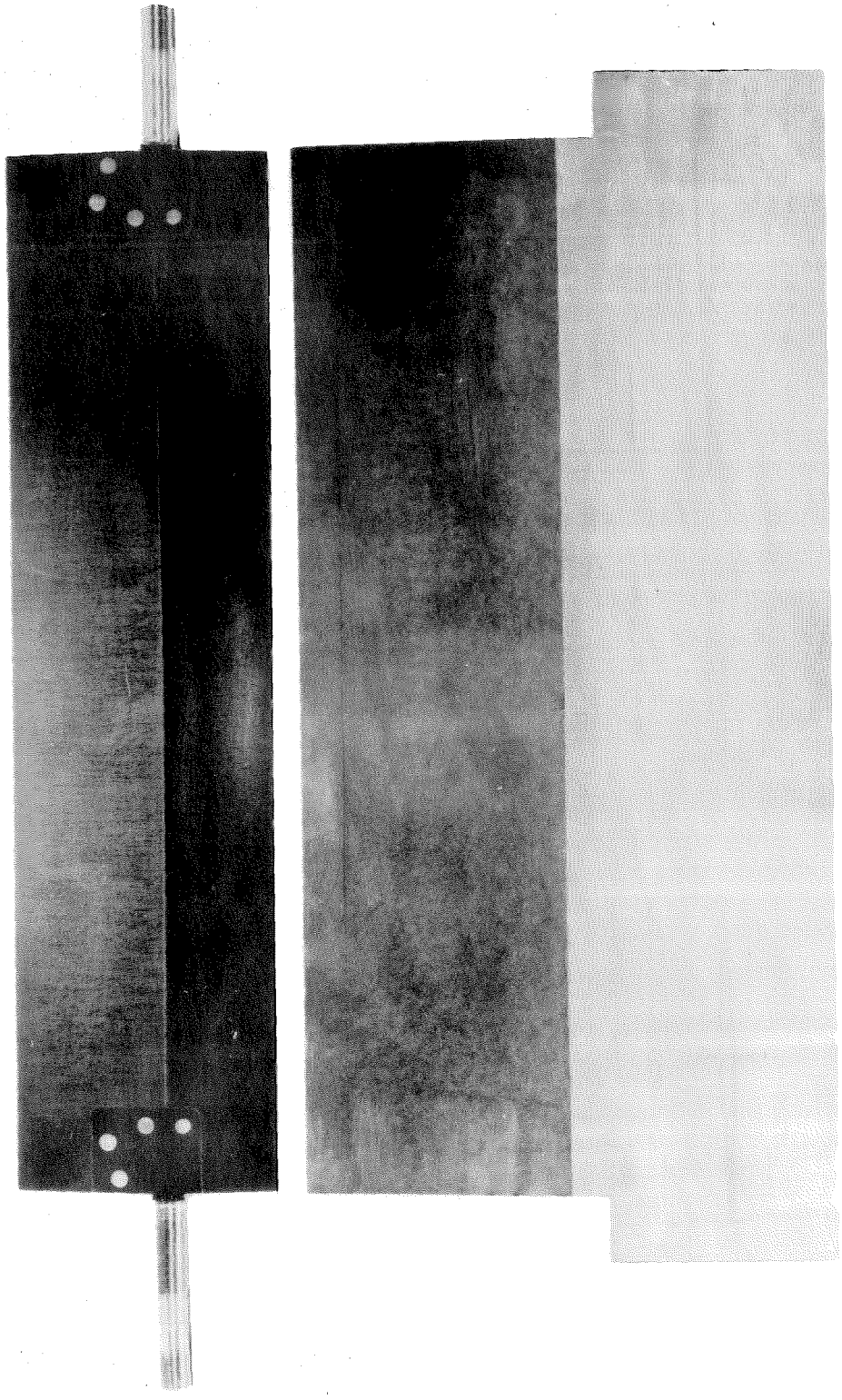

Figure 5. Photograph of Visual Model

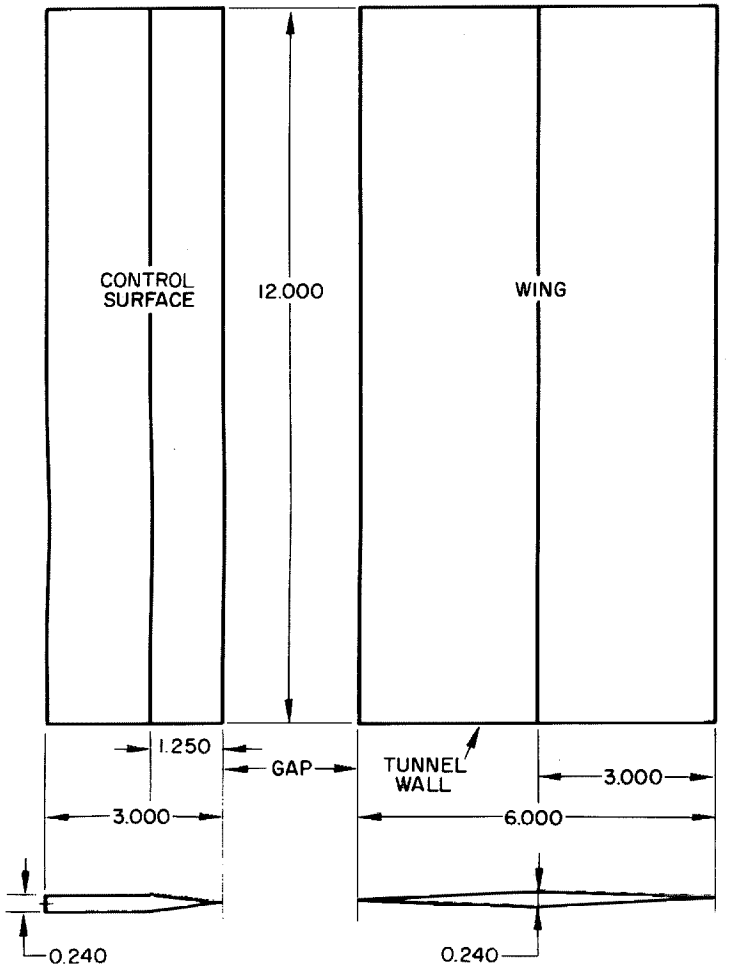

ALL DIMENSIONS IN INCHES
SHARP LEADING AND TRAILING EDGES HAVE 0.006" RADII
GAPS 0.020, 0.250, 0.500, 1.000, 2.000

Figure 6. Drawing of 6 Inch Chord Visual Model Configuration

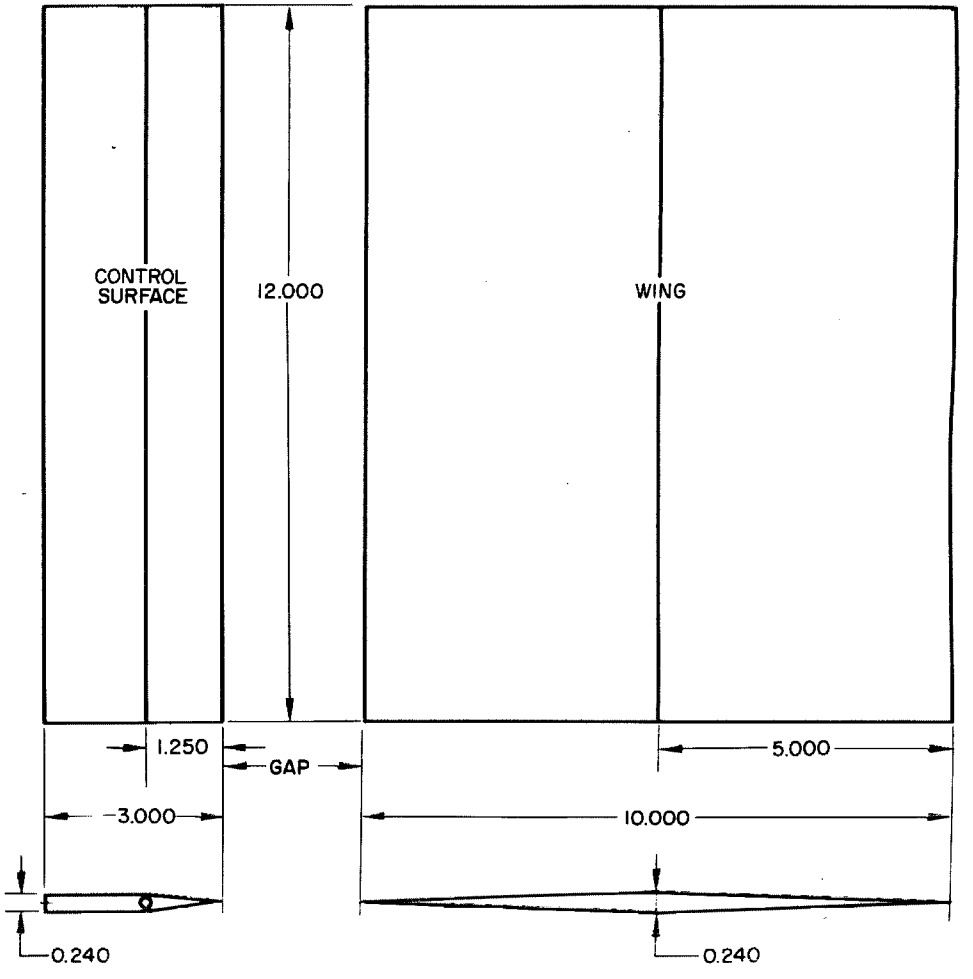

ALL DIMENSIONS IN INCHES
SHARP LEADING AND TRAILING EDGES HAVE 0.006" RADII
GAPS 0.020, 0.250, 0.500, 1.000, 2.000

Figure 7. Drawing of 10 Inch Chord Visual Model Configuration

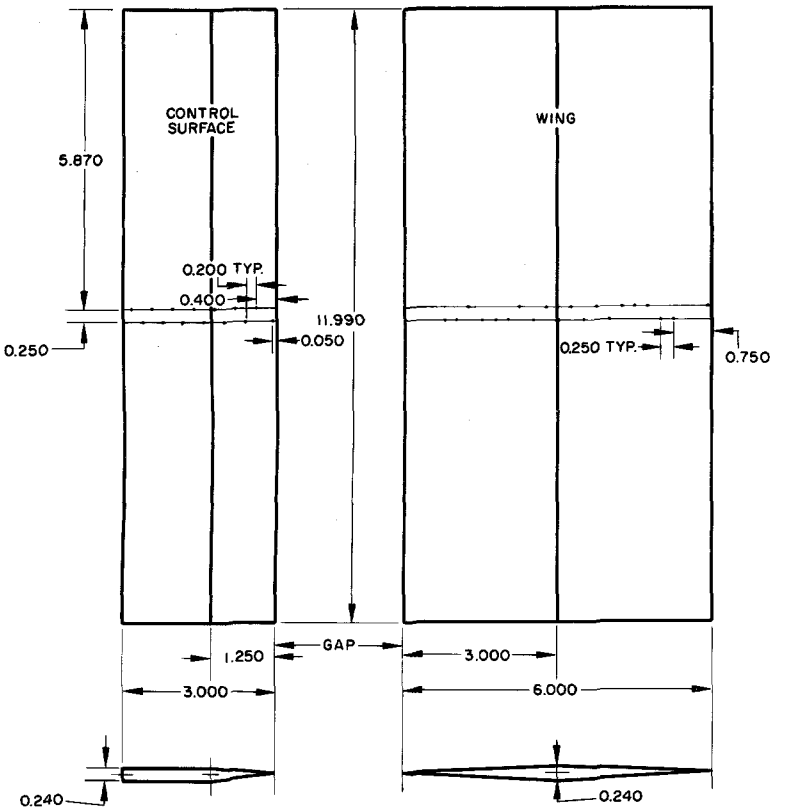

Figure 8. Drawing of Pressure Model Configuration

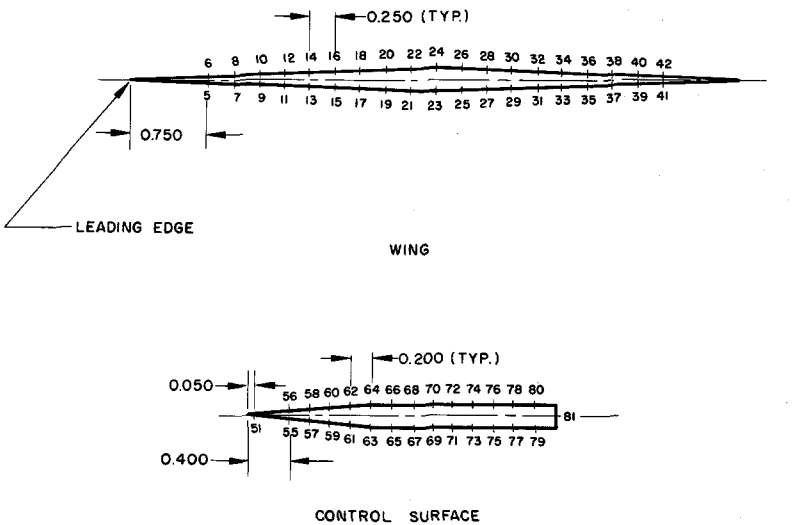

Figure 9. Drawing Showing Pressure Orifice Locations and Numbering System

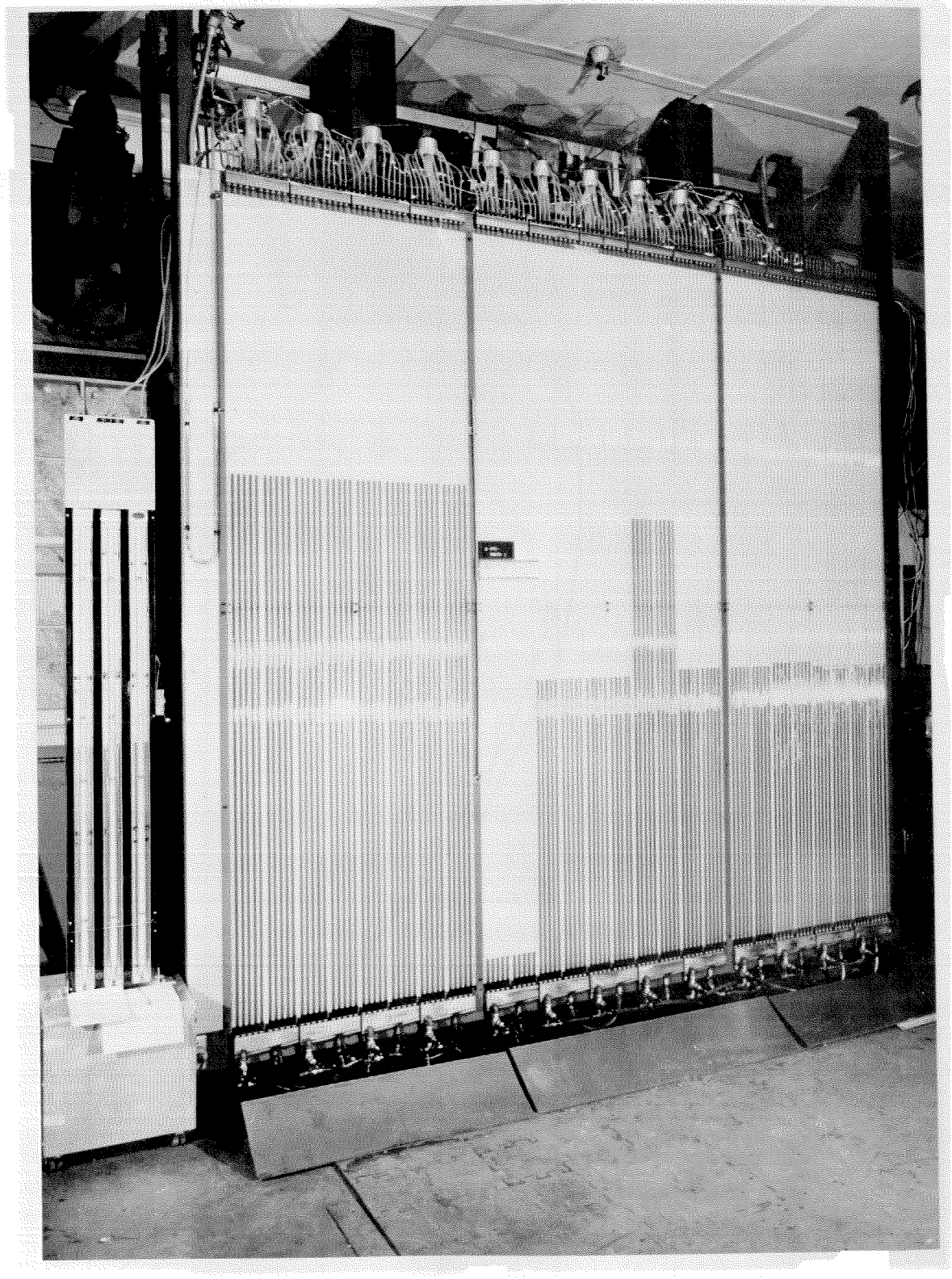

Figure 10. Photograph of Manometer Board

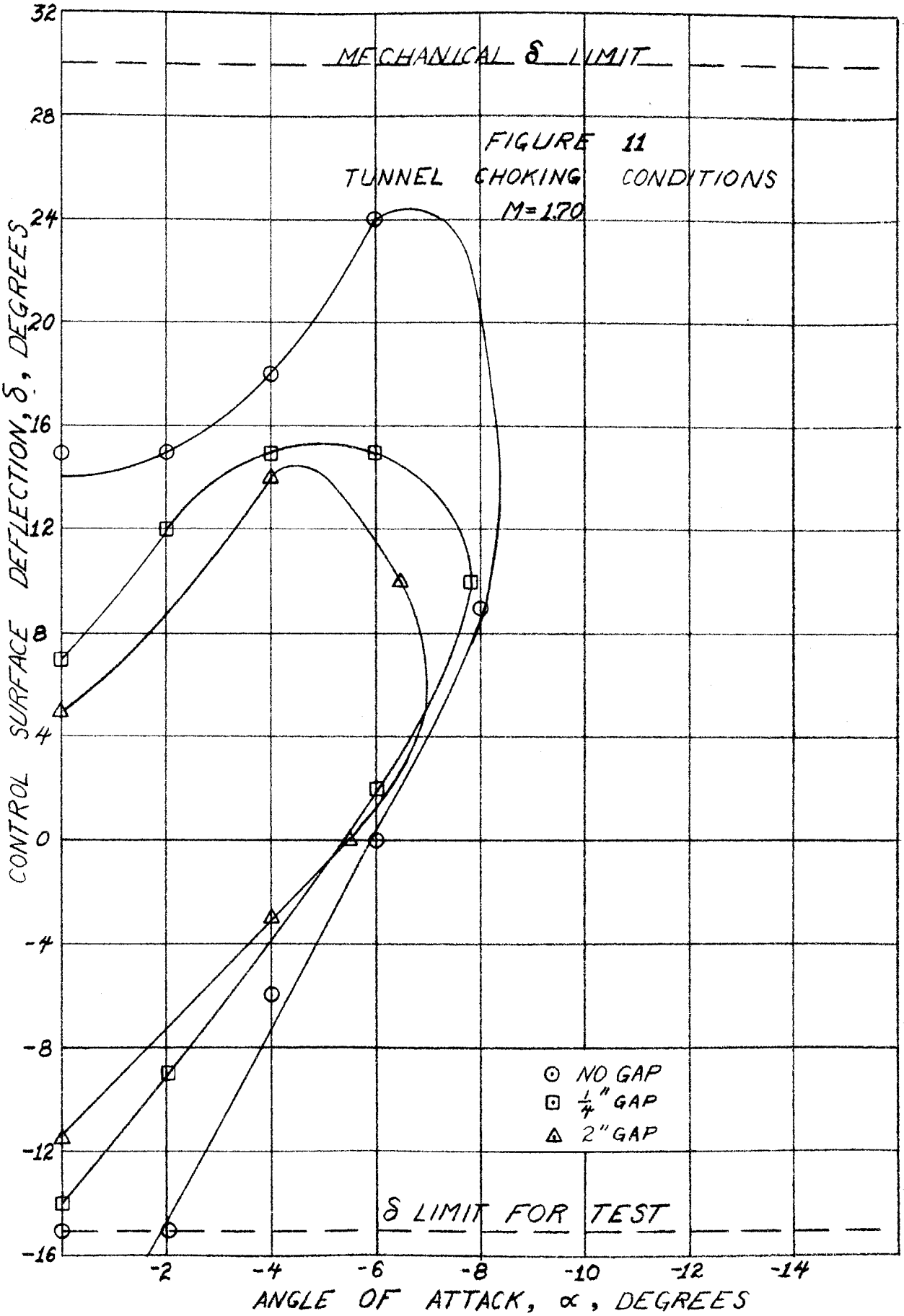
MECHANICAL δ LIMIT
FIGURE 11
TUNNEL CHOKING CONDITIONS
M=1.70
CONTROL SURFACE DEFLECTION, δ, DEGREES
32
28
24
20
16
12
8
4
0
-4
-8
-12
-16
NO GAP
¼" GAP
2" GAP
δ LIMIT FOR TEST
-2
-4
-6
-8
-10
-12
-14
ANGLE OF ATTACK, α, DEGREES

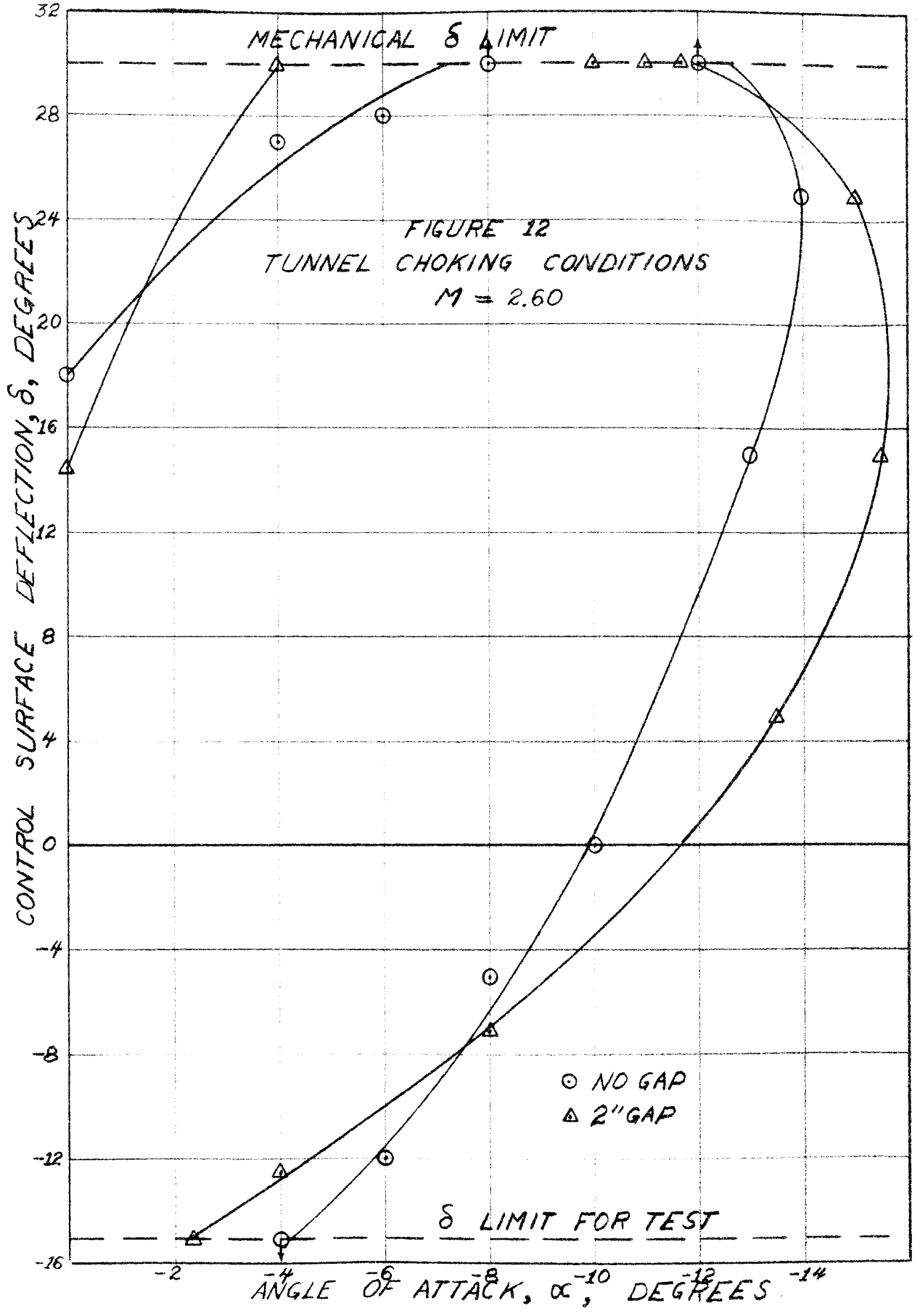
MECHANICAL δ LIMIT
FIGURE 12
TUNNEL CHOKING CONDITIONS
M = 2.60
CONTROL SURFACE DEFLECTION, δ, DEGREES
32
28
24
20
16
12
8
4
0
-4
-8
-12
-16
NO GAP
2" GAP
δ LIMIT FOR TEST
-2
-4
-6
-8
-10
-12
-14
ANGLE OF ATTACK, α, DEGREES

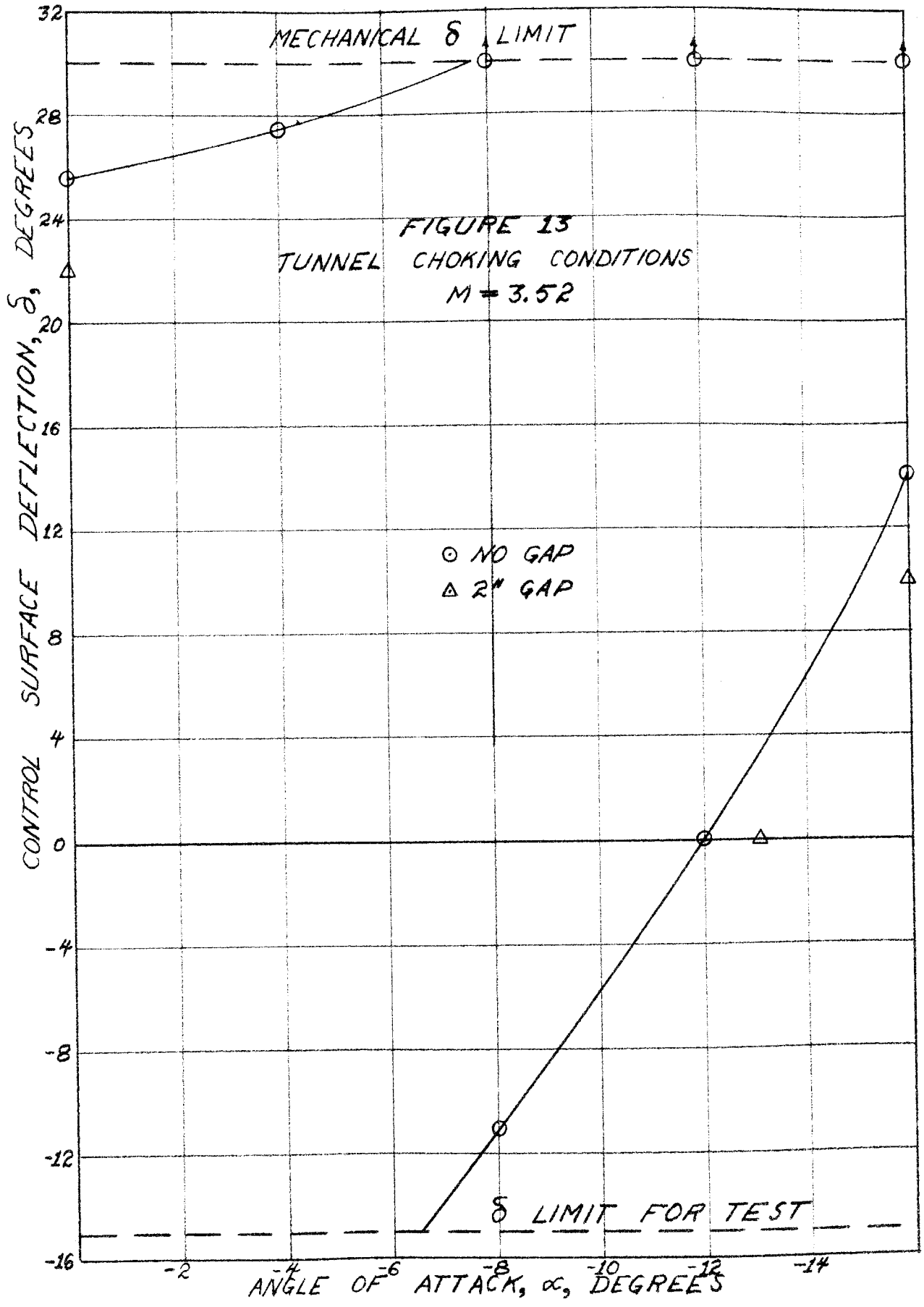
MECHANICAL δ LIMIT
FIGURE 13
TUNNEL CHOKING CONDITIONS
M = 3.52
⊙ NO GAP
△ 2" GAP
δ LIMIT FOR TEST
CONTROL SURFACE DEFLECTION, δ, DEGREES
ANGLE OF ATTACK, α, DEGREES
32
28
24
20
16
12
8
4
0
-4
-8
-12
-16
-2
-4
-6
-8
-10
-12
-14

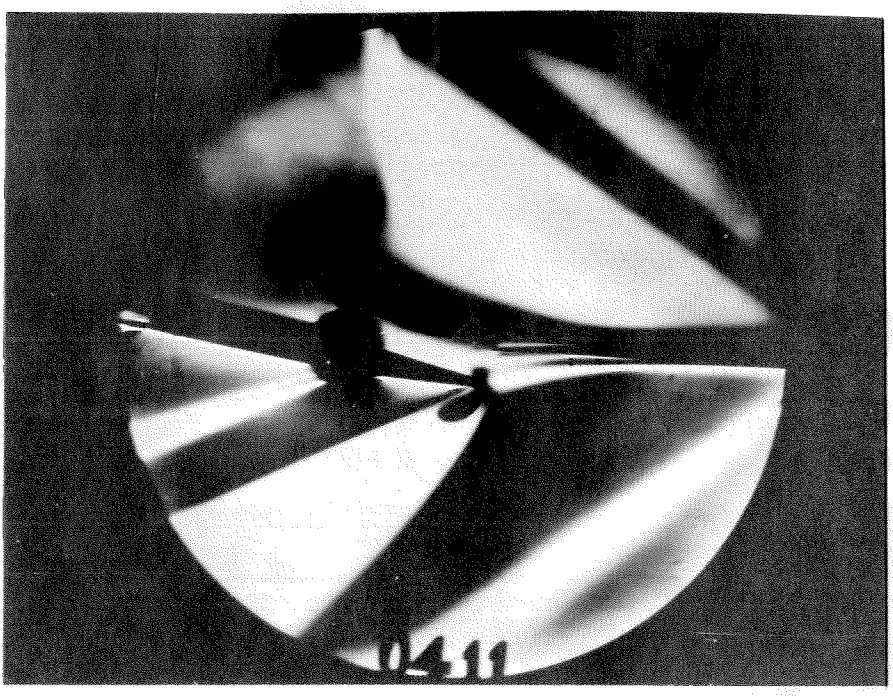

Figure 14. Sample of Schlieren Picture Taken with Standard J. P. L. System. First Visual Test

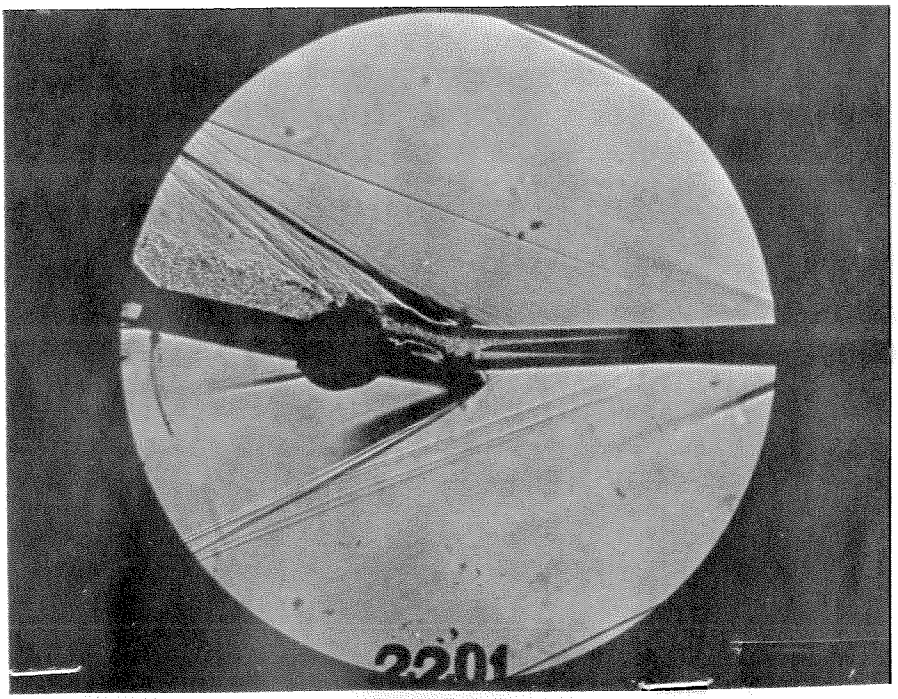

Figure 15. Sample of Shadowgraph Picture Taken with Standard J. P. L. System. First Visual Test

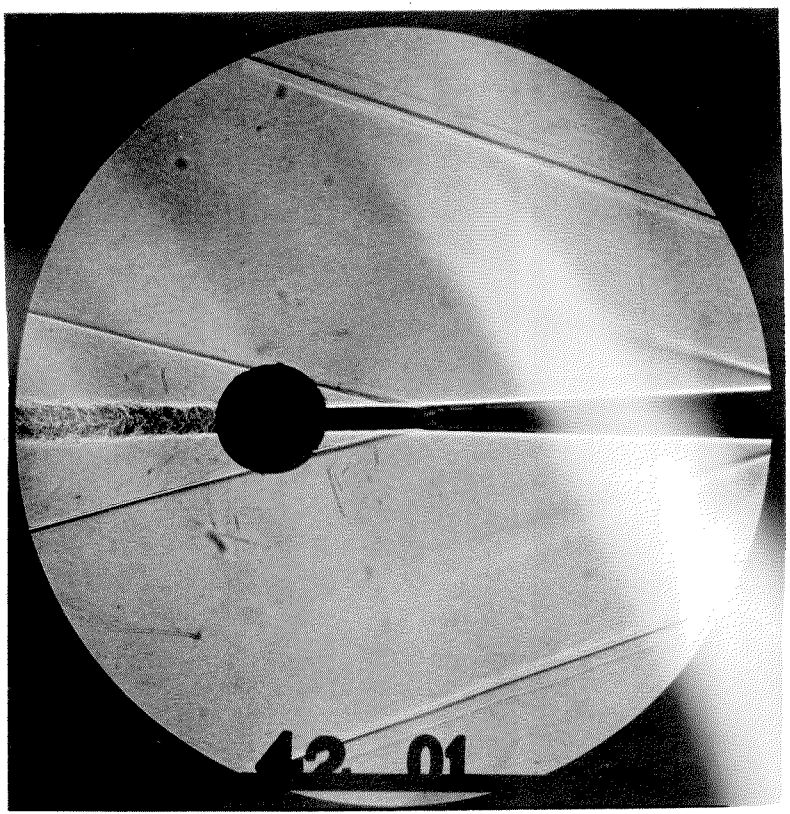

Figure 16. Shadowgraph, Wing Alone, M = 3.52, RN/L = 0.60 x 10^6, $\alpha = 0^o$

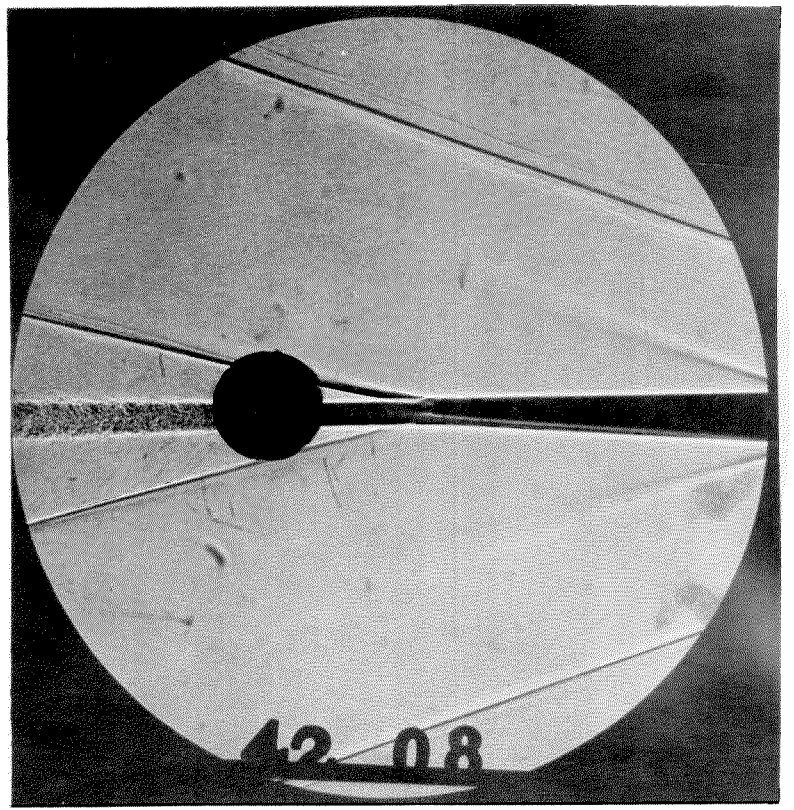

Figure 17. Shadowgraph, Wing Alone, M = 3.52, RN/L = 0.60 x 10^6, $\alpha = -2$

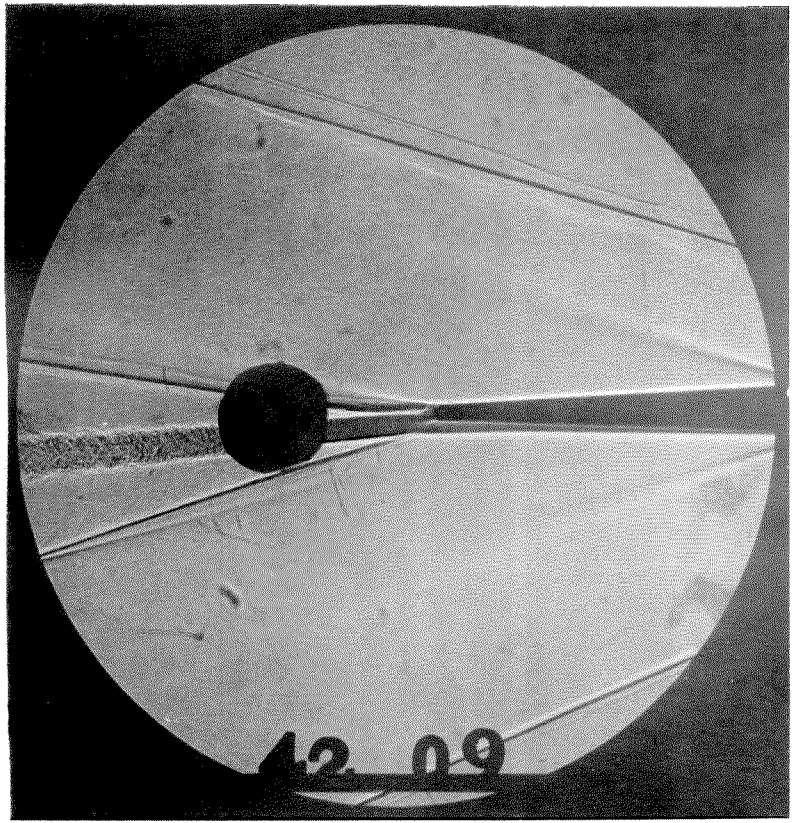

Figure 18. Shadowgraph, Wing Alone, M = 3.52, RN/L = 0.60 x 10^6, α = -4

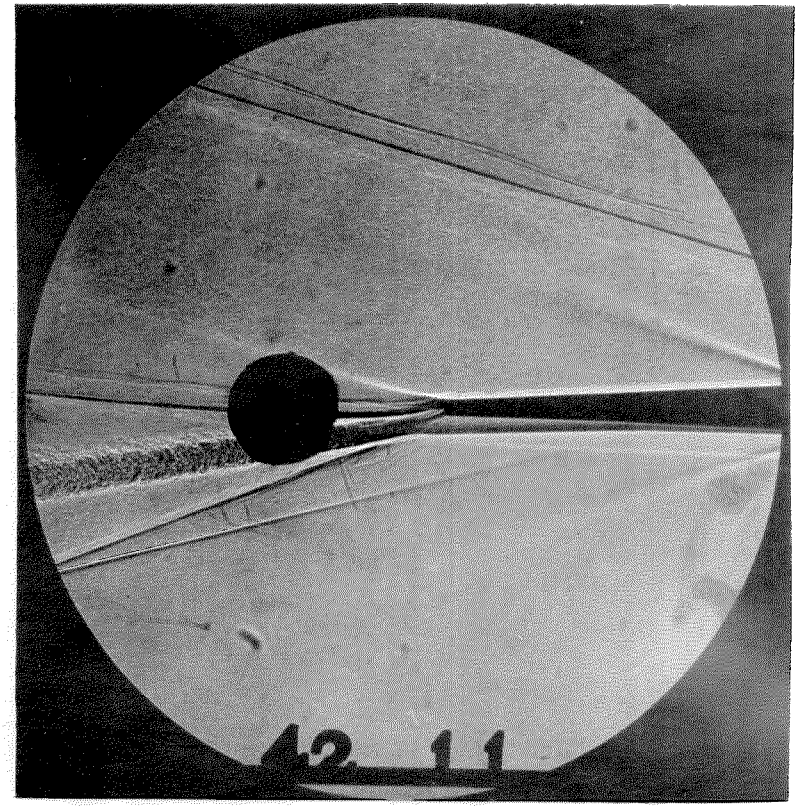

Figure 19. Shadowgraph, Wing Alone, M = 3.52, RN/L = 0.60 x 10^6, α = -8

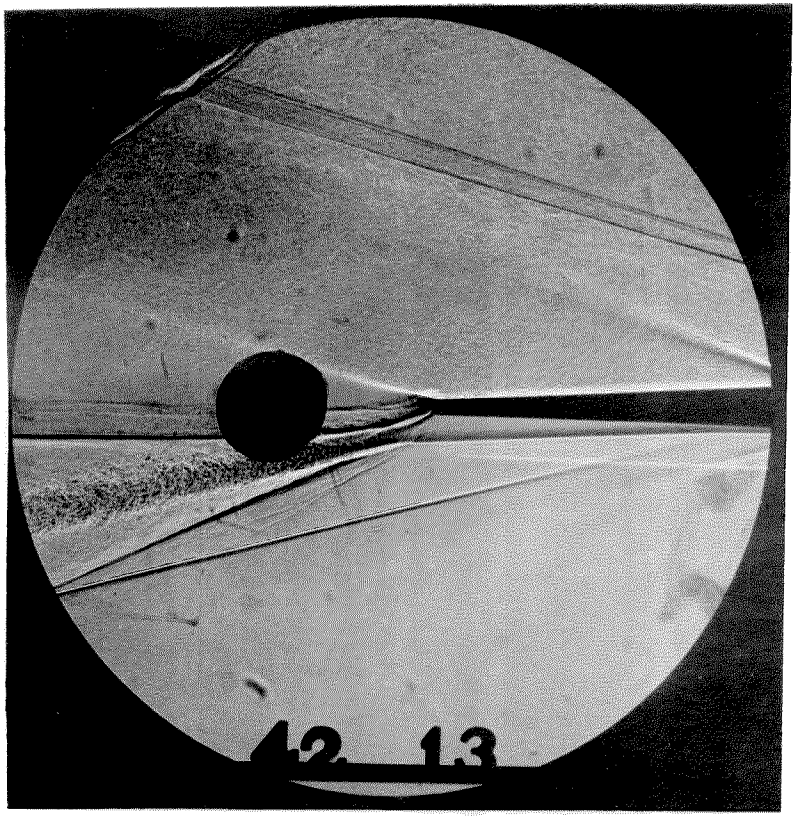

Figure 20. Shadowgraph, Wing Alone, M = 3.52, RN/L = 0.60 x 10^6, α = -12

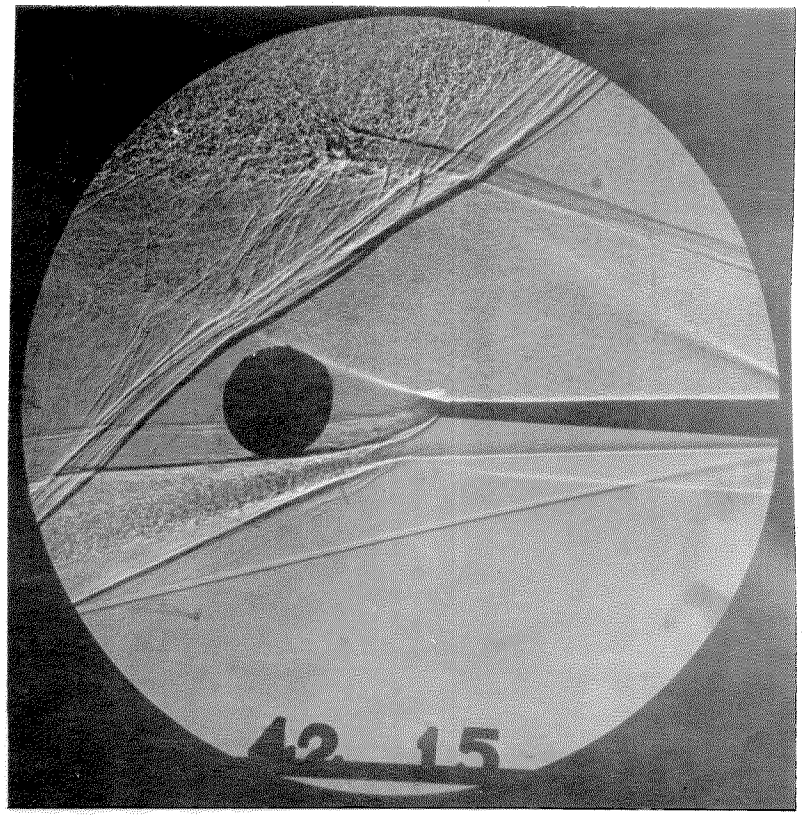

Figure 21. Shadowgraph, Wing Alone, M = 3.52, RN/L = 0.60 x 10^6, α = -16

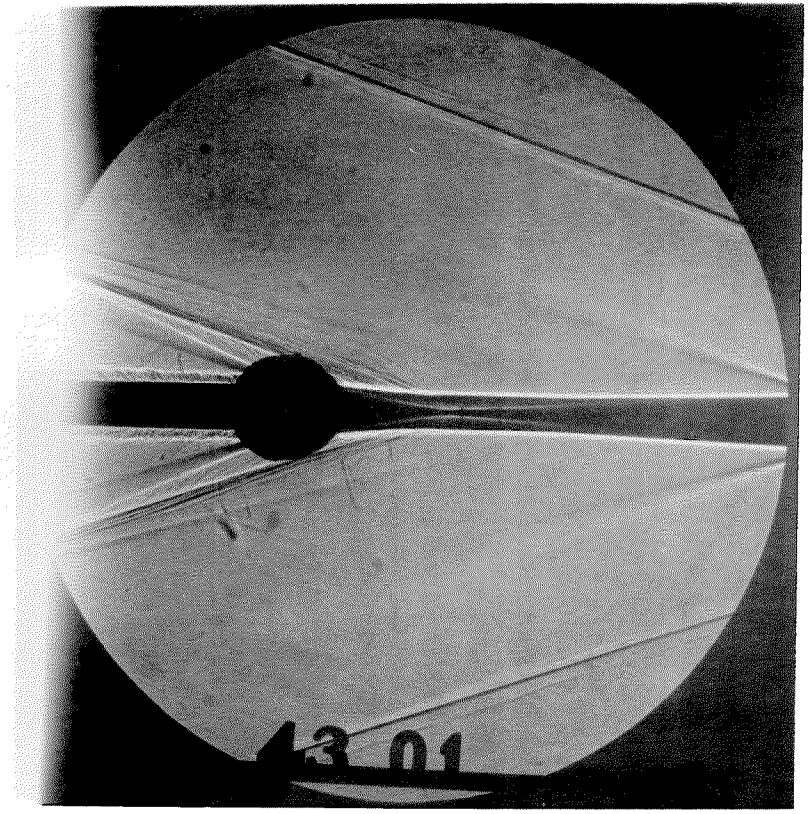

Figure 22. Shadowgraph, Control Surface Model, M = 3.52, RN/L = 0.57 x 10^6, $\alpha = 0^o$, $\delta = 0^o$

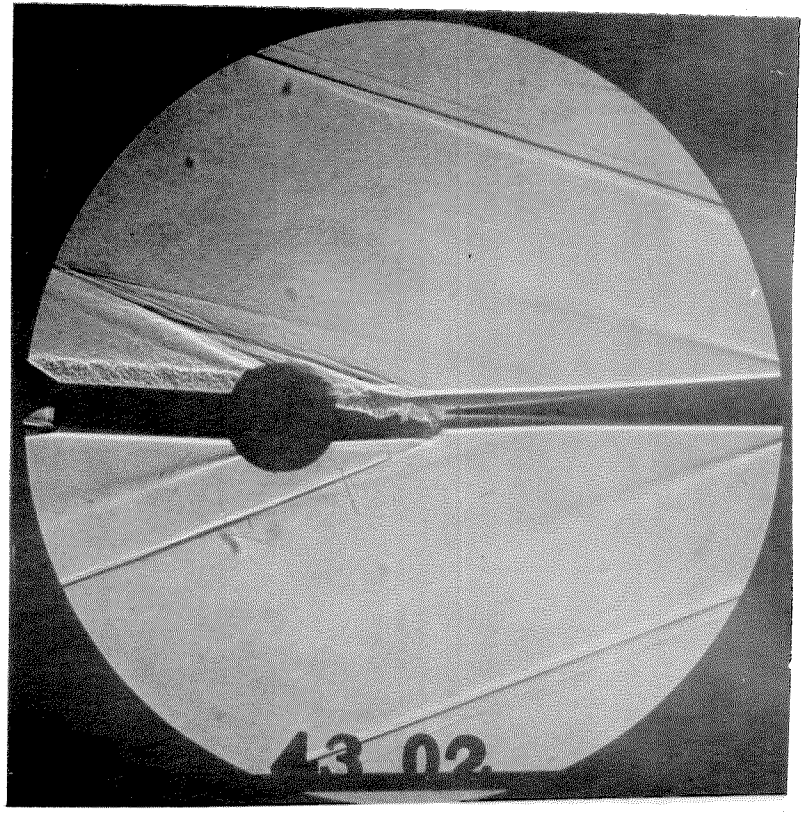

Figure 23. Shadowgraph, Control Surface Model, M = 3.52, RN/L = 0.57 x 10^6, $\alpha = 0^o$, $\delta = -5^o$

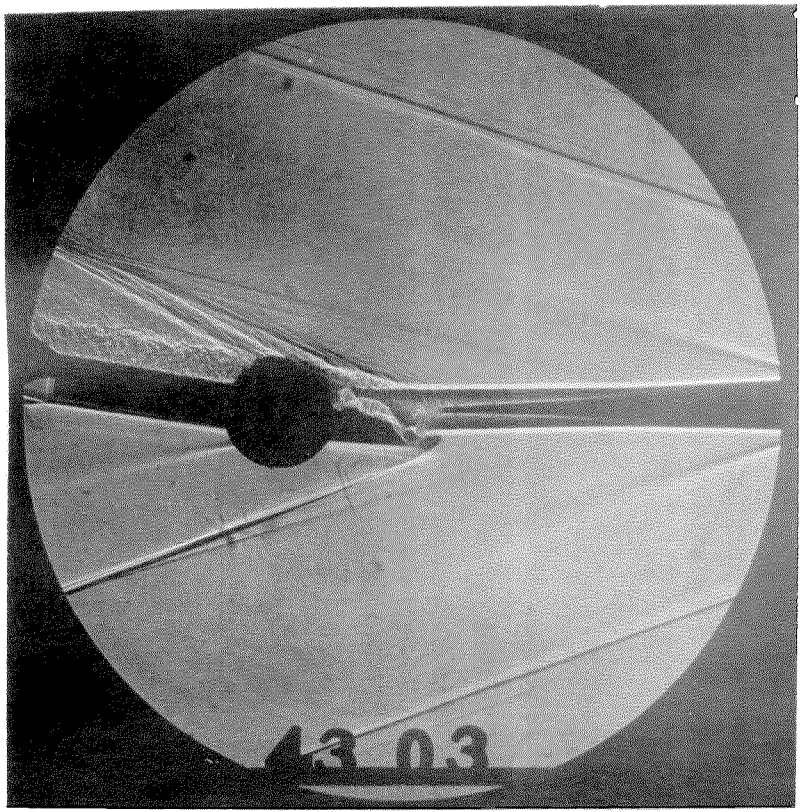

Figure 24. Shadowgraph, Control Surface Model, $M = 3.52$, $RN/L = 0.57 \times 10^6$, $\alpha = 0^\circ$, $\delta = -10^\circ$

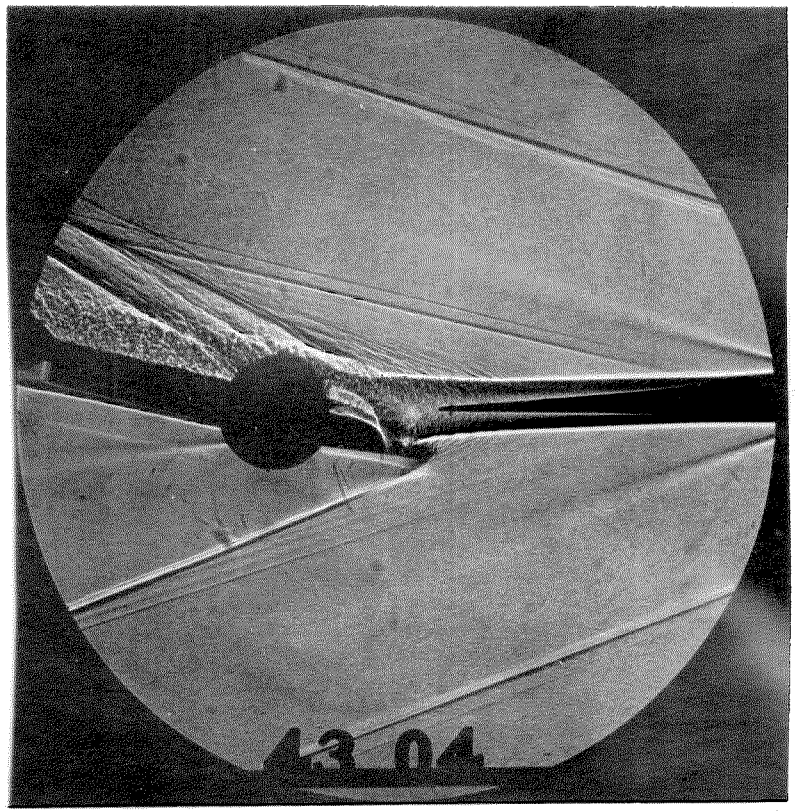

Figure 25. Shadowgraph, Control Surface Model, $M = 3.52$, $RN/L = 0.57 \times 10^6$, $\alpha = 0^\circ$, $\delta = -15^\circ$

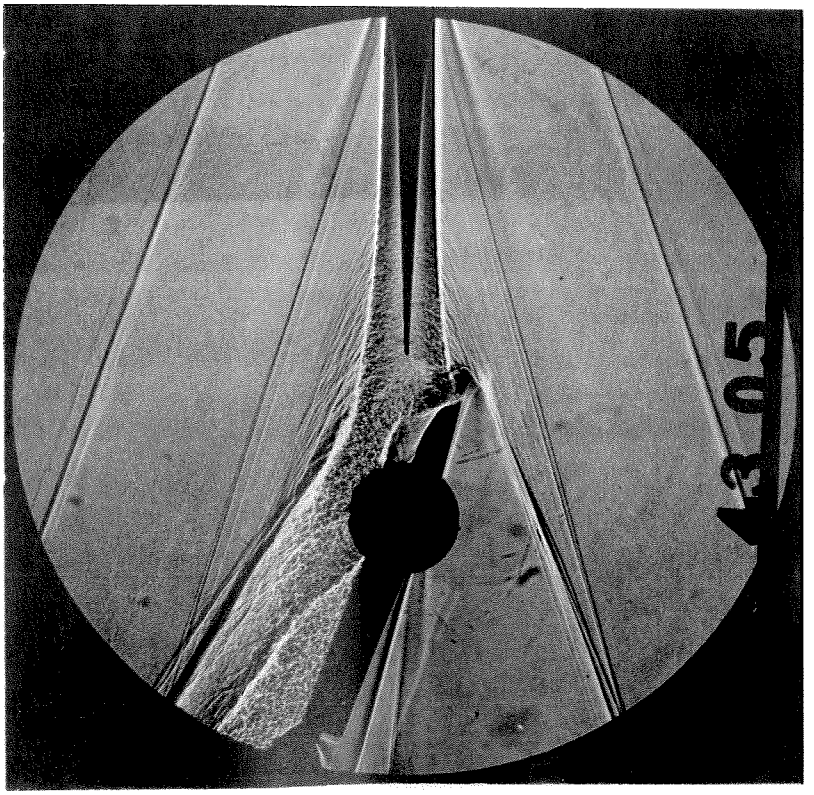

Figure 26. Shadowgraph, Control Surface Model, $M = 3.52$, $RN/L = 0.57 \times 10^6$, $\alpha = 0^\circ$, $\delta = -20^\circ$

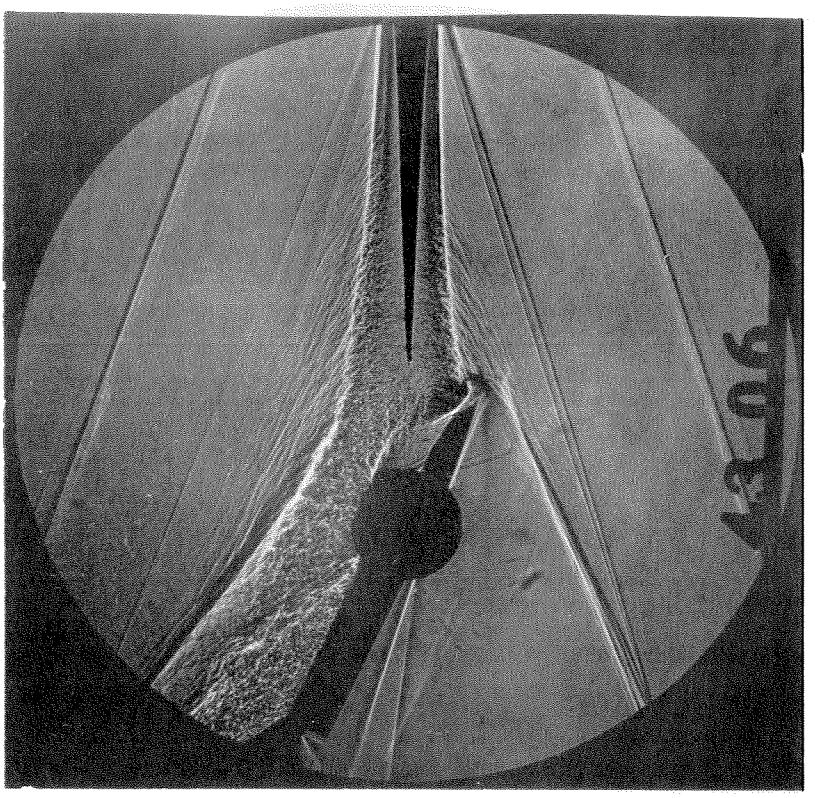

Figure 27. Shadowgraph, Control Surface Model, $M = 3.52$, $RN/L = 0.57 \times 10^6$, $\alpha = 0^\circ$, $\delta = -25^\circ$

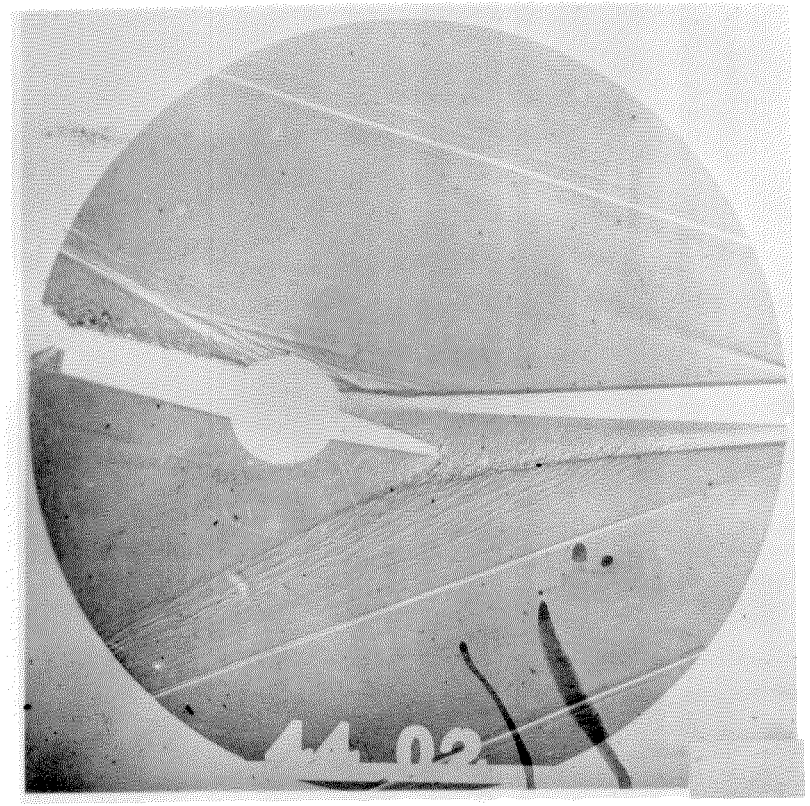

Figure 28. Shadowgraph, Control Surface Model, $M = 3.52$, $RN/L = 0.57 \times 10^6$, $\alpha = -4^\circ$, $\delta = -15^\circ$

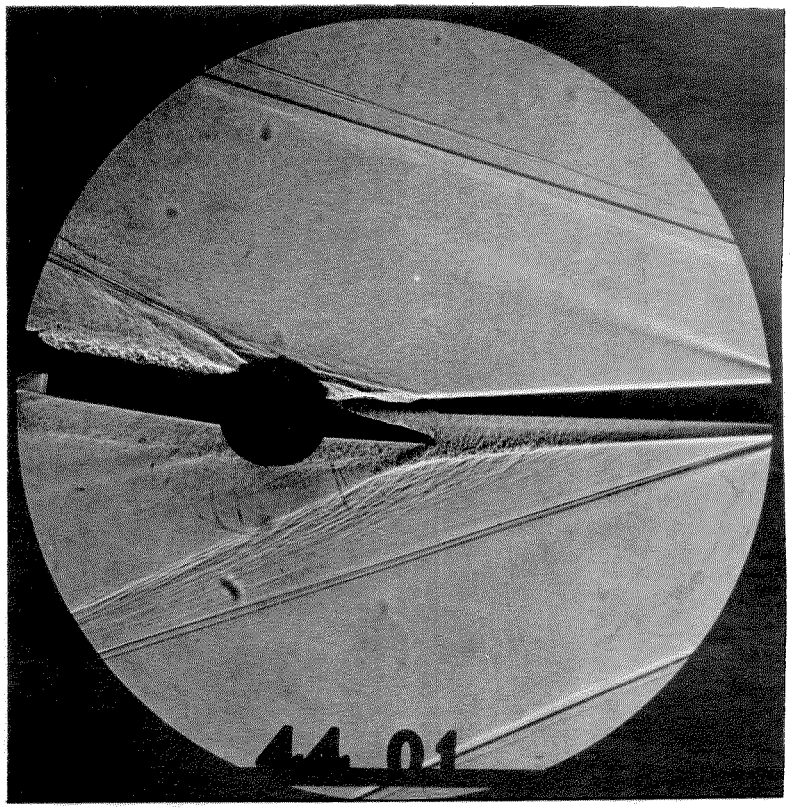

Figure 29. Shadowgraph, Control Surface Model, $M = 3.52$, $RN/L = 0.57 \times 10^6$, $\alpha = -4^\circ$, $\delta = -10^\circ$

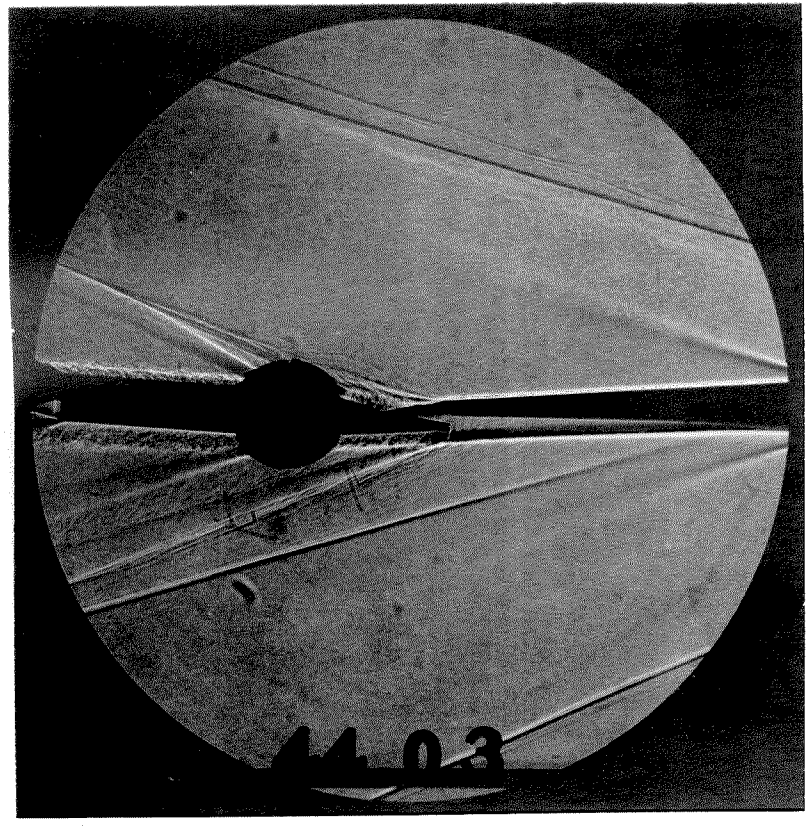

Figure 30. Shadowgraph, Control Surface Model, $M = 3.52$, $RN/L = 0.57 \times 10^6$, $\alpha = -4^\circ$, $\delta = -5^\circ$

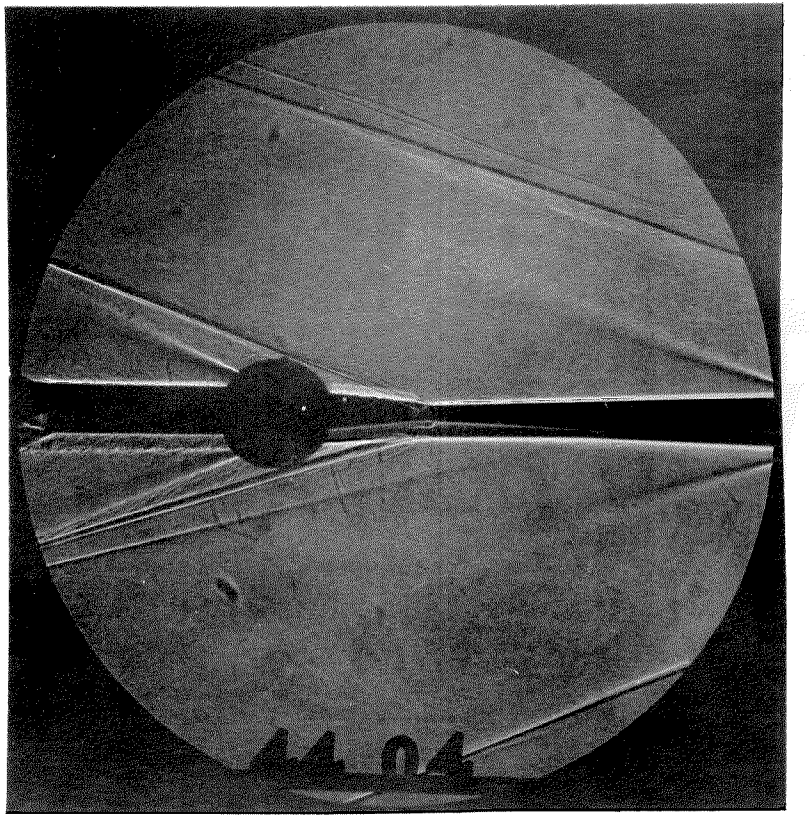

Figure 31. Shadowgraph, Control Surface Model, $M = 3.52$, $RN/L = 0.57 \times 10^6$, $\alpha = -4^\circ$, $\delta = 0^\circ$

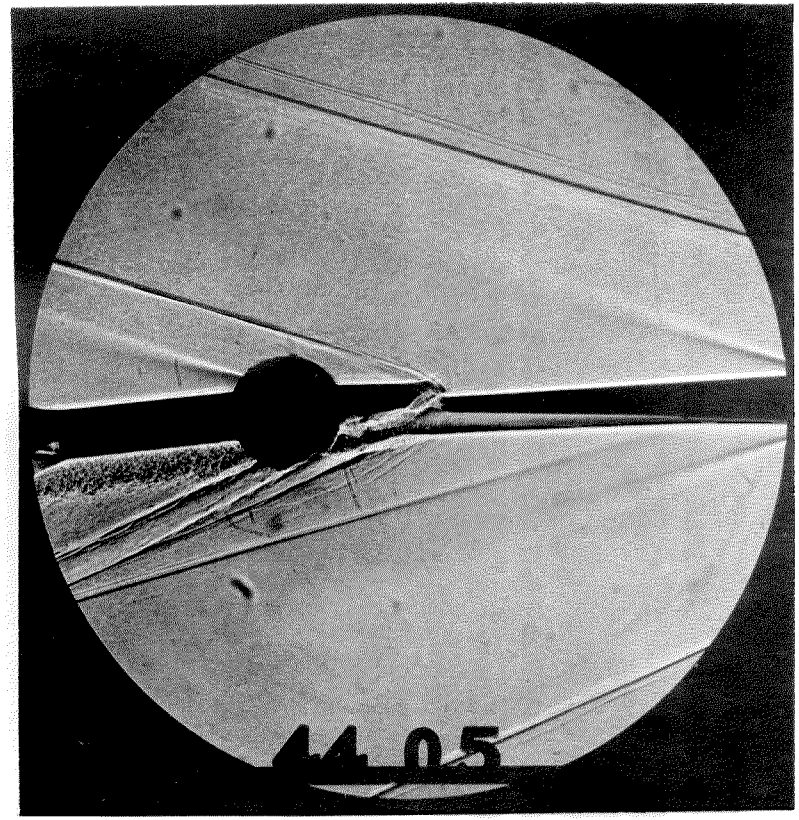

Figure 32. Shadowgraph, Control Surface Model, M = 3.52, RN/L = 0.57 x 10^6, $\alpha = -4^o$, $\delta = 5^o$

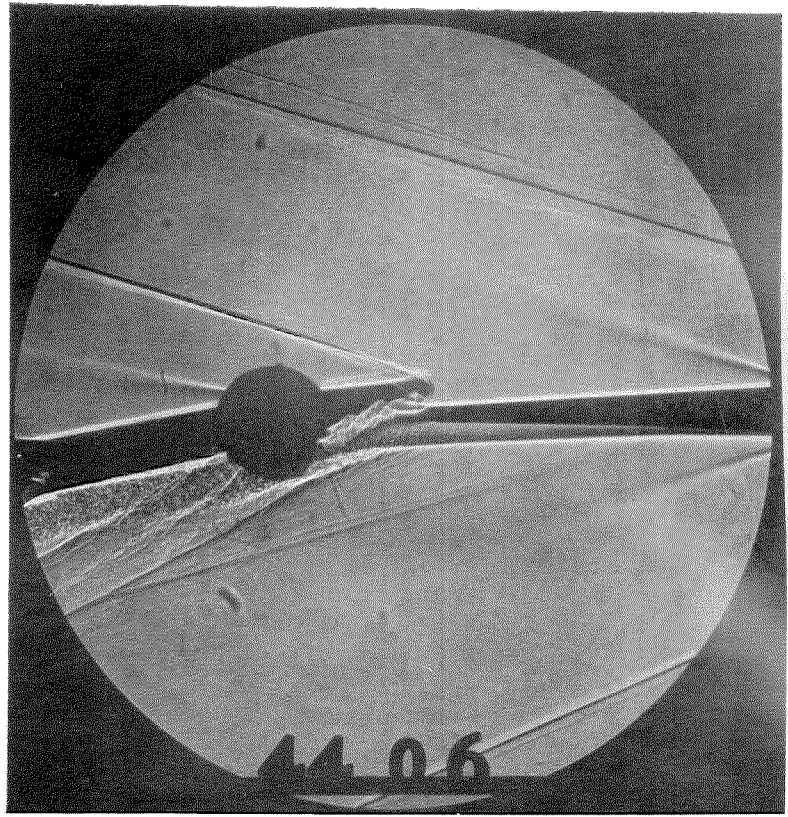

Figure 33. Shadowgraph, Control Surface Model, M = 3.52, RN/L = 0.57 x 10^6, $\alpha = -4^o$, $\delta = 10^o$

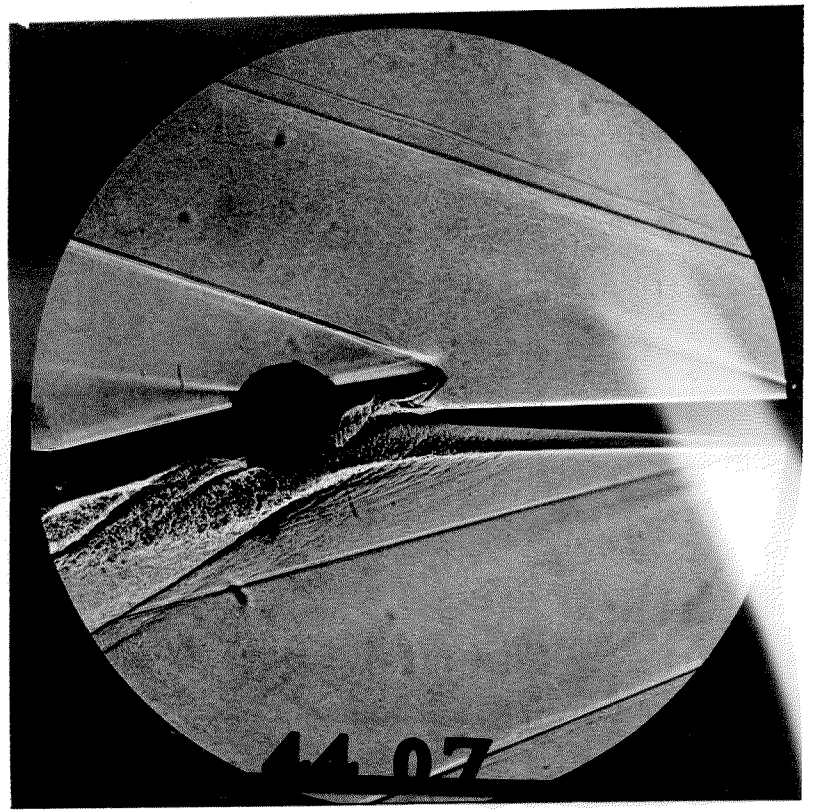

Figure 34. Shadowgraph, Control Surface Model, M = 3.52, RN/L = 0.57 x 10^6, α = -4°, δ = 15°

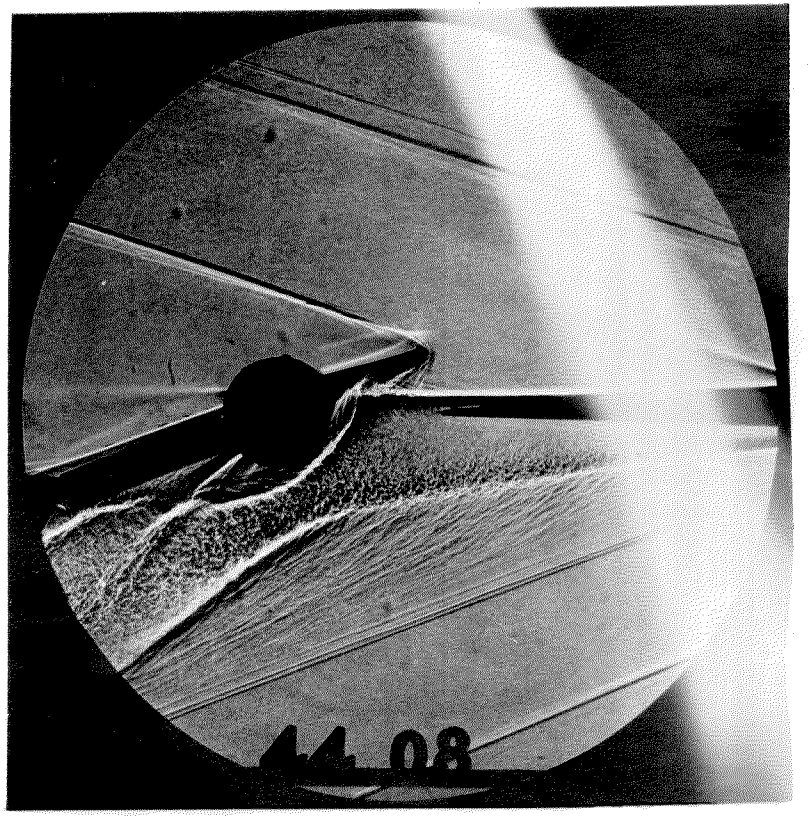

Figure 35. Shadowgraph, Control Surface Model, M = 3.52, RN/L = 0.57 x 10^6, α = -4°, δ = 20°

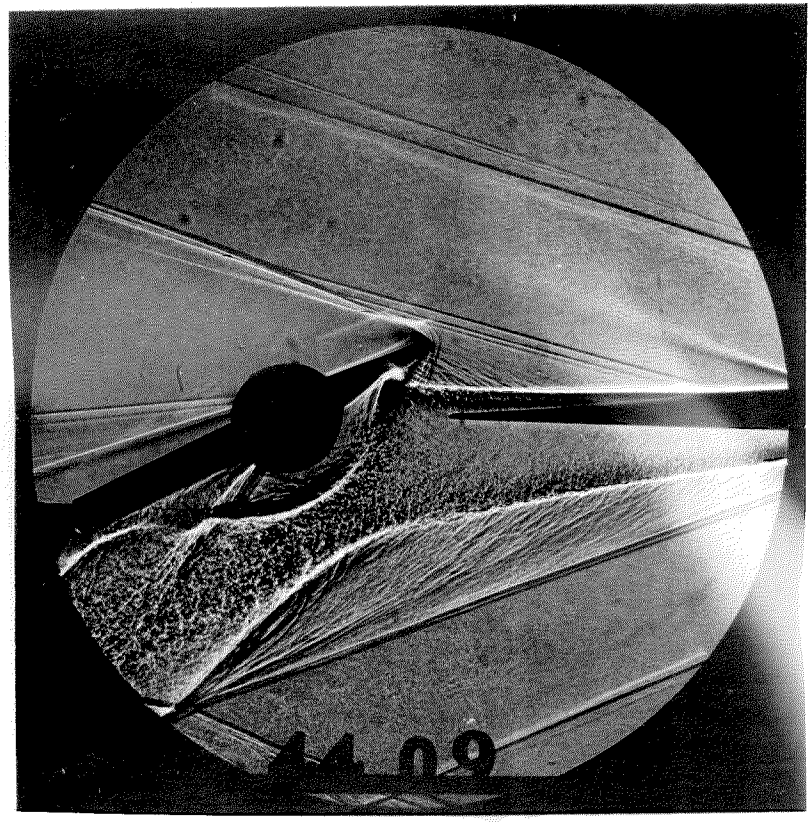

Figure 36. Shadowgraph, Control Surface Model, $M = 3.52$, $RN/L = 0.57 \times 10^6$, $\alpha = -4^\circ$, $\delta = 25^\circ$

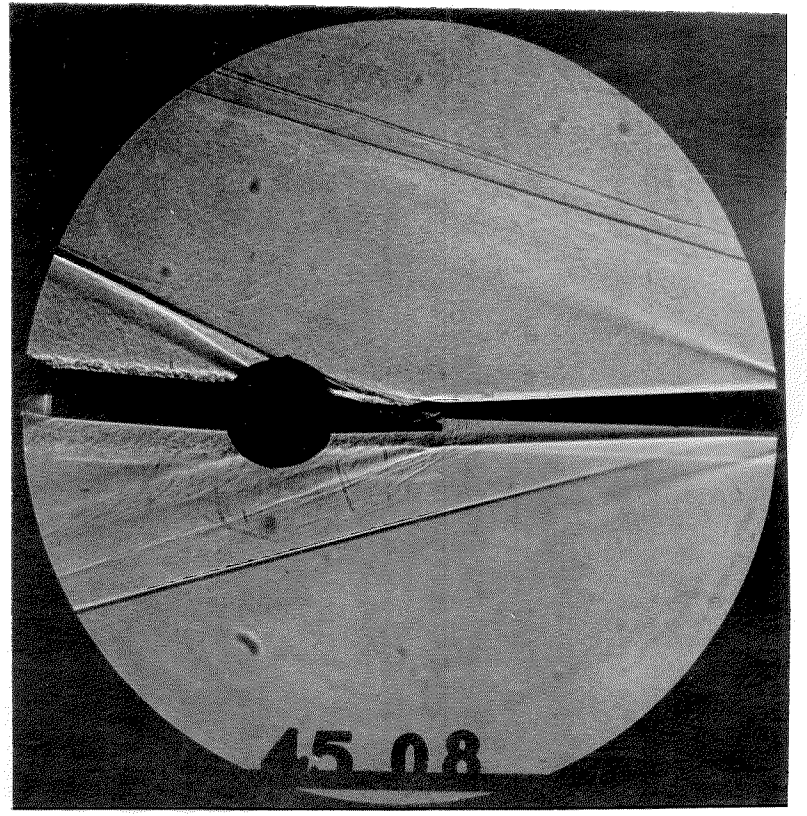

Figure 37. Shadowgraph, Control Surface Model, $M = 3.52$, $RN/L = 0.57 \times 10^6$, $\alpha = -8^\circ$, $\delta = -5^\circ$

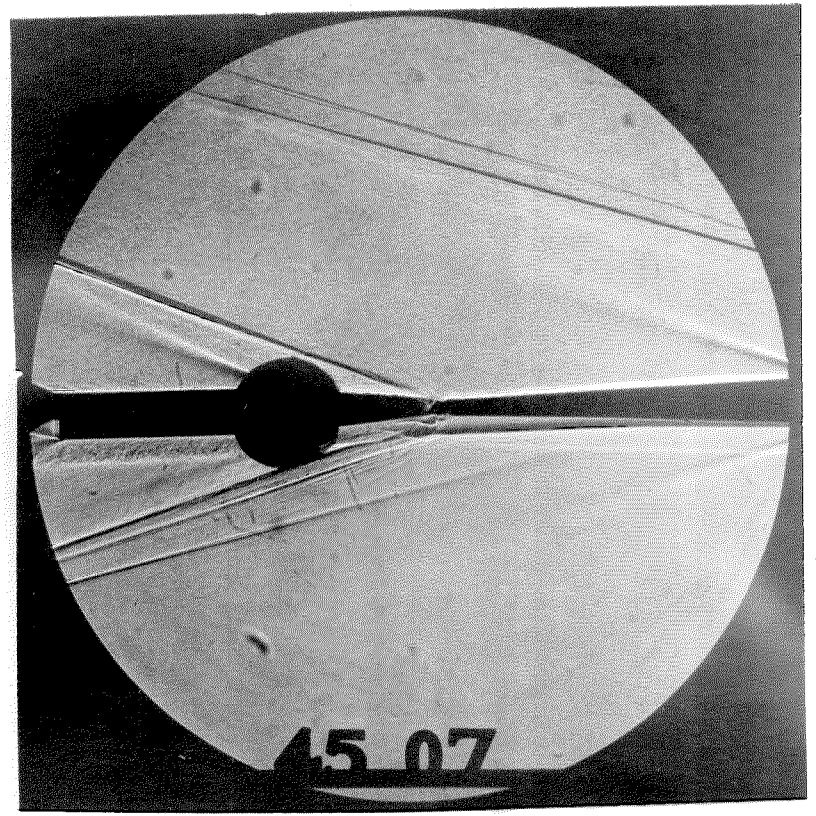

Figure 38. Shadowgraph, Control Surface Model, M = 3.52, RN/L = 0.57×10^6, $\alpha = -8^\circ$, $\delta = 0^\circ$

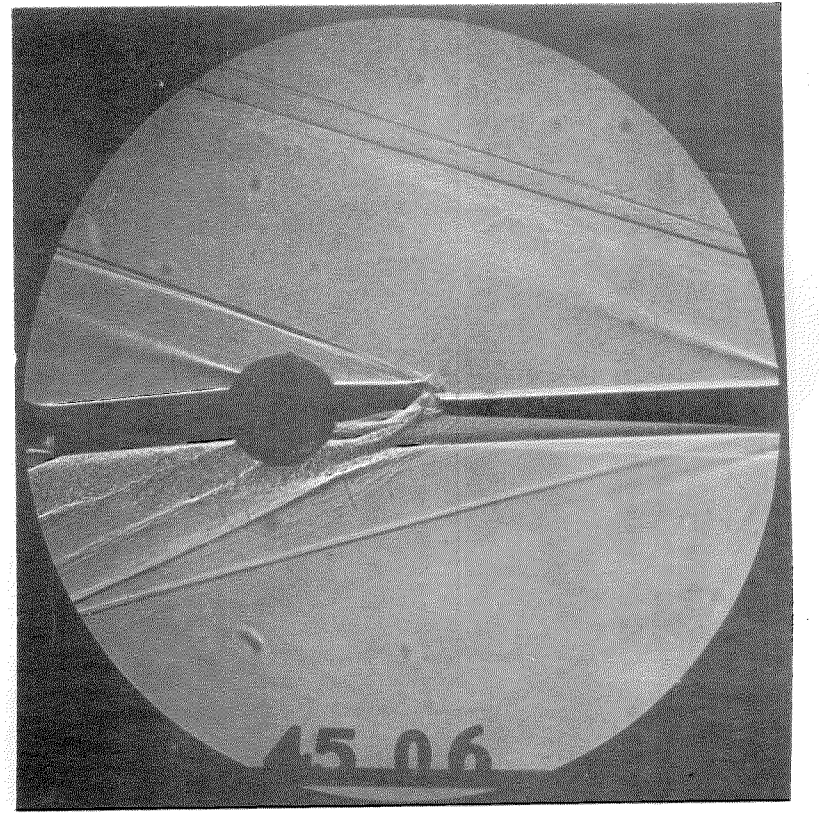

Figure 39. Shadowgraph, Control Surface Model, M = 3.52, RN/L = 0.57×10^6, $\alpha = -8^\circ$, $\delta = 5^\circ$

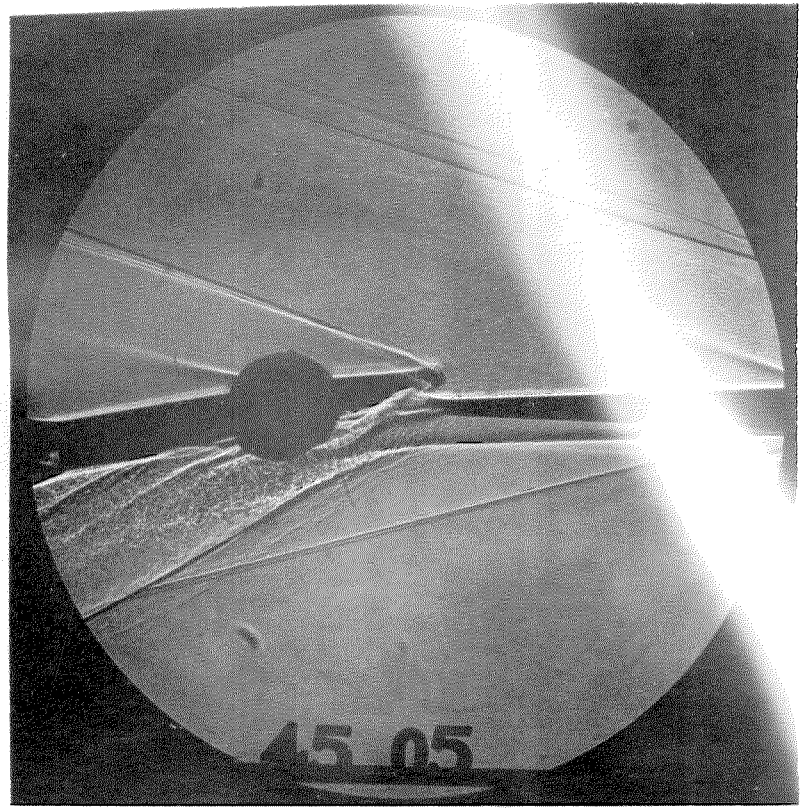

Figure 40. Shadowgraph, Control Surface Model, $M = 3.52$, $RN/L = 0.57 \times 10^6$, $\alpha = -8^\circ$, $\delta = 10^\circ$

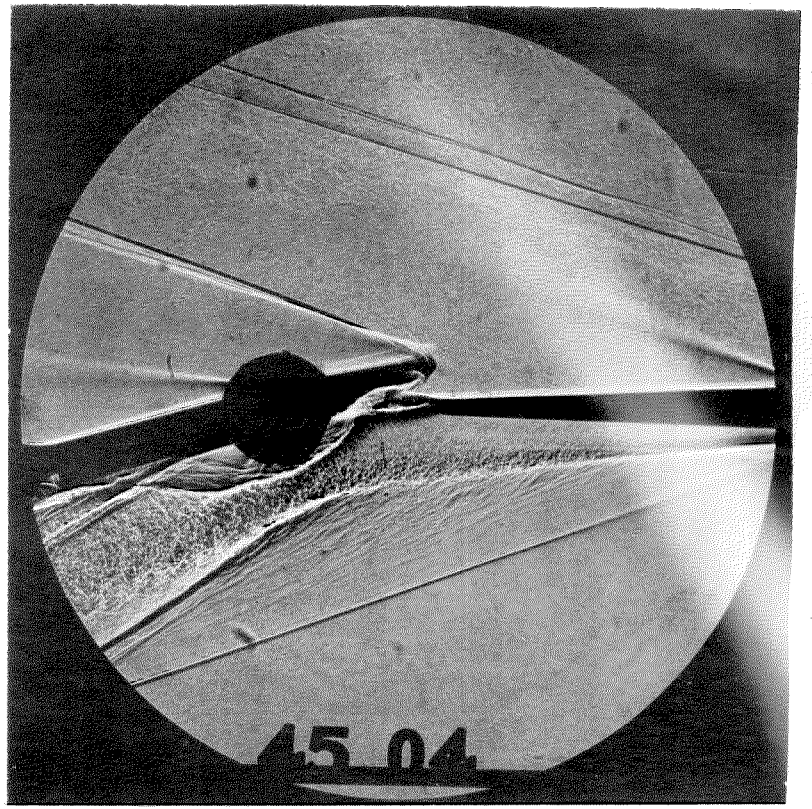

Figure 41. Shadowgraph, Control Surface Model, $M = 3.52$, $RN/L = 0.57 \times 10^6$, $\alpha = -8^\circ$, $\delta = 15^\circ$

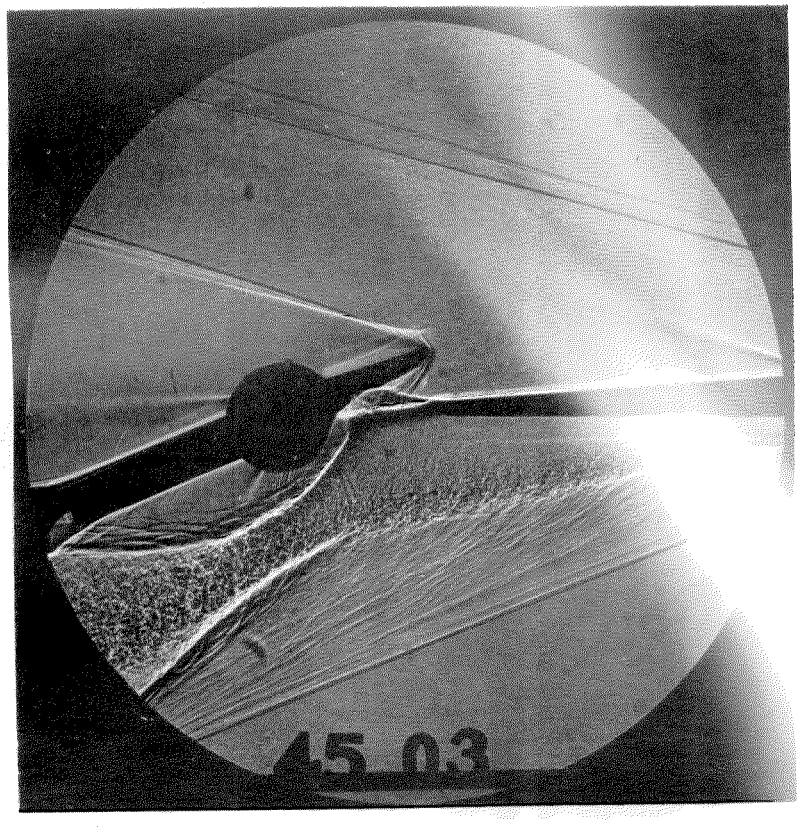

Figure 42. Shadowgraph, Control Surface Model, M = 3.52, RN/L = 0.57 x 10^6, α = -8°, δ = 20°

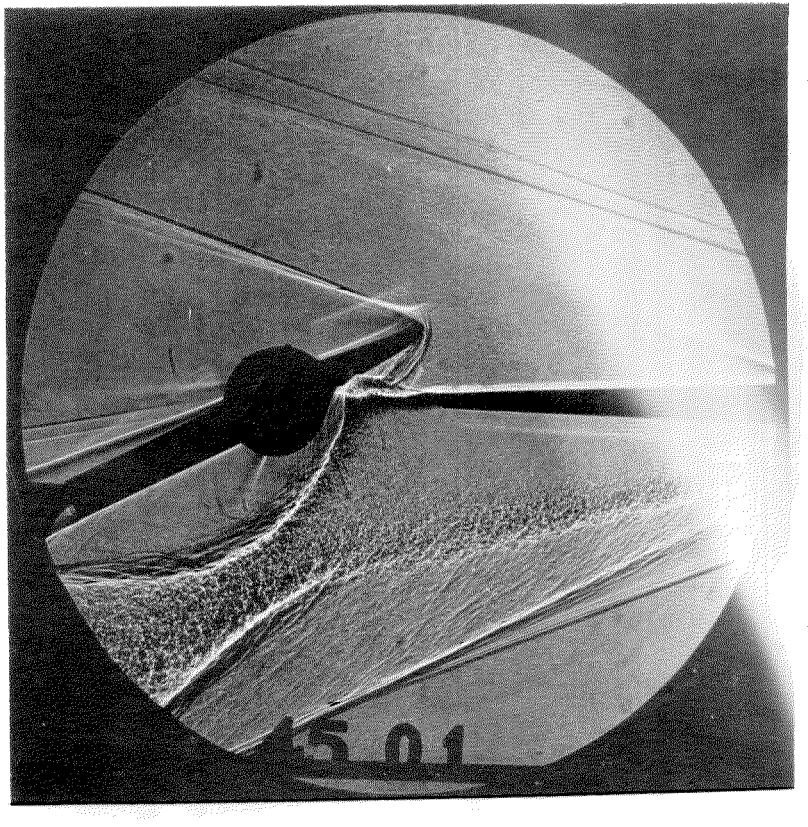

Figure 43. Shadowgraph, Control Surface Model, M = 3.52, RN/L = 0.57 x 10^6, α = -8°, δ = 25°

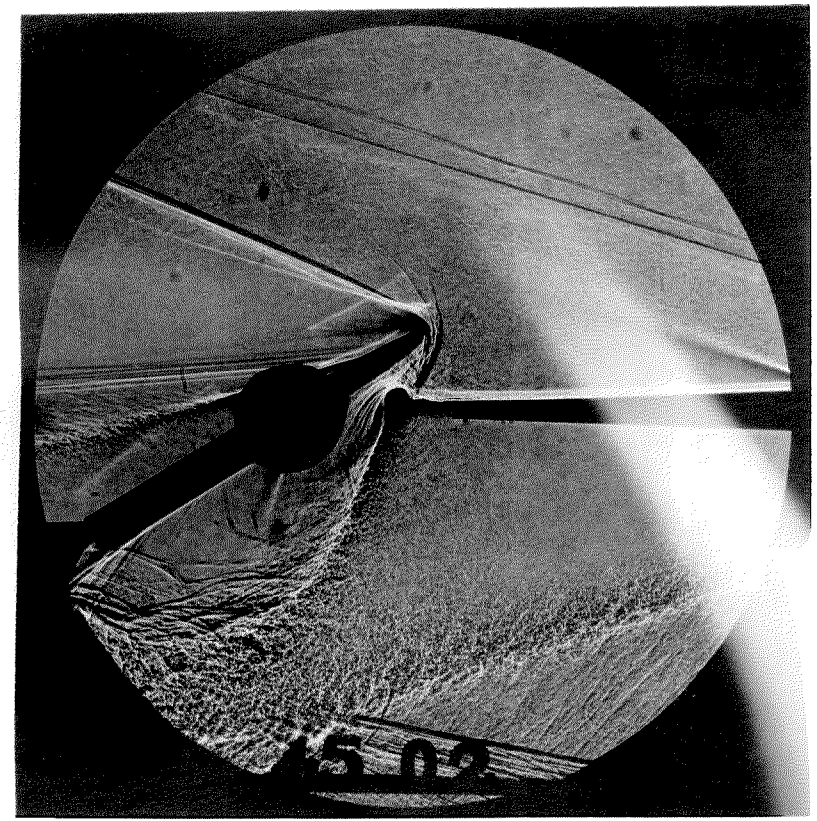

Figure 44. Shadowgraph, Control Surface Model, M = 3.52, RN/L = 0.57 x 10^6, α = -8°, δ = 30°

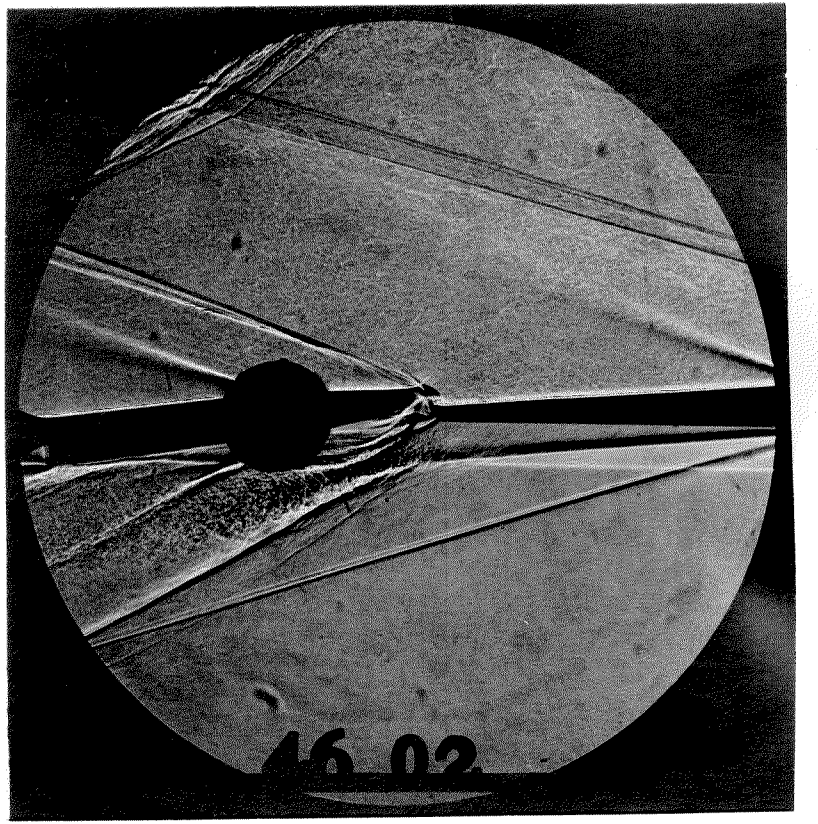

Figure 45. Shadowgraph, Control Surface Model, M = 3.52, RN/L = 0.57 x 10^6, α = -12°, δ = 5°

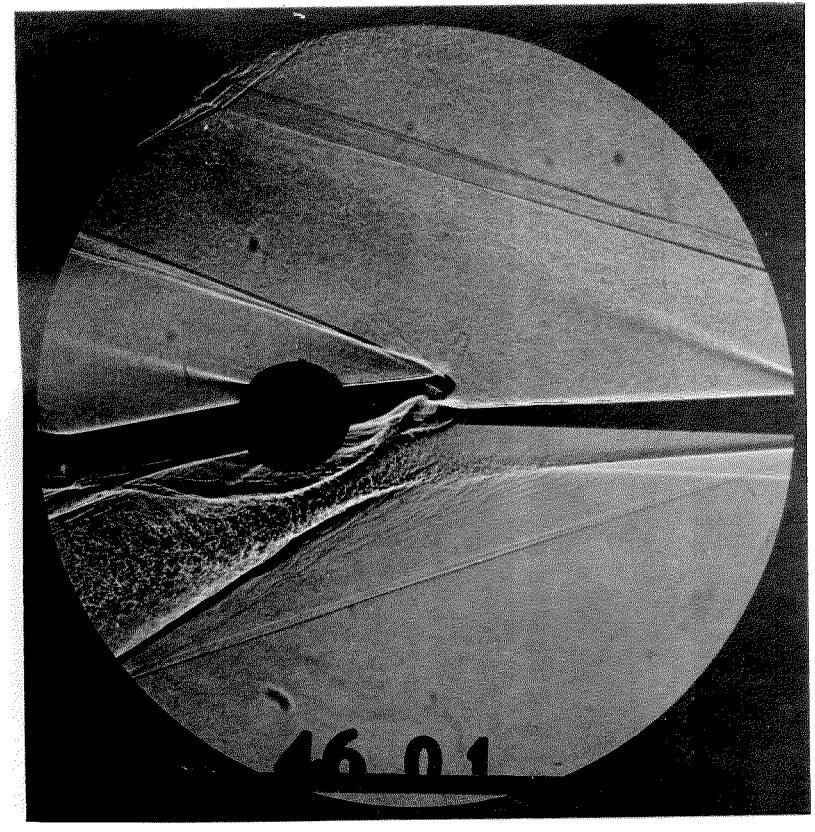

Figure 46. Shadowgraph, Control Surface Model, M = 3.52, RN/L = 0.57 x 10^6, α = -12°, δ = 10°

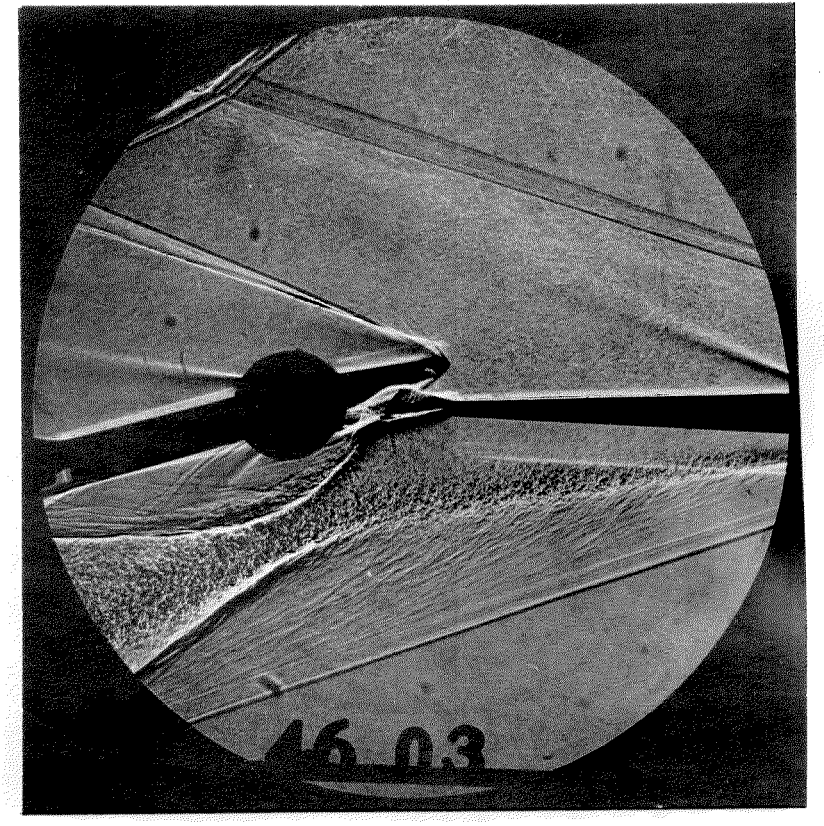

Figure 47. Shadowgraph, Control Surface Model, M = 3.52, RN/L = 0.57 x 10^6, α = -12°, δ = 15°

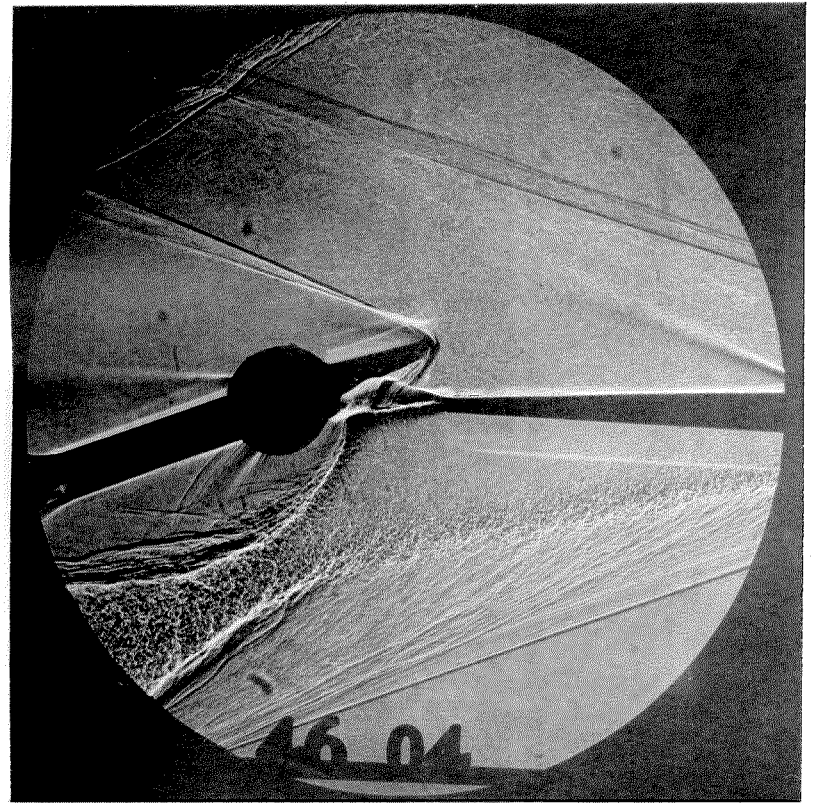

Figure 48. Shadowgraph, Control Surface Model, M = 3.52, RN/L = 0.57 x 10^6, α = -12°, δ = 20°

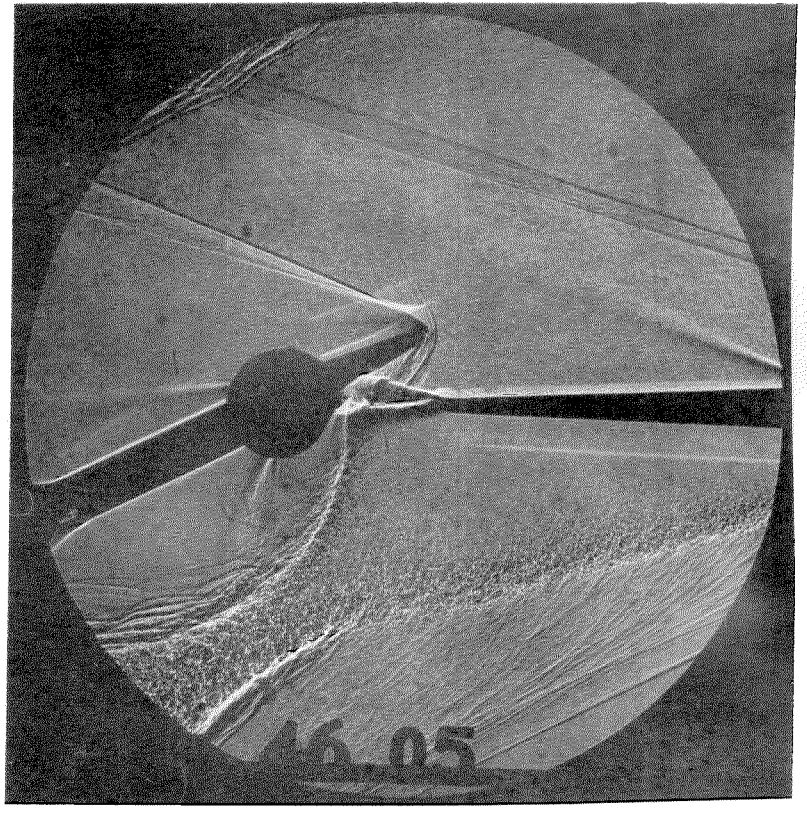

Figure 49. Shadowgraph, Control Surface Model, M = 3.52, RN/L = 0.57 x 10^6, α = -12°, δ = 25°

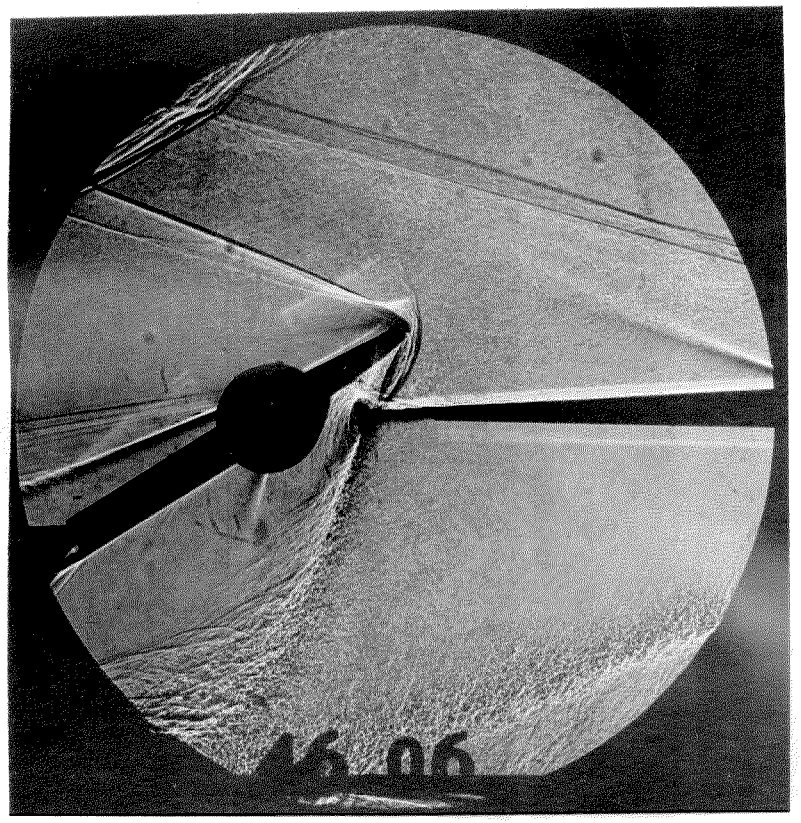

Figure 50. Shadowgraph, Control Surface Model, $M = 3.52$, $RN/L = 0.57 \times 10^6$, $\alpha = -12^\circ$, $\delta = 30^\circ$

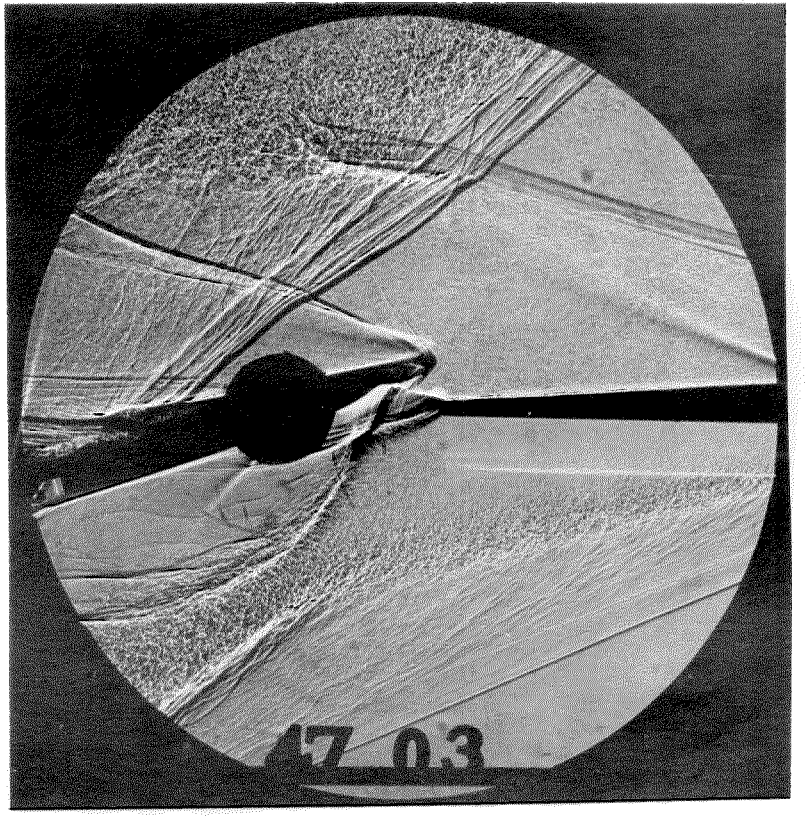

Figure 51. Shadowgraph, Control Surface Model, $M = 3.52$, $RN/L = 0.57 \times 10^6$, $\alpha = -16^\circ$, $\delta = 15^\circ$

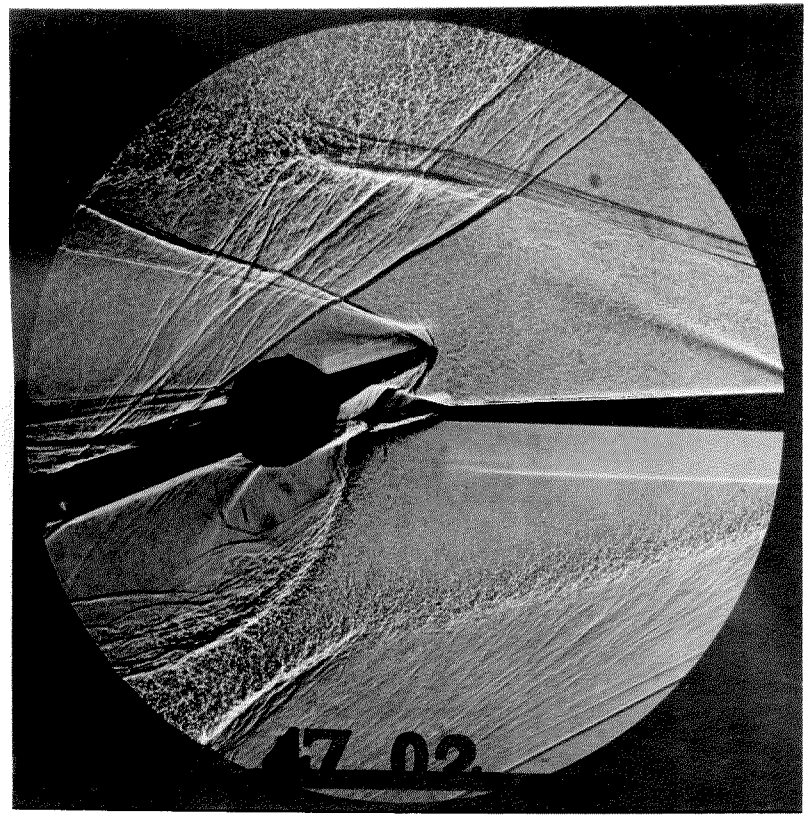

Figure 52. Shadowgraph, Control Surface Model, M = 3.52, RN/L = 0.57 x 10^6, α = -16°, δ = 20°

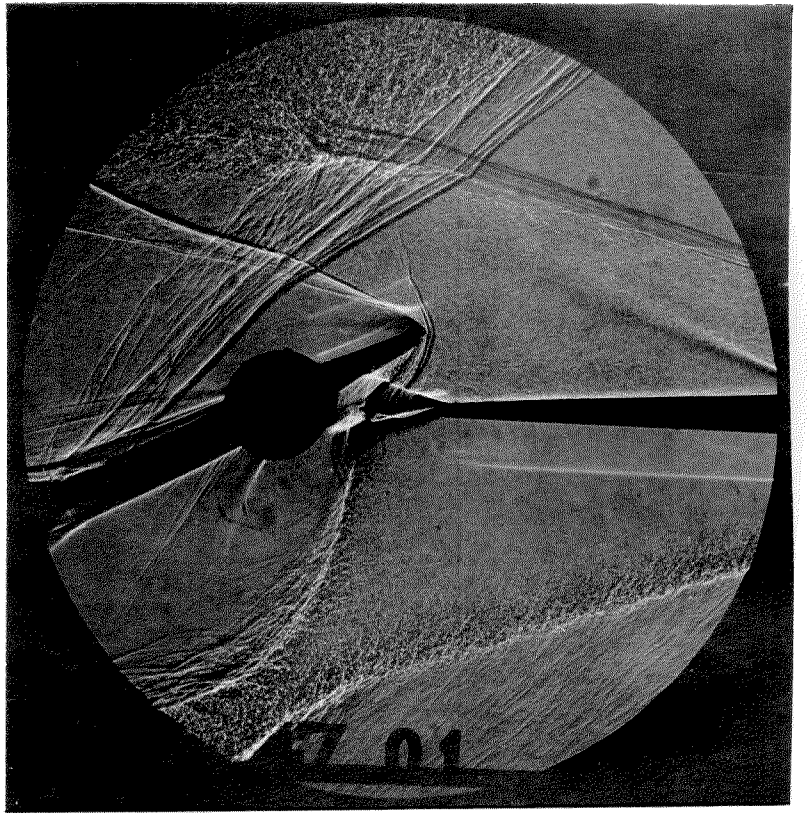

Figure 53. Shadowgraph, Control Surface Model, M = 3.52, RN/L = 0.57 x 10^6, α = -16°, δ = 25°

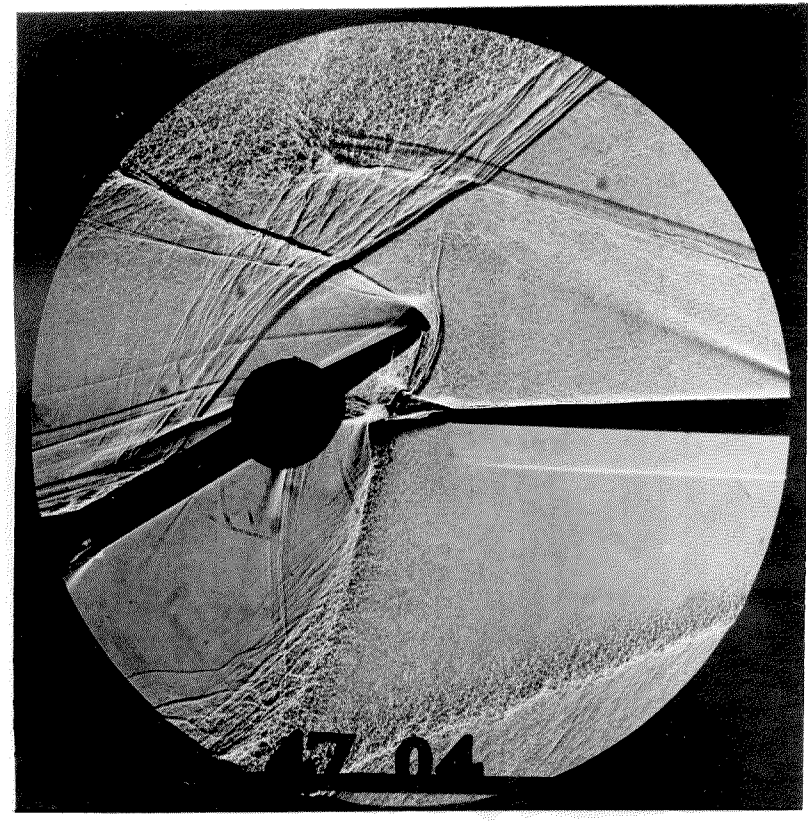

Figure 54. Shadowgraph, Control Surface Model, $M = 3.52$, $RN/L = 0.57 \times 10^6$, $\alpha = -16^\circ$, $\delta = 30^\circ$

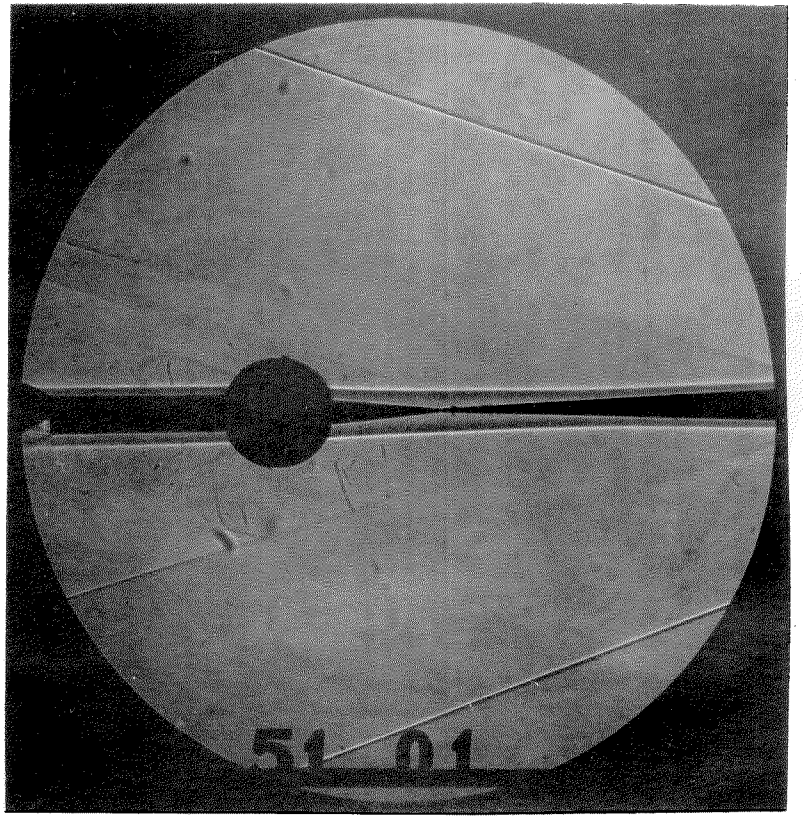

Figure 55. Shadowgraph, Control Surface Model, $M = 3.52$, $RN/L = 0.15 \times 10^6$, $\alpha = 0^\circ$, $\delta = 0^\circ$

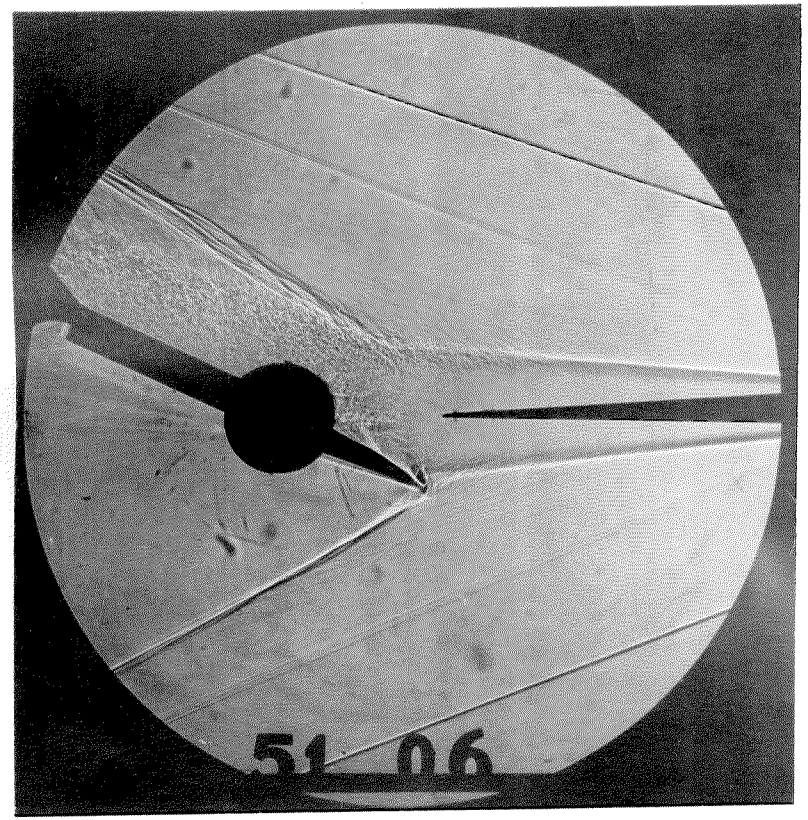

Figure 56. Shadowgraph, Control Surface Model, $M = 3.52$, $RN/L = 0.15 \times 10^6$, $\alpha = 0^\circ$, $\delta = -25^\circ$

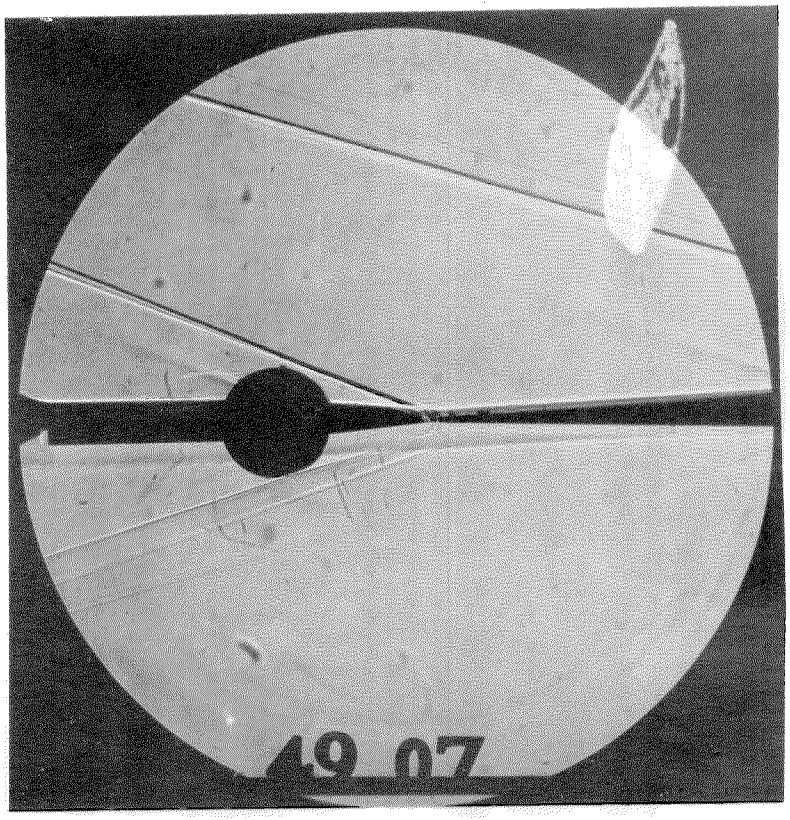

Figure 57. Shadowgraph, Control Surface Model, $M = 3.52$, $RN/L = 0.15 \times 10^6$, $\alpha = -8^\circ$, $\delta = 0^\circ$

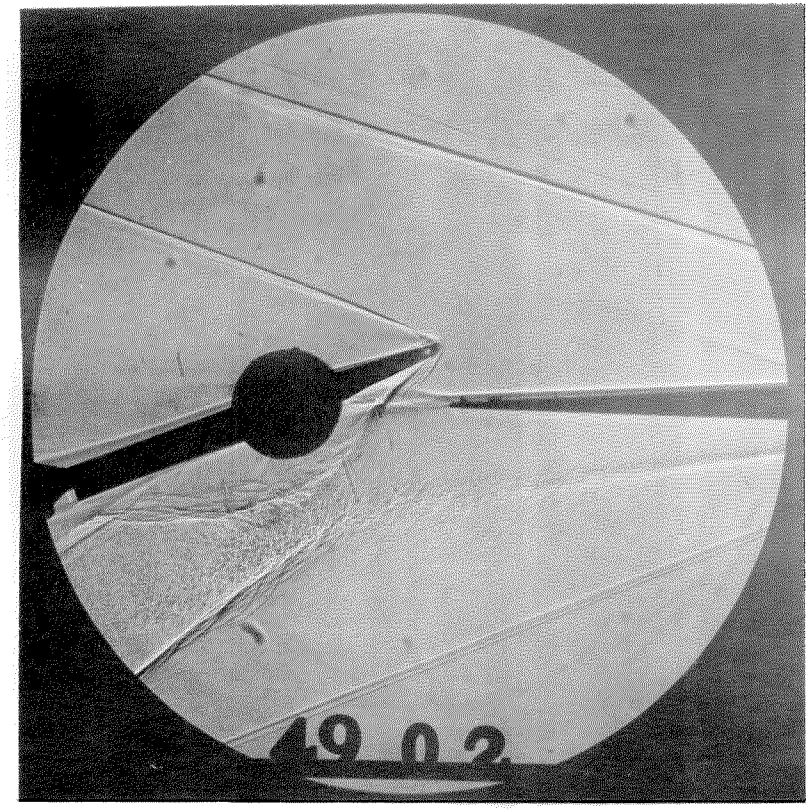

Figure 58. Shadowgraph, Control Surface Model, M = 3.52, RN/L = 0.15 x 10^6, α = -8°, δ = 20°

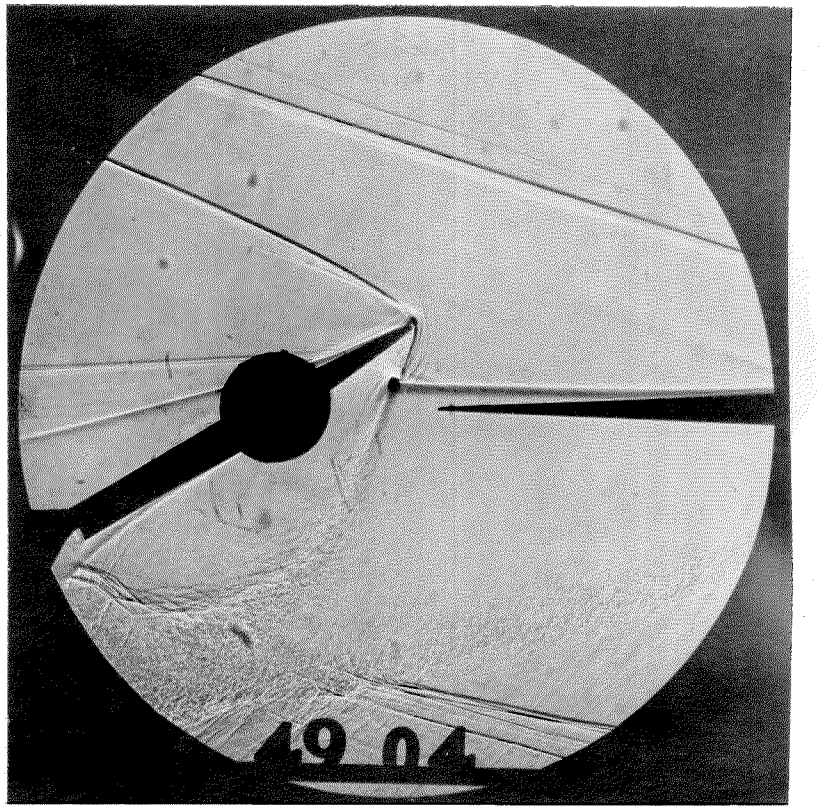

Figure 59. Shadowgraph, Control Surface Model, M = 3.52, RN/L = 0.15 x 10^6, α = -8°, δ = 25°

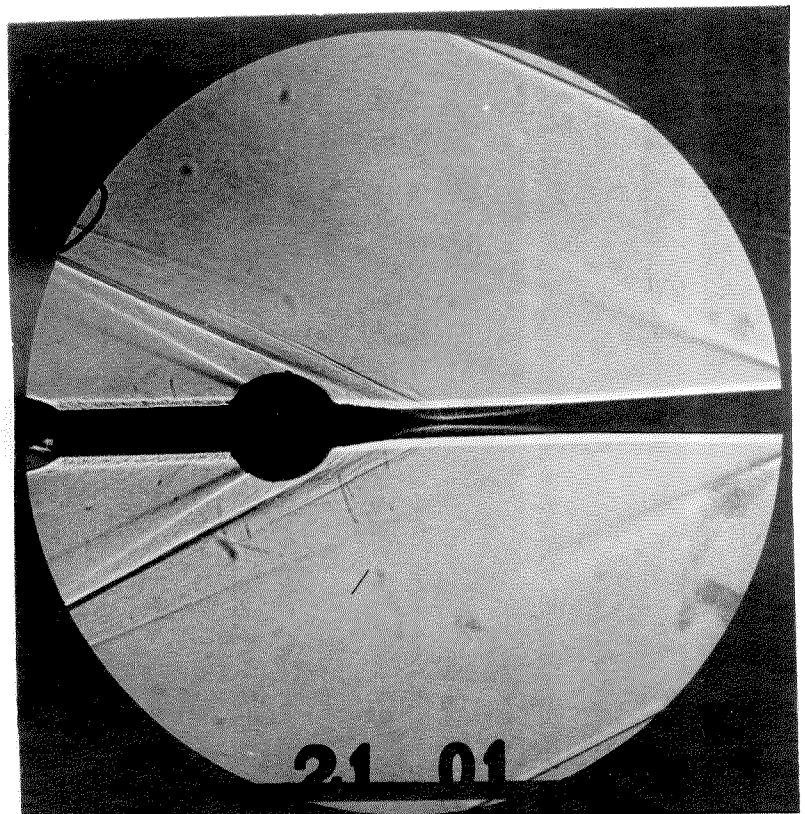

Figure 60. Shadowgraph, Control Surface Model, $M = 2.60$, $RN/L = 0.44 \times 10^6$, $\alpha = 0^\circ$, $\delta = 0^\circ$

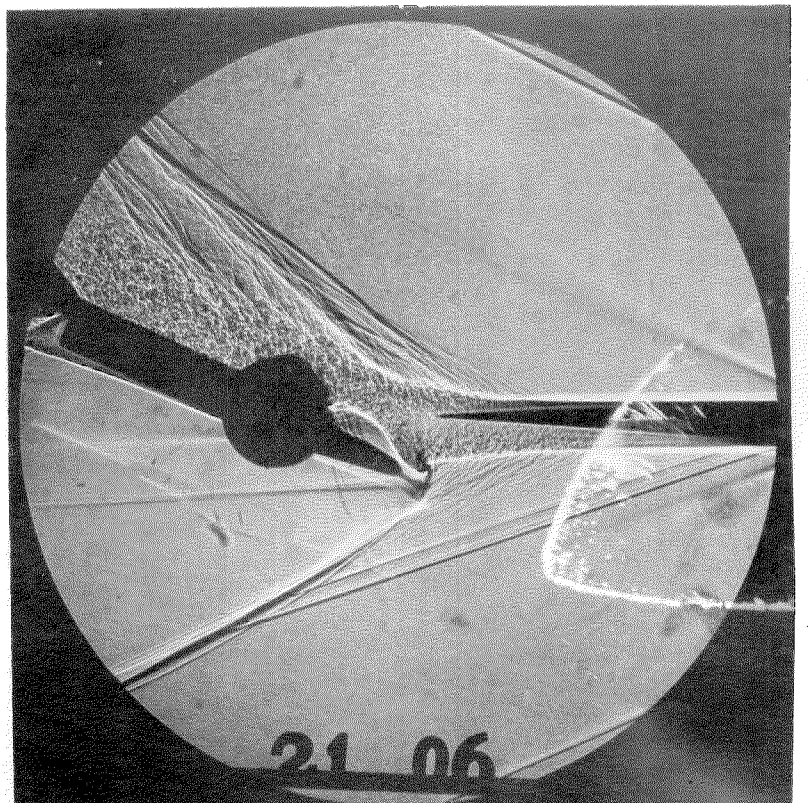

Figure 61. Shadowgraph, Control Surface Model, $M = 2.60$, $RN/L = 0.44 \times 10^6$, $\alpha = 0^\circ$, $\delta = -25^\circ$

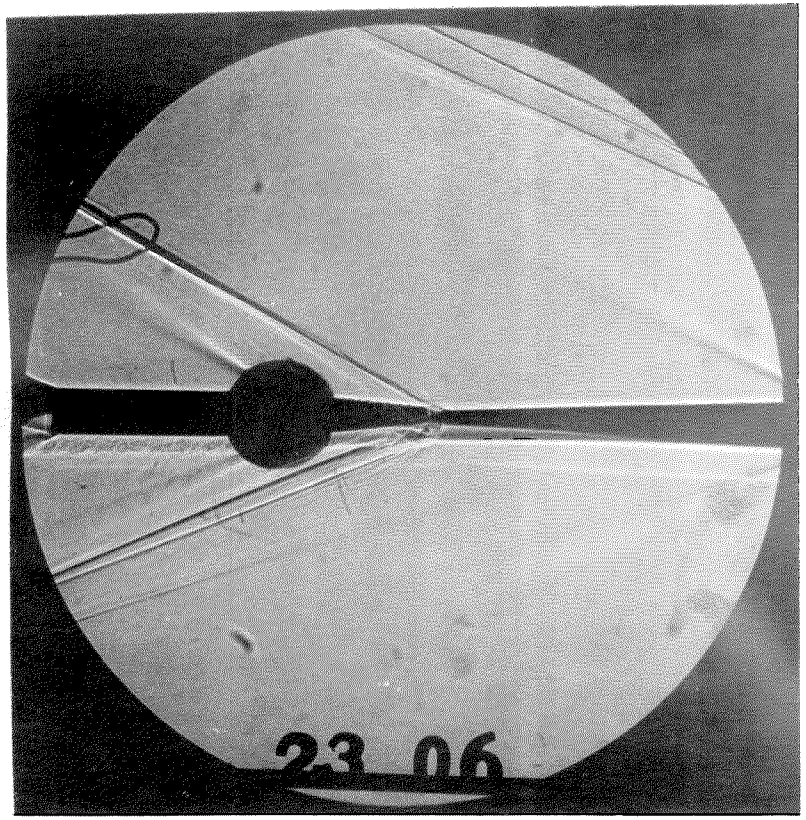

Figure 62. Shadowgraph, Control Surface Model, $M = 2.60$, $RN/L = 0.43 \times 10^6$, $\alpha = -8^\circ$, $\delta = 0^\circ$

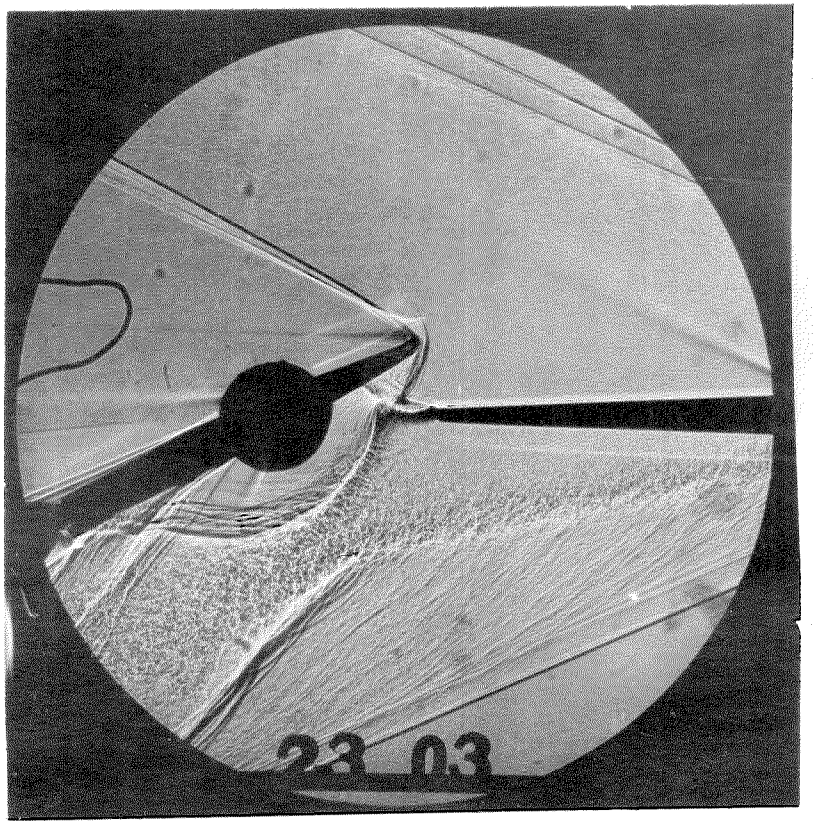

Figure 63. Shadowgraph, Control Surface Model, $M = 2.60$, $RN/L = 0.43 \times 10^6$, $\alpha = -8^\circ$, $\delta = 25^\circ$

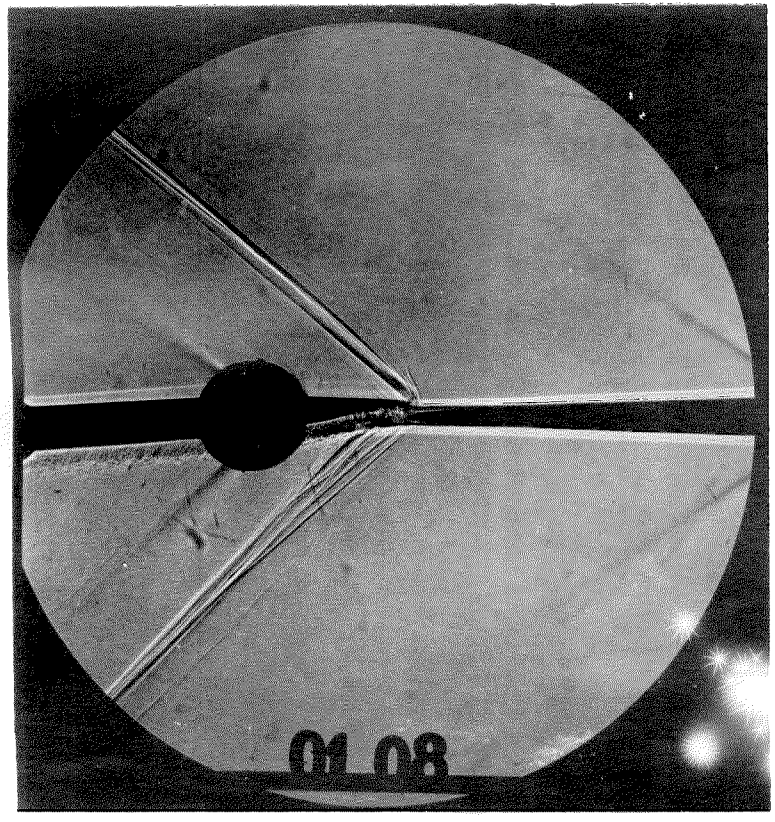

Figure 64. Shadowgraph, Control Surface Model, $M = 1.70$, $RN/L = 0.37 \times 10^6$, $\alpha = 0^\circ$, $\delta = 4^\circ$

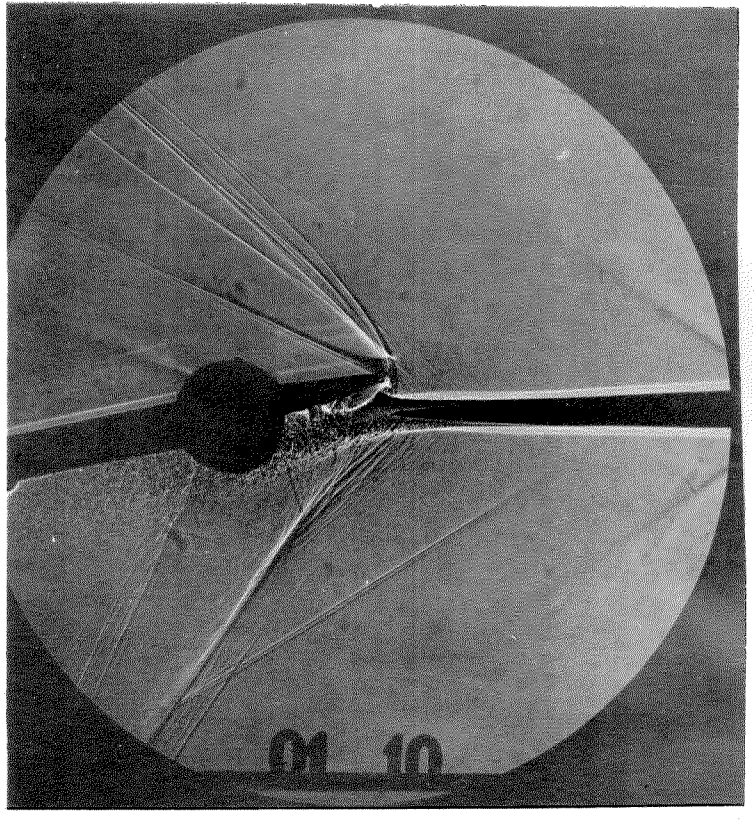

Figure 65. Shadowgraph, Control Surface Model, $M = 1.70$, $RN/L = 0.37 \times 10^6$, $\alpha = 0^\circ$, $\delta = 12^\circ$

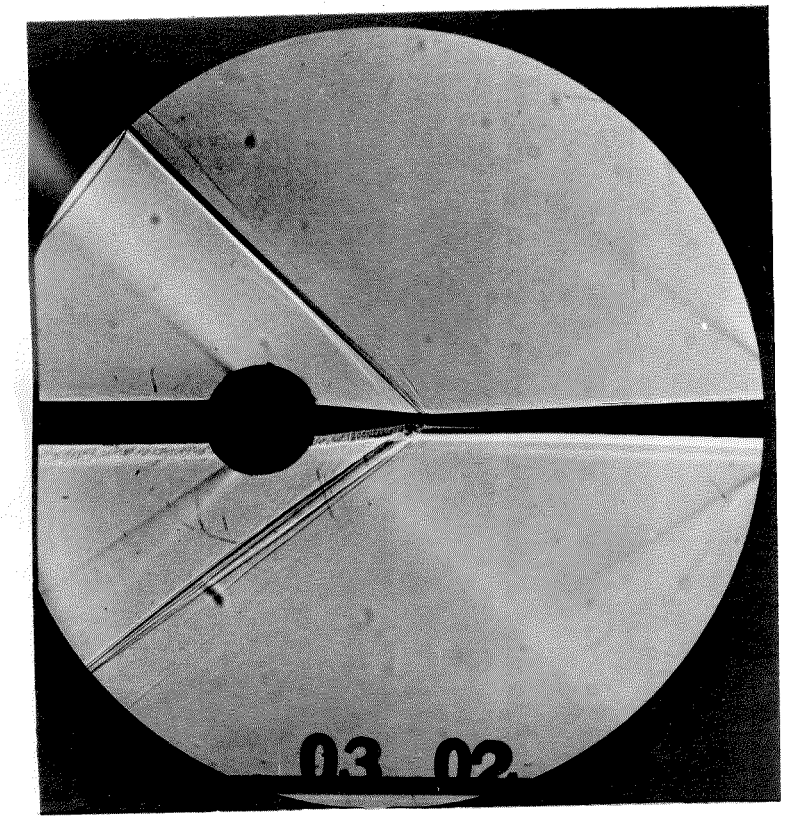

Figure 66. Shadowgraph, Control Surface Model, M = 1.70, RN/L = 0.37×10^6, $\alpha = -4^\circ$, $\delta = 0^\circ$

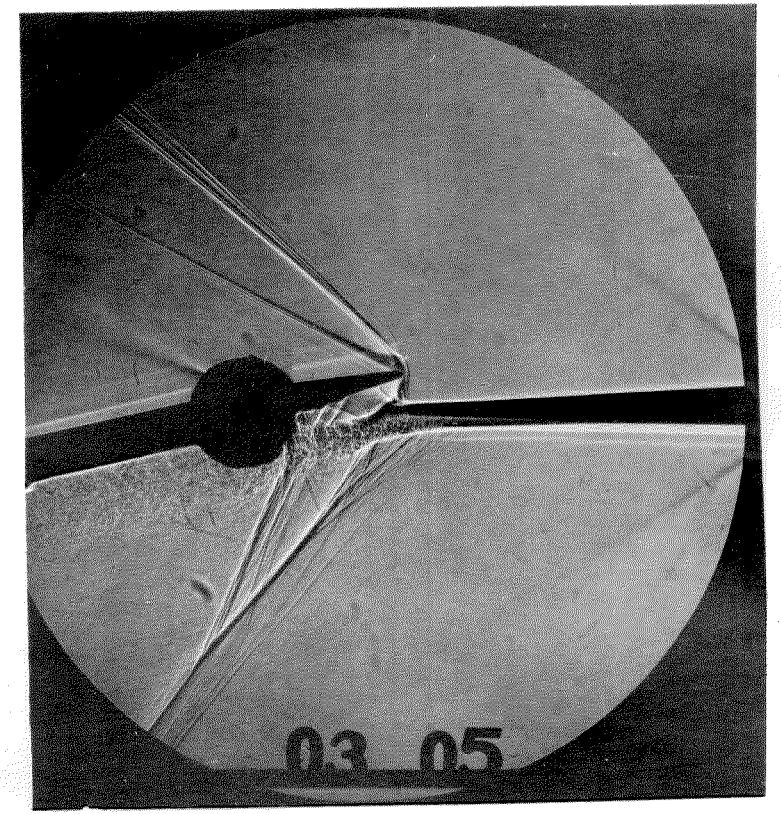

Figure 67. Shadowgraph, Control Surface Model, M = 1.70, RN/L = 0.37×10^6, $\alpha = -4^\circ$, $\delta = 12^\circ$

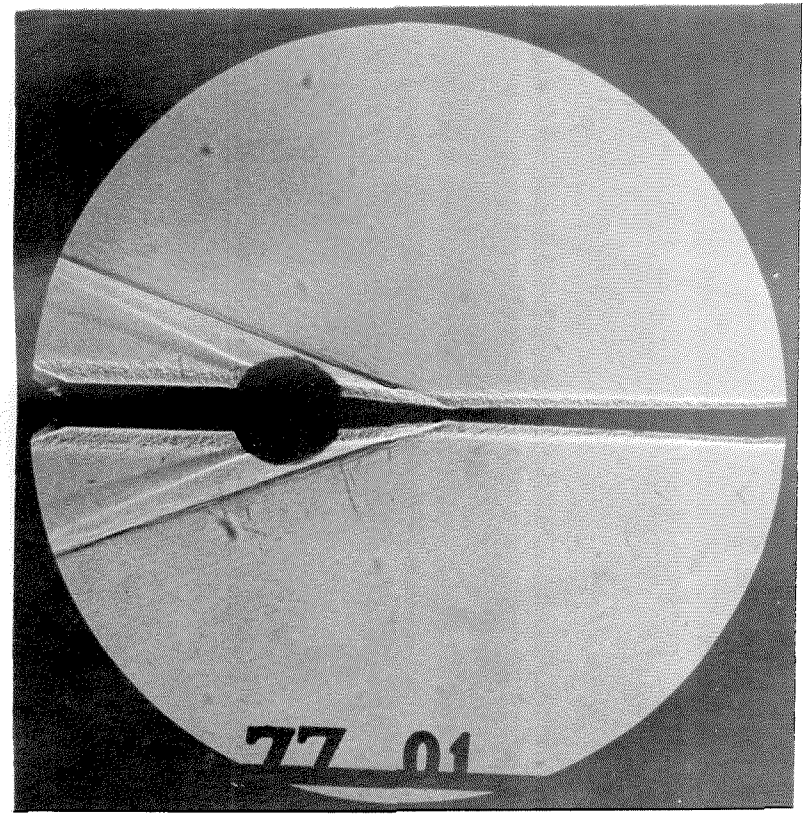

Figure 68. Shadowgraph, Control Surface Model, Turbulent Flow, 10" Wing, M = 3.52, RN/L = 0.57 x 10^6, $\alpha = 0^o$, $\delta = 0^o$

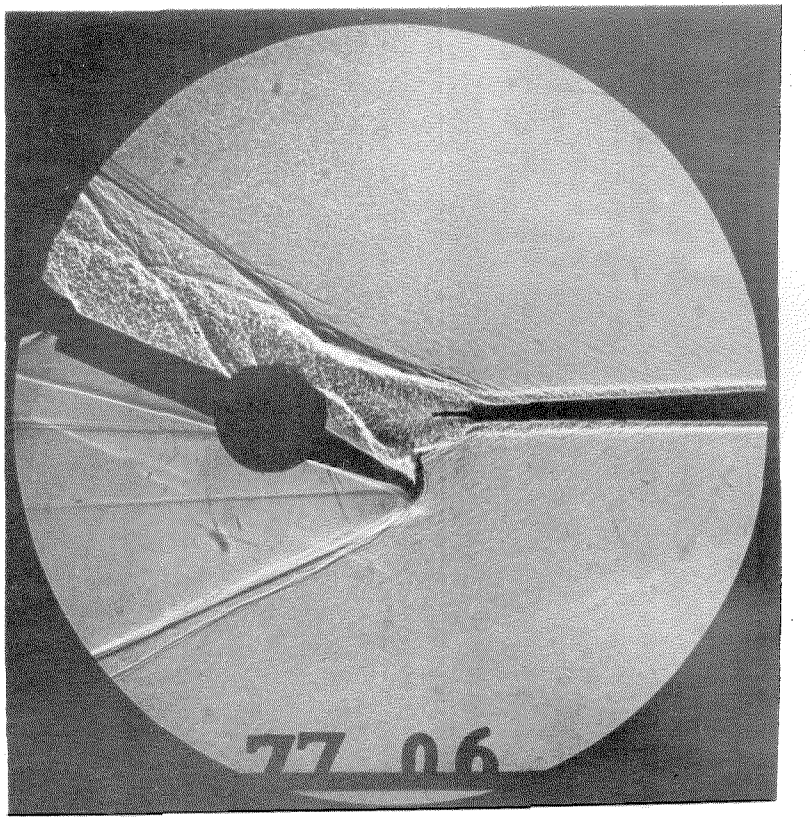

Figure 69. Shadowgraph, Control Surface Model, Turbulent Flow, 10" Wing, M = 3.52, RN/L = 0.57 x 10^6, $\alpha = 0^o$, $\delta = -25^o$

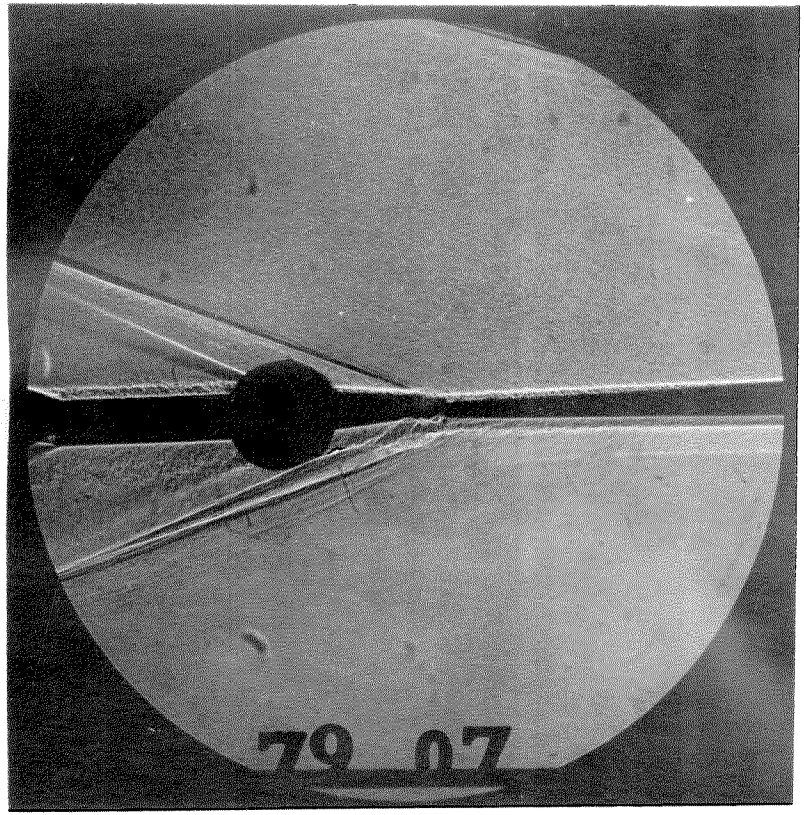

Figure 70. Shadowgraph, Control Surface Model, Turbulent Flow, 10" Wing, M = 3.52, RN/L = 0.56×10^6, $\alpha = -8^\circ$, $\delta = 0^\circ$

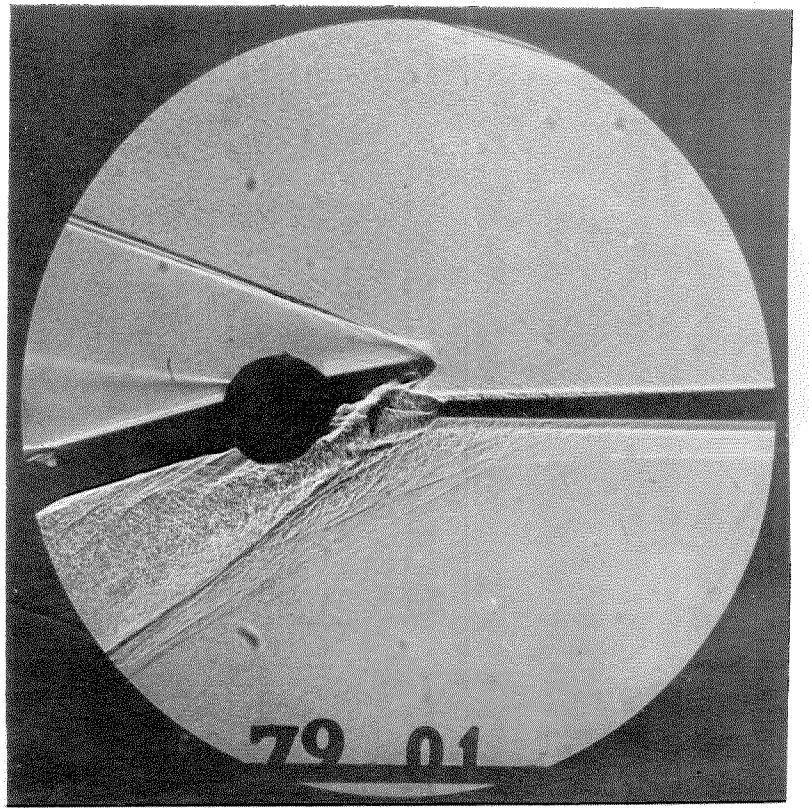

Figure 71. Shadowgraph, Control Surface Model, Turbulent Flow, 10" Wing, M = 3.52, RN/L = 0.56×10^6, $\alpha = -8^\circ$, $\delta = 15^\circ$

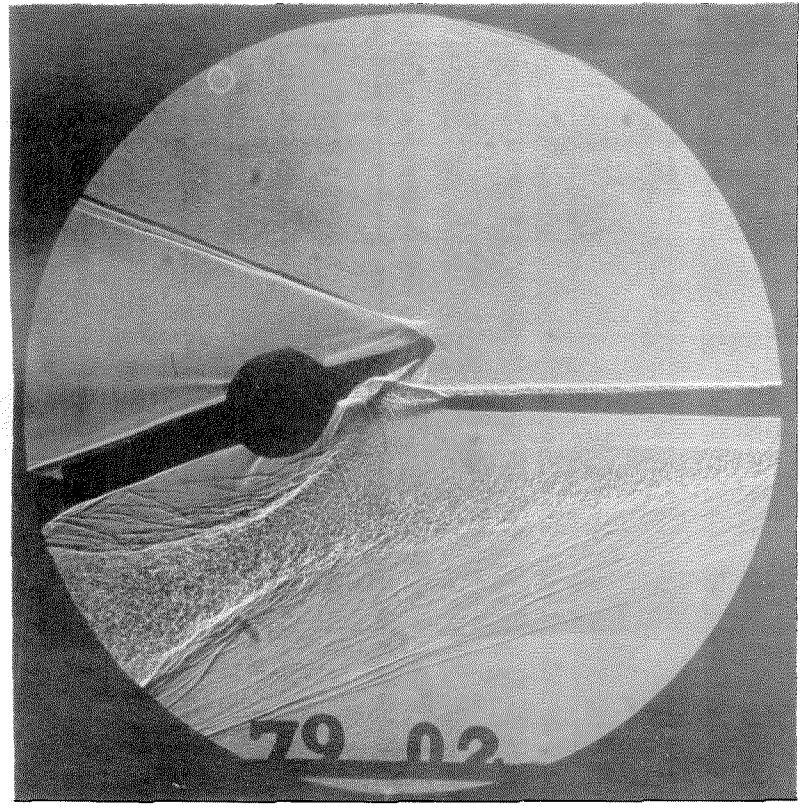

Figure 72. Shadowgraph, Control Surface Model, Turbulent Flow, 10" Wing, M = 3.52, RN/L = 0.56 x 10^6, α = -8°, δ = 20°

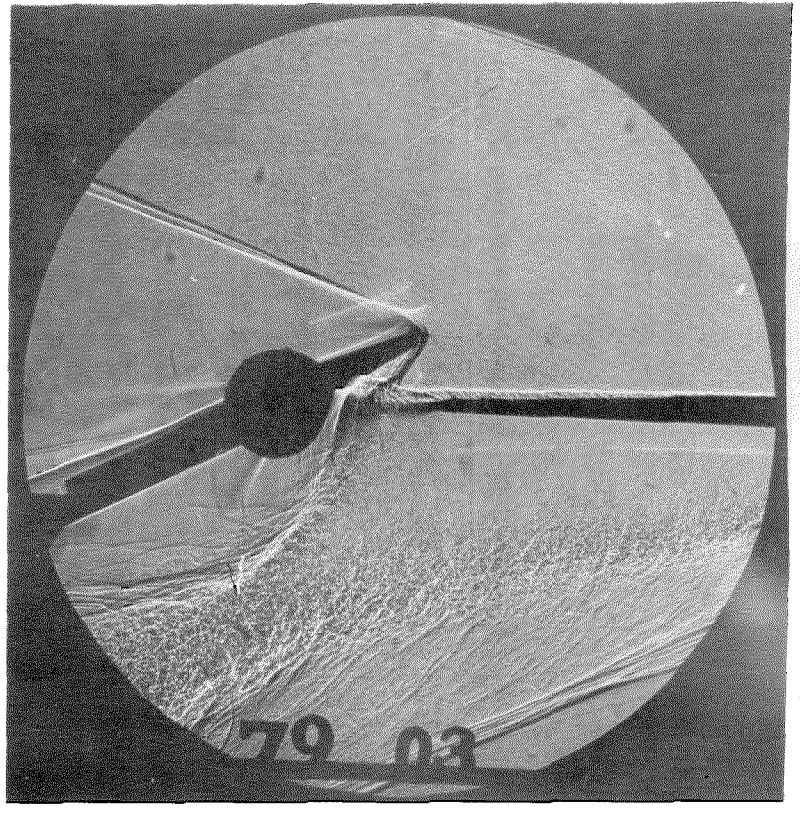

Figure 73. Shadowgraph, Control Surface Model, Turbulent Flow, 10" Wing, M = 3.52, RN/L = 0.56 x 10^6, α = -8°, δ = 25°

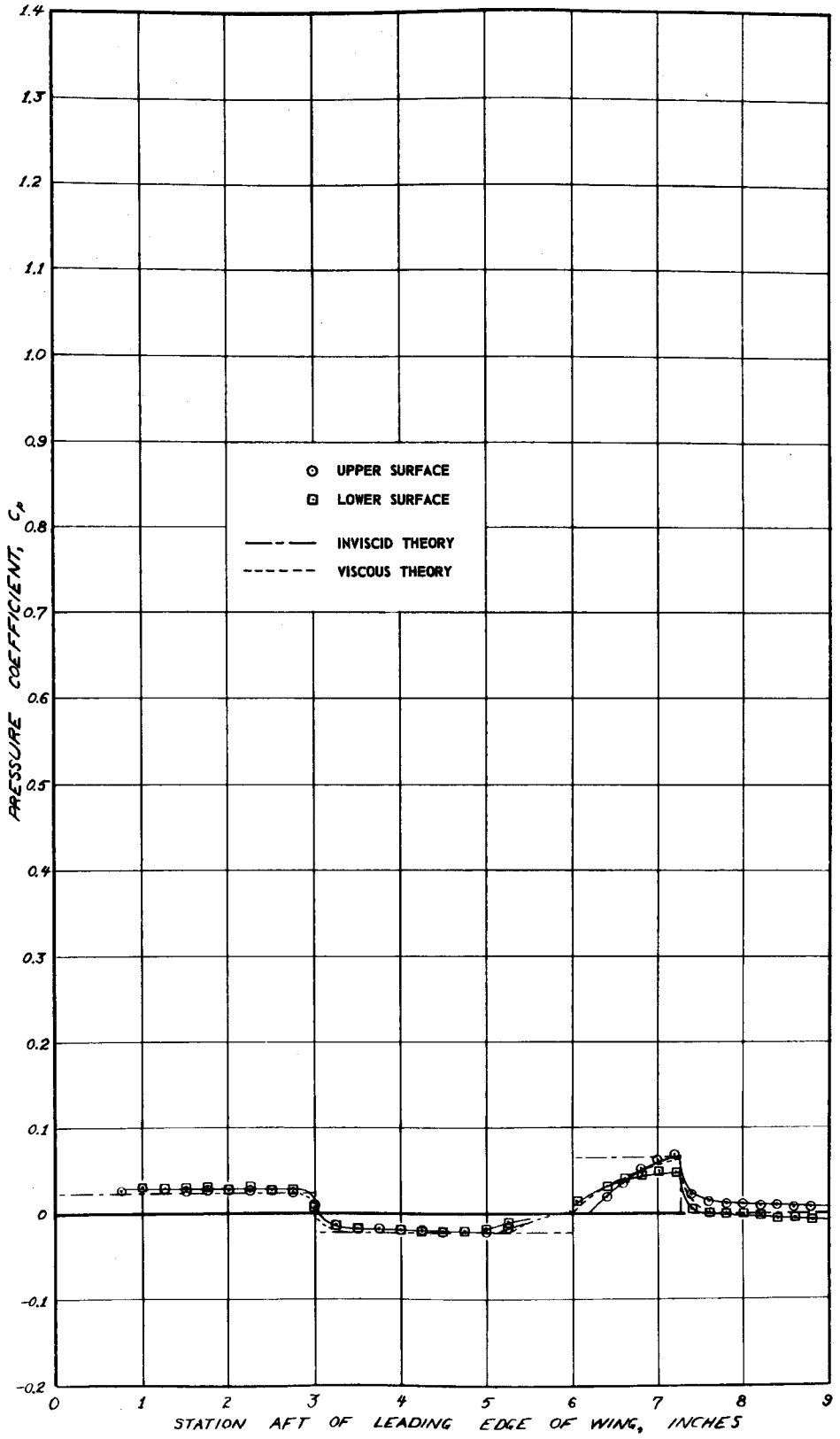

Figure 74. Pressure Distribution, M = 3.52, RN/L = 0.54×10^6, $\alpha = 0^\circ$, $\delta = 0^\circ$

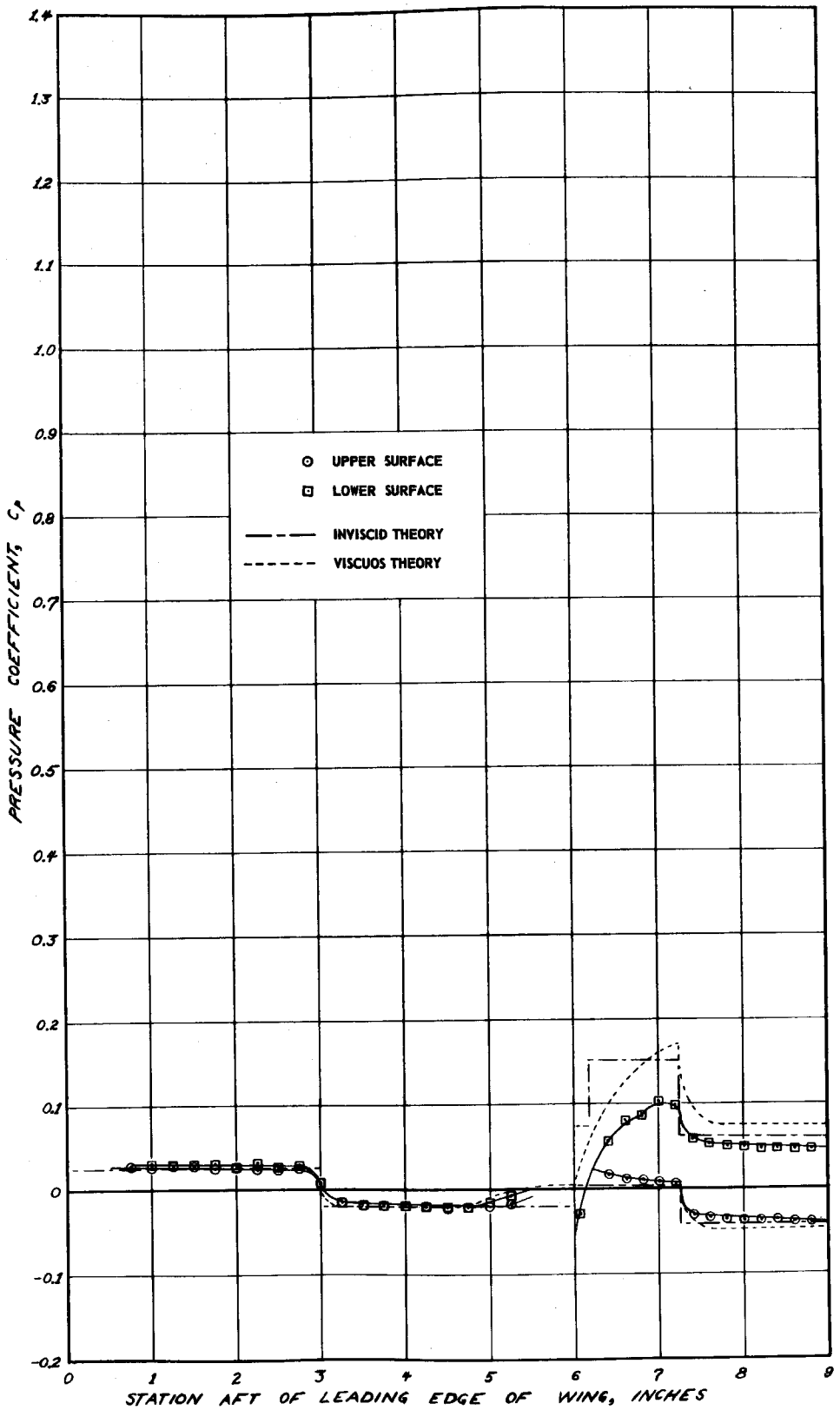

Figure 75. Pressure Distribution, M = 3.52, RN/L = 0.54×10^6, $\alpha = 0^\circ$, $\delta = 5^\circ$

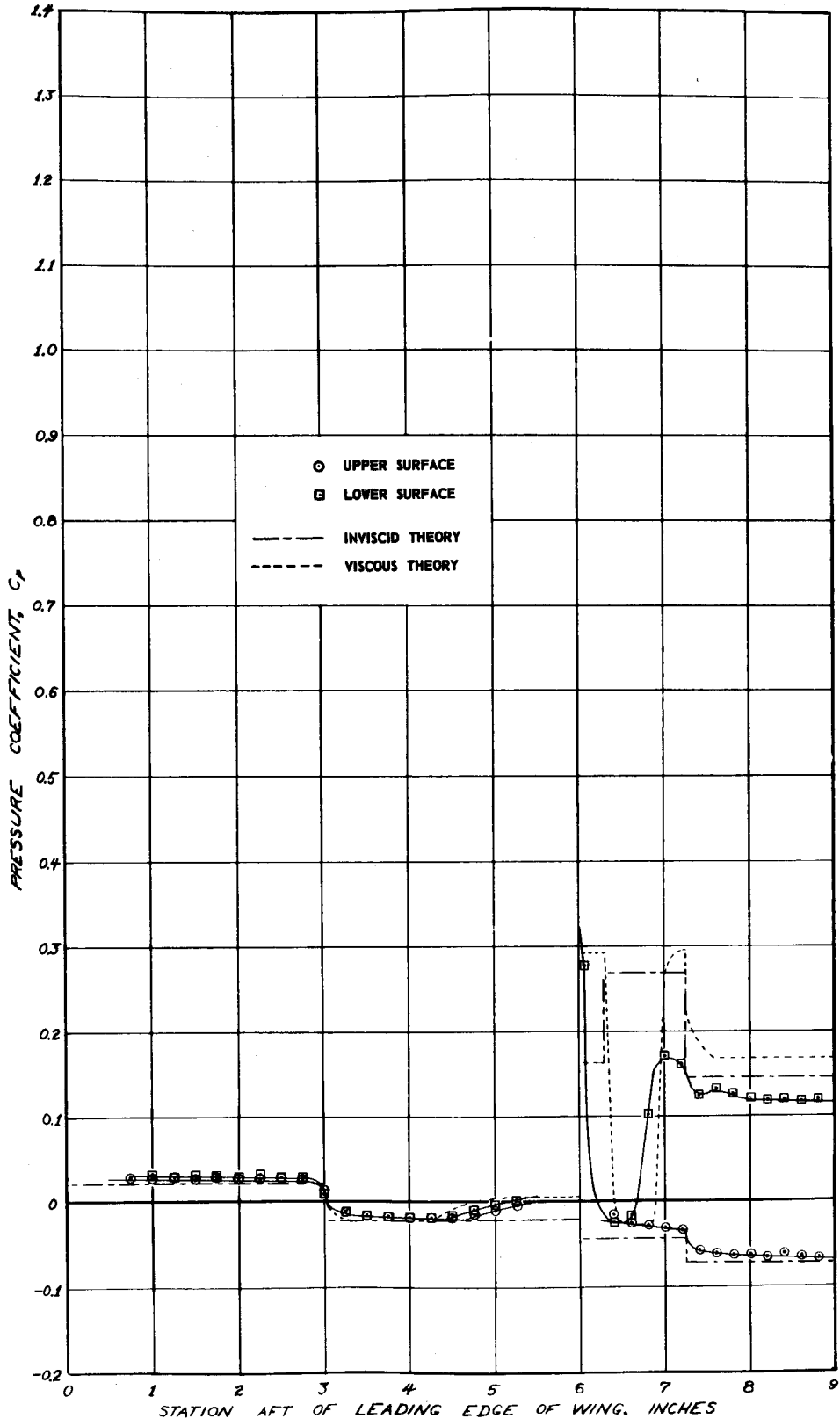

Figure 76. Pressure Distribution, M = 3.52, RN/L = 0.54×10^6, $\alpha = 0^\circ$, $\delta = 10^\circ$

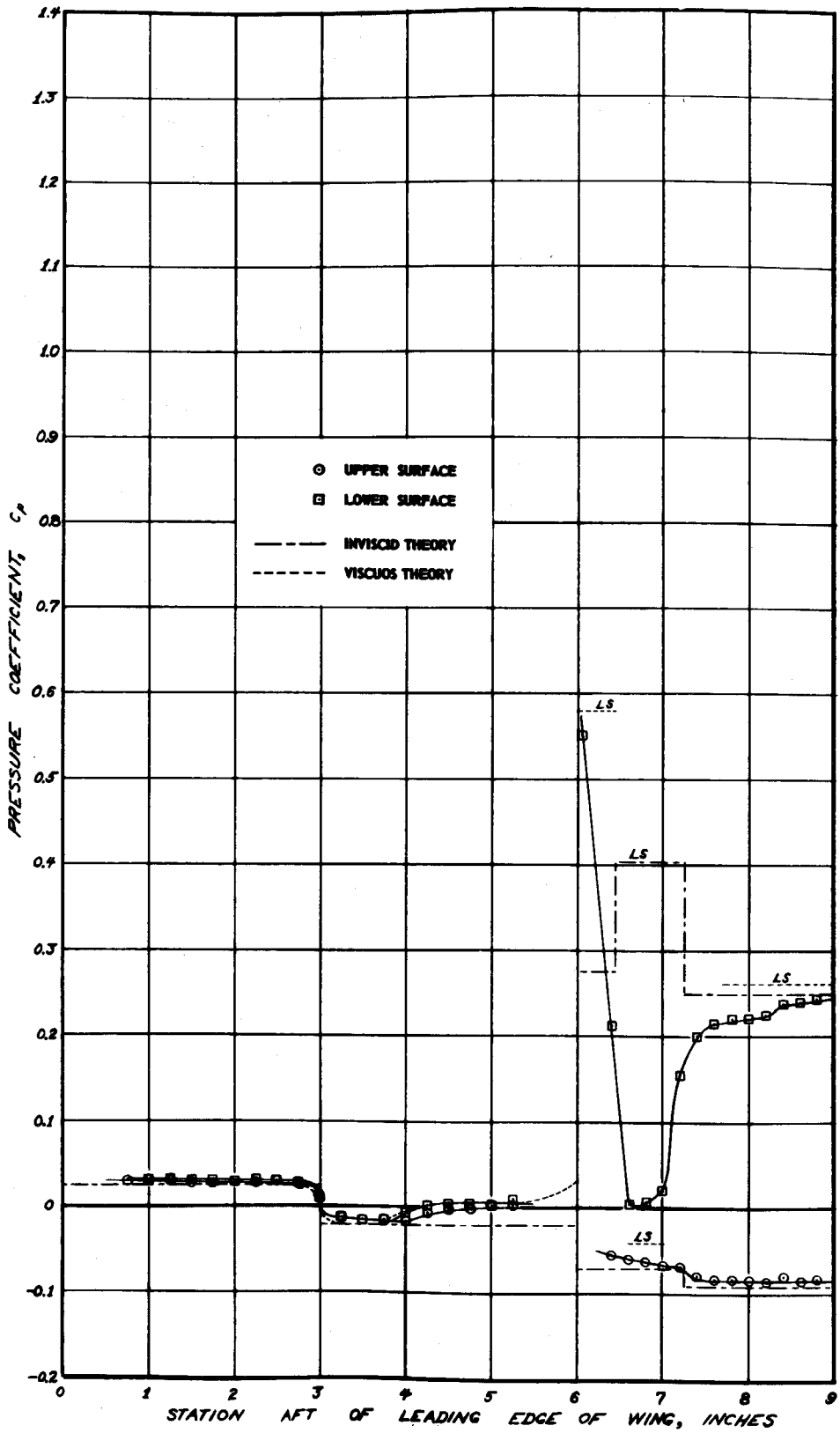

Figure 77. Pressure Distribution, M = 3.52, RN/L = 0.54×10^6, $\alpha = 0^\circ$, $\delta = 15^\circ$

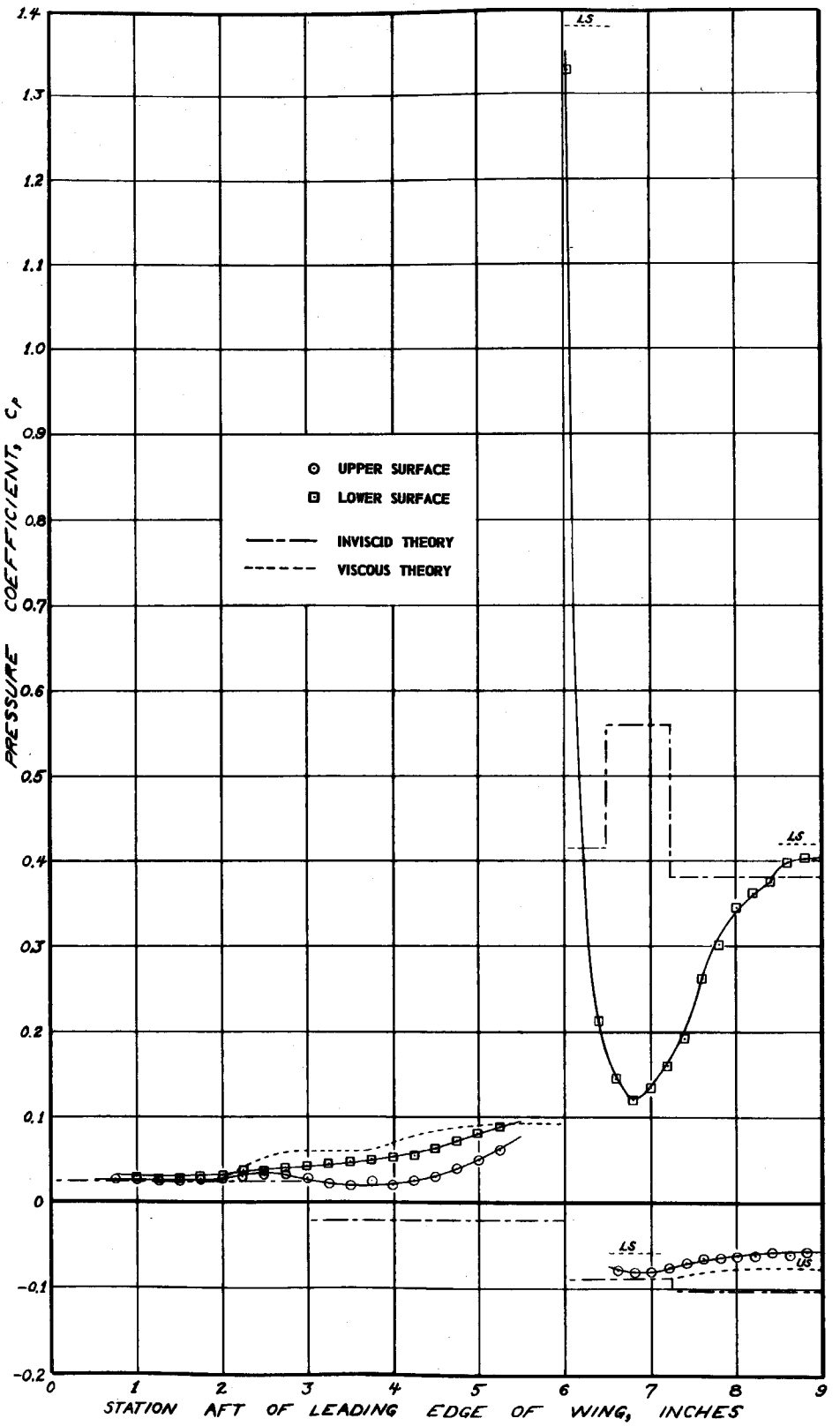

Figure 78. Pressure Distribution, M = 3.52, RN/L = 0.54×10^6, $\alpha = 0^\circ$, $\delta = 20^\circ$

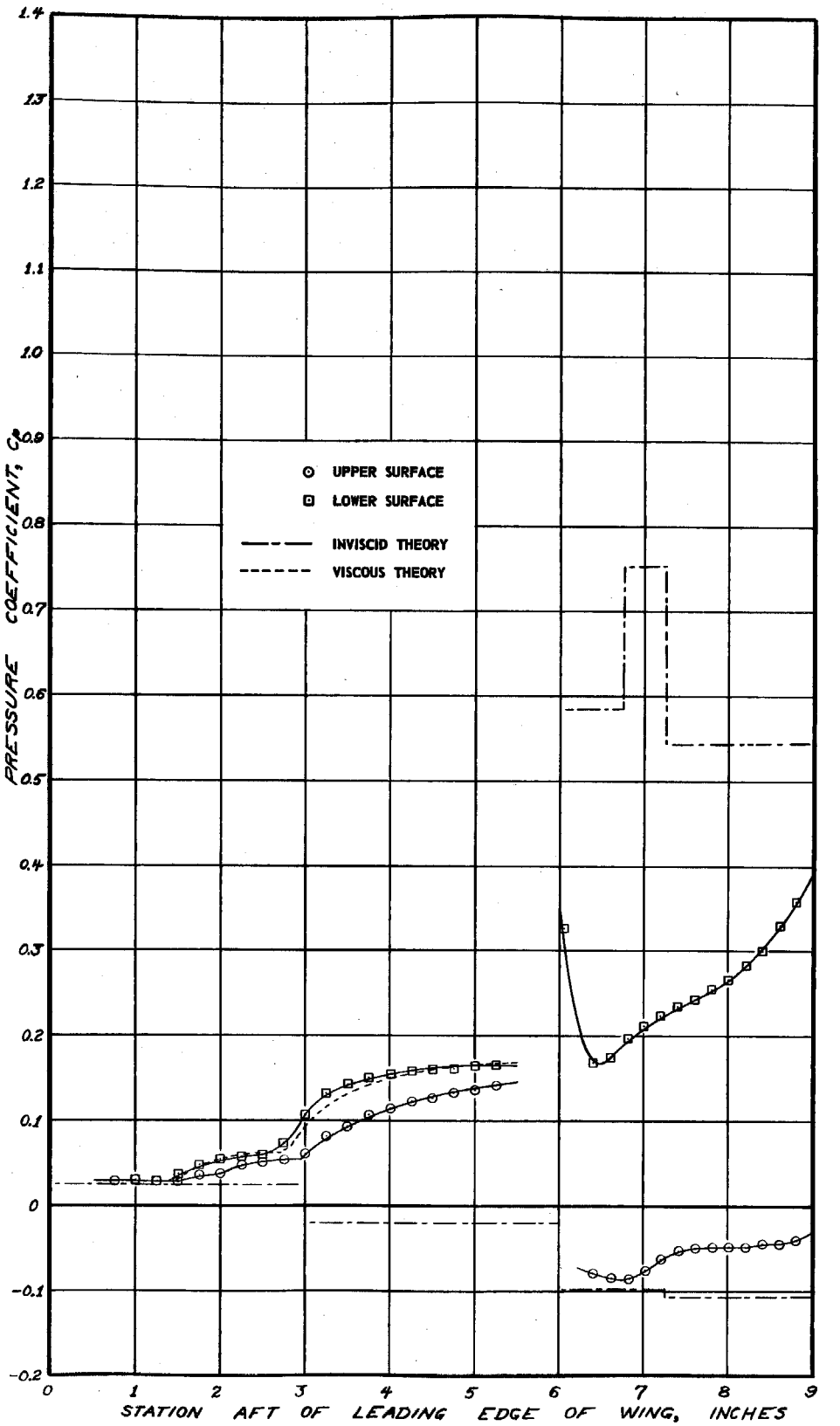

Figure 79. Pressure Distribution, M = 3.52, RN/L = 0.54×10^6, $\alpha = 0^\circ$, $\delta = 25^\circ$

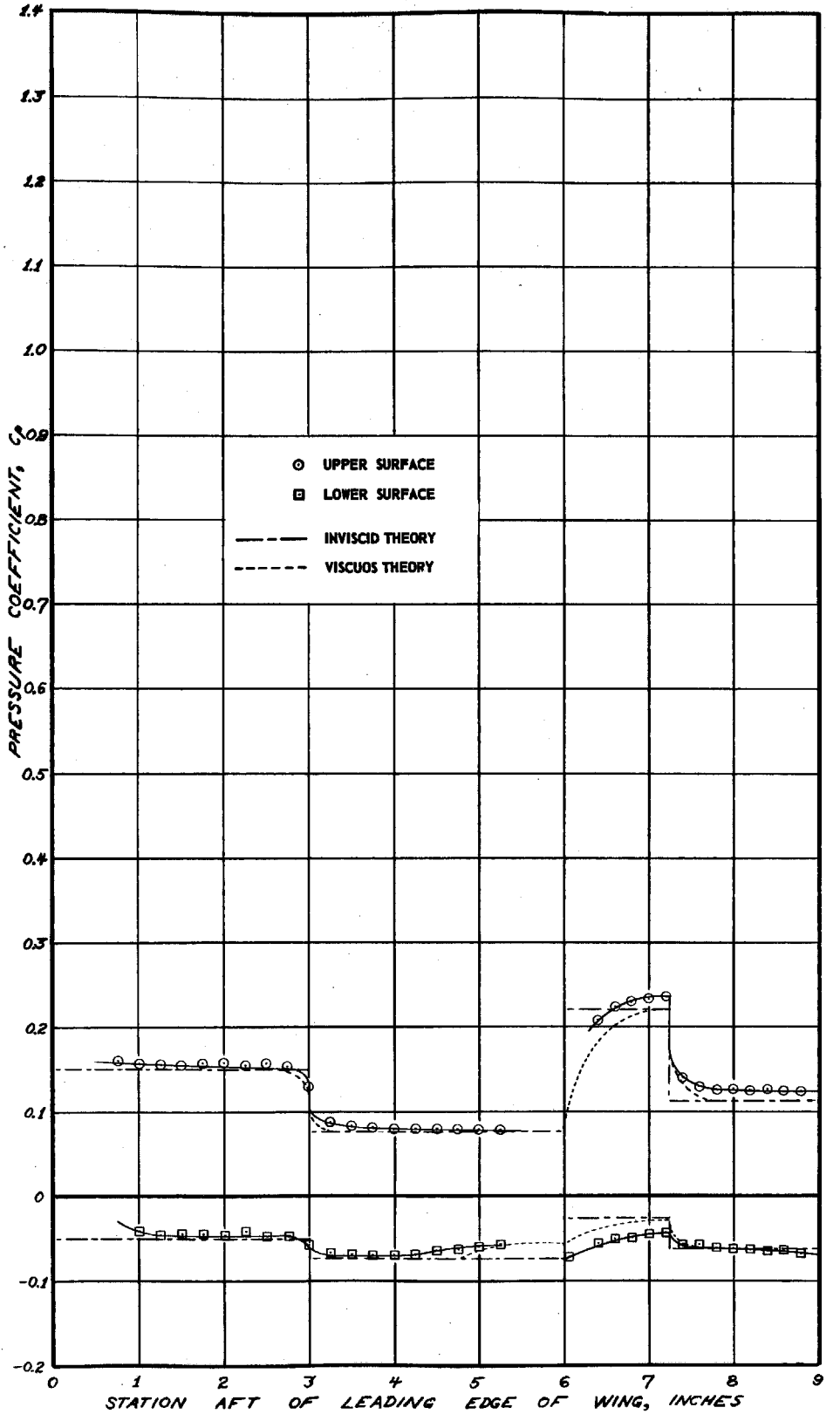

Figure 80. Pressure Distribution, M = 3.52, RN/L = 0.54×10^6, $\alpha = -8^o$, $\delta = 0^o$

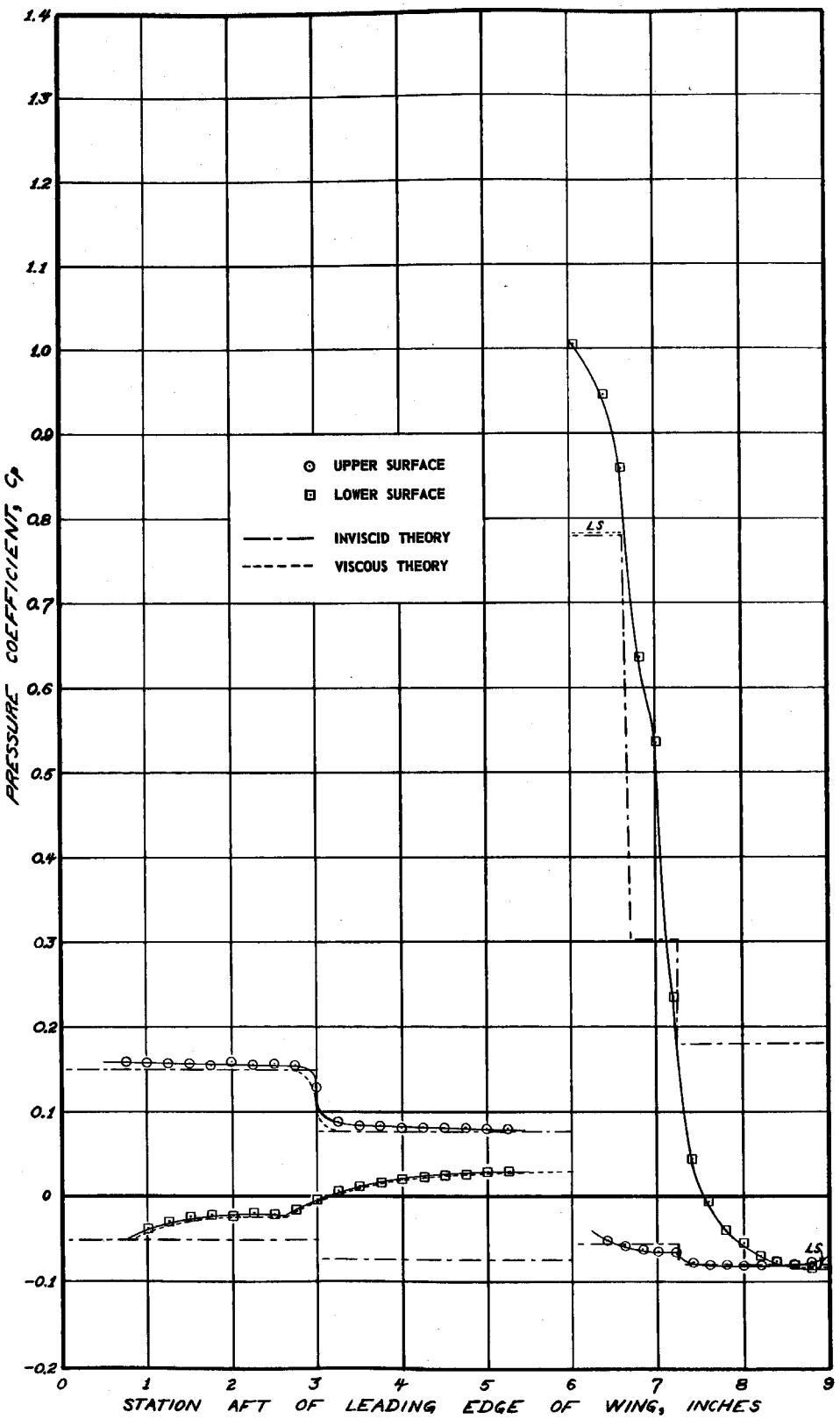

Figure 81. Pressure Distribution, M = 3.52, RN/L = 0.54×10^6, $\alpha = -8^\circ$, $\delta = 20^\circ$

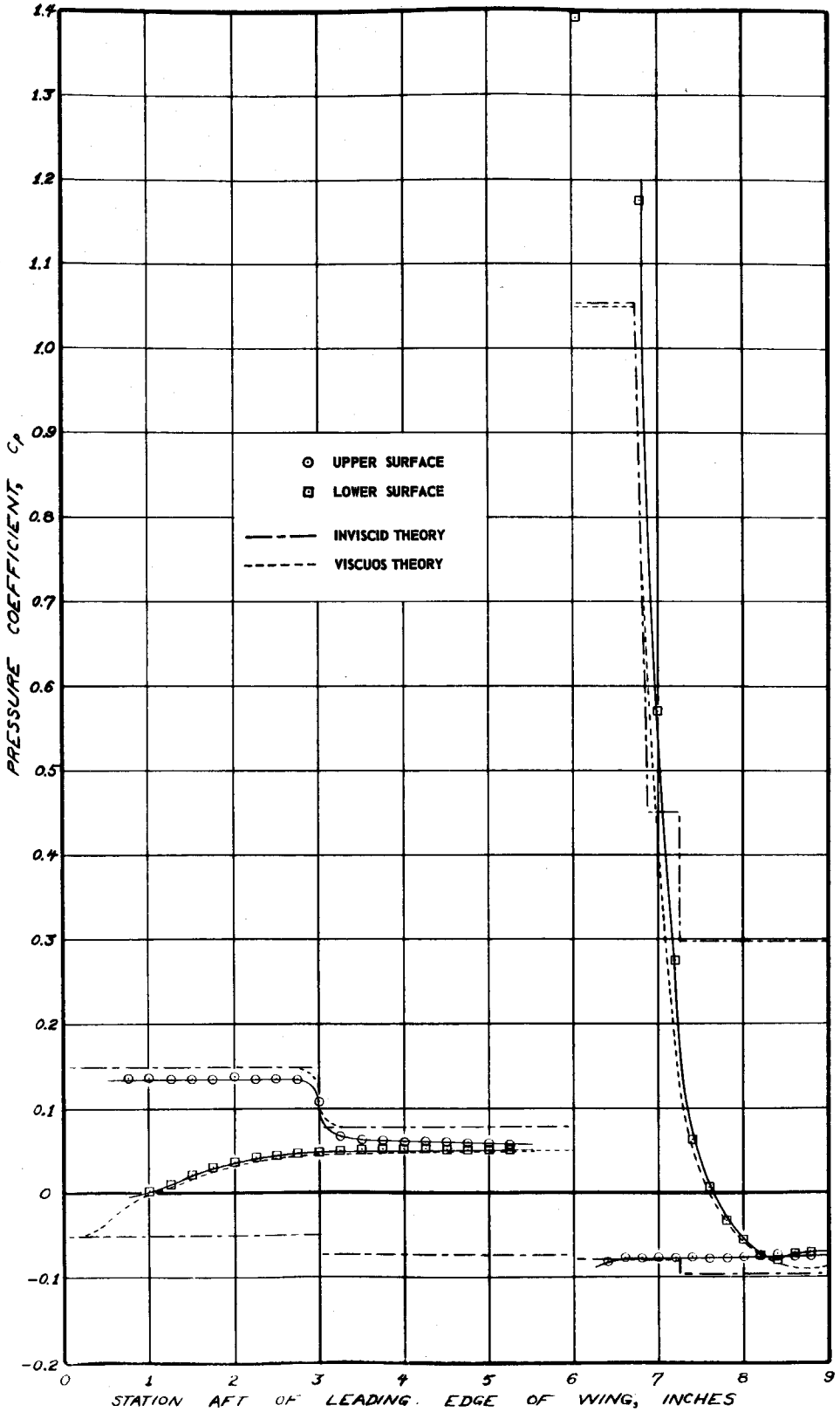

Figure 82. Pressure Distribution, M = 3.52, RN/L = 0.54×10^6, $\alpha = -8^\circ$, $\delta = 25^\circ$

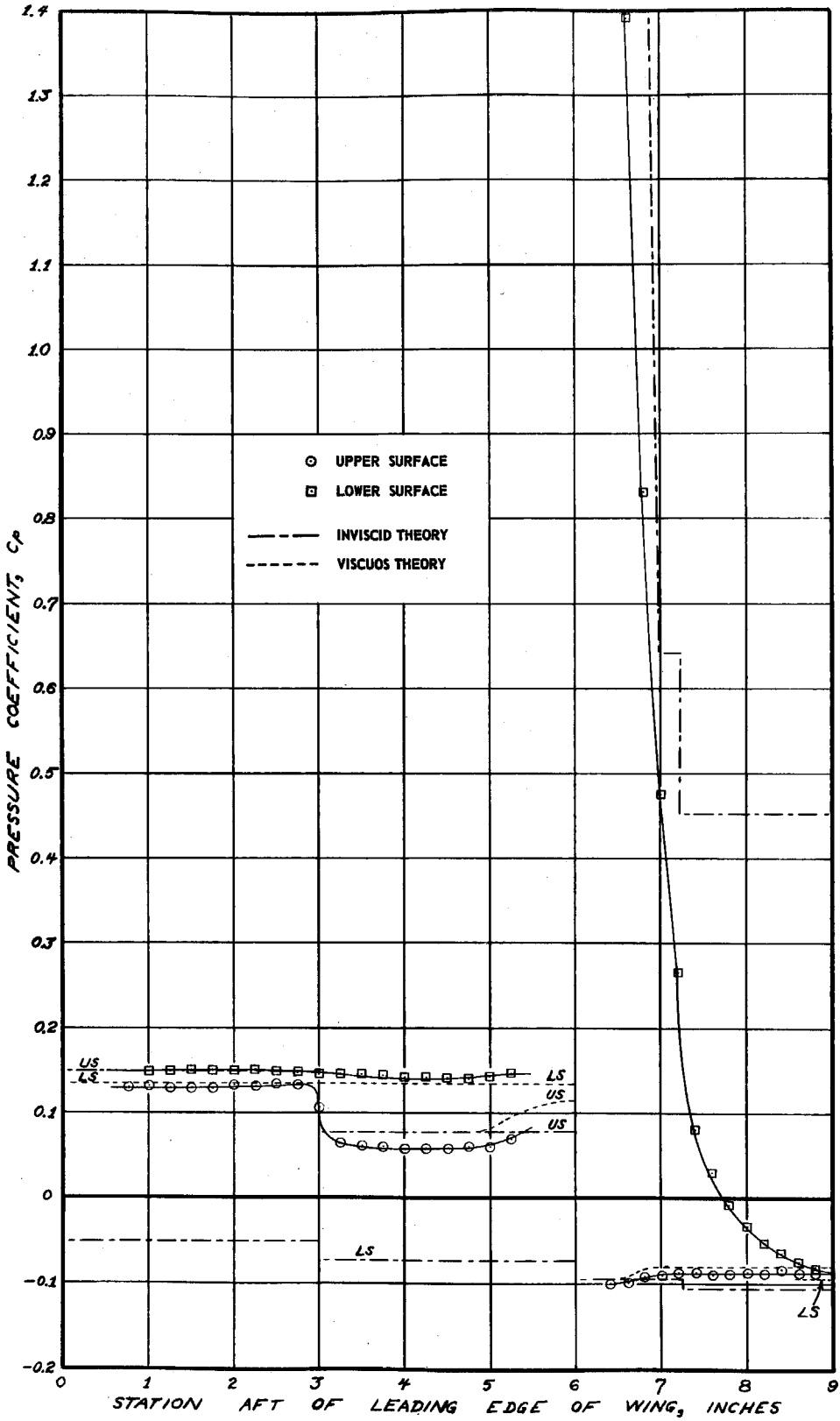

Figure 83. Pressure Distribution, M = 3.52, RN/L = 0.54×10^6, $\alpha = -8^\circ$, $\delta = 30^\circ$

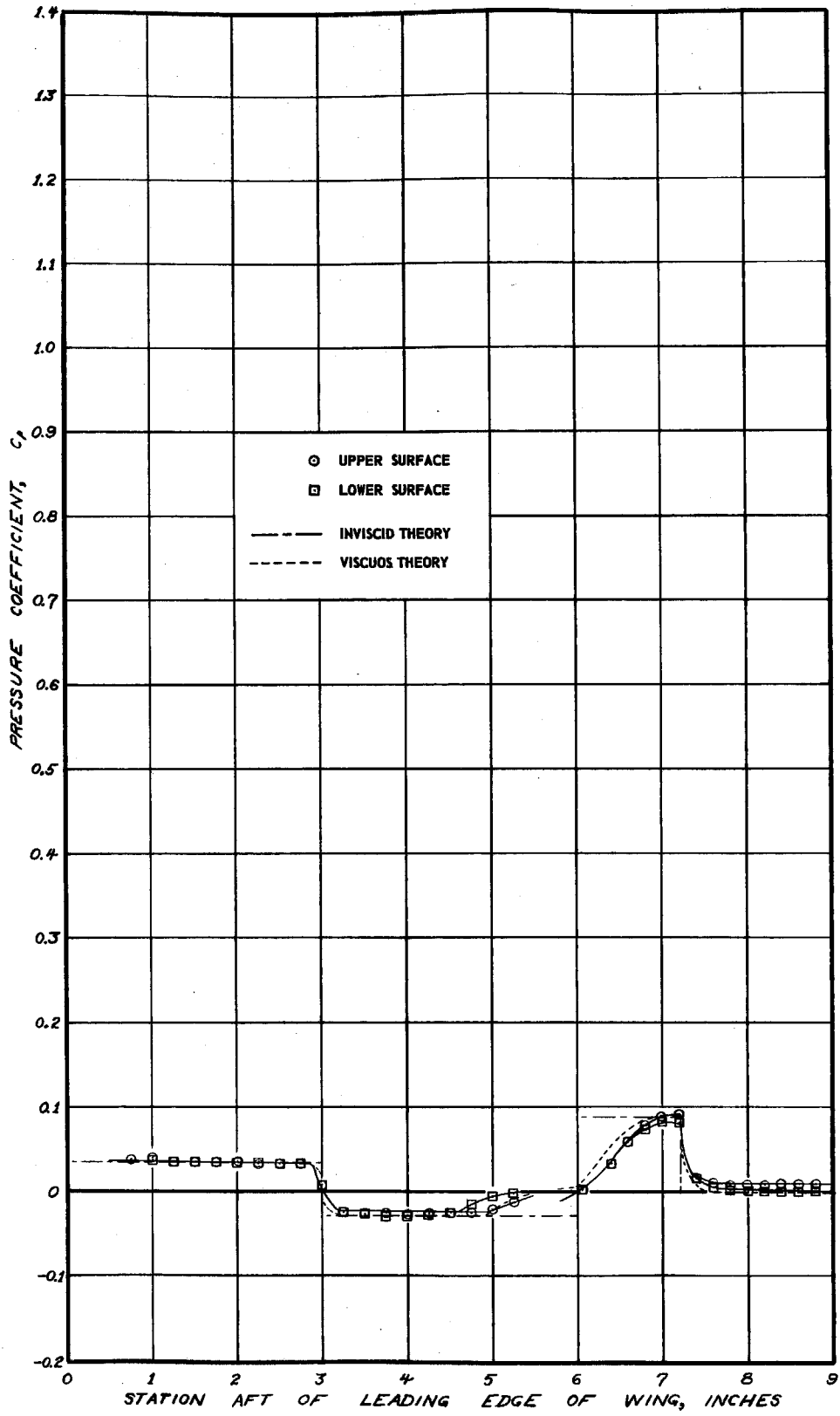

Figure 84. Pressure Distribution, M = 2.60, RN/L = 0.41×10^6, $\alpha = 0^\circ$, $\delta = 0^\circ$

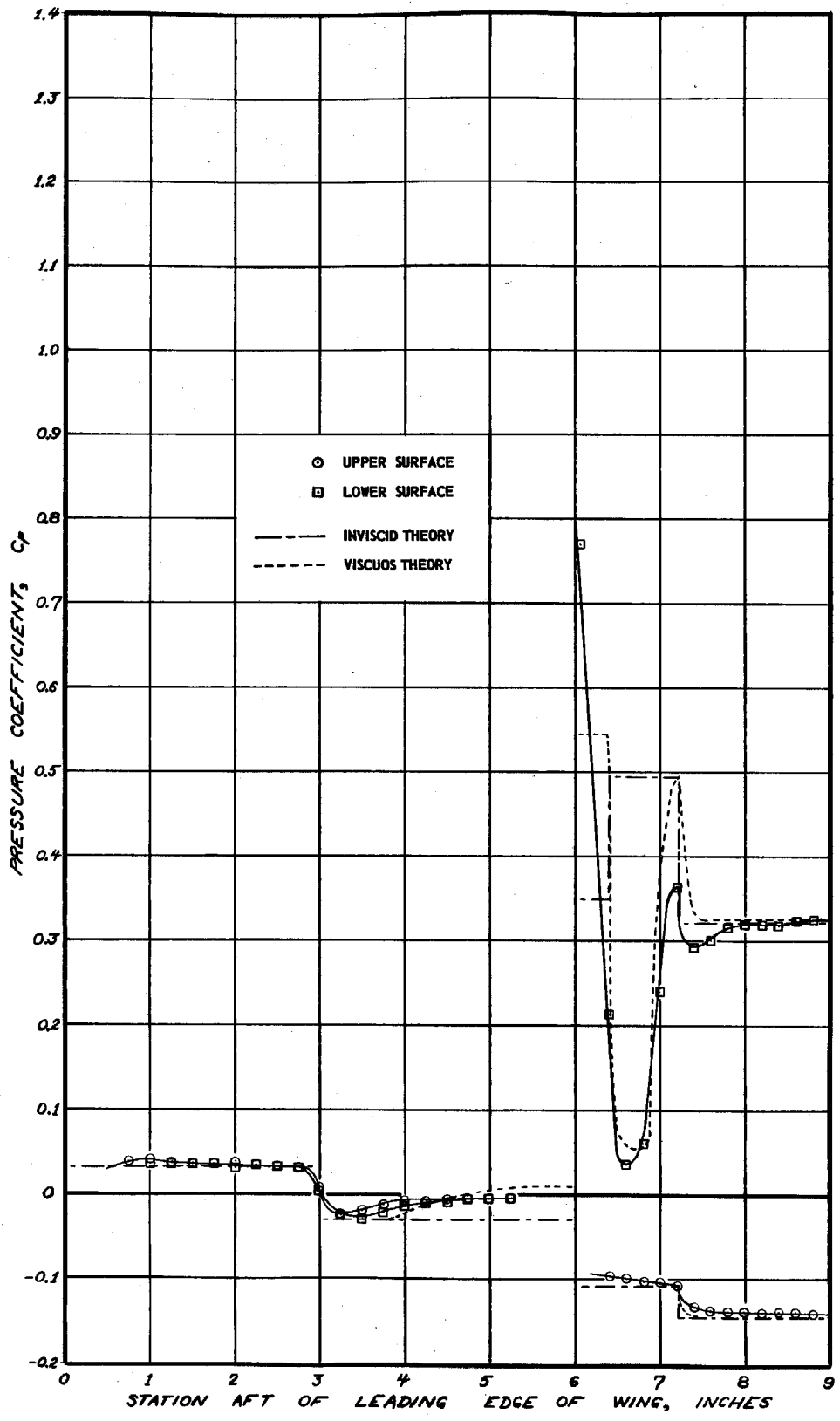

Figure 85. Pressure Distribution, M = 2.60, RN/L = 0.41×10^6, $\alpha = 0^\circ$, $\delta = 15^\circ$

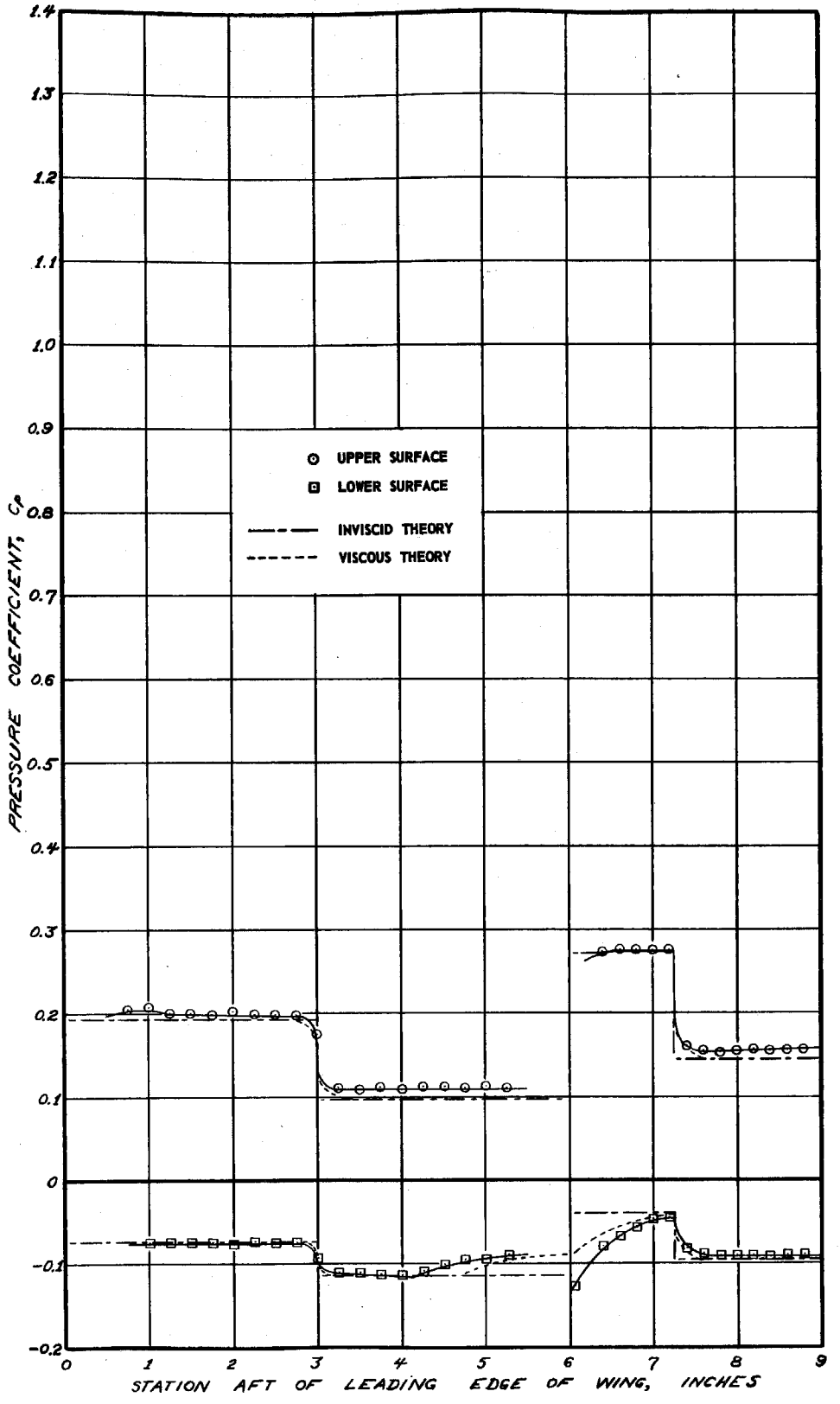

Figure 86. Pressure Distribution, M = 2.60, RN/L = 0.41×10^6, $\alpha = -8^\circ$, $\delta = 0^\circ$

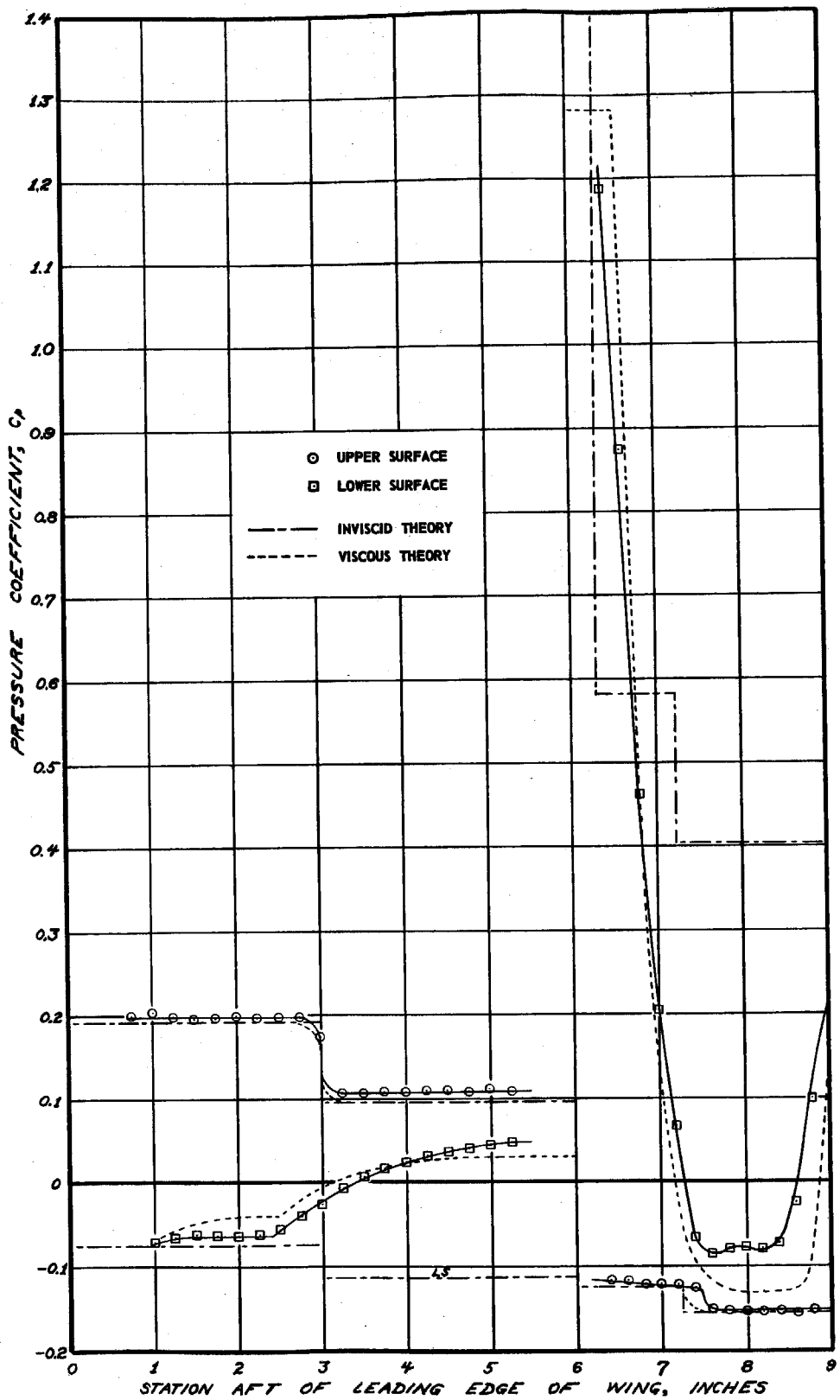

Figure 87. Pressure Distribution, M = 2.60, RN/L = 0.41×10^6, $\alpha = -8^\circ$, $\delta = 25^\circ$

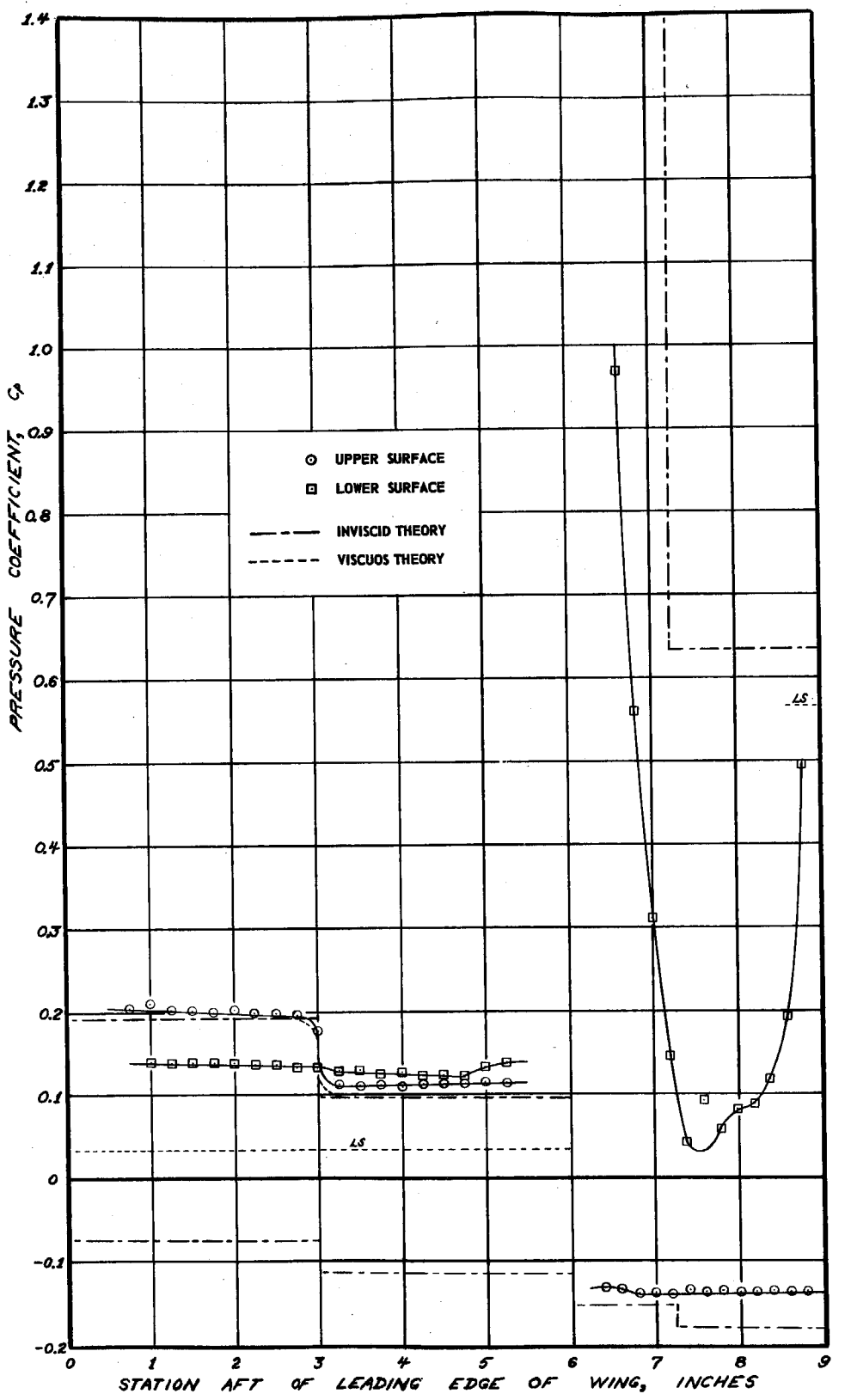

Figure 88. Pressure Distribution, M = 2.60, RN/L = 0.41×10^6, $\alpha = -8^\circ$, $\delta = 30^\circ$

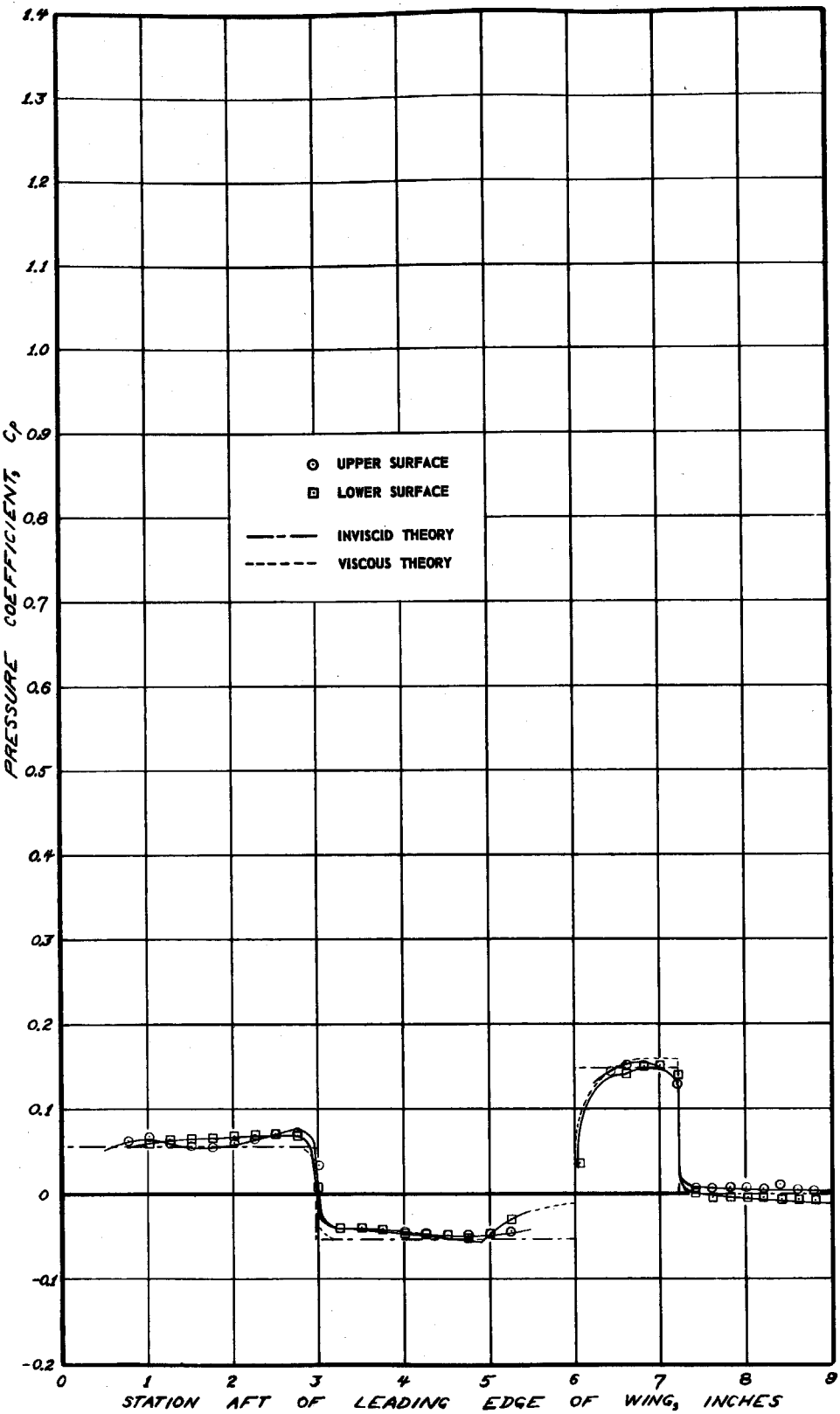

Figure 89. Pressure Distribution, M = 1.70, RN/L = 0.37×10^6, $\alpha = 0^\circ$, $\delta = 0^\circ$

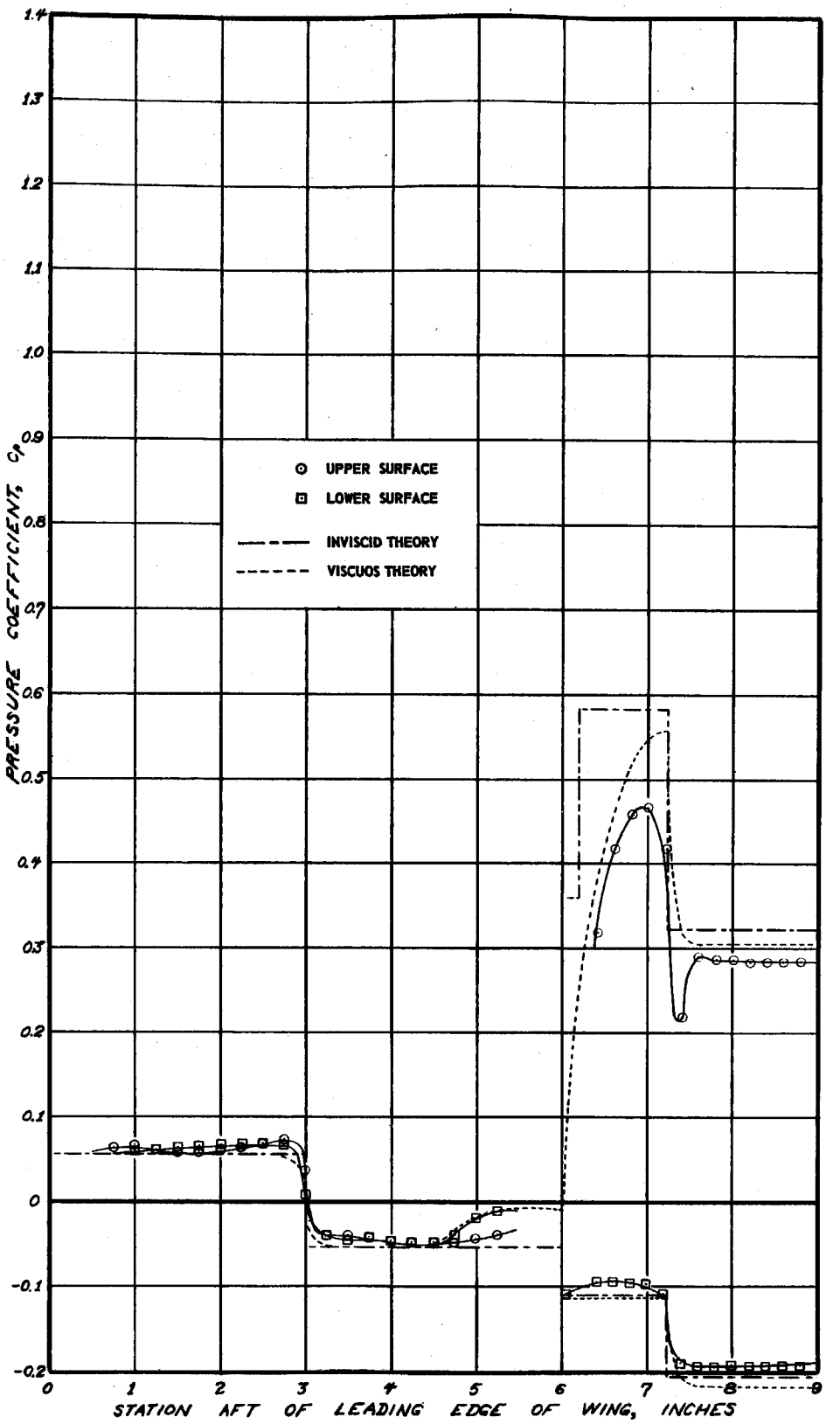

Figure 90. Pressure Distribution, M = 1.70, RN/L = 0.37×10^6, $\alpha = 0^\circ$, $\delta = -10^\circ$

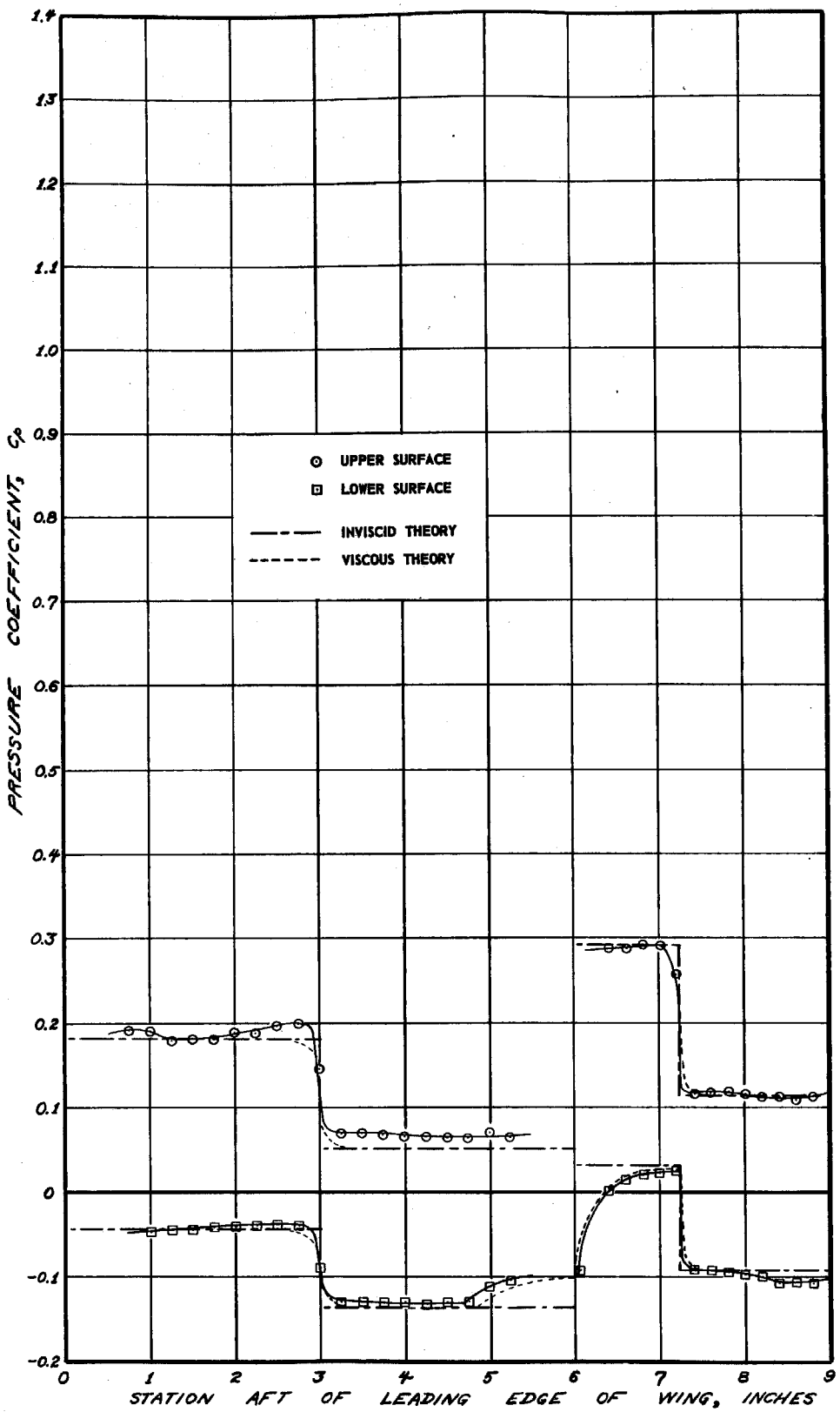

Figure 91. Pressure Distribution, M = 1.70, RN/L = 0.37×10^6, $\alpha = -4^o$, $\delta = 0^o$

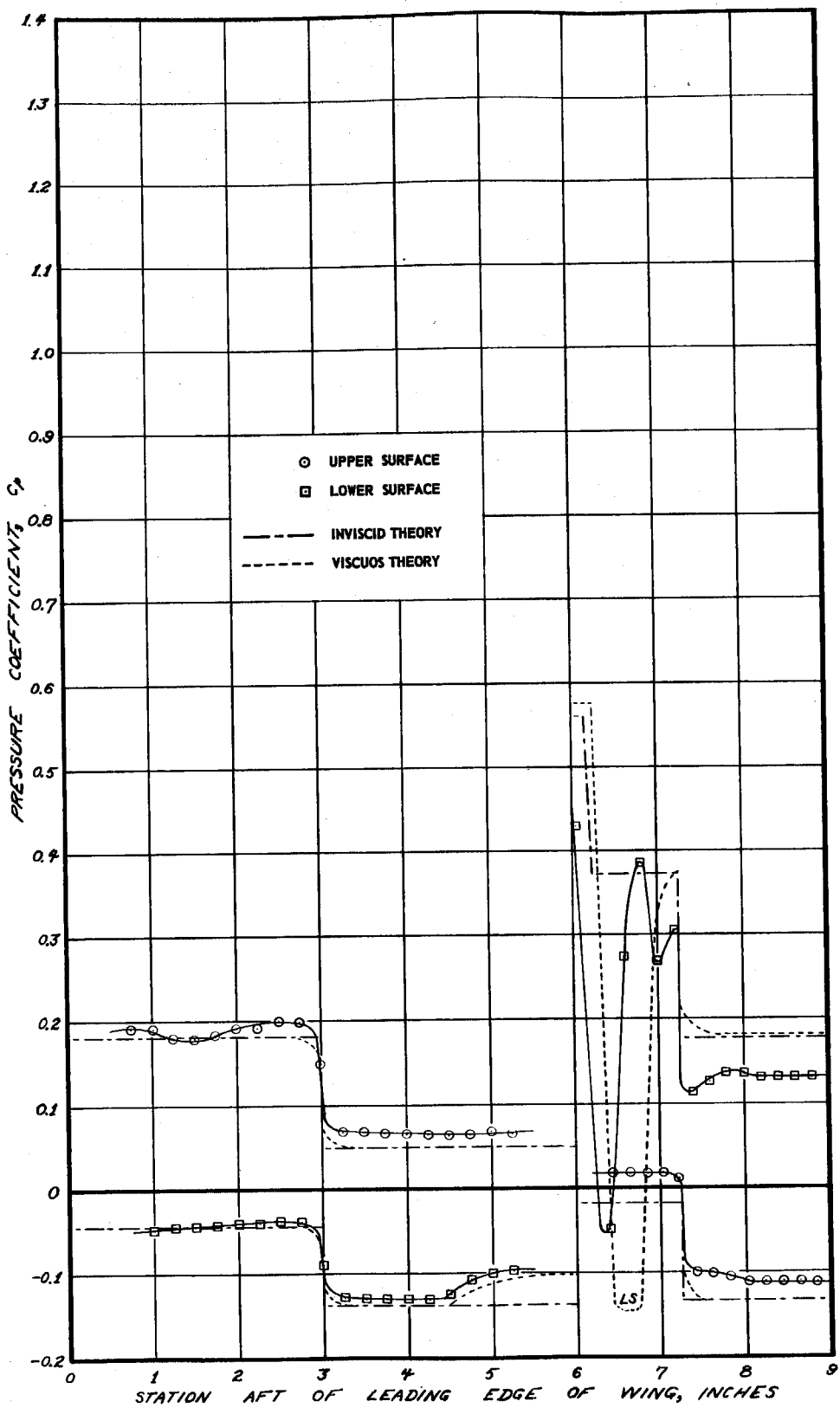

Figure 92. Pressure Distribution, M = 1.70, RN/L = 0.37×10^6, $\alpha = -4^\circ$, $\delta = 10^\circ$

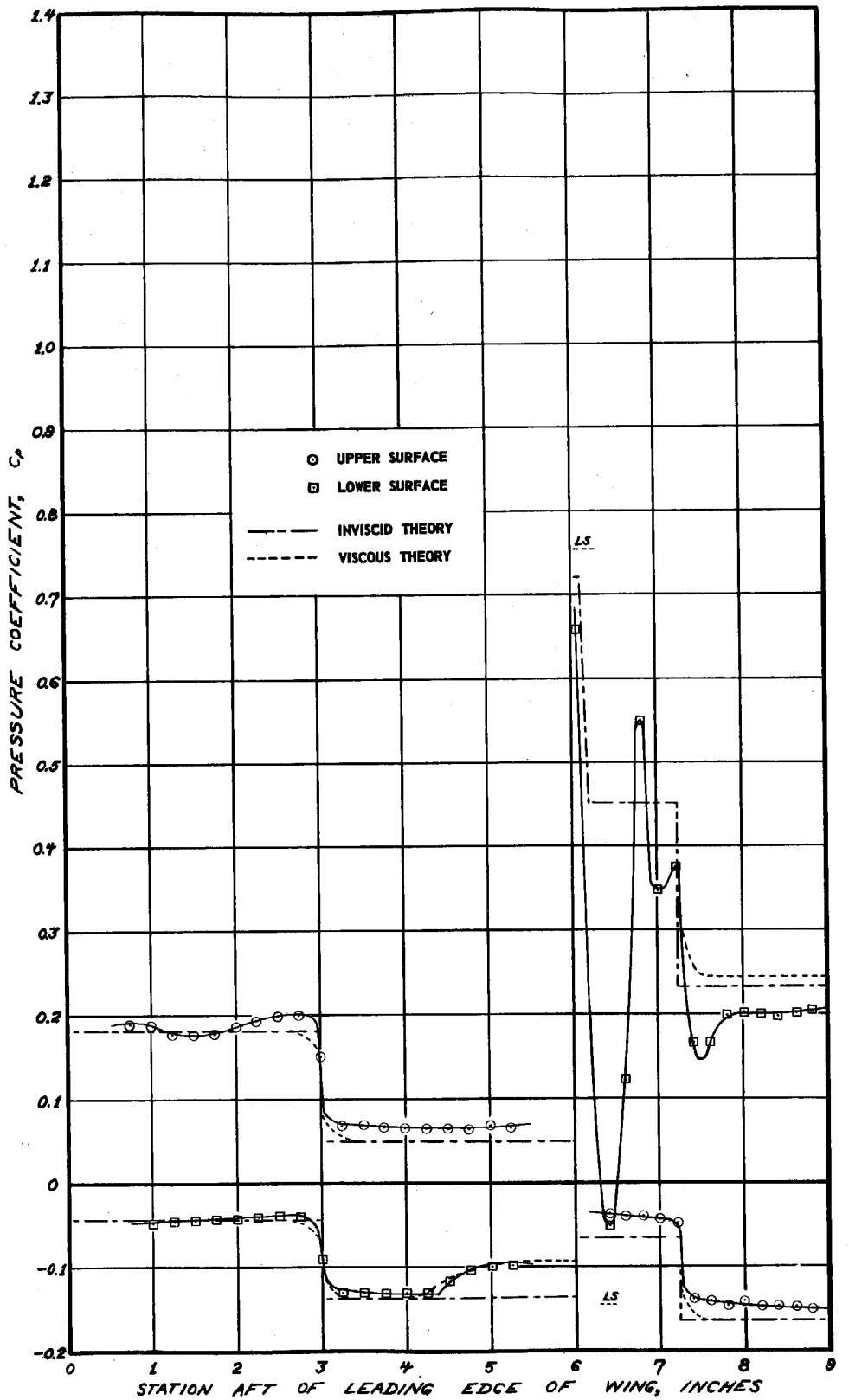

Figure 93. Pressure Distribution, M = 1.70, RN/L = 0.37×10^6, $\alpha = -4^\circ$, $\delta = 12^\circ$

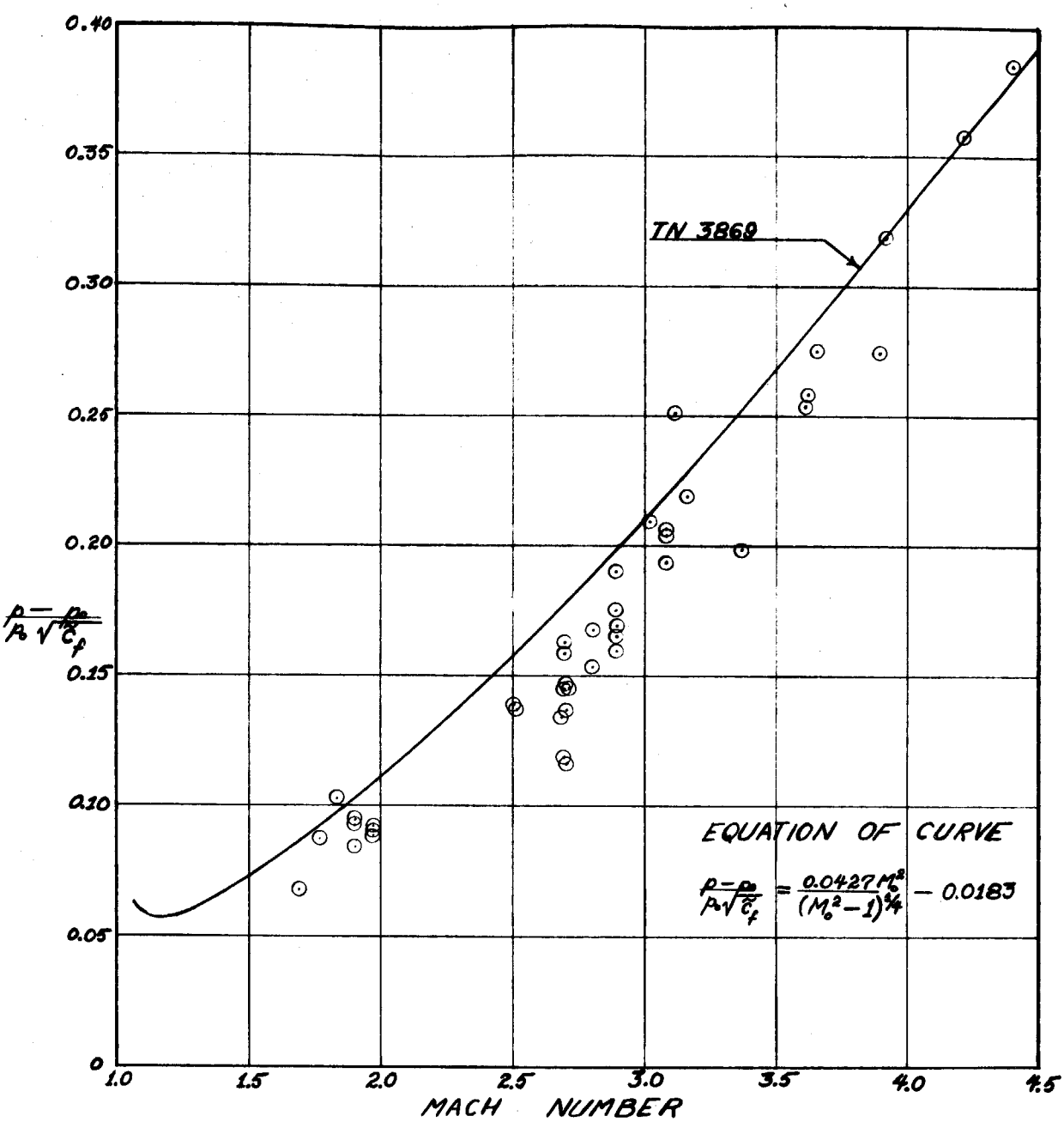

Figure 94. Pressure Rise Resulting from Shock Induced Separation of a Laminar Boundary Layer. Comparison of Results from the Current Tests with Those of Chapman, TN-3869

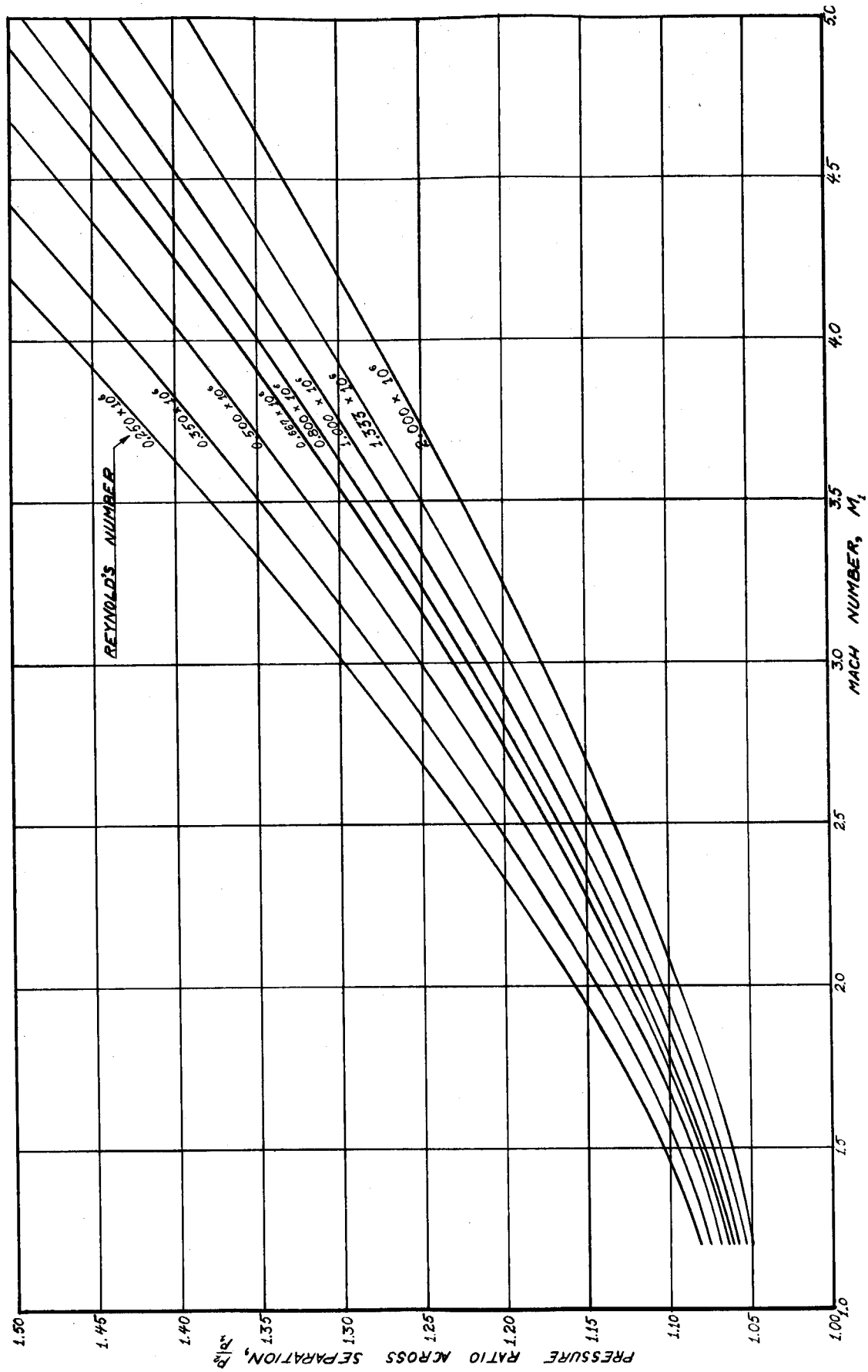

Figure 95. Pressure Rise Resulting from Shock Induced Separation of a Laminar Boundary Layer

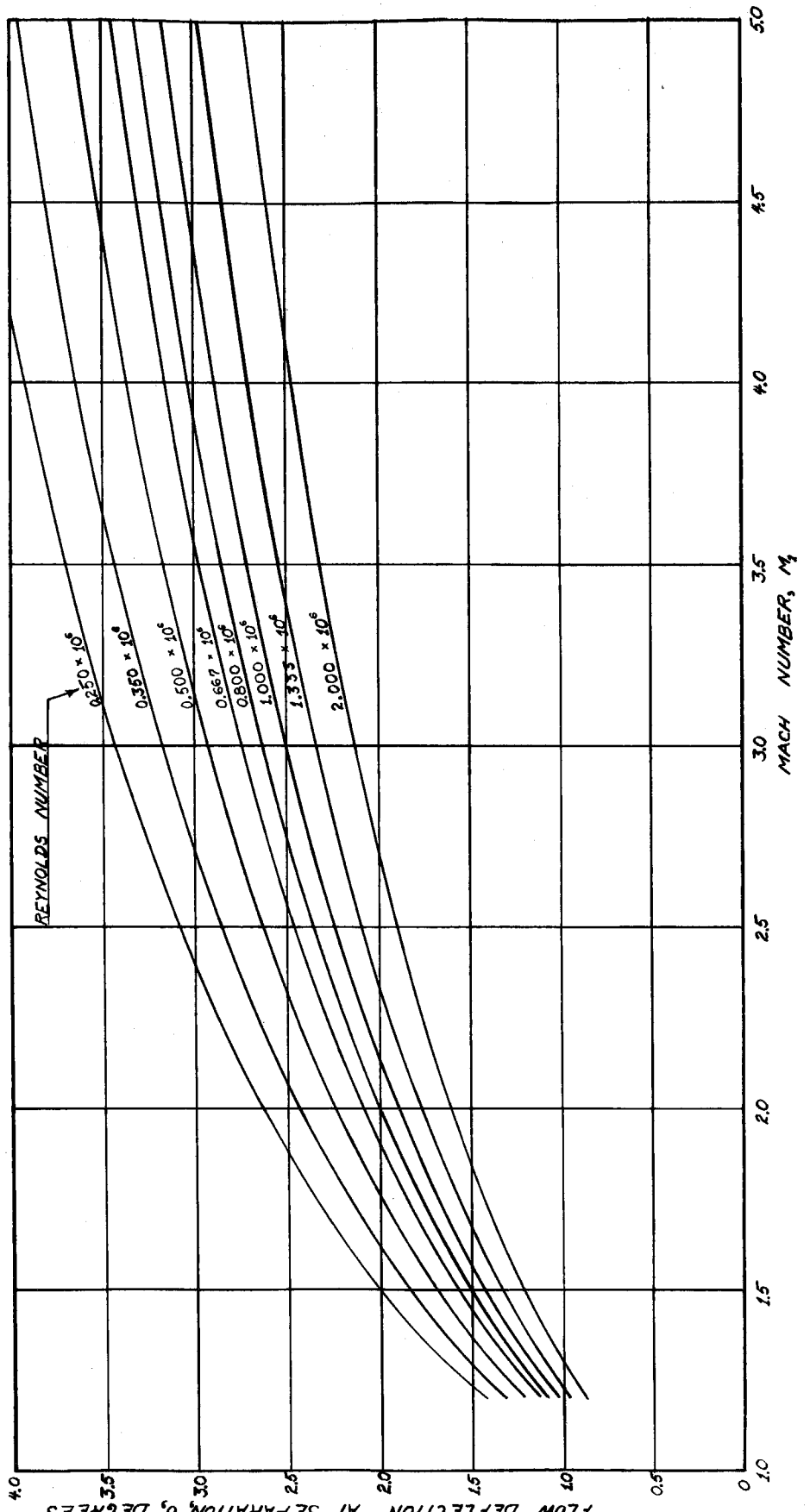

Figure 96. Flow Deflection Resulting from Shock Induced Separation of a Laminar Boundary Layer

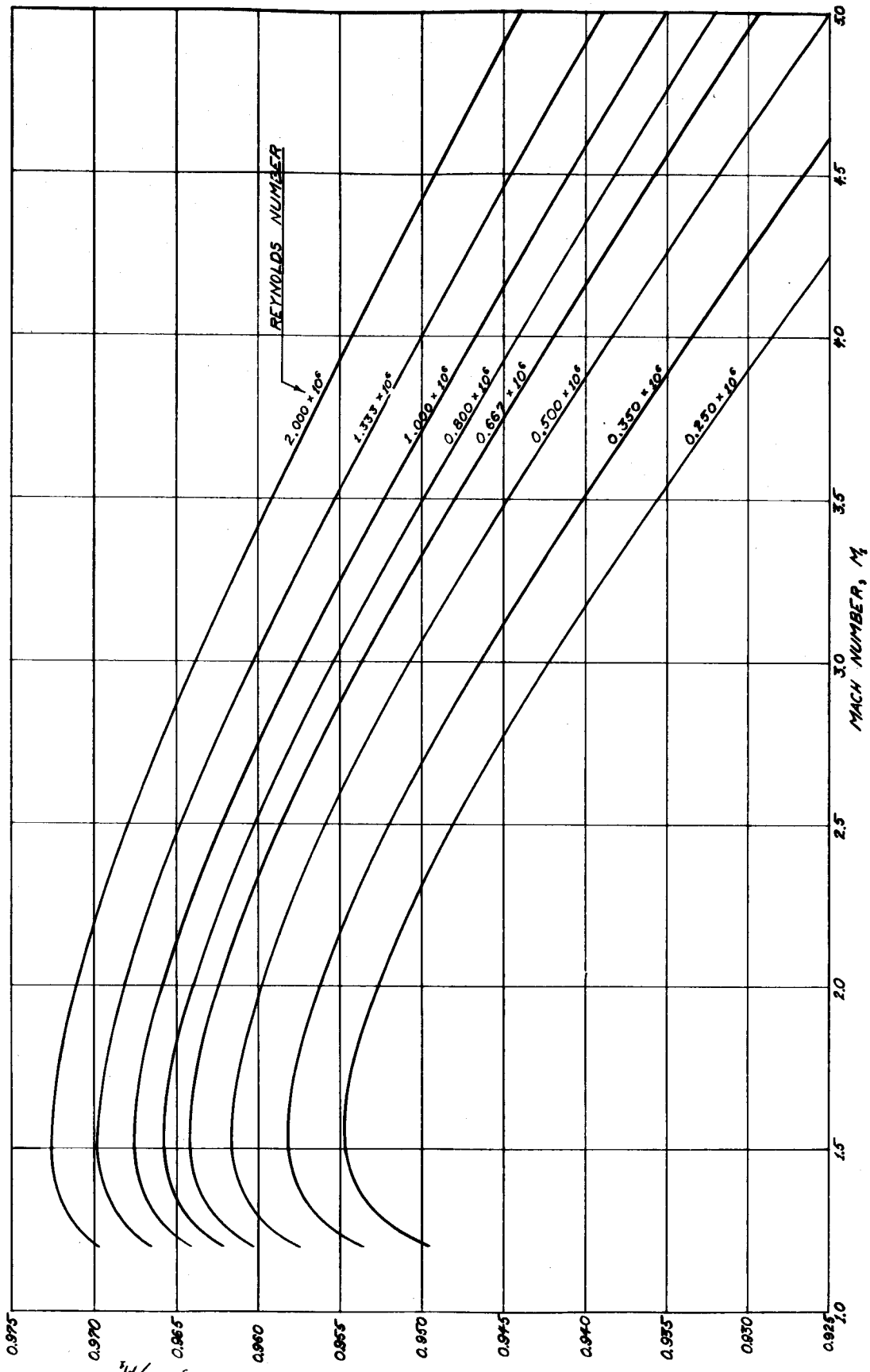

Figure 97. Mach Number Resulting from Shock Induced Separation of a Laminar Boundary Layer

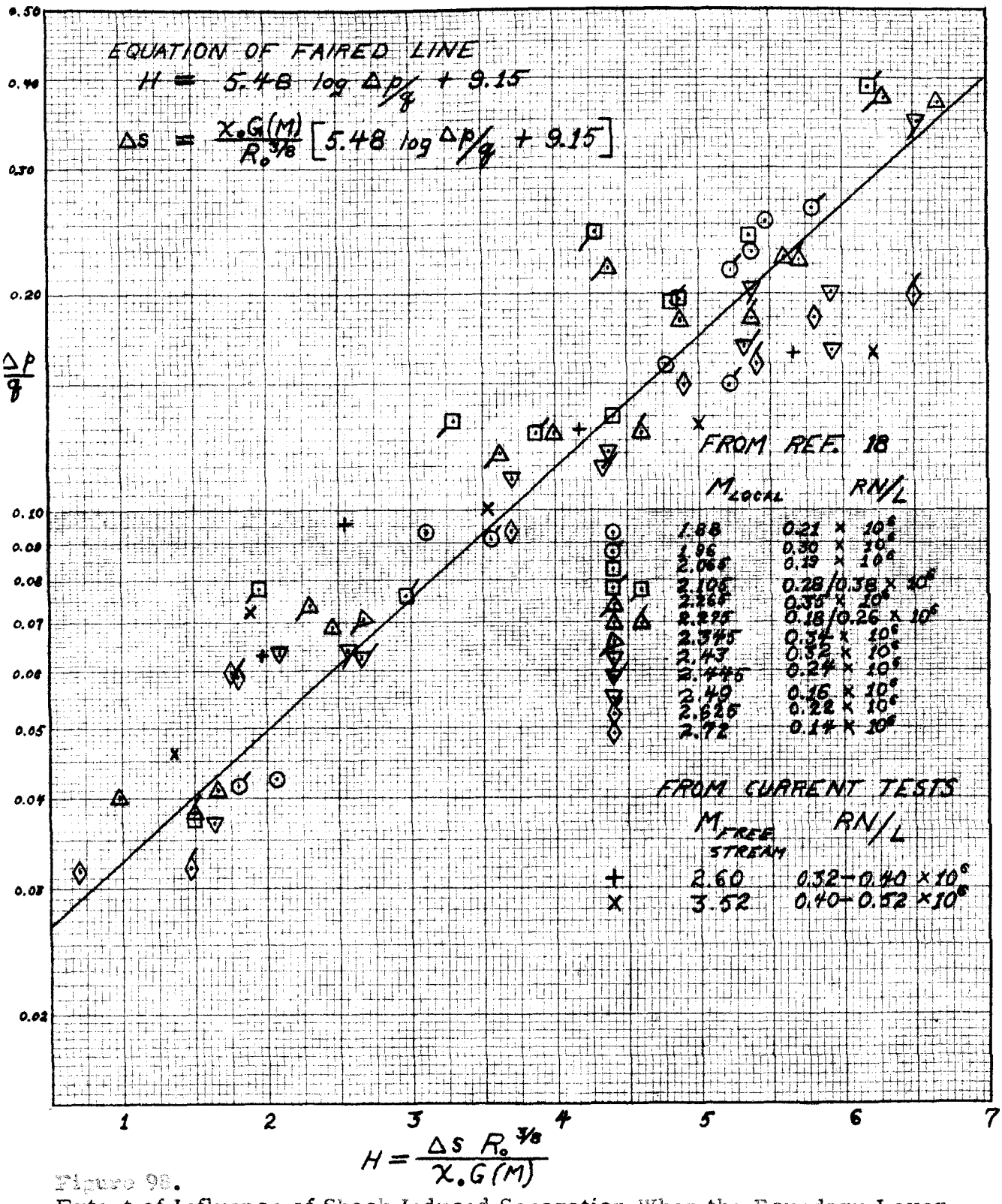

Figure 98.
Extent of Influence of Shock Induced Separation When the Boundary Layer is Laminar.

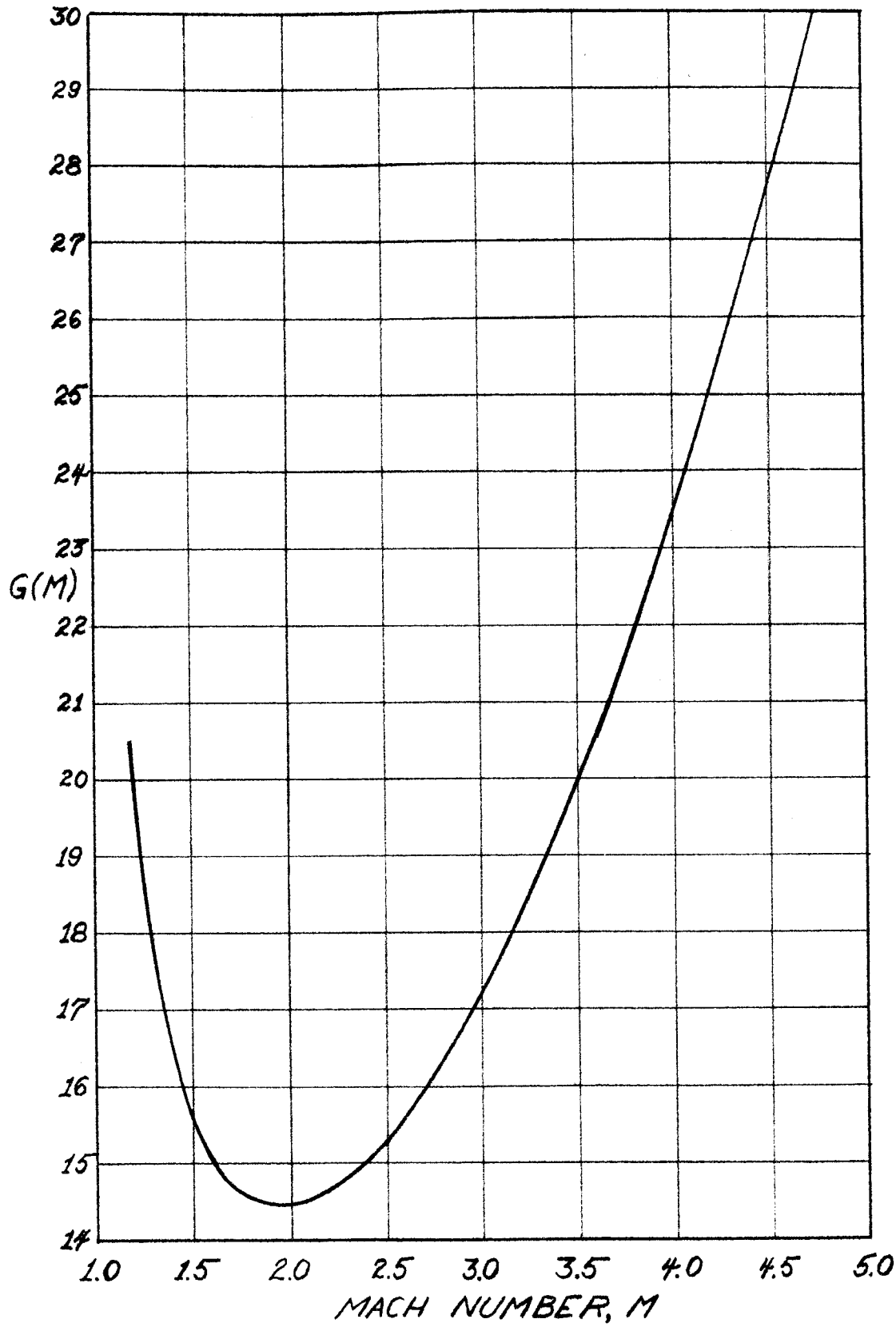

Figure 99. Mach Number Parameter Used in Locating Separation Point.

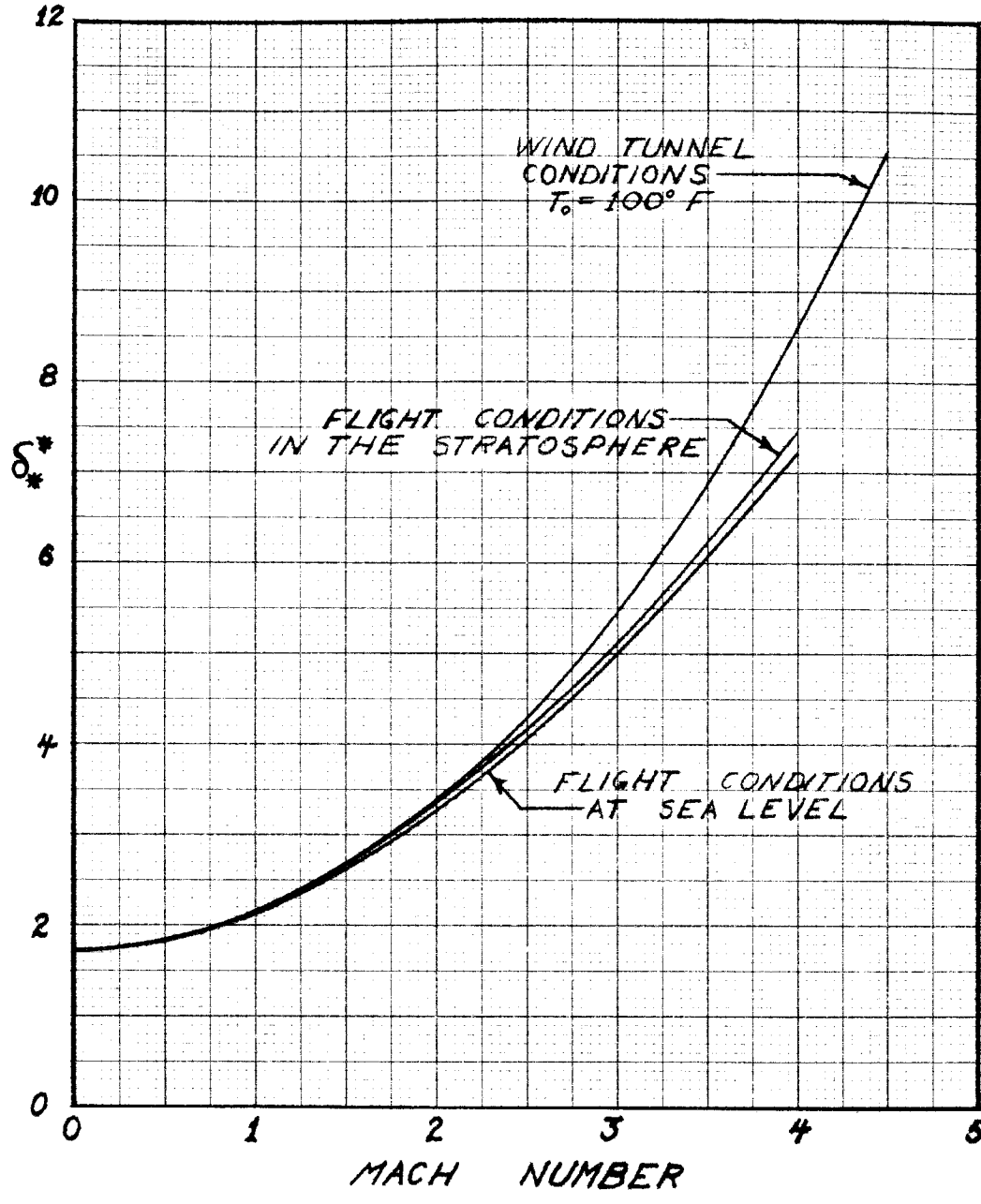

Figure 100. Displacement Thickness Parameter for Laminar Boundary Layer.

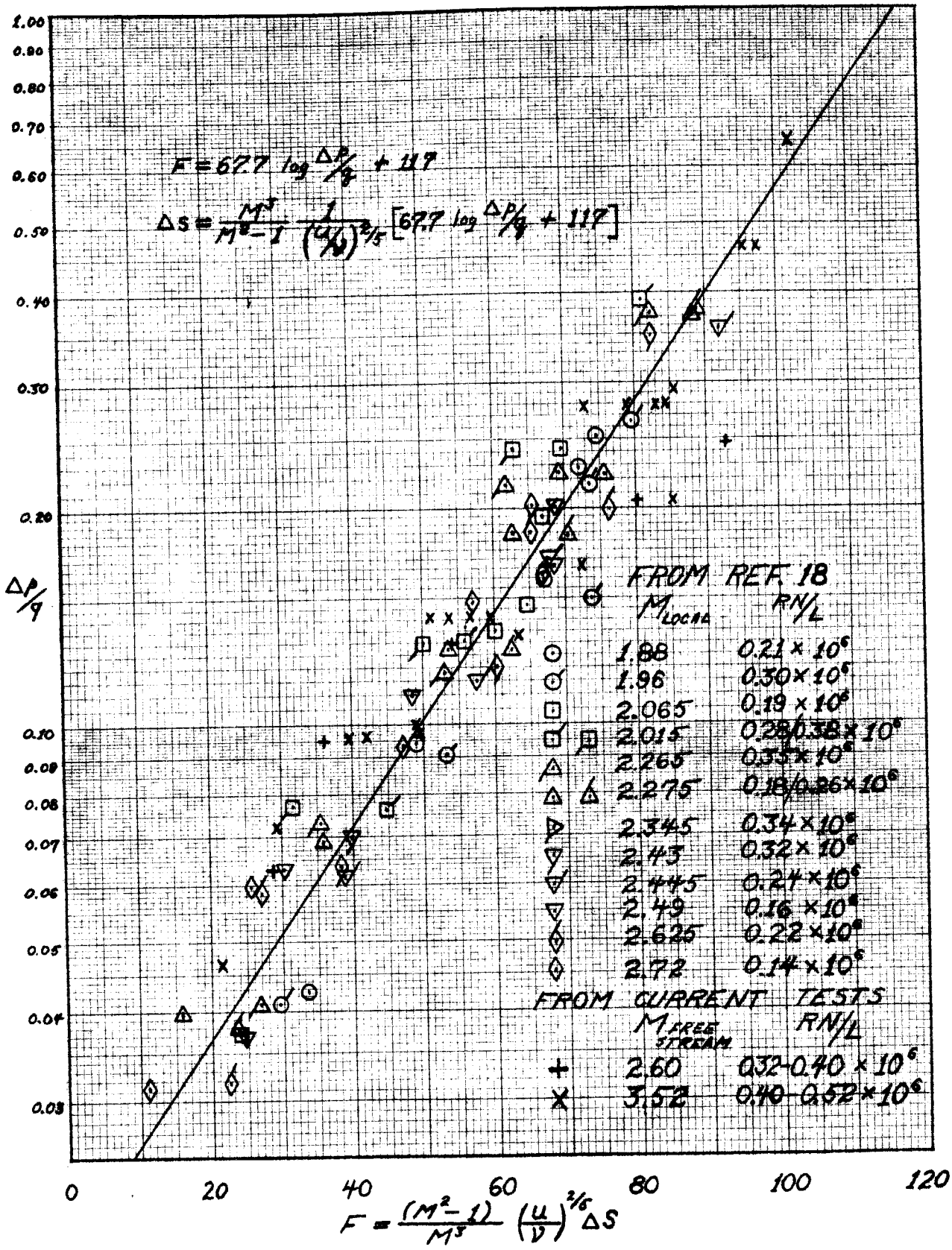

Figure 101. Alternate Method of Finding Extent of Influence of Shock Induced Separation when the Boundary Layer is Laminar.

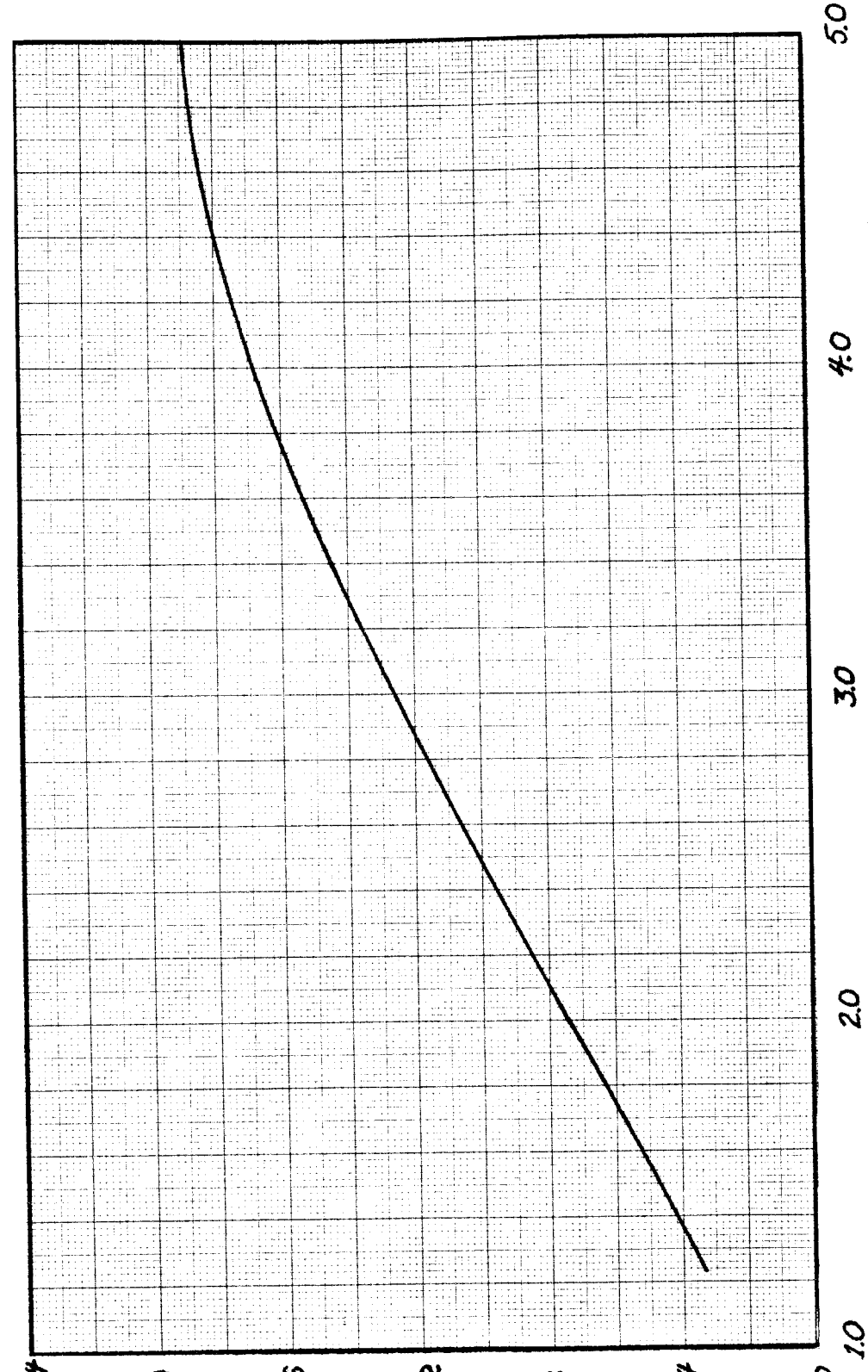

Figure 102. Pressure Rise Resulting From Shock Induced Separation of a Turbulent Boundary Layer.

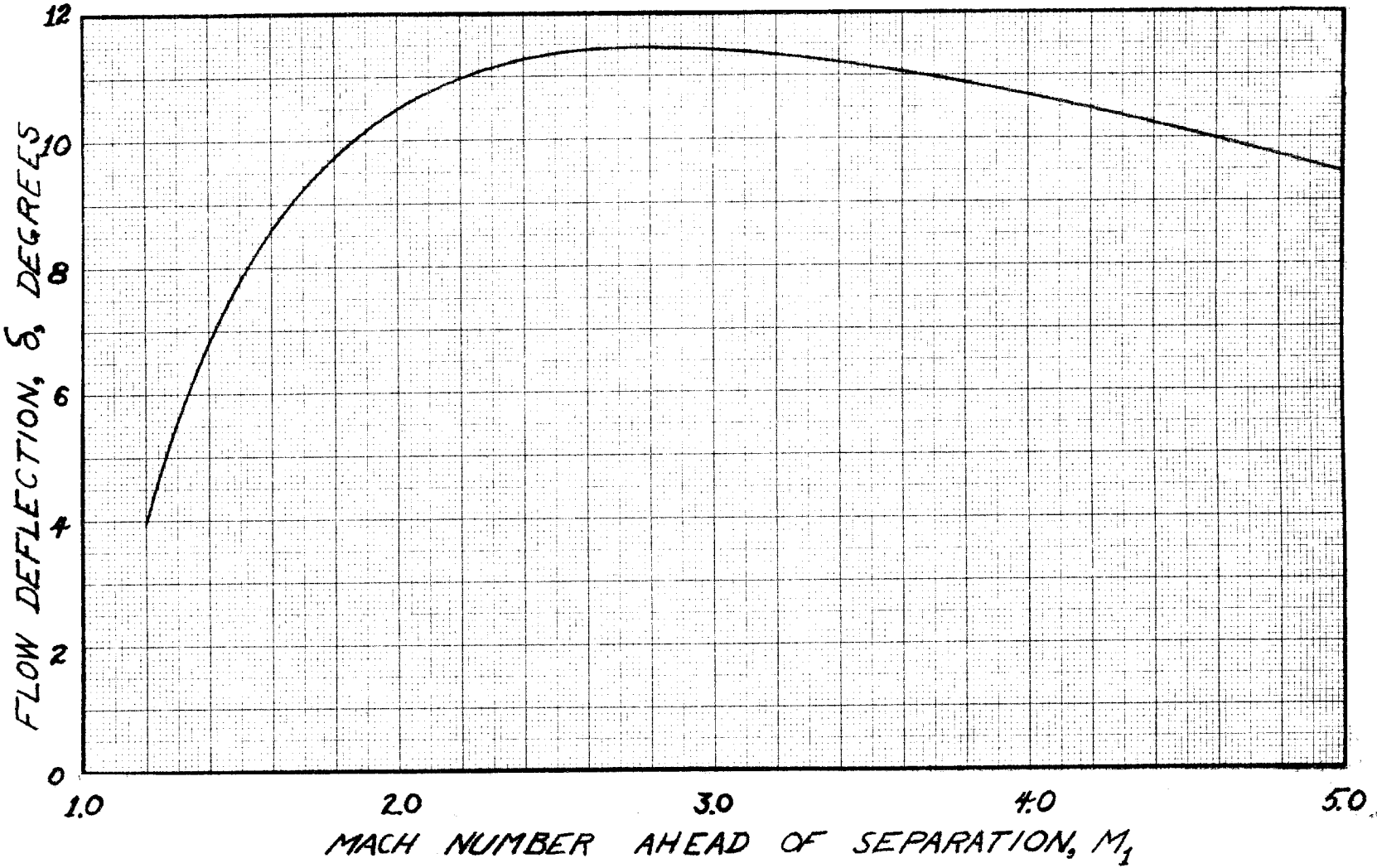

Figure 103. Flow Deflection Resulting From Shock Induced Separation of a Turbulent Boundary Layer.

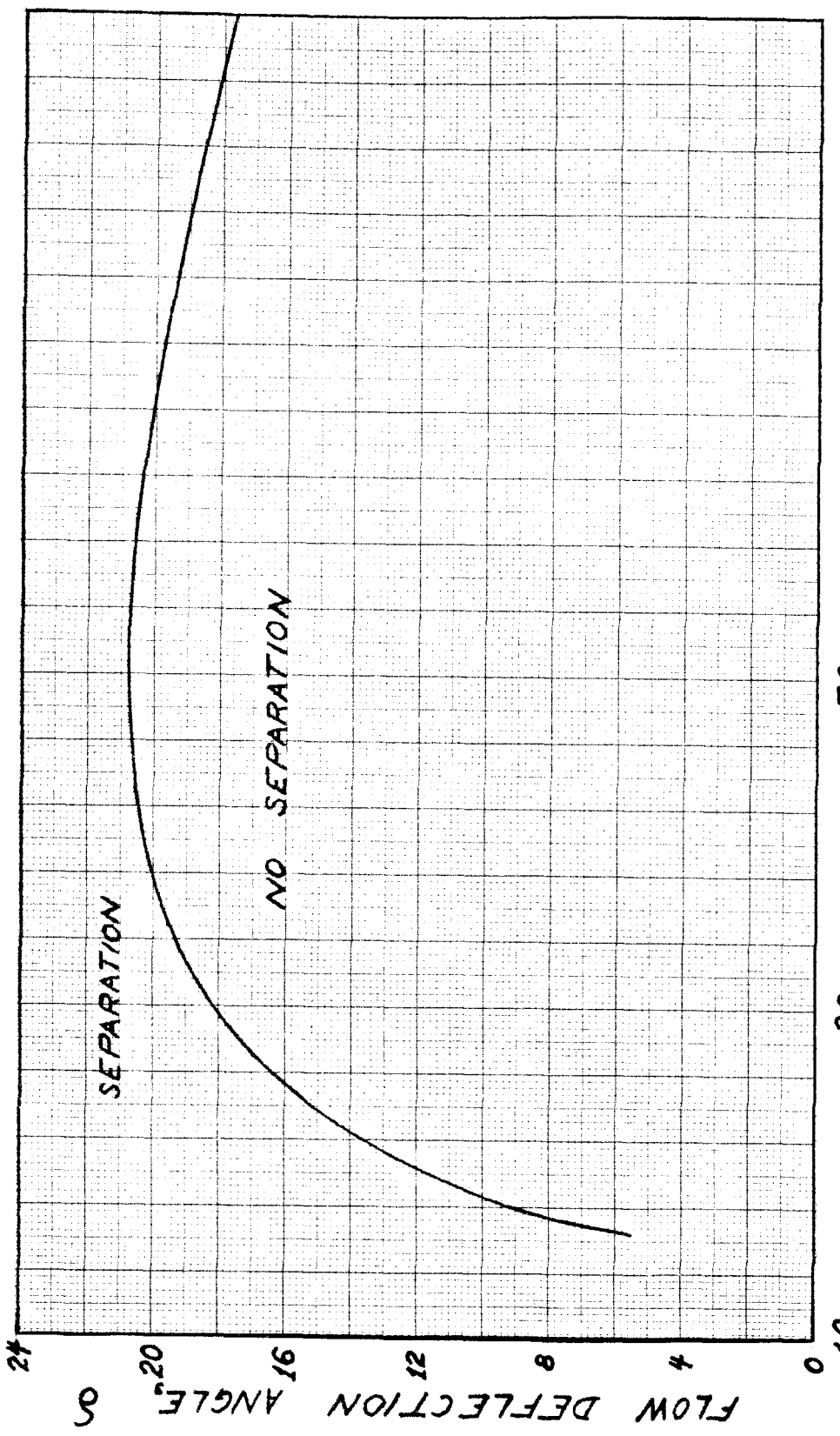

Figure 104. Flow Deflection that Causes Separation of a Turbulent Boundary Layer.

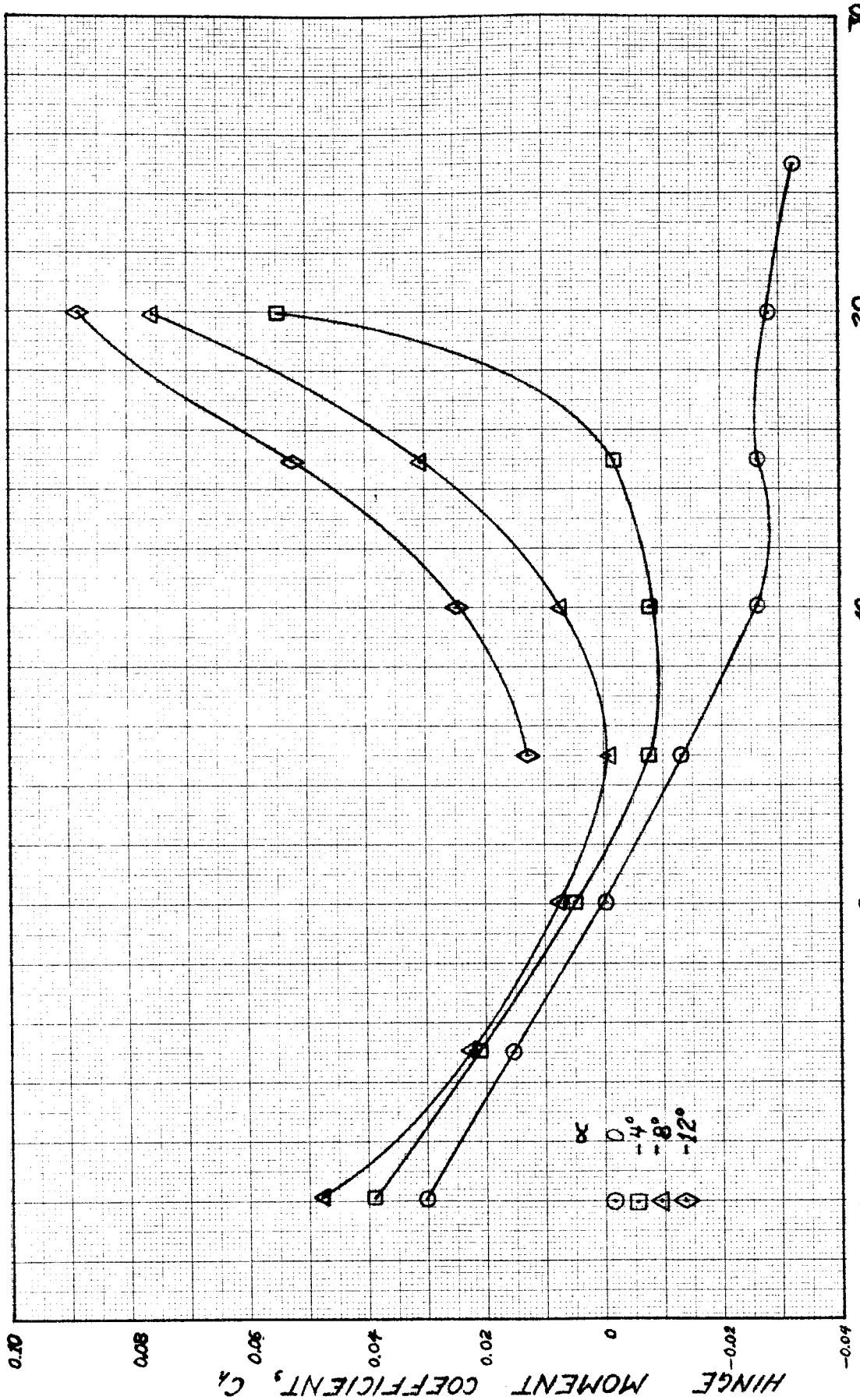

Figure 105. Hinge Moment Coefficients Obtained by Integrating the Pressure Distributions at Mach Number 3.52.

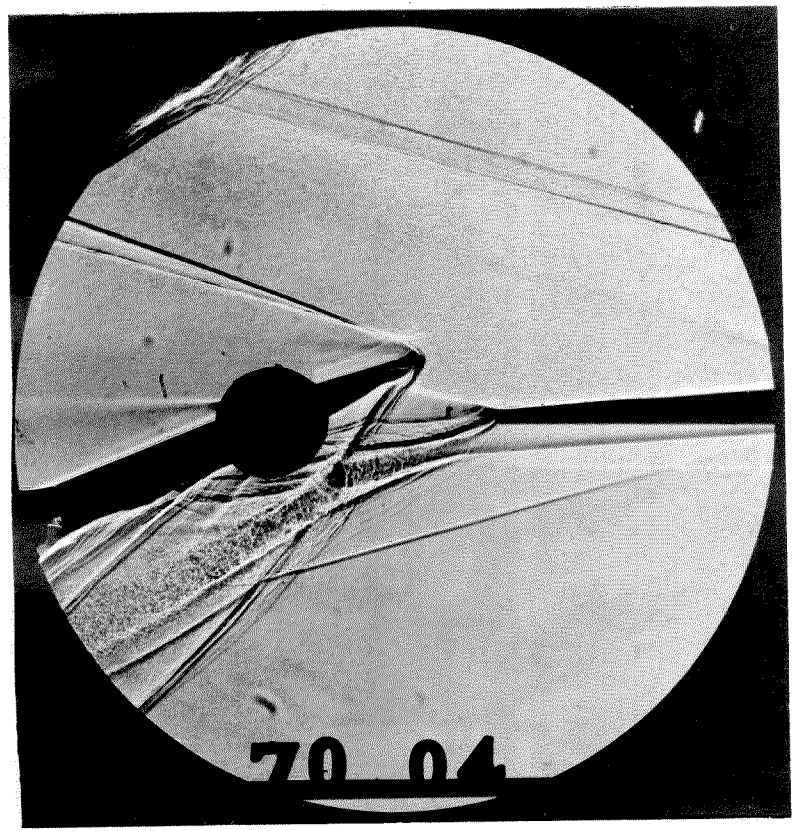

Figure 106. Shadowgraph, Control Surface Model, $\frac{1}{2}$" Gap, M = 3.52, RN/L = .57x10^6, $\alpha = -12^o$, $\delta = 20^o$

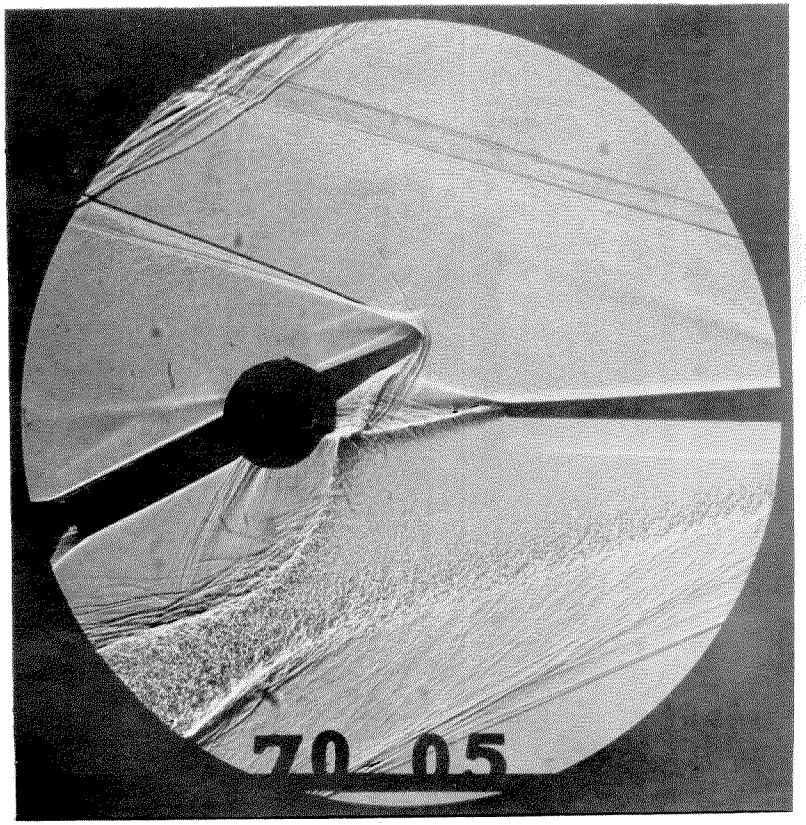

Figure 107. Shadowgraph, Control Surface Model, $\frac{1}{2}$" Gap, M = 3.52, RN/L = .57 x 10^6, $\alpha = -12^o$, $\delta = 25^o$

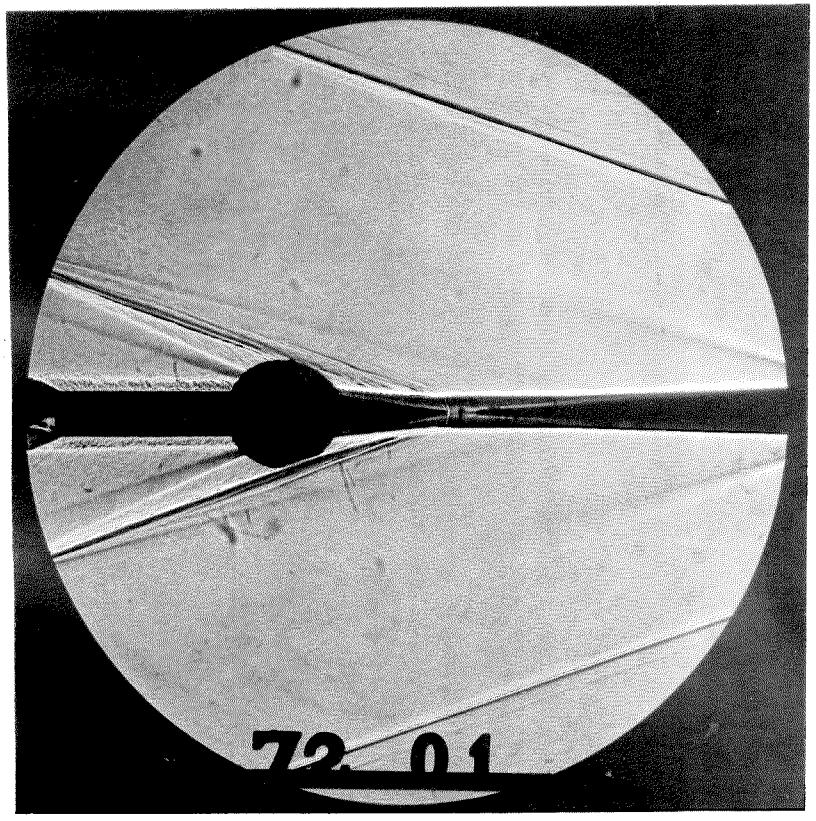

Figure 108. Shadowgraph, Control Surface Model, 1/4" Gap, M = 3.52, RN/L = 0.57 x 10^6, $\alpha = 0^o$, $\delta = 0^o$

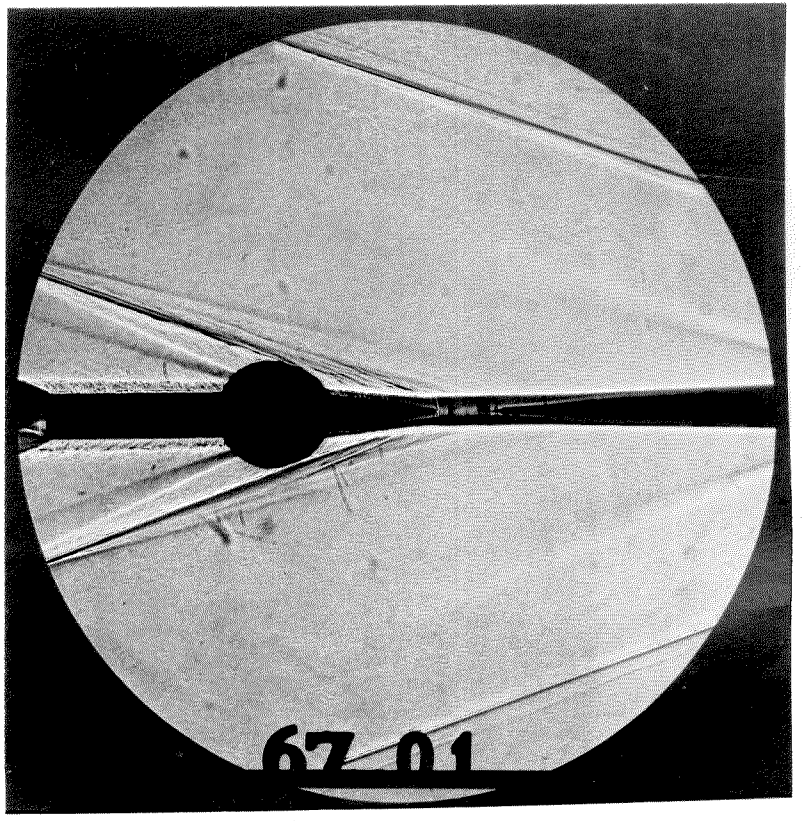

Figure 109. Shadowgraph, Control Surface Model, 1/2" Gap, M = 3.52, RN/L = 0.57 x 10^6, $\alpha = 0^o$, $\delta = 0^o$

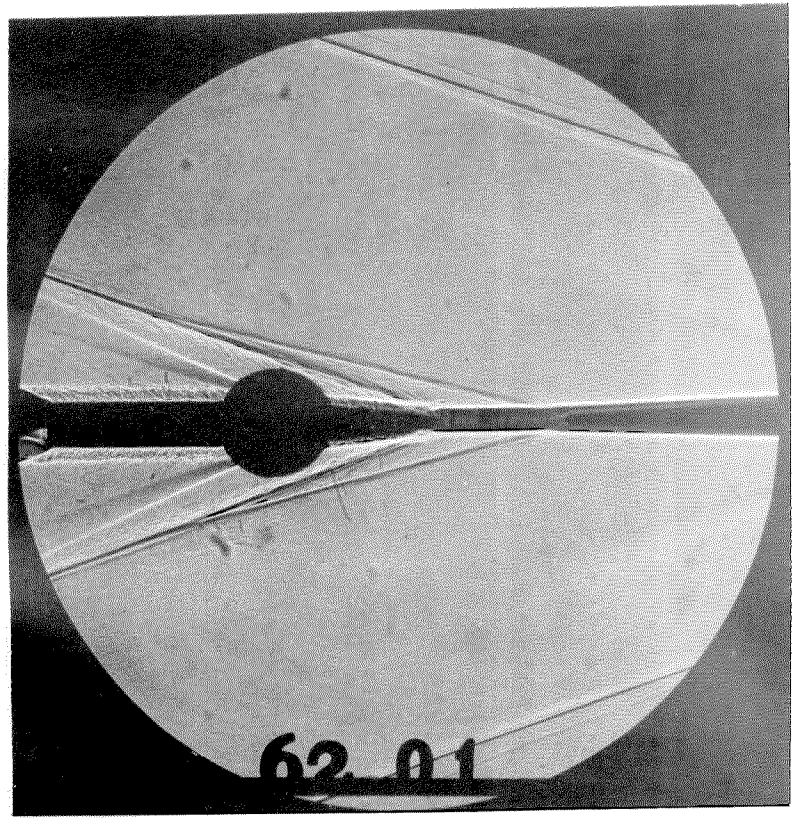

Figure 110. Shadowgraph, Control Surface Model, 1" Gap, M = 3.52, RN/L = 0.57×10^6, $\alpha = 0^\circ$, $\delta = 0^\circ$

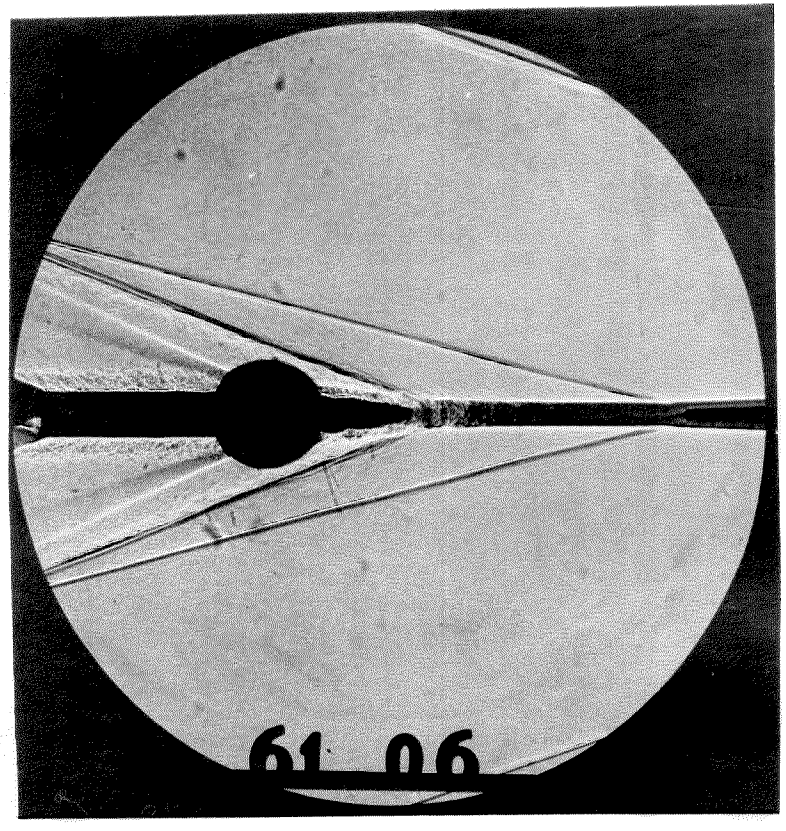

Figure 111. Shadowgraph, Control Surface Model, 2" Gap, M = 3.52, RN/L = 0.57×10^6, $\alpha = 0^\circ$, $\delta = 0^\circ$

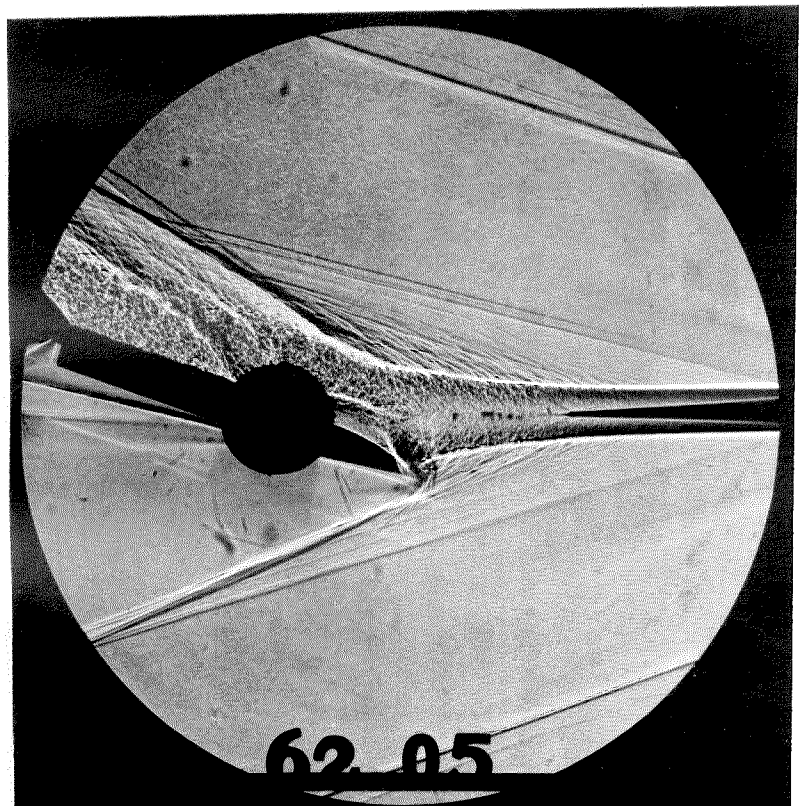

Figure 112. Shadowgraph, Control Surface Model, 1" Gap, M = 3.52, RN/L = 0.57×10^6, $\alpha = 0^\circ$, $\delta = -20^\circ$

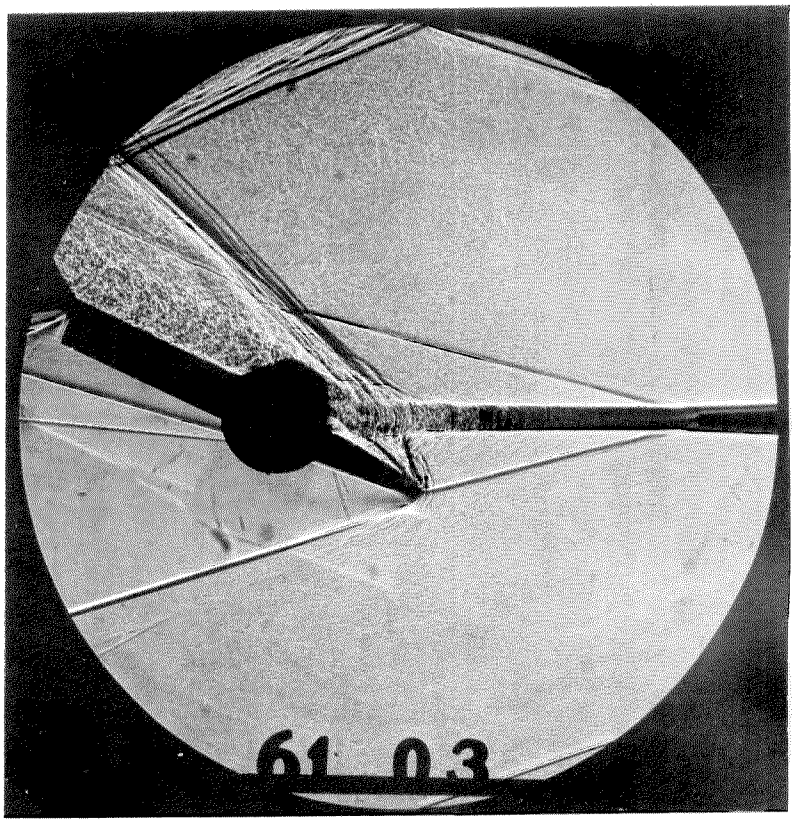

Figure 113. Shadowgraph, Control Surface Model, 2" Gap, M = 3.52, RN/L = 0.57×10^6, $\alpha = 0^\circ$, $\delta = -25^\circ$

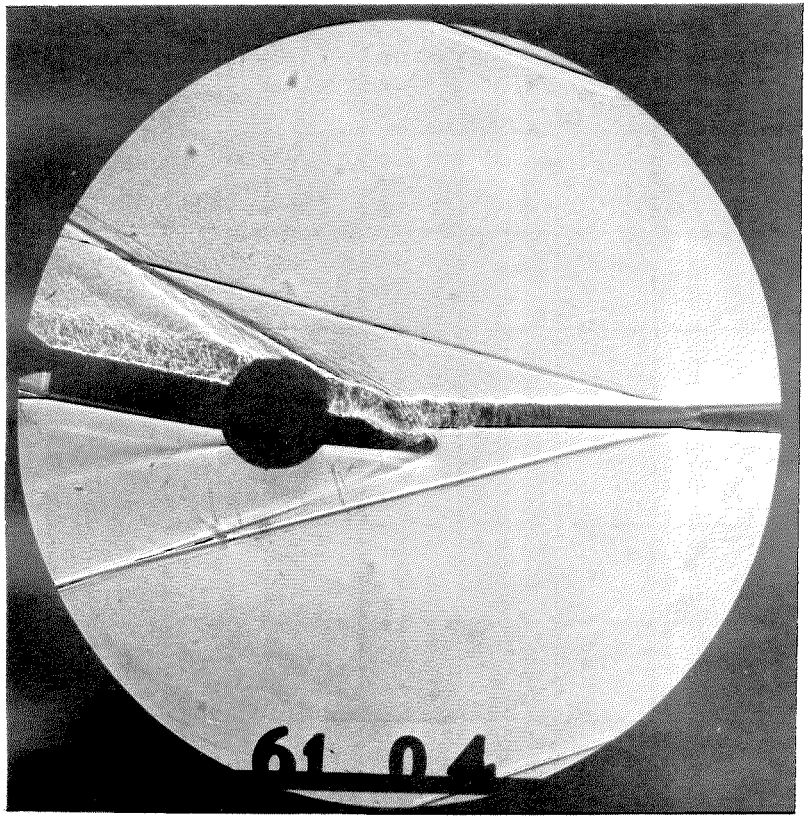

Figure 114. Shadowgraph, Control Surface Model, 2" Gap, M=3.52, RN/L = 0.57×10^6, $\alpha = 0^o$, $\delta = -10^o$

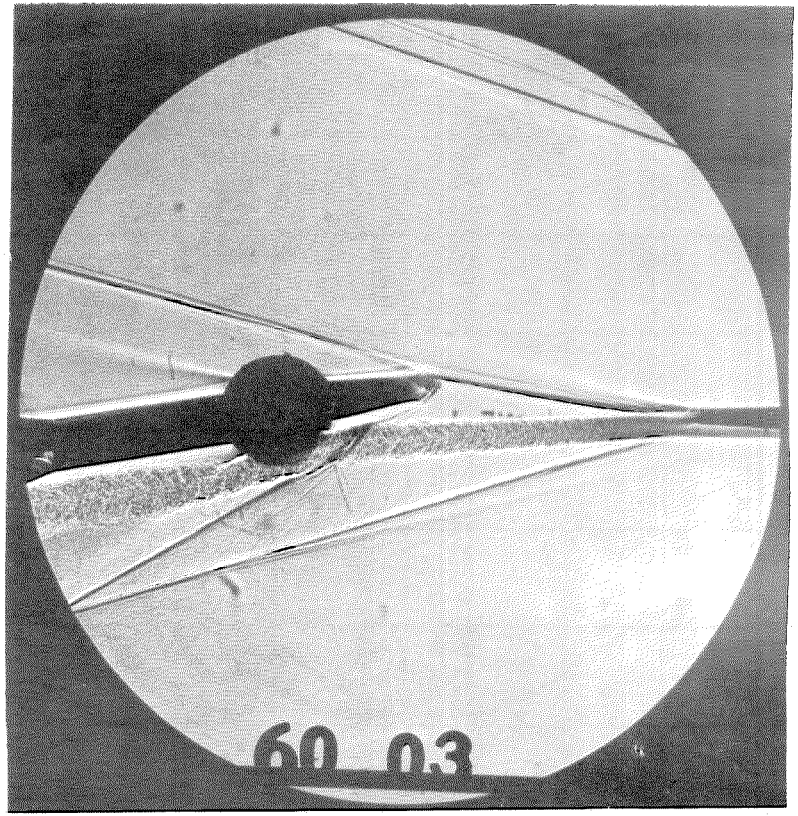

Figure 115. Shadowgraph, Control Surface Model, 2" Gap, M = 3.52, RN/L = 0.57×10^6, $\alpha = -4^o$, $\delta = 10^o$

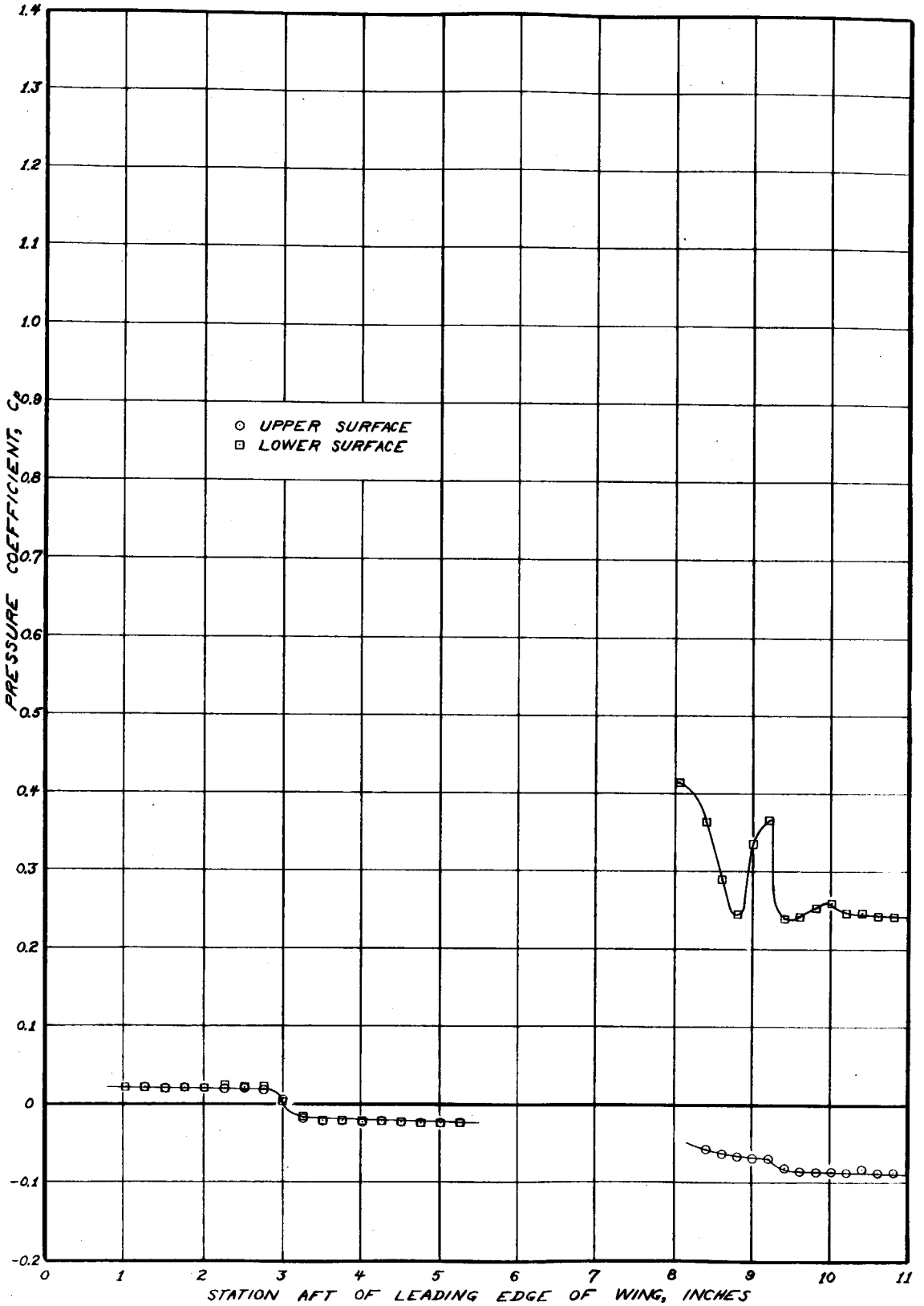

Figure 116. Pressure Distribution, 2" Gap, M = 3.52, RN/L = 0.54 x 10^6, $\alpha = 0^o$, $\delta = 15^o$

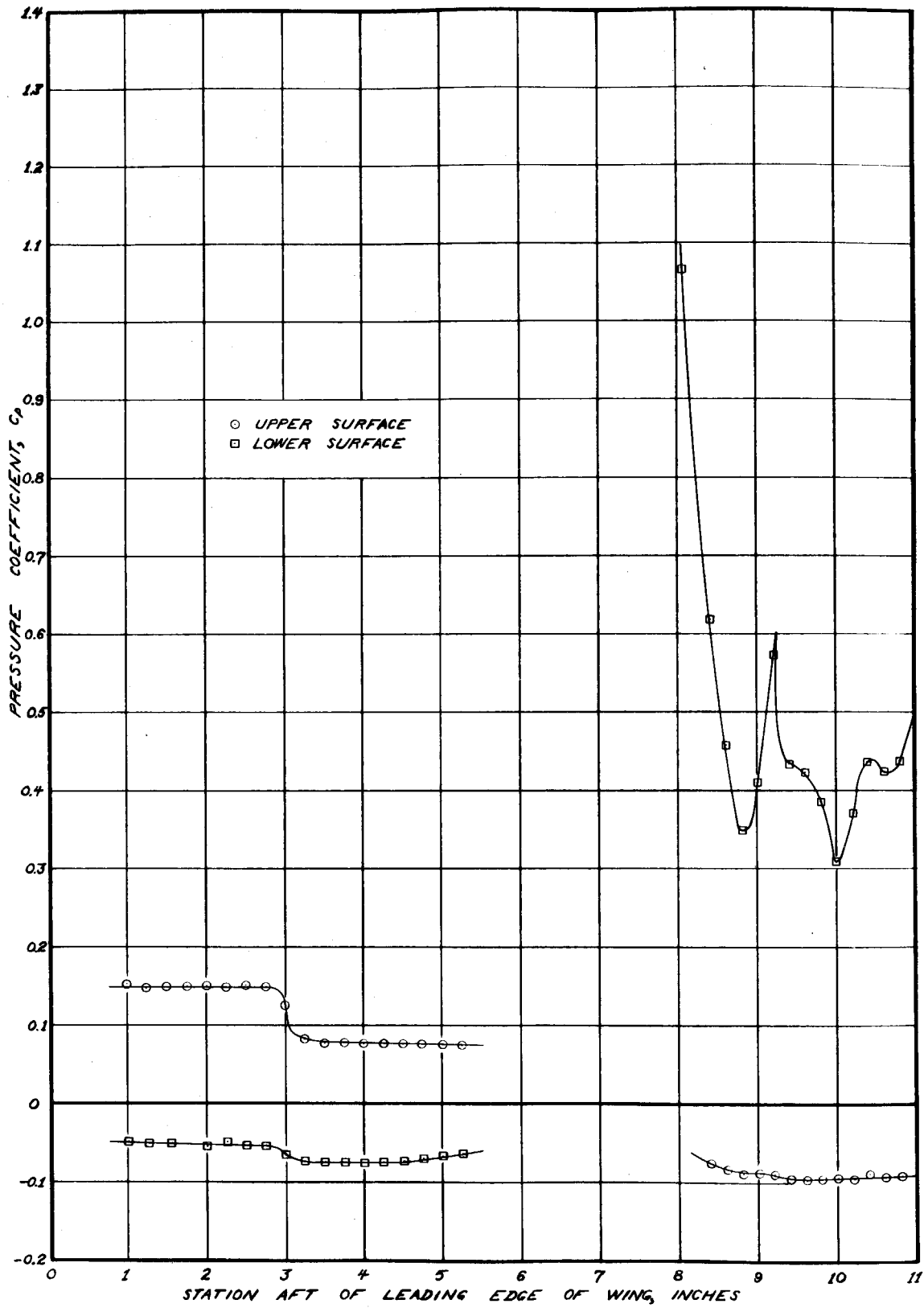

Figure 117. Pressure Distribution, 2" Gap, M = 3.52, RN/L = 0.54 x 10^6, $\alpha = -8^\circ$, $\delta = 25^\circ$

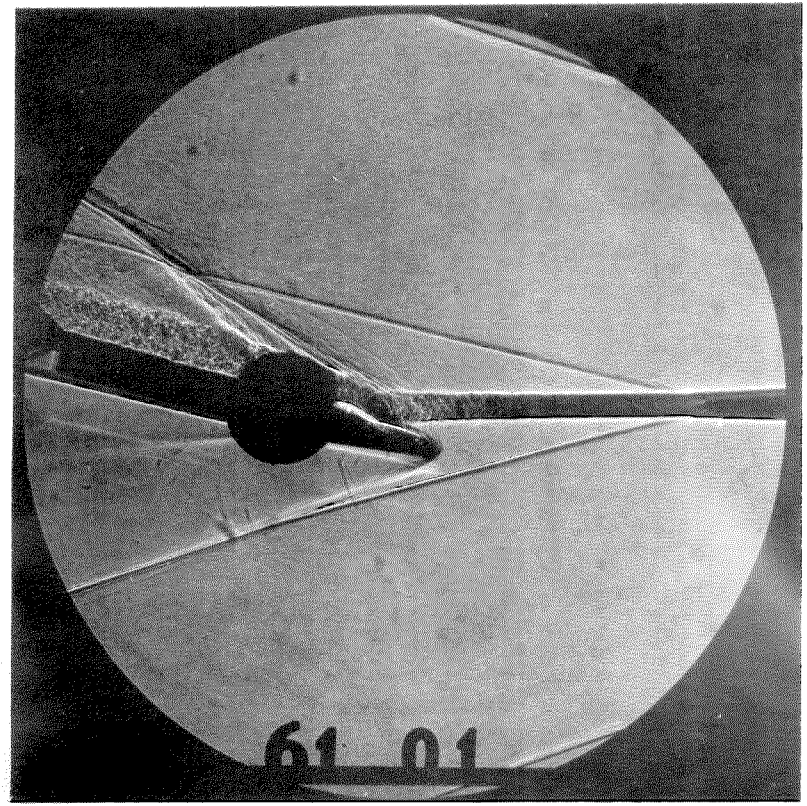

Figure 118. Shadowgraph, Control Surface Model, 2" Gap, M = 3.52, RN/L = 0.57×10^6, $\alpha = 0^\circ$, $\delta = 15^\circ$

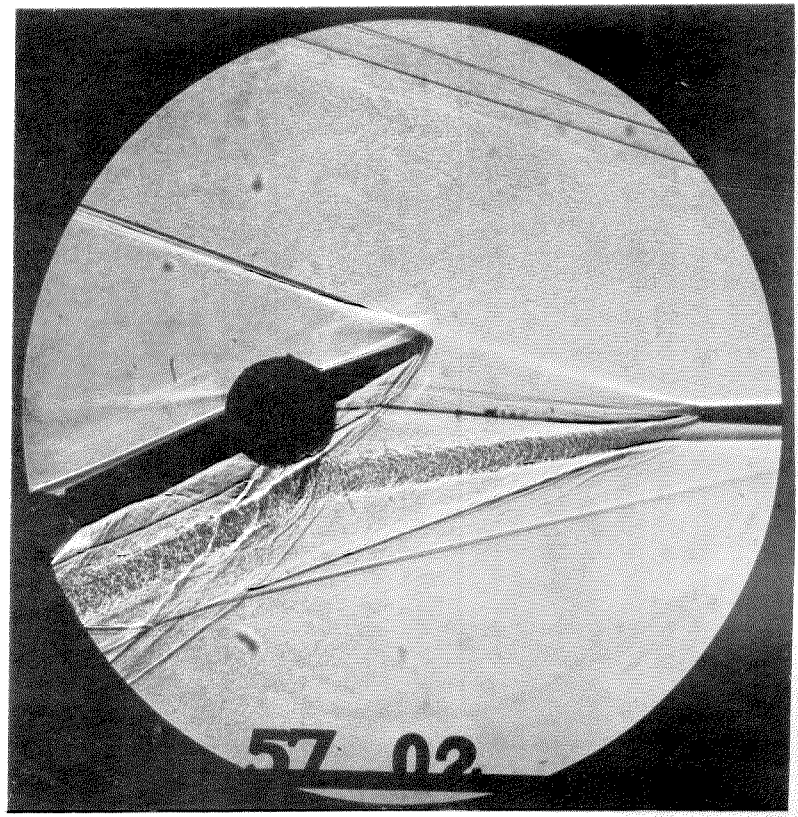

Figure 119. Shadowgraph, Control Surface Model, 2" Gap, M = 3.52, RN/L = 0.57×10^6, $\alpha = -8^\circ$, $\delta = 25^\circ$

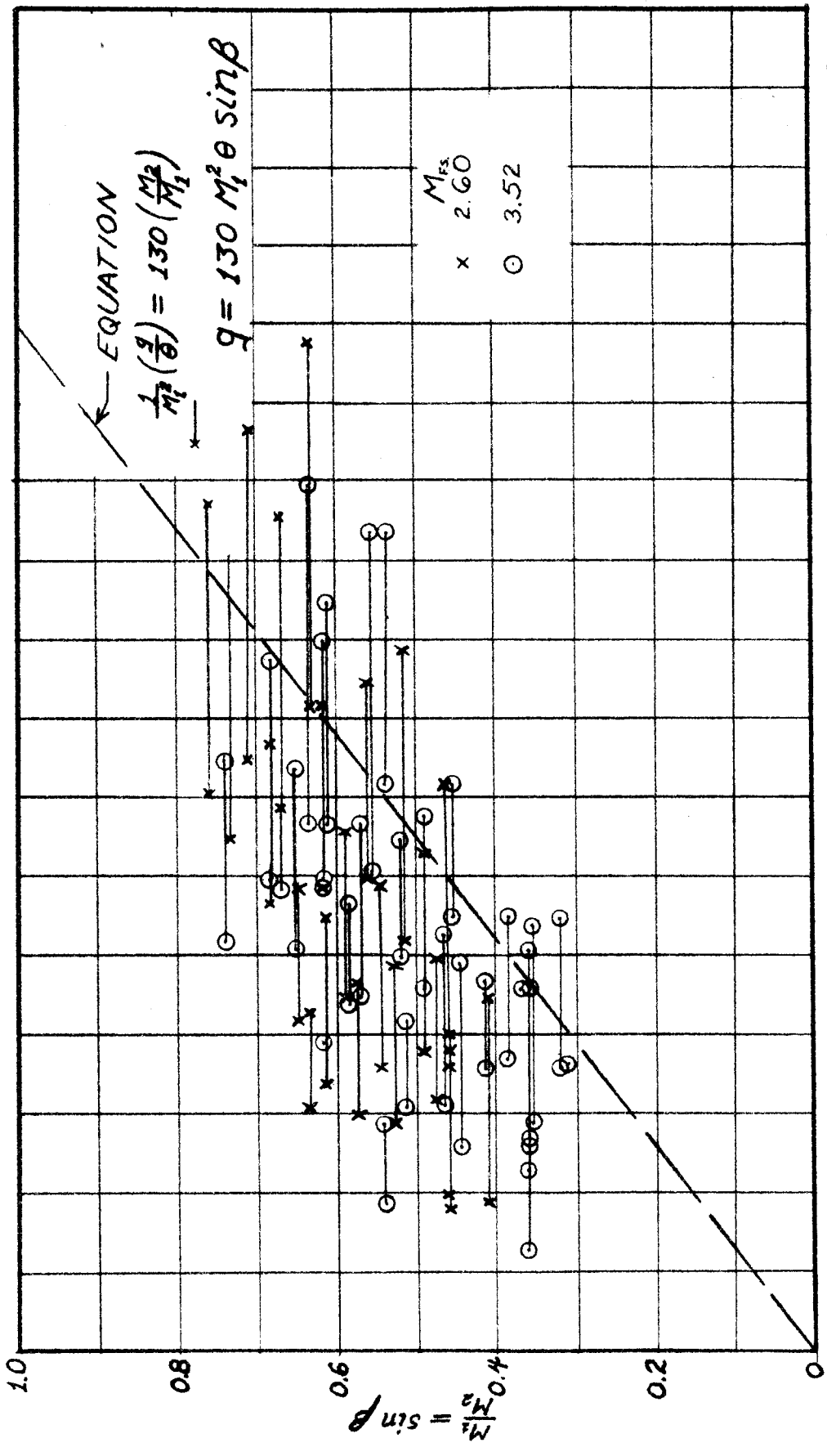

Figure 120. Correlation of Cap Size Required to Prevent Separation of a Laminar Boundary Layer.

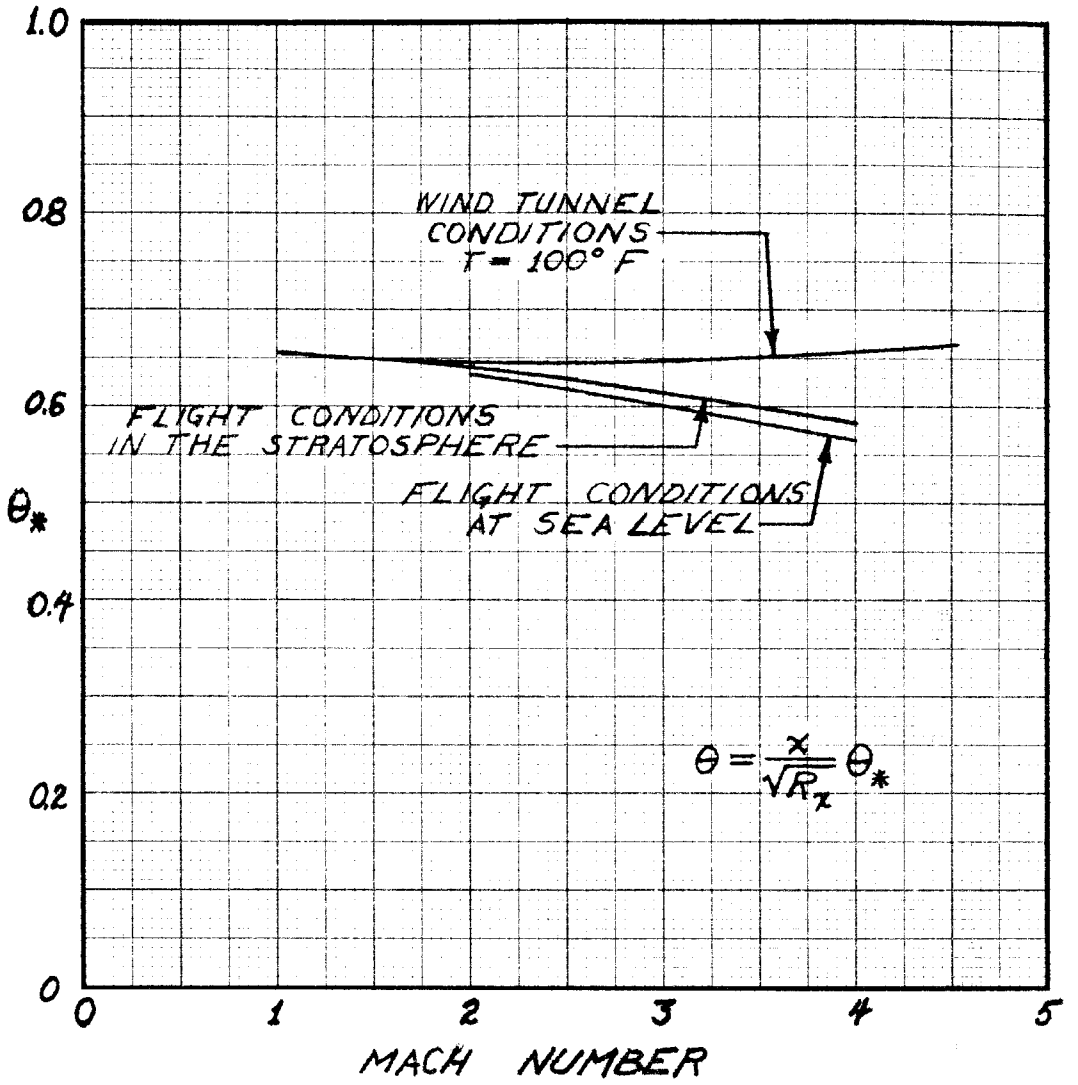

Figure 121. Momentum Thickness Parameter for a Laminar Boundary Layer.

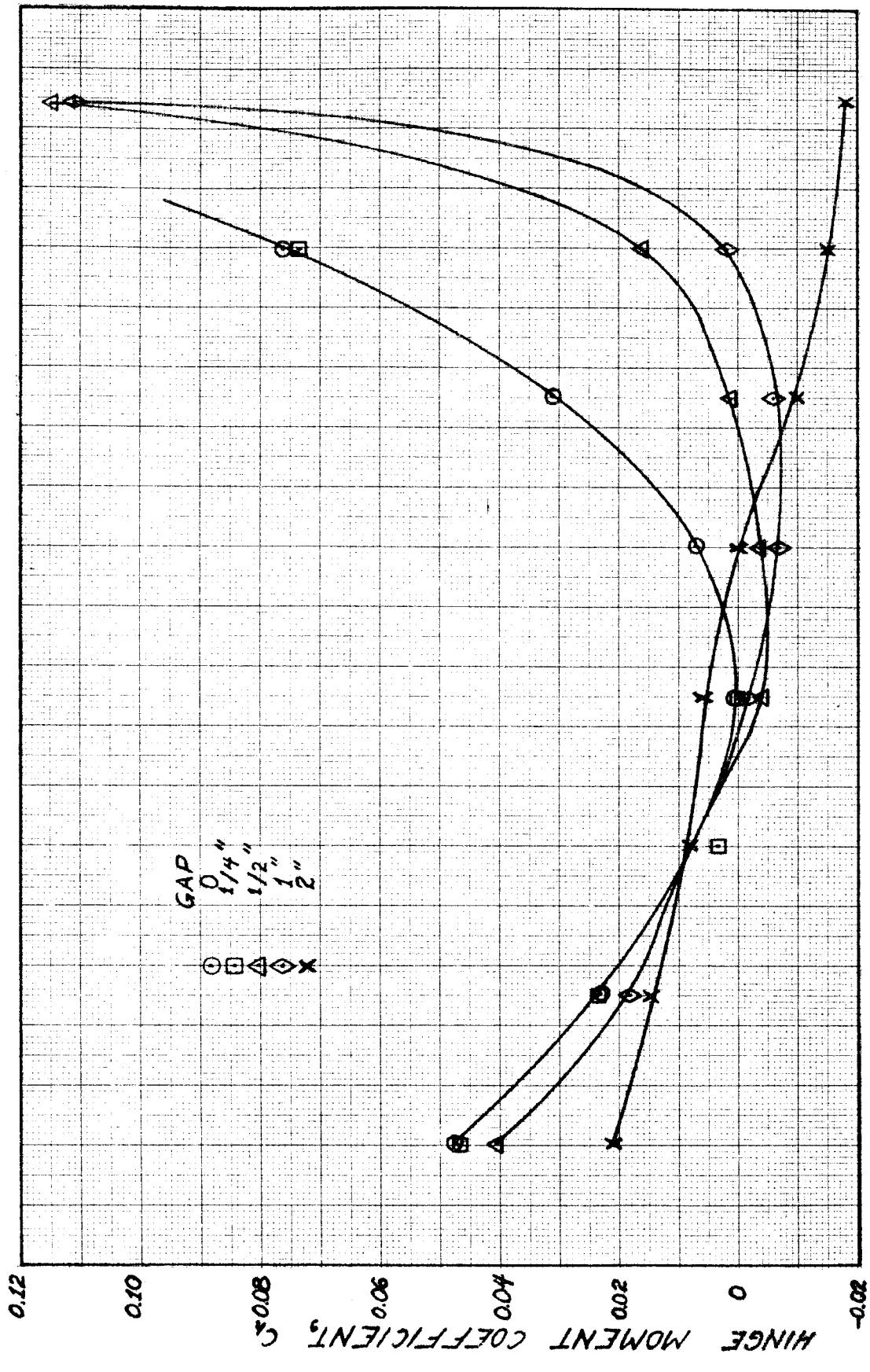

Figure 122. Effect of Gap on Hinge Moment Coefficients at Mach Number 3.52, $\alpha = -8^{\circ}$.